UAB
Universitat Autònoma de Barcelona

EXPERIMENTAL MODELS IN NON-ALCOHOLIC STEATOHEPATITIS AND EFFECTS OF THERAPEUTIC STRATEGIES BASED ON GUT MICROBIOTA

AURORA BARBERÁ BELLÉS

ADVERTIMENT. L'accés als continguts d'aquesta tesi doctoral i la seva utilització ha de respectar els drets de la persona autora. Pot ser utilitzada per a consulta o estudi personal, així com en activitats o materials d'investigació i docència en els termes establerts a l'art. 32 del Text Refós de la Llei de Propietat Intel·lectual (RDL 1/1996). Per altres utilitzacions es requereix l'autorització prèvia i expressa de la persona autora. En qualsevol cas, en la utilització dels seus continguts caldrà indicar de forma clara el nom i cognoms de la persona autora i el títol de la tesi doctoral. No s'autoritza la seva reproducció o altres formes d'explotació efectuades amb finalitats de lucre ni la seva comunicació pública des d'un lloc aliè al servei TDX. Tampoc s'autoritza la presentació del seu contingut en una finestra o marc aliè a TDX (framing). Aquesta reserva de drets afecta tant als continguts de la tesi com als seus resums i índexs.

ADVERTENCIA. El acceso a los contenidos de esta tesis doctoral y su utilización debe respetar los derechos de la persona autora. Puede ser utilizada para consulta o estudio personal, así como en actividades o materiales de investigación y docencia en los términos establecidos en el art. 32 del Texto Refundido de la Ley de Propiedad Intelectual (RDL 1/1996). Para otros usos se requiere la autorización previa y expresa de la persona autora. En cualquier caso, en la utilización de sus contenidos se deberá indicar de forma clara el nombre y apellidos de la persona autora y el título de la tesis doctoral. No se autoriza su reproducción u otras formas de explotación efectuadas con fines lucrativos ni su comunicación pública desde un sitio ajeno al servicio TDR. Tampoco se autoriza la presentación de su contenido en una ventana o marco ajeno a TDR (framing). Esta reserva de derechos afecta tanto al contenido de la tesis como a sus resúmenes e índices.

WARNING. The access to the contents of this doctoral thesis and its use must respect the rights of the author. It can be used for reference or private study, as well as research and learning activities or materials in the terms established by the 32nd article of the Spanish Consolidated Copyright Act (RDL 1/1996). Express and previous authorization of the author is required for any other uses. In any case, when using its content, full name of the author and title of the thesis must be clearly indicated. Reproduction or other forms of for profit use or public communication from outside TDX service is not allowed. Presentation of its content in a window or frame external to TDX (framing) is not authorized either. These rights affect both the content of the thesis and its abstracts and indexes.

DOCTORAL THESIS

EXPERIMENTAL MODELS IN NON-ALCOHOLIC STEATOHEPATITIS AND EFFECTS OF THERAPEUTIC STRATEGIES BASED ON GUT MICROBIOTA

Author:

AURORA BARBERÁ BELLÉS

Doctoral thesis directors:

Dr María Martell Pérez-Alcalde

Dr Salvador Augustin Recio

Doctoral thesis tutor:

Dr Joan Genescà Ferrer

Doctoral program in Medicine

Department of Medicine

Universitat Autònoma de Barcelona

Barcelona, 2023

AGRADECIMIENTOS

Se cierra una etapa, aunque no una cualquiera, sino una que me ha enseñado mucho y que siempre recordaré con cariño. Esta tesis es hoy una realidad gracias a todas esas personas que me han acompañado y para quien solo tengo palabras de gratitud.

En primer lugar, quiero dar las gracias a María Martell, Salvador Augustin y Joan Genescà por darme la oportunidad de realizar mi tesis doctoral en vuestro grupo y por ser mi guía a lo largo de todo este camino. A María, gracias por tu plena dedicación y tiempo, por estar siempre dispuesta a aclararme cualquier tipo de duda y por tu implicación en mi formación y aprendizaje. A Salva, gracias por haberme ayudado a mejorar como científica y por aportar tus ideas, siempre brillantes. A Joan, gracias por dar siempre tu punto de vista crítico y por haberme enseñado tanto a través de tu gran experiencia y conocimiento. También quiero dar las gracias a Juanma Pericàs y Meritxell Ventura por vuestras aportaciones durante nuestras reuniones, me han servido de mucho.

A Imma, has sido una parte fundamental en la realización de este trabajo, gracias porque contigo he aprendido mucho, tanto en el laboratorio como en el estabulario. Gracias también por haber sido tan atenta conmigo, voy a guardarte siempre un enorme cariño.

A Mar, mi fiel compañera desde los inicios, gracias por ser mi apoyo en todo momento y por todas las experiencias vividas en estos años. Me llevo una amiga para siempre.

A todos mis compañeros que han pasado por el laboratorio, Diana, Miren, Federico, Carla, Jéssica, Pol y María, me he sentido siempre muy bien acompañada por vosotros, gracias por haber aportado tanto en este trabajo.

A Mónica, Elena y Meri, gracias por echarme una mano siempre que lo he necesitado, por ser mi fuente de desahogo y por todos los ratitos que hemos pasado juntas dentro

y fuera del VHIR. También quiero dar las gracias a Qian, Sofía, Mer y Josep por haber amenizado mi día a día, sacándome siempre una sonrisa.

A mis amigas de tantos años, Rocío y Mar, gracias por siempre estar dispuestas a escuchar mis dramas, por ayudarme a desconectar en cada plan. Es una suerte que nuestros caminos hayan coincidido en Barcelona. A mis amigas y compañeras de piso durante dos años, Àurea y Sara, mil gracias por haberme acogido tan bien y por darme tan buenos consejos. Gracias también a mis queridas amigas Bea, Elia, Lucía, Marina, Judith, Carmen y Espe por haberme hecho sentir vuestro apoyo y cariño a pesar de la distancia. Volver a casa siempre ha supuesto un chute de energía gracias a vosotras.

A Miquel, mi apoyo incondicional y mi compañero de vida, gracias por estar en mis subidas y sobre todo en mis bajadas. Convivir con una doctoranda no habrá sido fácil, así que gracias por tu paciencia y por ser tan comprensivo.

A mis padres, mi hermana y mis abuelos, sois mis pilares y la razón de seguir persiguiendo todos mis sueños. Gracias a vosotros he podido llegar donde estoy ahora. Siempre me habéis dado el impulso que necesitaba para seguir adelante.

Mi más sincera gratitud a todos por haber formado parte de este camino.

¡Me siento muy afortunada!

ABBREVIATIONS

AAA	Aromatic amino acids
AdipoR2	Adiponectin receptor 2
Akt	Protein kinase B
ALD	Alcoholic liver disease
ALT	Alanine aminotransferase
AP	Alkaline phosphatase
AST	Aspartate aminotransferase
Ath	Atherogenic
BA	Bile acid
BCAA	Branched-chain amino acids
BER	Balanced error rate
CD	Control diet
CDAA	Choline-deficient L-amino acid-defined
CDD	Choline-deficient diet
CK	Cytokeratin
CLD	Chronic liver disease
COL1A1	Collagen type I alpha 1 chain
CON	Consortium of nine bacterial strains
CRN	NASH-Clinical Research Network

DAMPs	Damage-associated molecular patterns
eNOS	Endothelial nitric oxide synthase
ER	Endoplasmic reticulum
FFA	Free fatty acids
FGF19	Fibroblast growth factor 19
FMT	Fecal microbiota transplantation
FXR	Farnesoid X receptor
GAPDH	Glyceraldehyde-3-phosphate dehydrogenase
GLP-1	Glucagon-like peptide 1
H&E	Hematoxylin and eosin
HbA1c	Glycated hemoglobin
HBC	Hepatitis C virus
HBV	Hepatitis B virus
HCC	Hepatocellular carcinoma
HDL	High-density lipoprotein
HFCS	High-fructose corn syrup
HFD	High-fat diet
HFGFD	High-fat glucose-fructose diet
HFHC/GF	High-fat high-cholesterol glucose-fructose diet
HOMA-IR	Homeostasis model of insulin resistance index

HSC	Hepatic stellate cells
HSP	Heat shock protein
IHVR	Intrahepatic vascular resistance
iNOS	Inducible nitric oxide synthase
IR	Insulin resistance
IRS	Insulin receptor substrate
KC	Kupffer cells
KLF2	Kruppel-like factor 2
LDL	Low-density lipoprotein
LepR	Leptin receptor
LPS	Lipopolysaccharide
LSEC	Liver sinusoidal endothelial cells
MAFLD	Metabolic dysfunction-associated fatty liver disease
MAP	Mean arterial pressure
MCDD	Methionine-choline deficient diet
MDD	Methionine-deficient diet
NAFL	Non-alcoholic fatty liver
NAFLD	Non-alcoholic fatty liver disease
NAS	NAFLD activity score
NASH	Non-alcoholic steatohepatitis

NO	Nitric oxide
PAMPs	Pathogen-associated molecular patterns
PBF	Portal vein flow
PH	Portal hypertension
PI3K	Phosphatidylinositol 3-kinase
PP	Portal pressure
PPAR	Peroxisome proliferator–activated receptor
PYY	Peptide YY
ROS	Reactive oxygen species
RT-qPCR	Quantitative reverse-transcription polymerase chain reaction
S14	Spot14
SCFA	Short-chain fatty acids
SEM	Scanning electron microscope
SEM	Standard error of the mean
Shh	Sonic hedgehog
SMABF	Superior mesenteric artery blood flow
SMAR	Superior mesenteric artery resistance
STZ	Streptozotocin
TG	Triglycerides
TLM	Telmisartan

TLR	Toll-like receptor
TMAO	Trimethylamine N-oxide
TNF-α	Tumor necrosis factor-alpha
VEGF	Vascular endothelial growth factor
VEH	Vehicle
VIP	Variable importance
VLDL	Very low-density lipoprotein
WMS	Whole metagenome shotgun
ZO-1	Zonula occludens-1
α-SMA	Alpha-smooth muscle actin

TABLE OF CONTENTS

SUMMARY

Non-alcoholic fatty liver disease (NAFLD) and its progressive form non-alcoholic steatohepatitis (NASH), are currently a major public health concern. The current lack of approved therapies encourages to search for new treatments that allow reversing the progression of NASH, and there is an ongoing challenge to identify preclinical models that best mimic human pathology. The gut microbiota has gained much attention in the past few years because of its association with metabolic disorders, including NAFLD. Therefore, the use of gut microbial approaches could be considered for treatment or prevention of NAFLD.

This thesis follows previous work of our group, in which a rat model of NASH without fibrosis induced by a high-fat glucose-fructose diet (HFGFD) for 8 weeks, allowed us to elucidate the link between insulin resistance (IR), endothelial dysfunction and the gut microbiota in the development of portal hypertension (PH). Here, we first aimed to evaluate the persistence of PH and underlying mechanisms in a 36-week HFGFD-induced rat model. We found that, liver fat *per se* (in the absence of endothelial dysfunction or fibrosis), is able to induce PH due to a marked increase in the hepatocyte area that promotes the mechanical reduction of the hepatic sinusoidal area.

Second, considering that our group demonstrated an amelioration on PH by fecal microbiota transplantation (FMT), we used a microbial consortia of defined composition, as a more patient-friendly approach, to test its effects in two *in vivo* rodent models of NASH: an 8-week HFGFD-induced rat model, and the STAM™ mouse model. In the NASH rats, an improvement of PH and endothelial function was observed. Gut microbial compositional changes also revealed that the consortium achieved a more defined and richer replacement of the gut microbiome than FMT. Moreover, liver transcriptomics suggested a beneficial modulation of pro-fibrogenic pathways. An improvement in histological liver fibrosis was then confirmed in the STAM™ study,

significantly reducing collagen- and fibronectin-positive areas in liver sections at 12 weeks. The bacterial consortium also improved the NAFLD activity score (NAS), consistent with a decrease in steatosis and ballooning. Inflammation (as measured through macrophage F4/80 positive area) and apoptosis (reduction in serum cytokeratin 18 levels) were also reduced. Therefore, administration of a specific bacterial consortium of defined composition can ameliorate NASH, PH and fibrosis, and delay disease progression.

Finally, we developed a rat model (termed FIBRO-SH rat model) following a high-fat high-cholesterol glucose-fructose diet (HFHC/GF) during 16 weeks in order to reproduce the full NAFLD phenotype with fibrosis. The 16-week HFHC/GF intervention was able to induce increased NAS with marked histological liver fibrosis, significant PH and endothelial dysfunction promoted by hepatic IR. In conclusion, the FIBRO-SH rat model could become a suitable model for basic research on the advanced stages of NAFLD and for testing anti-fibrotic therapies in this pathology.

RESUMEN

La enfermedad de hígado graso no alcohólico (EHGNA) y su forma progresiva, la esteatohepatitis no alcohólica (EHNA), constituyen hoy en día, un importante problema de salud pública. Actualmente no existen terapias aprobadas que permitan revertir la progresión de la EHNA por lo que nos vemos en la necesidad de buscar nuevos tratamientos y de identificar y desarrollar nuevos modelos preclínicos que imiten lo mejor posible la patología en humanos. La microbiota intestinal ha sido objeto de gran interés en los últimos años debido a su asociación con los trastornos metabólicos, incluyendo la EHGNA. Por lo tanto, el uso de terapias basadas en microbiota intestinal para el tratamiento o la prevención de la EHGNA, se ha considerado como una aproximación interesante.

Esta tesis es la continuación de un trabajo previo de nuestro grupo, en el que un modelo de EHNA en rata inducido por una dieta de 8 semanas alta en grasas y en glucosa y fructosa (HFGFD), nos permitió dilucidar el vínculo entre la resistencia a la insulina (IR), la disfunción endotelial y la microbiota intestinal en el desarrollo de la hipertensión portal (HP), en ausencia de fibrosis. En primer lugar, nos propusimos evaluar la persistencia de la HP y los mecanismos subyacentes en un modelo de rata inducido por la dieta HFGFD durante 36 semanas. Encontramos que, la grasa hepática *per se* (en ausencia de disfunción endotelial o fibrosis), es capaz de inducir HP debido a un marcado aumento del área de los hepatocitos que promueve la reducción mecánica del área sinusoidal hepática.

En segundo lugar, teniendo en cuenta que nuestro grupo demostró una mejora de la HP mediante el trasplante de microbiota fecal (TMF), utilizamos una combinación microbiana de composición definida, como una alternativa más confortable para el paciente, para probar sus efectos en dos modelos *in vivo* de EHNA en roedores: un

modelo de rata inducido por la dieta HFGFD durante 8 semanas y el modelo de ratón STAM^{TM}. En las ratas con EHNA, se observó una mejora de la HP y de la función endotelial. Los cambios en la composición microbiana intestinal también revelaron que la combinación bacteriana logró una sustitución más definida y rica de la microbiota que el TMF. Además, la transcriptómica hepática sugirió una regulación beneficiosa de las vías profibrogénicas. En el modelo de ratón STAM^{TM}, se confirmó la mejora de la fibrosis histológica, reduciéndose significativamente las áreas positivas en colágeno y fibronectina en hígado a las 12 semanas. La combinación bacteriana también disminuyó la actividad EHGNA (NAS, del inglés *NAFLD Activity Score*), en consonancia con una disminución de la esteatosis y de la balonización hepatocitaria. Además, disminuyó la inflamación (mediante la reducción del área positiva F4/80 de los macrófagos) y la apoptosis (mediante la reducción de los niveles séricos de citoquetatina-18). Por lo tanto, la administración de una combinación bacteriana específica de composición definida puede mejorar la EHNA, la HP y la fibrosis, y retrasar la progresión de la enfermedad.

Por último, desarrollamos un modelo de rata (denominado modelo FIBRO-SH) que siguió una dieta alta en grasas, en colesterol y en glucosa y fructosa (HFHC/GF) durante 16 semanas para reproducir el fenotipo completo de EHGNA con fibrosis. La intervención de la dieta HFHC/GF durante 16 semanas fue capaz de inducir un aumento de la actividad de EHNA con una marcada fibrosis hepática, una HP significativa y disfunción endotelial promovida por IR hepática. En conclusión, el modelo FIBRO-SH podría convertirse en un modelo adecuado para la investigación básica de las fases avanzadas de la EHGNA y para probar terapias antifibróticas en esta patología.

1. INTRODUCTION

1. INTRODUCTION

1.1. Chronic liver diseases

Chronic liver disease (CLD) refers to a disease process that involves progressive destruction and regeneration of liver parenchyma leading to fibrosis and cirrhosis. Cirrhosis represents the final stage of liver fibrosis, characterized by disrupted liver architecture along with fibrotic bands, parenchymal nodules and vascular distortion (1). The major causes of CLDs include alcoholic liver disease (ALD), chronic hepatitis B virus (HBV) and hepatitis C virus (HCV) infections and non-alcoholic fatty liver disease (NAFLD). Other less frequent etiologies are the different types of cholangitis and autoimmune hepatitis (2).

NAFLD is emerging as the leading cause of CLD in the Western world. This is due, on the one hand, to increasing rates of obesity and type 2 diabetes and, on the other hand, to the widespread HBV vaccination and the development of highly effective antiviral treatments against HBV and HCV, which are strategies with a potentially positive impact on the burden of viral hepatitis (2).

1.1.1. Non-alcoholic fatty liver disease

1.1.1.1. Prevalence and epidemiology

NAFLD is an expanding health problem viewed as the hepatic manifestation of metabolic syndrome, as it is commonly associated with obesity, insulin resistance (IR), dyslipidemia and arterial hypertension (3). The prevalence of NAFLD is increasing in line with obesity and type 2 diabetes, with an estimated worldwide prevalence of 25%, but it is estimated to be at least twice as common among individuals who meet criteria for metabolic syndrome (4).

However, not all obese subjects develop NAFLD and, more importantly, NAFLD can be found in non-obese individuals, who might even have worse outcomes than obese individuals with NAFLD, with more rapid development of cirrhosis. The prevalence of NAFLD among non-obese patients is approximately 7%. Nonetheless, there may be regional variation, with a prevalence in the Asian population of around 20% (5,6).

Despite the high prevalence of NAFLD, only a subgroup of patients with NAFLD (about 20%) develop its progressive form non-alcoholic steatohepatitis (NASH), associated with inflammation and hepatocellular injury (7). The global prevalence of NASH has been estimated to range from 3% to 5%, with a heterogeneous distribution in relation to demographic characteristics, including ethnicity, age and gender. People with NASH are at much higher risk of clinically significant and progressive liver fibrosis, cirrhosis, and hepatocellular carcinoma (HCC) (4). Thus NAFLD is now a major cause of liver-related morbidity and mortality and is predicted to become the most frequent indication for liver transplantation (8).

1.1.1.2. Pathophysiology and progression

NAFLD is defined by the presence of fat in the hepatocytes (steatosis), mainly triglycerides (TG), greater than 5% of liver weight, in the absence of excessive alcohol consumption and other known causes of liver disease (9). Current nomenclature suggests that NAFLD is more of a diagnosis of exclusion than of inclusion and fails to reflect the critical role of a disordered metabolic system in the development of the disease. To address this issue, a new terminology has been proposed: metabolic dysfunction-associated fatty liver disease (MAFLD) (10). This new term acknowledges the principal state of systemic metabolic disorder and accounts for the possibility of other coexisting liver diseases, including alcohol use disorder. However, MAFLD is not the currently accepted nomenclature by the American Association for the Study of Liver Diseases or the European Association for the Study of Liver Diseases (11).

Histologically, NAFLD encompasses a broad spectrum of liver diseases ranging from simple hepatic steatosis (non-alcoholic fatty liver, NAFL), which represents a relatively benign state, to a necro-inflammatory subtype (NASH), which is additionally characterized by the presence of hepatocellular injury (ballooning) with or without fibrosis, and which may eventually progress to cirrhosis and HCC (12) (Figure 1).

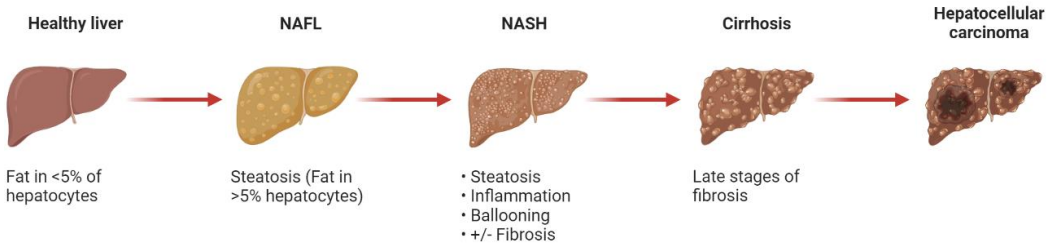

Figure 1. Non-alcoholic fatty liver disease (NAFLD) spectrum**.** NAFL, non-alcoholic fatty liver; NASH, non-alcoholic steatohepatitis.

The underlying mechanism for the development and progression of steatosis to NASH is complex and multifactorial. In this regard, NASH involves a complex interaction among a number of parallel hits resulting in a disturbed lipid homeostasis and an excessive accumulation of TG and other lipids in hepatocytes. Excessive fatty acid influx to the liver and IR are two important factors contributing to steatosis (13).

In the liver, dysregulation of lipid metabolism leads to the formation of lipotoxic lipids that contribute to mitochondrial dysfunction, overproduction of reactive oxygen species (ROS) and endoplasmic reticulum (ER) stress, resulting in hepatocyte injury, and subsequent activation of inflammatory and fibrogenic responses (14). Moreover, multiple extrahepatic factors such as dysfunctional adipose tissue, altered gut microbiota and genetic predisposition are also involved in the pathogenesis of NASH (13).

Different theories have been formulated on the development and progression of NAFLD, leading initially to the two-hit hypothesis. According to this, hepatic lipid

accumulation secondary to sedentary lifestyle, high-caloric intake, obesity and IR, acts as the first hit, sensitizing the liver to further insults acting as a second hit, which activates an inflammatory event with associated fibrogenesis (15). However, it was believed that this view was too simplistic to recapitulate the complexity of the human NAFLD where multiple parallel factors, acting synergistically in genetically predisposed individuals, are implicated in the development and progression of NAFLD. Consequently, the progression of NAFLD has been more recently explained by a multiple-hit hypothesis (16) (Figure 2).

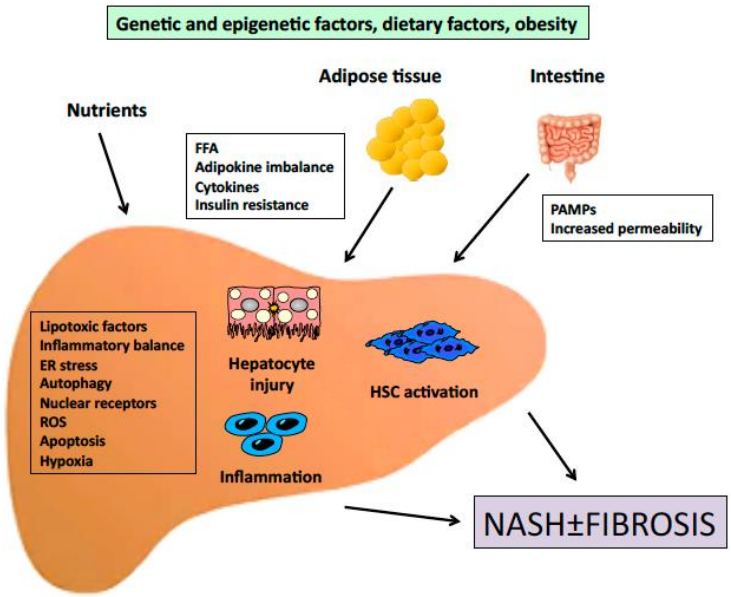

Figure 2. Outline of the pathogenesis of non-alcoholic steatohepatitis (NASH). ER, endoplasmic reticulum; FFA, free fatty acids; HSC; hepatic stellate cells; PAMPs, pathogen-associated molecular patterns; ROS, reactive oxygen species. From Caligiuri A *et al*., Int J Mol Sci. 2016 (17).

1.1.1.3. Risk factors influencing NASH development

Insulin resistance

Under physiological conditions, insulin binding to its receptor stimulates hepatic as well as peripheral glucose uptake and suppresses hepatic glucose production

(gluconeogenesis). In addition, it promotes *de novo* lipogenesis in the postprandial state and inhibits lipolysis in adipose tissue (18).

IR is a major component of NAFLD present in most patients and may be independent of the presence of obesity and type 2 diabetes (19). Dietary habits, environmental and genetic factors can lead to the development of IR, characterized by a lack of suppression of endogenous glucose production in insulin-sensitive tissues such as muscle, adipose tissue and liver (20).

IR leads to adipose tissue dysfunction with consequent alterations in the production and secretion of adipokines (decreased levels of adinopectin) and inflammatory cytokines (increased levels of tumor necrosis factor-alpha, TNF-α) that may profoundly affect not only the adipose tissue itself but also the liver (21). Moreover, due to IR, the adipose tissue becomes resistant to the anti-lipolytic effect of the insulin and causes an increase of lipolysis in adipocytes, leading to excess free fatty acids (FFA) release into the circulation and to a higher uptake by the hepatocytes, which is a driver of steatosis (22). In turn, the accumulation of FFA in the liver promotes hepatic IR, characterized by an increase in *de novo* lipogenesis and hepatic glucose production, which leads to decreased glycogen synthesis and increased gluconeogenesis, contributing to hyperinsulinemia (23).

Therefore, NAFLD should be looked at as a dynamic process that occurs between peripheral and hepatic metabolic alterations, where hepatic steatosis and IR potentiate each other (24).

Lipotoxicity

The hallmark of NAFLD is the accumulation of fat in the hepatocytes, in the form of lipid droplets containing TG. Increased delivery of FFA from insulin-resistant adipose tissue, intrahepatic *de novo* lipogenesis, and dietary fat and carbohydrate are the major

mechanisms underlying TG accumulation (25). Although TG represent the major lipid class contained in droplets, this form is currently considered as potentially protective with respect to cell toxicity. Thus, hepatocytes lipotoxicity is mainly caused by FFA and derived metabolites such as dyacylglycerols and ceramides (26,27).

The predominant fate of FFA in the liver is to either undergo mitochondrial β-oxidation or esterification into TG. These neutral lipids can be either stored in cytoplasmic lipid droplets, or secreted into bloodstream as very low-density lipoprotein (VLDL) particles (28). Hepatic lipotoxicity may occur when the hepatic capacity to oxidize, store and export FFA as TG is overwhelmed by FFA flux from the periphery or hepatic *de novo* lipogenesis (29). Another factor contributing to the increased intracellular FFA load may be the breakdown of hepatocellular TG by intracellular lipases and autophagy of lipid droplets (30,31).

The excessive cellular load of FFA leads to mitochondrial damage, oxidative stress, ER stress and hepatocellular dysfunction. The resulting cellular injury triggers immune-mediated hepatocellular damage and apoptotic/necrotic cell death mechanisms, leading to hepatic fibrogenesis and further development of cirrhosis (9).

Gut microbiota

The gut microbiota, i.e. the microbial community within the gastrointestinal tract, plays key physiological roles in host digestion, immunity and metabolism. In the past few years it has gained much attention and its association with metabolic syndrome-related disorders, namely NAFLD, is well documented (32–34). In this regard, numerous gut-derived metabolites, synthetized by microbes, have been implicated in disease progression. Among these, lipopolysaccharide (LPS), a gram-negative bacteria-derived endotoxin, exerts relevant metabolic and proinflammatory effects. However, some gut-derived metabolites may be of benefit to metabolic diseases. For instance, short-chain fatty acids (SCFA), i.e., acetate, butyrate and propionate, have demonstrated positive

effects, such as promoting the production of the anorexigenic peptides Peptide YY (PYY) and glucagon-like peptide 1 (GLP-1) (35). Moreover, SCFA have well-established barrier protective and anti-inflammatory properties in the intestine, which could prevent progression of NAFLD (36,37) (Figure 3). Conversely, colonic inflammation lowers the abundance of SCFA-producing bacteria: a reduction in the genus *Faecalibacterium*, containing butyrate producers, has been observed in NASH patients (38).

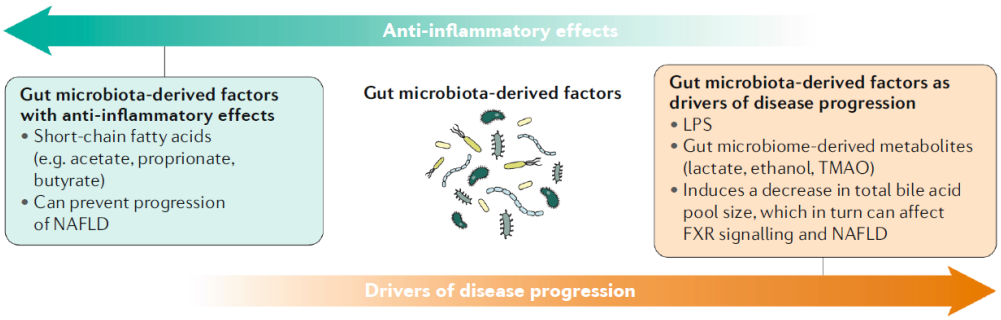

Figure 3. Gut-derived metabolites and factors that could drive progression of non-alcoholic fatty liver disease (NAFLD). FXR, farnesoid X receptor; LPS, lipopolysaccharide; TMAO, trimethylamine N-oxide. Adapted from Aron-Wisnewsky J *et al*., Nat Rev Gastroenterol Hepatol 2020 (37).

The liver and the gut have an intimate anatomical and functional relationship, often termed gut-liver axis, as the liver receives the majority of its blood supply from the intestines through the portal circulation. This makes the liver one of the most exposed organs to gut microbiota and gut-derived metabolites. In this sense, disturbance of the gut-liver axis plays a pivotal role in the pathogenesis of NAFLD (39).

Obesity, dietary intake and physical inactivity favor gut barrier disruption and dysbiosis, the latter referring to all imbalances between beneficial and pathogen bacteria or modifications in gut microbiota taxonomic composition and/or function. Consequently, there is an increase in intestinal permeability though the disruption of tight junction proteins such as zonula occludens-1 (ZO-1) and claudins. This pathologic microenvironment facilitates the systemic translocation of pathogenic bacteria, gut-

derived pathogen-associated molecular patterns (PAMPs; such as LPS and peptidoglycans), damage-associated molecular patterns (DAMPs) and bacterial metabolites, such as trimethylamine N-oxide (TMAO) and ethanol, into the mesenteric portal blood flow (endotoxemia). Upon arrival to the liver via portal vein, PAMPs/DAMPs and high levels of FFA activate inflammatory response though Toll-like receptor (TLR) signaling, which enhances the release of cytokines and chemokines, ultimately resulting in NAFLD progression (40) (Figure 4). Therefore, gut microbiota may play a critical role in the maintenance of gut-liver homeostasis and in the pathogenesis of liver diseases.

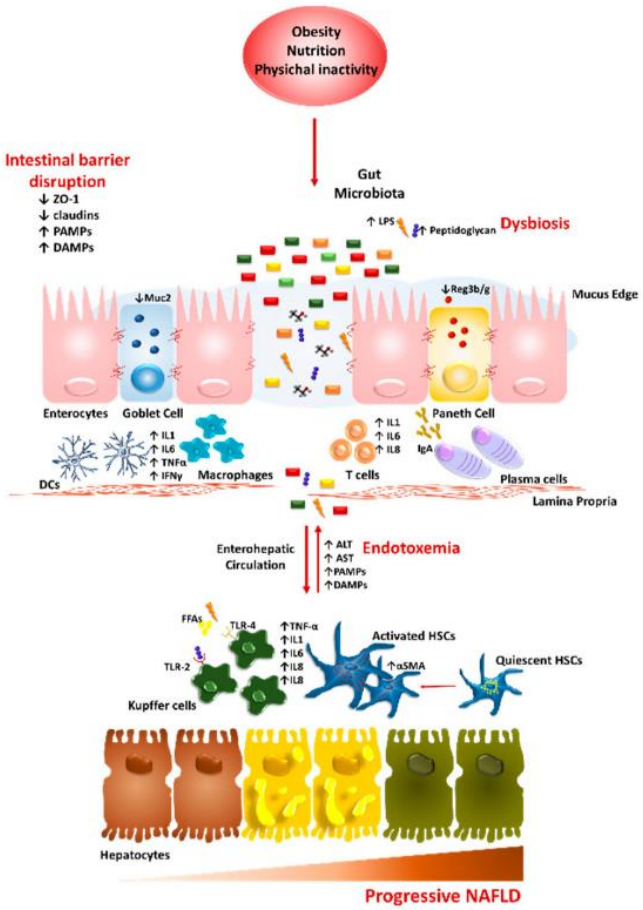

Figure 4. Role of gut-liver axis in progressive non-alcoholic fatty liver disease (NAFLD). Adapted from Meroni M *et al.*, Nutrients 2019 (40).

1.2. Portal hypertension

Portal hypertension (PH) is responsible for most of the complications associated with advanced NAFLD. It is defined as a complex syndrome, consequence of a pathological increase of the portal pressure gradient, which is the pressure difference between the portal vein and the inferior vena cava. Normal values of the portal pressure gradient are of 1-5 mmHg, values between 5 and 9 mmHg correspond to preclinical PH and values above 10 mmHg define what is being called clinically significant PH, since it represents the portal pressure gradient required threshold above which the associated clinical complications of PH may begin to appear. These complications include ascites, hepatorenal syndrome, hepatic encephalopathy and gastro-esophageal varices (41).

Any condition interfering with blood flow at any level within the portal system can arise PH. According to the anatomic location of the obstacle to blow flow, PH is classified as prehepatic (involving the splenic, mesenteric or portal vein, as in the case of portal vein thrombosis), intrahepatic (liver diseases such as cirrhosis) and posthepatic (diseases blocking the hepatic venous outflow, as in Budd-Chiari syndrome).

1.2.1. Physiopathology of portal hypertension

As in any vascular system, the portal pressure gradient (ΔP) is the result of the interaction between portal blood flow (Q) and the vascular resistance (R) that opposes that flow. Following Ohm´s law this relationship is defined as:

$$\Delta P = Q \times R$$

Therefore, PH is caused by an increase in portal blood flow, an increase in hepatic vascular resistance or a combination of both.

About 90% of cases of intrahepatic PH in Western countries are caused by cirrhosis in the liver. Other causes accounting for less than 10% of cases worldwide are frequently

referred to as *non-cirrhotic PH* (42). In liver cirrhosis, increased intrahepatic vascular resistance (IHVR) to portal blood flow is the primary factor increasing portal pressure (PP) and leading to PH. As the disease progresses, it affects extrahepatic vascular beds in the splanchnic and systemic circulation, leading to arterial vasodilatation and collateral vessel formation and the subsequent increase in portal venous inflow. This increase further exacerbates PH and eventually leads to the systemic hyperdynamic circulatory state characterized by decreased mean arterial pressure, decreased systemic vascular resistance and increased cardiac index (43) (Figure 5).

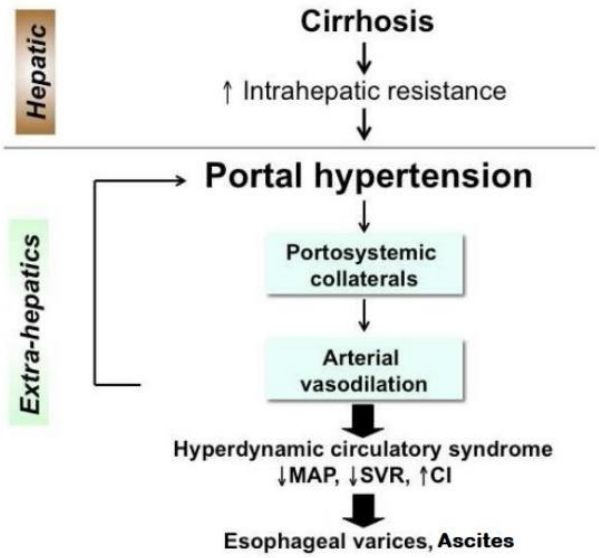

Figure 5. Pathophysiology of portal hypertension. CI, cardiac index; MAP, mean arterial pressure; SVR, systemic vascular resistance. From Iwakiri Y, Clin Liver Dis. 2014 (43).

By contrast, several studies have verified the presence of PH in NAFLD even when fibrosis is far less advanced or absent, both in humans and in animal models, raising the concern that PH may occur prior to the development of cirrhosis in patients with NAFLD (44–47). One of the factors contributing to the early development of PH is the presence of endothelial dysfunction, i.e. the impairment of the endothelium-dependent vasodilatation (48), with decreased nitric oxide (NO) production resulting in sinusoidal

vasoconstriction (49,50). Furthermore, experiments have shown that severe steatosis by itself may be also associated with the induction of significant PH (51,52). This induced increase in PP could result from pure structural changes such as sinusoidal narrowing by fat-laden enlarged hepatocytes (53,54).

1.2.2. Risk factors of portal hypertension development

Intrahepatic vascular resistance

Increased IHVR results from the combination of structural alterations in the vascular architecture of the liver caused by fibrosis, nodule formation, sinusoidal remodeling and vascular obstruction, and functional abnormalities leading to endothelial dysfunction and an increment in intrahepatic vascular tone (55). This latter dynamic and reversible component accounts at least 25% of the total increased IHVR in cirrhosis (48). It is a consequence of an imbalance between elevated production of vasoconstrictors (such as endothelin-1, angiotensin and thromboxane A2) and reduced release of vasodilators (of which the most important is NO). In response, there is active contraction of portal/septal myofibroblasts, activation of hepatic stellate cells (HSC) and active contraction of vascular smooth muscle cells. HSC also undergo important morphological and functional changes, including overexpression of alpha-smooth muscle actin (α-SMA), increased response to vasoconstrictors and fibrogenic activity (56).

Hepatic microcirculation and endothelial dysfunction

The vascular endothelium, representing the interface between blood and other tissues, is not only a physical barrier, but contributes to different physiological and pathological processes (57). In physiological conditions, the endothelium is able to generate vasodilatory factors in response to increases in blood volume, blood pressure or vasoconstrictor agents.

The intrahepatic microvascular unit is made up of several discrete units, including portal venules, hepatic arterioles, sinusoids and central veins. In addition to hepatocytes, the hepatic sinusoid consists mainly of three types of non-parenchymal cells (Figure 6). The liver sinusoidal endothelial cells (LSEC), HSC and the liver resident macrophages, known as Kupffer cells (KC). These cells are intimately associated with one another, where they have paracrine and autocrine effects (58). To note, between the endothelial cell lining and the apical membrane of hepatocytes is the space of Disse, which is involved in lymphatic drainage and provides a residence niche for HSC (59).

LSEC are highly specialized endothelial cells that form the wall of the hepatic sinusoids and act as the hepatic first defense barrier from injury. They differ anatomically and biologically from other endothelial cells by the presence of fenestrae in the cytoplasm and the absence of a basement membrane, which makes them highly permeable (60–62). In normal conditions, LSEC exert diverse effects on liver functions including blood clearance, vascular tone, immunity, hepatocyte growth and angiogenesis/sinusoidal remodeling. In pathological conditions, however, LSEC become dysfunctional, accompanied by insufficient release of vasodilators and increased levels of vasoconstrictors, resulting in impaired vasomotor control, inflammation, fibrosis, impaired liver regeneration and pathological angiogenic/sinusoidal remodeling, all of which contribute to increased IHVR and, therefore, to PH (60).

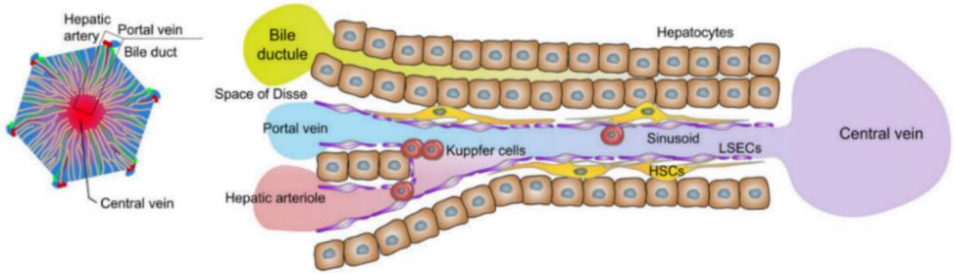

Figure 6. Representation of hepatic sinusoid morphology. Adapted from Iwakiri Y *et al.*, J Hepatol. 2014 (58).

NO is probably the most important vasodilator regulating vascular tone in the intrahepatic microcirculation. NO is generated by three isoforms of nitric oxide synthases (NOSs): neuronal NOS (nNOS), endothelial NOS (eNOS), and inducible NOS (iNOS), being eNOS and iNOS the major players in liver biology.

iNOS is induced in various liver cells including LSEC, hepatocytes, KC and HSC (among others) and contributes to pathological processes as it mainly acts as a pro-inflammatory mediator. This may be related to the microenvironments at the site of iNOS induction where generated NO can facilitate the formation of ROS. In contrast, eNOS is mainly expressed in LSEC and produces NO in response to stimuli such as flow shear stress, insulin, vascular endothelial growth factor (VEGF), or G protein-coupled receptor agonists. Therefore, eNOS-derived NO maintains hepatic vascular homeostasis and inhibits pathological conditions in the liver (63). NO production is also indispensable to maintain the quiescent phenotype of HSC, as well as in an autocrine manner, to maintain the fenestrae and differentiated phenotype of LSEC (64,65).

The activity of eNOS is tightly regulated at the transcriptional and post-transcriptional level (66). Kruppel-like factor 2 (KLF2) is a transcription factor that modulates the expression of multiple endothelial vasoprotective genes, including eNOS. Thus, KLF2 ~~e~~xpression confers endothelial protection against inflammation, thrombosis and excessive vasoconstriction (67). Furthermore, the eNOS signaling pathway can be regulated through different post-transcriptional mechanisms, with Akt-dependent eNOS phosphorylation playing an important role in its activation (68). In response to various forms of stimuli (such as insulin), protein kinase B (Akt) directly phosphorylates eNOS (at serine 1177) and enhances its ability to generate NO by a phosphatidylinositol 3-kinase (PI3K)-dependent mechanism, leading to vasodilation (68–70) (Figure 7A).

In the presence of IR (as it occurs in common NASH), the IRS/PI3K/Akt pathway is impaired, leading to a dysregulation in the activity of eNOS mainly through a reduction

of its constitutive phosphorylation and thus to a lower production of NO, which represents the main mechanism leading to endothelial dysfunction, increased IHVR and PH (49,70) (Figure 7B).

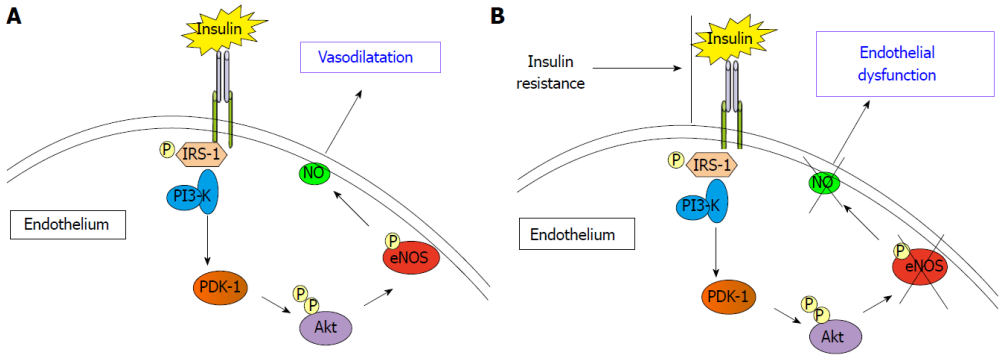

Figure 7. Insulin resistance and endothelial nitric oxide synthase (eNOS) activity. (A) The release of nitric oxide (NO) causes endothelium dependent vasodilation. (B) Insulin resistance causes the reduction of insulin-induced activation of eNOS. Adapted from Pasarín M *et al.*, WJG 2017 (70).

1.3. Animal models of NASH

Animal models represent a fundamental preclinical tool to understand the pathogenesis and underlying mechanisms in the onset and progression of NAFLD, and to define effective treatments and potential biomarkers (71). Numerous animal models of NAFLD/NASH have been reported to date; however, there is no ideal model that faithfully recapitulates the whole disease spectrum and metabolic features associated to human NASH. Thus, the recognition of the limitations from the different animal models is necessary to most effectively translate findings from such models to improved therapeutics in humans (72).

NAFLD/NASH animal models are essentially distinguished by their ability to mimic the etiology/natural history (diet-induced models) or histopathology (nutrient-deficiency models or diet-toxic-induced models). Also, genetic models are widely used in NASH

research. Consequently, available animal models of NASH have different utility and clinical translatability (73).

1.3.1. Genetic models

Among the most frequently used genetic models are those that exhibit defects in the leptin signaling pathways. The peptide hormone leptin is produced in adipocytes and participates in the hypothalamic regulation of feeding behavior by reducing food intake (74). Leptin function can be disabled by mutation of the gene resulting in a truncated inactive product (in ob/ob mice) or by resistance to leptin action due to mutation of the receptor gene (in db/db mice, Zucker rats) (75). Consequently, these models give rise to hyperphagia, obesity, hyperlipidemia and IR under normal dietary conditions. Although this is accompanied by the spontaneous development of liver steatosis, they do not progress to NASH unless challenged by additional stimuli such as feeding with high-caloric diets (76).

In addition to its role as a satiety hormone, leptin seems to be directly involved in liver fibrogenesis, as ob/ob mice are protected against fibrosis (77). In contrast, db/db mice and Zucker rats, having normal or elevated leptin levels, develop fibrosis when being challenged with an additional stimulus (76,78,79).

The main advantage of these models is that they show the typical features of metabolic syndrome. Moreover, the addition of a second hit can be used to study more advanced stages of the disease. However, congenital leptin deficiency and leptin resistance caused by gene mutations are extremely rare in humans. Thus these models have limited use for the study of NASH (80,81).

1.3.2. Dietary models

As only a minority of NAFLD patients exhibit genetic defects, the use of dietary models to induce NAFLD is more relevant to human disease than genetic models (82).

1.3.2.1. Nutrient-deficiency models

Several available animal models are based on diets low or lacking in certain essential nutrients. Among these, CDD (choline-deficient diet), MDD (methionine-deficient diet), MCDD (methionine-choline deficient diet), and semisynthetic CDAA (choline deficient, L-amino acid-defined; moderately low in methionine) are commonly used in preclinical NASH research. The diets can vary in fat content (10-20% fat kcal), and sucrose levels are typically high (40-60% carbohydrate kcal) (73).

Methionine and choline amino acids are methyl-group donors that are essential for lipid metabolism. In some particular situations, when choline is lacking in the diet, methionine can be used for the synthesis of choline (83). However, the deficiency of both components results in impaired hepatic β-oxidation and impaired VLDL production, resulting in hepatic fat accumulation, liver cell death, oxidative stress and changes in cytokines and adipokines (84).

The MCDD is one of the best described dietary models for NAFLD. It induces the histopathological features and fibrosis within only a few weeks of feeding (typically after 2-8 weeks). However, MCDD creates a metabolic profile contrary to that observed in human NASH. Animals fed an MCDD show significant weight loss, cachexia and lack of IR (85).

The CDAA diet is a variant of the MCDD, as it contains reduced methionine levels. Similar to the MCDD, the CDAA diet increases lipid synthesis, inflammation and causes liver injury. Animals fed CDAA diet require longer time than MCDD for these histological changes to progress, but the degree of NASH perhaps slightly more severe (86). In

addition, mice on the CDAA diet do not gain body weight and do not display IR (87). In contrast to MCDD and CDAA, the sufficient supply with methionine in CDD prevents a pronounced weight loss (88). Thus, in addition to the absence of metabolic syndrome in these models, such amino acid deficiency is not common in human diets, limiting their relevance when considering the etiology of NAFLD.

1.3.2.2. Diet-induced models

The clinical picture of NASH is currently best achieved through dietary interventions resembling Western diets. It should be noted that the time of onset and degree of diet-induced NAFLD may depend on the species (rats appear to be more sensitive than mice (89)), strain (Sprague-Dawley rats easily develop steatohepatitis, while Wistar rats are resistant (90,91)), and gender (males appear to be more sensitive than females as estrogen is protective against NASH (91), and estrogen replacement in estrogen-deficient mice improves steatosis (92)).

The diet-induced models apply a broad range of dietary regimens ranging from alternating contents and sources of fat to different amounts of cholesterol and additional supplements (93). The use of regular high-fat diets (HFD), with the majority of calories derived from fat (typically 30-60 kcal%), bring about a phenotype similar to human disease, characterized by obesity, IR and hyperlipidemia. However, it induces only minimal fibrosis after extended exposure (36-50 weeks) (86) and are therefore suboptimal models to investigate advanced stages of NASH (73,93). To overcome this limitation, several attempts have been made to use modified HFD supplemented with cholesterol and/or fructose to induce NASH and significant liver fibrosis within shorter time frame.

Diets with supplemented cholesterol content (up to 3% w/w) and cholic acids (atherogenic [Ath] diets) have initially been employed to study atherosclerosis; however, both cholesterol and cholate (the salt of cholic acid) induce important features

of human NASH, including progressive development of steatosis, inflammation, and fibrosis with hepatocellular ballooning (94,95). However, the Ath diet by itself does not induce weight gain, nor significant IR. The addition of a high-fat component to the Ath diet can ensure hepatic IR and further accelerate the progression to NASH (95).

Over-consumption of high-fructose corn syrup (HFCS, a mixture of fructose and glucose monosaccharides), primarily in the form of soft-drink consumption, has been associated with the development of obesity and NASH (96,97). Table sugar (sucrose) and HFCS are the two major dietary sources of fructose. HFCS-containing beverages have variable ratios, usually varying from a 55/45 or 65/35 fructose:glucose ratio (98). In animals, as well as in clinical studies, hepatic metabolism of fructose stimulates *de novo* lipogenesis and blocks hepatic β-fatty acid oxidation leading to fat accumulation in the liver, IR and hyperglycemia (99,100). In addition, fructose contributes to intestinal dysbiosis, leading to increased endotoxin levels in portal blood, subsequent KC activation and inflammation in the liver (101,102).

Altogether, diets that combine nutrient manipulations, such as diets with moderately elevated fat or moderately high fructose, and some dietary cholesterol can accurately model human Western diets and also cause NAFLD/NASH (103). In this line, our group developed a rat NASH model trying to include all the dietary variables discussed so far, i.e., a diet-induced model with high-fat, cholesterol-supplemented diet combined with a glucose-fructose beverage (HFGFD model). This model develops all the histological features of NASH as well as the aspects of metabolic syndrome such as obesity and IR after 8 weeks of feeding (50). Moreover, the administration of this diet to Sprague-Dawley male rats causes a decrease in the diversity of bacterial species in gut microbiota, reproducing the dysbiosis described in obese patients (104).

Besides that, the use of this diet-induced rat model allows to analyze the development of PH in the context of NAFLD. Although the main limitation of the model is the absence

of fibrosis, it can be used to study the functional component of the increase in PP, without interference from the structural component.

1.3.2.3. Diet and toxin-induced model (the STAM™ mouse model)

The administration of low doses of streptozotocin (STZ) in newborn animals lead to a chemical inflammation and destruction of the pancreatic islets, thus inducing diabetes. This method combined with HFD can establish a model for NAFLD (105,106). In the STAM™ mouse model, neonatal animals are exposed to one single low-dose of STZ two days after birth, followed by a HFD starting from 4 weeks of age. These mice developed simple steatosis at 6 weeks of age, NASH with inflammatory foci and ballooning at 8 weeks, progressive pericellular fibrosis starting at 8-12 weeks, and even HCC at 20 weeks of age (106). This model recapitulates several important histological aspects of human NAFLD, but differs from the human state as β-cell function loss is induced by STZ rather than a systemic, inflammatory, insulin resistant milieu (72). Furthermore, similar to nutrient-deficient diets, STZ cause weight loss in STAM mice (106). As a result, the STAM™ mouse model is mainly used in initial proof-of-concept studies on anti-fibrotic therapies (73).

1.4. Therapeutic options for NASH

Despite the rising prevalence and serious potential clinical consequences of NASH, there are currently no treatments approved for the disease. Weight loss, through physical activity and lifestyle changes, has been shown to improve hepatic steatosis and IR and therefore remains the most effective approach to improve NASH (107). However, only a small proportion of patients achieved the necessary weight loss to induce these changes, and the effect on weight loss on patients with more advanced NASH remains to be demonstrated. Thus, great preclinical and clinical efforts are being carried out to develop new drugs with the aim of reducing the progression of NASH (108).

Peroxisome proliferator–activated receptor gamma (PPARγ) ligands, such as pioglitazone, have been studied in several trials and improve insulin sensitivity, aminotransferases and all the histological features of NASH (109). However, their appeal is limited by some side effects such as weight gain, as shown in patients with type 2 diabetes (110). Furthermore, GLP-1 receptor and thyroid hormone receptor beta (THR-β) agonists are being evaluated as a means to reduce lipotoxic load regulating lipid metabolism (111,112). Vitamin E is a prototypic antioxidant, which has also been shown in several clinical trials to improve NASH histology. However, its appeal is limited by lack of efficacy in reducing liver fibrosis in a large randomized controlled trial (109,113).

To note, the success in discovering effective therapies for NASH will continue to rely upon fundamental biomedical investigation that links the microbiota, liver metabolism and response to injury, systemic consequences of obesity and metabolic syndrome (108).

1.4.1. Therapeutic strategies targeting the gut-liver axis

The growing interest on the gut-liver axis has opened avenues for the treatment or prevention of NAFLD. In this regard, different therapeutic strategies have been proposed to target the gut-liver axis, especially the gut microbiota (114,115) (Figure 8).

On the one hand, there are microbiota-based strategies aimed to alter the composition of gut microbiota (bugs as drugs). One is fecal microbiota transplantation (FMT), which involves the replacement of entire microbiota communities. A study performed by our group demonstrated that FMT from control lean rats recovers intrahepatic insulin sensitivity in rats with NASH (50). Probiotics (living bacteria), prebiotics (group of nutrients that enhance growth of specific bacteria) and synbiotics (combination of probiotics and prebiotics) are first-generation microbiota-based therapies; these may add or nurture beneficial bacterial strains to the commensal microbiota. The engineered bacteria, that have been classified as next-generation microbiota-based therapies, are

precisely designed to either produce a beneficial metabolite or metabolize toxic products (115).

Other strategies aimed at eliminating bacteria or pathogens that promote disease progression (drug the bug). These include bacteriophages and antibiotics. Collectively, it seems that antibiotics alleviate the severity of NAFLD by depletion or alteration of gut microbiota (116). However, its clinical use must be cautious as they are not specific and can have side effects because they also eliminate beneficial commensals.

Finally, microbe-derived metabolites and their related signaling pathways might be used in treatment of NAFLD (drugs from bugs). Supplementation with these molecules or their derivatives could replace some metabolic activities of the lost or reduced microbes. In this regard, given the associations between dysregulation of bile acid (BA) homeostasis and severity of NAFLD, targeting the BA pathway with fibroblast growth factor 19 (FGF19) analogs and farnesoid X receptor (FXR) agonists such as obeticholic acid, is one of the most promising approaches for the treatment of NASH (117). Another strategy would be the direct supplementation of SCFA, although their use is still open to many questions and data in patients are limited (115).

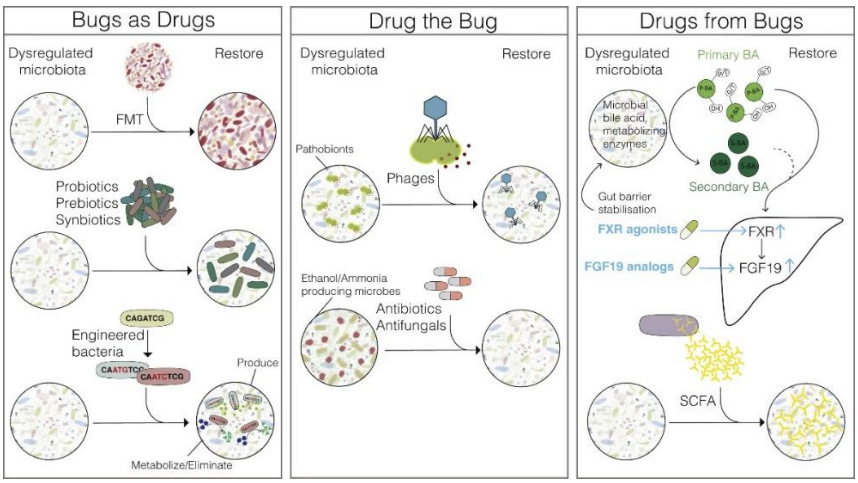

Figure 8. Targeting the gut microbiota for treatment of liver disease. Adapted from Lang S *et al.*, Cell Host Microbe 2020 (115).

2. HYPOTHESIS

2. HYPOTHESIS

Vital insights into the pathogenesis and underlying mechanisms in NAFLD have been gained from the study of existing animal models. However, none of the current available NAFLD models recapitulates adequately all the key elements of the human condition. In a previous study from our group (50), we developed and characterized a rat model induced by a high-fat glucose-fructose diet (HFGFD) for 8 weeks that was able to reproduce the key phenotypic features of the early stages of NASH: obesity, IR, intestinal dysbiosis, endothelial dysfunction and PH. Although this model failed to induce fibrosis, it helped at characterizing the link between IR, endothelial dysfunction and the gut microbiota in the development of PH in NASH. On the other hand, despite its high prevalence, there are no approved therapies for NASH. Thus, there is a high unmet medical need to develop new effective therapeutic modalities targeting these key NASH mechanisms. Given the recognized role of gut microbiota in NAFLD and associated comorbidities such as obesity and type 2 diabetes, the use of gut microbial approaches for the treatment or prevention of NAFLD is of great interest. In our previous study (50), FMT from lean to NASH rats restored the sensitivity to insulin and improved endothelial dysfunction, thereby leading to an improvement in PH. However, despite the observed protective effects, FMT is unlikely to become a long-term therapeutic option, especially considering the chronic and progressive nature of NASH. Consequently, microbial-based therapies of defined composition would represent a more patient-friendly approach.

In this context, the present doctoral thesis consists of three studies. Study 1 and 3 focus on the development of a rat model of NASH with diet-induced fibrosis, and study 2 on testing the effects of a 9-strain bacterial consortium on key mechanisms of NASH in two well-established rodent models of the disease: the 8-week HFGFD-induced rat model and the STAM^{TM} mouse model.

These are the proposed hypotheses:

- The extension in time from 8 to 36 weeks of the HFGFD intervention is able to elicit a fibrotic response and perpetuate endothelial dysfunction, thus leading to the progression of PH in the rat NASH model.
- The administration of a bacterial consortium of defined composition exerts protective effects on key mechanisms leading to PH and fibrosis in two animal models of NASH: the 8-week HFGFD-induced rat model and the STAM™ mouse model.
- An increase in dietary cholesterol intake with the addition of sodium cholate results in more advanced disease with the presence of NASH with fibrosis and PH in a rat model after 16 weeks of feeding.

3. AIMS

3. AIMS

The main aim of the present doctoral thesis is to develop a dietary model that fully recapitulates human NASH, including its later fibrotic stages, and to assess whether a consortium composed of a limited number of bacterial strains could induce similar benefits to those observed with FMT.

The secondary aims are:

- To develop and characterize the long-term effects of a known HFGFD on NASH histology and PH in rats, and to elucidate the specific mechanistic contributions of endothelial dysfunction and/or intrahepatic structural changes in the progression of PH over time in the NASH model.
- To test the efficacy of a bacterial consortium composed of nine human gut commensal strains capable of producing both butyrate and propionate, on a rat dietary model of NASH and PH and compared it to that of FMT from control lean rats.
- To test the same 9-strain bacterial consortium in the STAM^{TM} mouse model described to develop histological liver fibrosis.
- To assess whether a change in diet composition, i.e., increasing the amount of cholesterol and adding sodium cholate to the diet, is able to induce an advanced disease state in a relatively short period of 16 weeks in a rat model.

4. MATERIALS AND METHODS

4. MATERIALS AND METHODS

4.1. Experimental animal models of NASH

Rat experimental models of the three studies were developed in male Sprague-Dawley rats (Charles River Laboratories, L´Abresle, France) weighting 200-220 g at the beginning of the experiments. Animals were housed under a 12-hour light/dark cycle at constant temperature (24 ± 1 °C) and relative humidity (55 ± 10%). Body weight and food and drink consumption were monitored weekly. All three rat studies were approved by the Animal Experimentation Ethics Committee (CEEA) of the Vall d´Hebron Research Institute (VHIR, Barcelona, Spain) and authorized by e*l Departament d´Agricultura, Ramaderia i Pesca de la Generalitat* (file numbers: 9481, 11047 and 11376). Experiments in rats were conducted at the animal facilities of VHIR in accordance with the European Union Guidelines for Ethical Care of Experimental Animals (EC Directive 86/609/EEC for animal experiments).

The STAM™ mouse model used in study 2 was developed in male C57BL/6J mice (Japan SLC Inc., Hamamatsu, Japan). Mice were maintained in a SPF facility under controlled conditions of temperature (23 ± 3 °C), humidity (50 ± 20%), lighting (12-hour artificial light and dark cycles; light from 8:00 to 20:00), and air exchange. Body weight was recorded daily during the experimental period. Experiments performed in the STAM™ mouse model were conducted by SMC Laboratories (Tokyo, Japan) according to the following guidelines: Act on Welfare and Management of Animals (Ministry of the Environment, Act No. 105 of October 1, 1973, Japan; Standards Relating to the Care and Management of Laboratory Animals and Relief of Pain (Notice No.88 of the Ministry of the Environment, April 28, 2006, Japan) and Guidelines for Proper Conduct of Animal Experiments (Science Council of Japan, June 1, 2006).

4.1.1. The 8 and 36-week diet-induced rat models

Model development

Rats had *ad libitum* access to a high-fat glucose-fructose diet (HFGFD) with a caloric intake of 5.73 kcal/g during 8 weeks (Study 1 and 2) and for up to 36 weeks (Study 1). The HFGFD consisted of 30% fat (butter, coconut oil, palm oil, beef tallow) with mainly saturated fatty acids, supplemented with 1 g/kg cholesterol (Ssniff Spezialdiäten GmbH, Soest, Germany), and combined with a beverage of glucose-fructose (42 g/L, 45% glucose and 55% fructose) (PanReac AppliChem, Darmstadt, Germany) providing 157.72 kcal/L. Rats in the control group were fed with a control diet (CD) with a caloric intake of 2.89 kcal/g. The CD consisted of a 4% fat grain-based chow (Teklad 2014; Harlan laboratories, Indianapolis, IN, USA) and tap water.

For the characterization of rat models, liver hemodynamics and blood biochemistry were performed, and liver tissue was collected for histopathology, immunohistochemistry, and molecular pathway analyses. In addition, structural characteristics of all 8- and 36-weeks rat liver sections from study 1 were systematically analyzed using digital image analysis.

Treatment administration

In study 2, after 8 weeks of HFGFD intervention, rats were randomized into 3 treatment groups: HFGFD-vehicle (HFGFD-VEH, n = 13), HFGFD-consortium of nine human commensal bacterial strains (HFGFD-CON, n = 11), and HFGFD-transplanted with fecal microbiota from control lean rats (HFGFD-FMT, n = 11). HFGFD-VEH individuals received oral probing vehicle (sterile PBS), while individuals in HFGFD-CON and HFGFD-FMT groups were subjected to different microbiota-based treatments, which consisted of oral administration of a bacterial consortium of defined composition and FMT,

respectively (both procedures described below). The treatment period lasted 2 weeks during which animals were maintained on the original diet (Figure 9A).

At week 10, liver hemodynamics and blood biochemistry were performed, and liver tissue samples were collected for histological and molecular analyses. In addition, the cecum content was collected for shotgun sequencing of gut microbes. For metagenomics analysis, fecal samples were also obtained from a group of rats receiving regular diet so to compare HFGFD-induced changes on microbial composition with those of rats fed CD.

Bacterial consortium treatment

The consortium treatment started after 8 weeks of HFGFD intervention, and it consisted of the daily administration of the following nine human gut commensal strains: *Faecalibacterium prausnitzii*, *Butyricicocccus pullicaecorum*, *Roseburia inulinivorans*, *Akkermansia muciniphila*, *Lactiplantibacillus plantarum* (former *Lactobacillus plantarum*), *Anaerostipes caccae*, *Phocaeicola vulgatus* (former *Bacteroides vulgatus*), *Veillonella parvula*, and *Blautia obeum*.

On each dosing day, lyophilized bacterial consortium was washed and reconstituted in previously filtered DPBS (Dulbecco's phosphate buffered saline; Merck, Darmstadt, Germany) under anaerobic conditions (N_2:CO_2:H_2: 80:10:10). As a result of centrifugation at 5340 g at room temperature for 10 min, a concentrated liquid ready-to-use formulation in air-tight vials was obtained. Then 1 mL of this suspension was administered immediately per individual (corresponding to a daily dose of $2x10^9$ CFU of the total counts of the 9 strains), using a disposable oral probe (Biochrom Ltd, Cambridge, UK) and repeating the procedure every 24 h for 2 weeks. For individuals belonging to the vehicle group, the same procedure was followed, but sterile DPBS was administered instead. Rats receiving the bacterial consortium were housed individually throughout the treatment period to avoid cross-contamination.

Fecal microbiota transplantation treatment

Fecal microbiota transplantation (FMT) was also performed after 8 weeks of HFGFD intervention. To achieve higher homogeneity in the transplantation procedure, feces from 3 control (lean) rat donors were pooled to be used for transplantation. With the aim of reducing gastric acidity and thus increasing the survival of the microorganisms, omeprazole was administered orally at a dose of 50 mg/kg/day during the 3 days prior to intestinal decontamination. The preparation of omeprazole required grinding and filtering the contents of commercial capsules. To proceed with intestinal emptying (intestinal decontamination), rats were maintained isolated in fast grills to avoid coprophagia, and two oral doses of CitraFleet® (sodium picosulfate, 0.16 mg/mL and magnesium oxide 51.2 mg/mL) of 1 mL and 2 mL were administered 24 h and 12 h, respectively, before FMT. These administrations were accompanied by 2 mL of water each to ensure hydration. During the 24 h of intestinal decontamination, animals were fasted but with access to water. Recolonization was performed with a single administration using a disposable oral probe (Biochrom Ltd, Cambridge, UK), for which 100 mg of the fecal pool were dissolved in 2 mL of sterile DPBS. Feces were stored at 80 °C until resuspension, which was done by avoiding the use of a vortex.

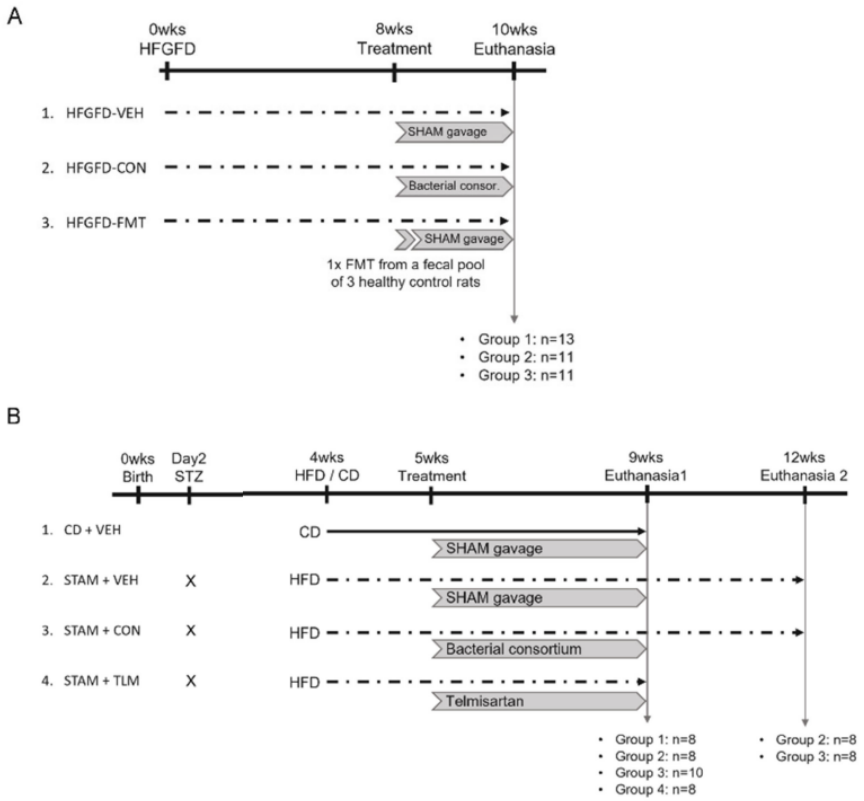

Figure 9. Experimental design in study 2. (A) 8-week diet-induced rat model of NASH. Rats were fed a high-fat glucose-fructose diet (HFGFD) for 8 weeks, after which they received either sham or bacterial consortium treatment for 2 additional weeks. HFGFD-VEH: group of NASH rats receiving sham gavage (vehicle); HFGFD-CON: group of NASH rats receiving the 9-strain bacterial consortium daily ($2x10^9$ CFU/day, total counts); HFGFD-FMT: group of NASH rats receiving fecal microbiota transplantation from control lean rats (1x transplantation followed by sham gavage). (B) STAM™ mouse model. C57BL/6J male mice were subcutaneously injected with 200 µg streptozotocin (STZ) two days after birth. At 4 weeks of age animals received high-fat diet (HFD) or regular control diet (CD). At 5 weeks of age treatment was initiated: control diet animals and STAM mice received sham gavage (CD+VEH and STAM+VEH, respectively) for a total of 4 weeks. In the two test groups, STAM animals received either the 9-strain consortium (10^9 CFU/day, total counts) (STAM+CON) or Telmisartan (10 mg/kg/day) (STAM+TLM) also for a total of 4 weeks. At 9 weeks of age animals were sacrificed (euthanasia 1). Two groups of STAM animals belonging to the vehicle control or the consortium groups were followed for an additional three weeks until sacrifice at 12 weeks of age (euthanasia 2).

4.1.2. The STAM™ mouse model

Model development

In study 2, mice were subcutaneously injected with a single dose of 200 µg streptozotocin (STZ, Merck, Darmstadt, Germany) 2 days after birth, to induce mild pancreatic islet inflammation and destruction. At 4 weeks of age, animals initiated a high-fat diet (HFD; 57 kcal% fat, Cat# HFD32, CLEA Japan Inc., Tokyo, Japan) or a regular control diet (CD; 5 kcal% fat, Rodent Diet CE-2, CLEA Japan Inc., Tokyo, Japan).

Treatment administration

Mice were randomized into 3 treatment groups based on their body weight the day before initiating the HFD. At 5 weeks of age (after one week on HFD), mice received either sham gavage (STAM+VEH, n = 16), the 9-strain bacterial consortium (STAM+CON, n = 18), or Telmisartan (STAM+TLM, n = 8), an angiotensin II receptor blocker that decreases hepatic fat accumulation and inhibits HSC activation and thus suppresses hepatic fibrogenesis (118). Vehicle (sterile PBS) and bacterial consortium were administered orally in a volume of 200 µL/mouse; the consortium was administered at the dose of 10^9 CFU/day (total counts of the nine strains) for a total of 4 weeks. Product suspensions were prepared as described above. Telmisartan was used as benchmark and administered orally at the daily dose of 10 mg/kg in a volume of 10 mL/kg for 4 weeks. For that, one tablet of Telmisartan (Micardis®; Boehringer Ingelheim GmbH, Ingelheim, Germany) was transferred into a mortar and triturated with pestle by adding pure water until obtaining a homogenous suspension of 1 mg/mL. All treatments were prepared freshly prior to administration. A control group fed CD and receiving sham gavage was also included in this study (CD+VEH, n = 8).

Animals belonging to the control (CD+VEH, n = 8) and STAM groups (STAM+VEH, STAM+CON, and STAM+TLM, n = 8, n = 10, or n = 8, respectively) were sacrificed after 4

weeks of treatment, i.e., at 9 weeks of age, which corresponds to a steatohepatitis/early fibrosis stage. In addition, two groups of STAM animals belonging to the vehicle (n = 8) and consortium (n = 8) groups were followed for three additional weeks and were sacrificed at 12 weeks of age, which corresponds to a stage of late fibrosis (Figure 9B). This was performed to investigate the potential of the bacterial consortium to delay disease progression upon cessation of treatment. Mice were sacrificed by exsanguination through direct cardiac puncture under isoflurane anesthesia (Pfizer Inc., New York, NY, USA). For model characterization, blood was collected for biochemistry, and whole liver for immunohistochemistry and histopathology.

4.1.3. The FIBRO-SH rat model

Model development

Rats in study 3 had *ad libitum* access to a high-fat high-cholesterol glucose-fructose diet (HFHC/GF, n = 12) with a caloric intake of 5.62 kcal/g during 16 weeks. The HFHC/GF consisted of 30% fat (butter, coconut oil, palm oil, beef tallow) with mainly saturated fatty acids, supplemented with 20 g/kg cholesterol and 5 g/kg sodium cholate (Ssniff Spezialdiäten GmbH, Soest, Germany), and combined with a glucose-fructose beverage (110 g/L, 45% glucose and 55% fructose) (PanReac AppliChem, Darmstadt, Germany) providing 438.48 kcal/L. Rats in the control group (CD, n = 6) were fed with a 4% fat grain-based chow (Teklad 2014; Harlan laboratories, Indianapolis, IN, USA) with a caloric intake of 2.89 kcal/g, and tap water.

This diet-induced model, termed FIBRO-SH rat model, ended at 16 weeks based on confirmation of fibrosis in liver biopsies performed in some individuals at week 12 of feeding (procedure described below). After 16 weeks of feeding, liver hemodynamics and blood biochemistry were performed, and liver tissue samples were collected for histological and molecular analyses.

Liver biopsy

Liver biopsies were performed on some individuals (HFHC/GF n = 4, CD n = 2) at 12 weeks of model development under constant anesthesia with inhaled isoflurane (5% induction and 2% maintenance; Baxter International Inc., Deerfield, IL, USA). Prior to the procedure, analgesia (0.1 mg/kg buprenorphine; Buprex®, Rb Pharmaceuticals Inc., Richmond, VA, USA) was administered subcutaneously with a 27 G needle to prevent painful stimulation. The intervention started by making a 3 cm longitudinal incision in the abdominal skin slightly on the left side of the animal. A 3 cm incision in the abdominal wall was made to visualize the left-lateral lobe (LLL) of the liver. The LLL was then externalized through the incision with the aid of sterile cotton swabs. A sterile saline-soaked piece of gauze was placed underneath the LLL to allow a sterile and hydrated surface for the liver to lie on. A small piece of the LLL of the liver (1-2 cm^3) was cut with sterile scissors and collected for histopathology. A sterile hemostatic absorbable gelatin sponge (Equispon®; Equimedical BV, Zwanenburg, Netherlands) of the same size was inserted into the cut portion of the liver using sterile forceps and contact with the liver was maintained until it adhered to the surface and hemostasis was achieved. The liver was then placed back to the abdominal cavity taking care to not disturb the sponge. To complete the procedure, the abdominal wall and skin were sutured with Ethicon® 4-0 coated absorbable silk thread (Johnson & Johnson, New Brunswick, NJ, USA) and prophylactic antibiotic treatment (10 mg/kg Gobemicin®; Laboratorios Normon S.A., Madrid, Spain) was administered intramuscularly with a 27 G needle. A second and a third dose of 0.1 mg/kg buprenorphine was administered subcutaneously 24 and 48 h post-surgery.

4.2. Liver hemodynamics

The hemodynamic measurements were performed in fasted rats from all three studies at the time of sacrifice either under intraperitoneal anesthesia with 100 mg/kg ketamine

(Ketolar®, Pfizer, NY, USA) and 5 mg/kg midazolam (B. Braun, Melsungen, Germany) (Study 1 and 2) or under constant anesthesia with inhaled isoflurane (5% induction and 2% maintenance; Baxter International Inc., Deerfield, IL, USA) (Study 3). Intraperitoneal anesthetized animals were given a booster dose (0.2 mL of 50% ketamine and midazolam) in case the anesthetic effect was lost. The surgical regions (inner part of the leg and abdomen) were shaved and the animal was placed in supine position. The temperature of the animal was maintained at 37 °C with the help of a heated blanket (Panlab, Cornellà de LLobregat, Spain) and a rectal probe throughout the recording. Measurements were recorded using the PowerLab data acquisition unit (Harvard Apparatus, Holliston, MA, USA) associated with Chart 5.0 software.

Mean arterial pressure

Mean arterial pressure (MAP, mmHg) was determined by intravascular cannulation of the right femoral artery of the animal with a polyethylene PE-catheter (PE50) (BD Intramedic™ Polyethylene Tubing (Non-Sterile), Franklin Lakes, NJ, USA) connected to a high-sensitivity signal transducer (Harvard Apparatus, Holliston, MA, USA). Initially, an incision was made in the right groin of the animal opening the way until locating the bundle composed of femoral vein, artery and nerve. Once the femoral artery was freed from the nerve, vein and connective tissue, a small incision in the artery with a 23 G needle was done. The catheter was then introduced into the artery and immobilized with a 2-knot ligature (Silkam* 3-0 coated non-absorbable suture thread; B. Braun, Melsungen, Germany).

Heart rate

Heart rate (BPM, beats per minute) was measured from the mean arterial pressure record to know the state of consciousness of the animal at all times. We always tried to keep BPM between 300 and 350.

Portal pressure

Portal pressure (PP, mmHg) was measured by intravascular cannulation of the ileocolic vein with a PE50 polyethylene catheter connected to a high-sensitivity signal transducer (Harvard Apparatus, Holliston, MA, USA). After an abdominal incision and exposing the mesentery, the catheter was introduced into the ileocolic vein and immobilized with one drop of cyanoacrylate glue.

Mesenteric flow

Superior mesenteric artery flow (SMABF, mL / [min · 100 g]) was measured using a 1 mm Doppler perivascular ultrasonic transit-time flow probe (Transonic Systems Inc., Ithaca, NY, USA). After the abdominal incision, the superior mesenteric artery (SMA) was isolated from connective tissue and the surrounding fat. Subsequently, an ultrasound transmission gel was applied to the probe to facilitate signal transmission, and finally the dissected artery was clamped with the probe.

Portal flow

Portal vein flow (PBF, mL / [min · 100 g]) was also measured using a 1 mm Doppler perivascular ultrasonic transit-time flow probe (Transonic Systems Inc., Ithaca, NY, USA). Once the portal vein was isolated, an ultrasound transmission gel was applied to the probe to facilitate signal transmission, and finally the vein was clamped with the probe.

Mesenteric resistance

Superior mesenteric artery resistance (SMAR, mmHg / mL · min · 100 g) was determined by the following formula:

$$SMAR = \frac{(MAP\text{-}PP)}{SMABF}$$

Intrahepatic vascular resistance

Intrahepatic vascular resistance (IHVR, mmHg / mL · min · 100 g) was determined by the following formula:

$$IHVR = \frac{PP}{PBF}$$

4.3. Blood biochemistry

4.3.1. Blood biochemistry on all rat models

Fasting rat blood samples were taken from the cava vein immediately after registration of the hemodynamic parameters. Part of the sample was stored in plastic tubes without anticoagulant (BD Vacutainer® SST™ II Advance, Franklin Lakes, NJ, USA) to be analyzed by standard techniques in the Clinical Biochemistry Laboratory of the Vall d´Hebron University Hospital. The serum levels of glucose, bilirubin, aspartate aminotransferase (AST), alanine aminotransferase (ALT), total cholesterol, high-density lipoprotein (HDL), low-density lipoprotein (LDL), triglycerides (TG) and albumin were analyzed.

Another part of the blood sample was collected in an *Eppendorf* tube and centrifuged at 4,000 g at 4 °C for 10 min. Serum was collected and stored at -20 °C for further analysis of insulin levels.

Measurement of insulin levels

The insulin levels were quantified following the ELISA commercial kit protocol (Merck, Darmstadt, Germany) with duplicates for each sample. The 96-well plate readings were performed at 450 nm and 590 nm with the Synergy MX spectrophotometer (Biotek, Winooski, VT, USA) and the Gen 5 v2.9 software. Insulin resistance was estimated by applying the homeostasis model of insulin resistance index (HOMA-IR) which is calculated with the following formula:

$$\text{HOMA-IR} = \frac{\text{Fasting serum insulin (ng/mL)} \cdot \text{Fasting serum glucose (mg/dL)}}{405}$$

4.3.2. Blood biochemistry on the STAM™ mouse model

In the STAM™ mice in study 2, non-fasting blood was drawn from the facial vein for the quantification of glycated hemoglobin (HbA1c), cytokeratin (CK)-18, and biochemistry. HbA1c levels were quantified in whole blood by DCN2000+ (Siemens Healthcare Diagnostics, Malvern, PA, USA). Serum CK-18 levels were measured by using the Mouse Cytokeratin 18-M30 ELISA kit (Cusabio Biotech Co., Ltd, China). Serum ALT and TG levels were measured by FUJI DRI-CHEM 7000 (Fujifilm Corporation). Serum total cholesterol, HDL and LDL levels were quantified by HPLC at Skylight Biotech Inc. (Japan).

4.4. Histological analysis

4.4.1. Histological stains: H&E and Sirius red

Animal liver samples were extracted, fixed in 4% formalin for 24 h (rats) or in Bouin´s solution (Sigma-Aldrich Japan, Japan) (mice), embedded in liquid paraffin at 65 °C and included in blocks. Paraffin-embedded blocks were then sectioned in 4 µm thick slices. In all three studies, processing of rat liver samples for histological analysis, including the hematoxylin and eosin (H&E) staining, was performed by the Anatomic Pathology Service of the Vall d´Hebron University Hospital to evaluate liver parenchyma.

To detect collagen fibers, i.e. liver fibrosis, 0.4 µm rat and mouse liver sections were hydrated and stained with 0.1% Sirius red (Merck, Darmstadt, Germany) for 1 h at room temperature with gentle agitation. After staining, they were washed twice with acidified water, dried at room temperature and mounted with DPX rapid mounting medium (PanReac AppliChem, Darmstadt, Germany). Ten fields from each Sirius red-stained liver section were randomly captured at 10× magnification with an optical microscope

Olympus BX61 (Olympus, Hamburg, Germany) equipped with a digital camera. The proportion of Sirius red-stained area per total area was measured using a Java-based image processing software (Image J; National Institute of Health, Bethesda, MD, USA) and expressed as Sirius red-positive area (%).

4.4.2. NASH histological diagnosis

All stained liver sections were examined by an expert liver pathologist blinded to the interventions performed on the animals.

The diagnosis of NASH was established based on the presence of all three characteristic patterns of the disease, which include the coexistence of steatosis, lobular inflammation, and hepatocellular ballooning. The degree of steatosis, inflammation and ballooning was scored according to the NASH-Clinical Research Network (NASH-CRN) system (119) (Table 1). The unweighted sum of these histological components, called NAFLD Activity Score (NAS), classifies the pathology according to its severity, being essential for the diagnosis of NASH not only that the sum of the scores is equal to or greater than three (NAS ≥ 3), but also that the concurrence of the three histological features is established. The degree of fibrosis was also scored according to the NASH-CRN system (Table 1).

Table 1. NASH-Clinical Research Network (CRN) scoring system (119).

Histological feature	Definition	Score
Steatosis	<5%	0
	5%-33%	1
	34%-66%	2
	>66%	3
Lobular inflammation	None	0
	<2 foci	1
	2-4 foci	2
	>4 foci	3
Hepatocellular ballooning	None	0
	Few ballooned cells	1
	Many ballooned cells	2
Fibrosis	None	0
	Perisinusoidal or periportal	1
	Mild, zone 3, perisinusoidal	1A
	Moderate, zone 3, perisinusoidal	1B
	Portal/periportal	1C
	Portal/periportal and perisinusoidal	2
	Bridging fibrosis	3
	Cirrhosis	4

4.5. Immunohistochemistry

4.5.1. Immunohistochemistry on the 8- and 36-week diet-induced rat models

In study 1, formalin-fixed, paraffin-embedded liver tissue from 8- and 36-week rats was cut into 4 µm sections, dewaxed and hydrated. Paraffin-embedded liver sections were used for CD34 and sonic hedgehog (Shh) immunohistochemistry. First, antigen retrieval

was performed by heating in 1X Tris-EDTA solution plus 0.05% Tween® 20 (Merck, Darmstadt, Germany) for 30 min at 95 °C. After cooling and washing with 1X PBS, sections were incubated for 10 min in 3% H_2O_2 to block endogenous peroxidase. Sections were blocked with 5% goat serum (Merck, Darmstadt, Germany) diluted with 1X PBS for 30 min and subsequently incubated with primary antibodies overnight at 4 °C in a humidified chamber. The primary antibodies and the dilutions used are indicated in Table 2. Following successive wash steps, secondary antibody was applied for 30 min (EnVision™ Dual Link System-HRP; Dako, Glostrup, Denmark). Peroxidase solution (Vector® Vip SK-4600, Vector laboratories, Inc., Burlingame, CA, USA) was used for detection and liver sections were then counterstained with Harris hematoxylin solution (PanReac AppliChem, Darmstadt, Germany) for 10 s, dehydrated and mounted with DPX rapid mounting medium (PanReac AppliChem, Darmstadt, Germany).

Table 2. Primary antibodies used for immunohistochemistry on the 8- and 36-week diet-induced rat models.

Primary antibodies			
Ab	**Reference code**	**Manufacturer**	**Dilution**
Anti-CD34	ab185732	Abcam, MA, USA	1/200
Anti-Shh	E-1 sc-365112	Santa Cruz Biotechnology, TX, USA	1/50

Ab, antibody; Shh, sonic hedgehog.

Digital images were randomly captured from all stained samples using an optical Olympus BX61 microscope (Olympus, Hamburg, Germany) equipped with a digital camera. For CD34, ten vision fields per sample were imaged at 20× magnification and for Shh, twelve vision fields per sample were imaged at 40× magnification. Stained area quantification was done blind to the group origin of the sample using Image J software. The results were reported as the median of all quantified areas for each sample and finally for each group.

4.5.2. Immunohistochemistry on the STAM™ mouse model

In study 2, mouse liver specimens were stored at -80 °C embedded in Optimal Cutting Temperature (O.C.T., Sakura Finetek Japan, Japan) compound for immunohistochemistry and fixed in acetone. O.C.T.-embedded specimens were used for F4/80 and fibronectin immunohistochemistry. First, endogenous peroxidase activity was blocked using 0.03% H_2O_2 for 5 min, followed by incubation with Block Ace (Dainippon Sumitomo Pharma Co. Ltd., Japan) for 10 min. Then, sections were incubated with primary antibodies overnight at 4 °C. After incubation with secondary antibody for 30 min at room temperature, enzyme-substrate reactions were performed using 3, 3'-diaminobenzidine/H_2O_2 solution (Nichirei Bioscience Inc., Japan). The primary and secondary antibodies used, as well as the dilutions, are detailed in Table 3.

Table 3. Primary and secondary antibodies used for immunohistochemistry on the STAM™ mouse model.

Primary antibodies			
Ab	**Reference code**	**Manufacturer**	**Dilution**
Anti-F4/80	Monoclonal Antibody T-2006	BMA Biomedicals, Basel, Switzerland	1/1000
Anti-Fibronectin	ab2413	Abcam, MA, USA	1/200
Secondary antibodies			
Ab	**Manufacturer**		**Dilution**
Anti-rat IgG-biotinylated	Vector Laboratories Inc., CA, USA		1/200
Anti-rabbit IgG-HRP	Vector Laboratories Inc., CA, USA		1/25

Ab, antibody.

Bright field images of immunostained sections were captured around the central vein using a digital camera (DFC295; Leica, Wetzlar, Germany) at 200× magnification.

4.6. Digital image analysis

In study 1, a complete digital image analysis to measure the intrahepatic structural changes from 8- and 36-week rat liver H&E sections was performed. Images were obtained with an optical microscope Olympus BX61 (Olympus, Hamburg, Germany) equipped with a digital camera. Measurements were made blindly to the group origin of the samples using Image J software.

4.6.1. Sinusoidal and fat area

Sinusoidal and fat area were measured by selecting 21 randomly non-overlapping areas per sample imaged at 20× magnification. To measure the areas, a threshold was assigned in order to mark the hepatic sinusoids on the one hand and the liver fat on the other, as shown in Figure 10.

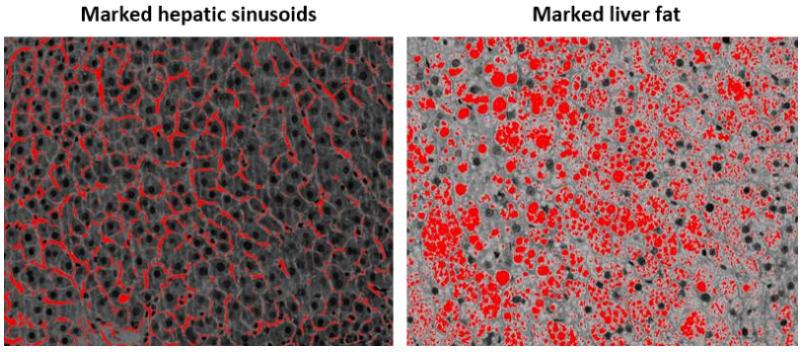

Figure 10. Images illustrating the measurement of the area (in red) of hepatic sinusoids and liver fat (20× magnification).

The result was reported as the median of all measurements for each sample and finally for each group.

4.6.2. Hepatocyte area

Hepatocyte area was measured by selecting 10 randomly non-overlapping areas per sample imaged at 40× magnification. Twenty hepatocytes were randomly selected for each image. Hepatocyte areas were measured in two perpendicular dimensions (as already described by Hall *et al*. (120)) and were then calculated as an oval using the following formula:

$$\text{Cell area } (\mu m^2) = \pi \cdot \left(\frac{\text{max lobule diameter}}{2}\right) \cdot \left(\frac{\text{perpendicular lobule diameter}}{2}\right)$$

The result was first reported as the median of all hepatocyte areas for each sample and finally as the median for each group.

4.6.3. Number of hepatocytes

As in the case of the sinusoidal and the fat area, 21 randomly selected non-overlapping areas per sample were imaged at 20× magnification to then calculate the number of hepatocytes by counting their nucleus. The result was reported as the median of the number of hepatocytes for each sample and finally for each group.

4.7. Scanning electron microscopy

For an in-depth exploration of the intrahepatic structural characteristics (namely the sinusoids) of the 36-week rat liver sections, scanning electron microscopy (SEM) was used. For that, livers were perfused via the portal vein with 1% heparin to flush blood from the liver, and then with fixative containing 2.5% glutaraldehyde, 2% paraformaldehyde, 2 mmol/L calcium chloride, 2% sucrose, and 0.1 mol/L cacodylate buffer. From each liver, a total of 10 blocks of tissue (1 × 1 × 5 mm) were taken from the left and right lobes to have representative samples of the entire liver.

To be able to proceed to the sample treatment and exploration by SEM, the samples were taken to the Electron Microscopy Service at the *Universitat Autònoma de Barcelona*. At first, samples were osmicated (1% OsO_4/0.1 mol/L cacodylate buffer [pH 7.3]) for 2 to 3 h and dehydrated in an ethanol gradient to 100%. Tissue pieces were then critical-point–dried using a Baltec CPD030, mounted on aluminum SEM stubs and sputter-coated with gold.

The hepatic tissue was examined on a Zeiss EVO® MA10 Scanning Microscope (ZEISS, Jena, Germany). Five to six blocks of tissue were examined per animal and images were taken at 500× for a general view and 1,500× magnification to a more detailed exploration of the tissue.

4.8. Molecular biology techniques

4.8.1. Western blot

Protein extraction

For the analysis of hepatic proteins, rat livers from all three studies were perfused with saline for exsanguination. They were then fragmented and directly frozen in liquid nitrogen and stored at -80 °C. Frozen liver samples were crushed cold, avoiding defrosting, until turning them manually into dust. They were then homogenized in Triton-lysis buffer (400 µL/sample), sonicated 3 times of 10 s at maximum power and after leaving them for 10 min on ice, they were centrifuged at 14,000 rpm for 10 min at 4 °C. The supernatant was transferred to a new *Eppendorf* and kept at 20 °C for subsequent total protein quantification.

Protein quantification

Supernatant total protein concentration was quantified by BCA™ protein assay kit (Thermo Fisher Scientific, Waltham, MA, USA) following kit´s instructions. 1/30 dilution

was used in liver samples. BSA known concentrations were used as standard curve. The total protein concentration was determined by a colorimetric reaction (color change of the sample from green to purple) reading at 652 nm with Nanodrop (Thermo Fisher Scientific, Waltham, MA, USA).

SDS-PAGE electrophoresis and electrotransfer

Electrophoresis was performed with the XCell SureLock™ Mini-Cell Electrophoresis System in a 10% NuPAGE® Bis-Tris (Thermo Fisher Scientific, Waltham, MA, USA) sodium dodecyl sulphate-polyacrylamide gel electrophoresis (SDS-PAGE).

The sample solutions were prepared as indicated in Table 4 and boiled at 95 °C for 10 min before loading the gel. A total of 11 µL of sample solution was loaded into each gel well. The protein ladder Precision plus Protein™ Dual Color Standards (Bio-Rad. Hercules, CA, USA) was ready-to-use and 5 µL were directly loaded into the gel well. Gels were run at 200 V and 120 mA.

Table 4. Sample preparation for NUPAGE® Electrophoresis Gel Loading.

Reagent	Volume (µL)
Protein extraction	X (60 µg)
dH_2O	7.8 µL - X
NuPAGE® LDS sample buffer (4X)	3 µL
NuPAGE® LDS reducing agent (10X)	1.2 µL

dH_2O, distilled water; Total volume = 12 µL (11 µL/well were loaded); NuPAGE® reagents are from Thermo Fisher Scientific (Waltham, MA, USA).

The transfer was performed with the XCell II™ Blot Module (Thermo Fisher Scientific, Waltham, MA, USA) onto polyvinylidine fluoride (PVDF) membranes with a pore size of 0.45 µm (Thermo Fisher Scientific, Waltham, MA, USA) previously hydrated with

methanol (30 s), dH2O (5 min) and transfer buffer (5 min). The transfer was performed at 30 V and 400 mA on ice.

Immunodetection

Once the transfer was done, membranes were stained with Ponceau S solution (Merck, Darmstadt, Germany) for 5 min to ensure that proteins were properly transferred. All incubations and washes were carried out with constant shaking. Membranes were washed with 1X TTBS three times for 10 min, and blocked for 1 h at room temperature with 5% bovine serum albumin (BSA) (Merck, Darmstadt, Germany) or with 5% PhosphoBLOCKER™ (Cell Biolabs, Inc., San Diego, CA, USA) in the case of phosphorylated proteins.

After blocking, membranes were incubated with primary antibodies overnight at 4 °C. They were then washed three times with 1X TTBS for 10 min, incubated with the corresponding secondary antibody (peroxidase-coupled) for 1 h at room temperature and washed three more times with 1X TTBS for 10 min. The primary and secondary antibodies used, as well as the dilutions, are detailed in Table 5.

Washed membranes were revealed with the ECL prime kit (GE Healthcare, Little Chalfont, UK) on the Odyssey®Fc imaging system (LI-COR, Lincoln, NE, USA) and quantified with Image Studio Lite software (LI-COR, Lincoln, NE, USA). The protein expression was normalized to glyceraldehyde-3-phosphate dehydrogenase (GAPDH) used as loading control.

Table 5. Primary and secondary antibodies for Western blot.

Primary antibodies				
Protein	**MW (kDa)**	**Species (Ab)**	**Manufacturer**	**Dilution**
GAPDH	37	Mouse	Ambion, TX, USA	1/5,000 in 1X TTBS
KLF2	40	Rabbit	Santa Cruz Biotechnology, TX, USA	1/200 in 1X TTBS
P-Akt	60	Goat	Cell Signaling, MA, USA	1/500 in 5% PhosphoBLOCKER™
P-eNOS	140	Rabbit	Cell Signaling, MA, USA	1/250 in 5% BSA
Secondary antibodies				
Ab			**Manufacturer**	**Dilution**
Anti-goat IgG-HRP			Santa Cruz biotechnology, TX, USA	1/30,000
Anti-mouse IgG-HRP			GE Healthcare, IL, USA	1/30,000
Anti-rabbit IgG-HRP			Cell Signaling, MA, USA	1/30,000

Ab, antibody; GAPDH, glyceraldehyde-3-phosphate dehydrogenase; KLF2, Kruppel-like factor 2; MW molecular weight; P-Akt, phosphorylated protein kinase B; P-eNOS, phosphorylated endothelial nitric oxide synthase. GAPDH was used as loading control. All secondary antibodies were diluted in 1X TTBS except P-Akt that was diluted in 5% PhosphoBLOCKER™.

4.8.2. Gene expression analysis

RNA extraction and reverse transcription

Rat liver samples from all three studies were maintained at least 24 h in RNA*later Stabilization Solution* (Thermo Fisher Scientific, Waltham, MA, USA) and then stored at -80 °C until further use. Total RNA was extracted using RNeasy Mini-Kit (QIAGEN, Venlo, Netherlands) and 1 µL RNA was finally quantified reading at 260 nm with Nanodrop (Thermo Fisher Scientific, Waltham, MA, USA).

Once the RNA was isolated, the reverse transcription to complementary DNA (cDNA) was performed with the *High-Capacity cDNA Reverse Transcription Kit* (Thermo Fisher Scientific, Waltham, MA, USA). All reagents and its corresponding volumes are detailed in Table 6.

Table 6. Sample preparation for High-Capacity cDNA Reverse Transcription.

Reagent	**Volume (µL)**
10X RT buffer	2
25X dNTP Mix (100 mM)	0.8
10X RT Random Primers	2
MultiScribe™ Reverse Transcriptase	1
RNase Inhibitor	1
RNase-free H_2O	3.2
RNA	X (1 µg)

Total volume = 20 µL. All reagents are from Thermo Fisher Scientific (Waltham, MA, USA).

RT-qPCR

Quantitative reverse-transcription polymerase chain reaction (RT-qPCR) was performed in 384-well plates with triplicates for each rat liver sample. The sample reagents and the probes used for RT-qPCR are indicated in Table 7 and Table 8, respectively. The quantification of gene expression was performed using 7900HT Fast Real-Time PCR system (Thermo Fisher Scientific, Waltham, MA, USA), based on a standard protocol of 40 cycles at 95 °C-60 °C. The data analysis was performed using the Relative Quantification qPCR Application in Thermofisher Cloud (Thermo Fisher Scientific, Waltham, MA, USA). For results calculation, the $2^{-\Delta\Delta Ct}$ method was used. The relative gene expression was normalized to β-Actin used as loading control.

Table 7. Sample preparation for RT-qPCR.

Reagent	Volume (µL)
Taqman universal PCR master mix	4.5
Specific probe	0.5
cDNA	5 (20 ng)

Taqman universal PCR master mix is from Thermo Fisher Scientific (Waltham, MA, USA).

Table 8. Probes used for RT-qPCR.

Probes			
Symbol	**Full name**	**Other nomenclatures**	**Reference code**
Actb	Actin, beta	β-Actin	Rn00667869_m1
Acta2	Actin, alpha 2, smooth muscle, aorta	α-SMA	Rn01759928_g1
Adipor2	Adiponectin receptor 2	AdipoR2	Rn01463173_m1
Col1a1	Collagen, type I, alpha 1	COL1A1	Rn01463848_m1
Irs1	Insulin receptor substrate 1	IRS-1	Rn02132493_s1
Irs2	Insulin receptor substrate 2	IRS-2	Rn01482270_s1
Lepr	Leptin receptor	LepR	Rn01433205_m1
Nos2	Nitric oxide synthase 2, inducible	iNOS	Rn00561646_m1

All probes are from Thermo Fisher Scientific (Waltham, MA, USA). β-Actin was used as loading control. All probes are marked with FAM-MGB fluorophore.

4.8.3. Cecal whole metagenome shotgun sequencing

Genomic DNA was extracted from approximately 0.2 g of cecum content of each rat in study 2 using the ZymobioMics DNA Miniprep Kit (Zymo Research, Irvine, CA, USA) according to manufacturer's instructions and quantified using the Qubit™ Flex Fluorometer (Thermo Fisher Scientific, Wilmington, DE, USA) and used for whole metagenome shotgun (WMS) sequencing. WMS sequencing, taxonomic- and pathway profiling were performed by CosmosID (Rockville, MD, USA). As result, 2x150bp Illumina reads were mapped to a proprietary microbial genome database for taxonomic profiling

(121) and to UniRef90 and MetaCyc for pathway profiling (122). Treatment-induced microbial composition modulation was assessed with both unsupervised analysis (multi-dimensional scaling using UniFrac distances), and supervised analysis (sparse partial least-squares discriminant analysis, sPLS-DA), using the R packages phyloseq (123) and mixOmics (124), respectively. Classifier performance for the latter was appreciated through the balanced error rate (BER): $BER = 0.5 \cdot (FP / (TN + FP) + FN / (TP + FN))$. Microbiome features, comprising diversity estimates and inferred metabolite biosynthesis capacity were treated as non-normally distributed and non-parametric Wilcoxon signed-rank testing was performed to compute statistical significance of group comparison.

4.8.4. Liver transcriptomics

Liver transcriptomics was performed on rats in study 2. For this, RNA extraction, RNA library preparations, and HiSeq Sequencing reactions were conducted at GENEWIZ, LLC. (South Plainfield, NJ, USA).

RNA extraction

Total RNA was extracted from fresh frozen liver tissue samples using the Qiagen RNeasy Plus Universal Mini-Kit following manufacturer's instructions (Qiagen, Hilden, Germany). RNA samples were quantified using Qubit 2.0 Fluorometer (Life Technologies, Carlsbad, CA, USA), and RNA integrity was measured using the RNA Screen Tape on Agilent 2200 TapeStation (Agilent Technologies, Palo Alto, CA, USA).

RNA library preparations

RNA sequencing libraries were prepared using TruSeq Stranded mRNA library prep kit following manufacturer's protocol (Illumina, Cat# RS-122-2101). First, mRNAs were enriched with Oligo d(T) beads. Enriched mRNAs were fragmented for 8 min at 94 °C.

Subsequently, first strand and second strand cDNA were synthesized. The second strand of cDNA was marked by incorporating dUTP's during synthesis. cDNA fragments were adenylated at 3'ends and indexed adapters were ligated to cDNA fragments. Limited cycle PCR was used for library enrichment. The incorporated dUTP's in second strand cDNA quenched the amplification thus preserving strand specificity. Sequencing libraries were validated using DNA Analysis Screen Tape on the Agilent 2200 TapeStation (Agilent Technologies, Palo Alto, CA, USA), and quantified by using Qubit 2.0 Fluorometer (Invitrogen, Carlsbad, CA, USA) as well as by quantitative PCR (KAPA Biosystems, Wilmington, MA, USA). The pooled libraries were clustered on 7 lanes of a flowcell.

HiSeq sequencing

After clustering, the flowcell was loaded on the Illumina HiSeq instrument (4000 or equivalent) according to manufacturer's instructions and sequenced using a 2x150bp Paired End (PE) configuration. Image analysis and base calling were conducted by the HiSeq Control Software (HCS). Raw sequence data (.bcl files) generated from Illumina HiSeq was converted into fastq files and de-multiplexed using Illumina's bcl2fastq 2.17 software. One mismatch was allowed for index sequence identification.

Gene expression profiling

Strand-specific gene expression profiling was achieved through mapping of Illumina 2x150bp reads to the Ensembl *Rattus norvegicus* Rnor_6.0 transcriptome and processing the alignments with feature Counts from the subread package (125). Rat Ensembl gene (version 104) IDs were mapped to human Ensembl gene equivalents and HUGO Gene Nomenclature Committee (HGNC) symbols through Ensembl Biomart. Resulting uniquely mapping fragment counts were taken into differential gene expression analysis with the R package DESeq2 (126) to obtain differential expressed genes with Benjamini & Hochberg false discovery rate (FDR) adjusted P-values. Outlier

analysis was performed with orthogonal partial least squares analysis using the R package ropls (127). Simultaneously, sPLS-DA was performed to estimate variable importance (VIP). Liver genes discriminant for treatment vs. vehicle contrasts were retained as having a VIP>1 and FDR adjusted P-value<0.1. Functional over-representation analysis (ORA) in these genes was performed with the R package clusterProfiler (128), using the functional annotation database WikiPathways (WP) (129), MetaCyc (MC) (130), Reactome (RT) (131), and Biocarta (BC) (132). The Harmonizome database (133) provides curated and ranked disease gene associations, including a Fatty Liver gene set of 11,463 genes. The top 1,000 fatty liver associated genes were used to select disease related genes from differential gene expression analysis.

4.9. Statistical analysis

Statistical analyses were performed using GraphPad Prism software (GraphPad Software, San Diego, CA, USA). Continuous variables were tested for normality using the D'Agostino-Pearson normality test and were documented as mean ± standard error of the mean (SEM). Continuous variables were compared by Student's t-test or One Way ANOVA with Dunnett's multiple comparisons' test. A P-value ≤ 0.05 was considered statistically significant.

5. RESULTS

5. RESULTS

5.1. STUDY 1: Characterization of short- and long-term HFGFD-induced rat models

Metabolic, histological and hemodynamic features were evaluated in order to characterize the short- (8 weeks) and long-term (36 weeks) rat models after the HFGFD intervention.

The 36-week HFGFD intervention further worsened the altered metabolic profile of the 8-week NASH model

HFGFD intervention markedly increased the body weight of rats compared to CD at both time points (Table 9). The 36-week HFGFD (36w-HFGFD) intervention was associated with a significant increase in fasting glucose levels as compared to 36-week controls and 8-week groups. This intervention also associated a significant increase in fasting insulin as well as in insulin resistance (HOMA-IR) as compared to the 8-week intervention. These changes did not reach statistical significance when compared to 36-week controls (36w-CD) because of the marked raise in insulin plasma levels in these sedentary 36w-CD individuals. Serum transaminases (ALT and AST) were also significantly increased in the 36w-HFGFD group compared to 36w-CD and 8-week groups. The same significant differences between the 8- and 36-week HFGFD interventions were observed with fasting blood concentrations of total cholesterol and HDL-cholesterol (Table 9). Overall, the expected disturbed metabolic profile of the model was further worsened with the long-term time extension of the HFGFD intervention.

Table 9. Body weight and biochemical parameters in CD and HFGFD rats after 8 and 36 weeks of dietary intervention.

	8 weeks		36 weeks	
	CD (n = 10)	**HFGFD (n = 10)**	**CD (n = 14)**	**HFGFD (n = 15)**
BW (g)	461 ± 12.83	493 ± 16.61	654 ± 21.9†††	798 ± 29.46$^{***\#\#\#}$
Glucose (mg/dL)	140.88 ± 8.72	181.22 ± 27.78	179 ± 11.87†	227.53 ± 10.67$^{*\#}$
Insulin (ng/mL)	4.23 ± 7.05	7.96 ± 7.25	15.44 ± 2.76††	25.98 ± 6.38$^{\#}$
HOMA-IR	1.97 ± 3.4	3.83 ± 4.1	7.57 ± 1.2†	13.75 ± 3.82$^{\#}$
Albumin (g/dL)	2.55 ± 0.09	2.87 ± 0.05**	2.8 ± 0.04††	2.8 ± 0.05
Bilirubin (mg/dL)	0.09 ± 0.01	0.1 ± 0.02	0.14 ± 0.02†	0.13 ± 0.02
AST (IU/L)	117.29 ± 6.36	170.14 ± 21.3*	206 ± 30.87†	447 ± 193.09$^{*\#}$
ALT (IU/L)	33.22 ± 6.3	45.67 ± 3.57	66.5 ± 7.99††	206 ± 75.69$^{*\#\#}$
TG (mg/dL)	37.11 ± 3.23	45.33 ± 5.1	42.21 ± 3.63	52 ± 16.121
Cholesterol (mg/dL)	85 ± 5.45	80.22 ± 4.13	119.5 ± 10.14††	104 ± 9.37$^{\#\#}$
Cholesterol HDL (mg/dL)	47.21 ± 2.59	45.56 ± 1.76	67 ± 5.89††	58 ± 4.83$^{\#\#}$
Cholesterol LDL (mg/dL)	27.2 ± 1.22	25.6 ± 4.07	41.5 ± 4.32††	35 ± 3.76

Values are expressed as mean ± SEM. ALT, alanine aminotransferase; AST, aspartate aminotransferase; BW, body weight; CD, control diet; HDL, high-density lipoprotein; HFGFD, high-fat glucose-fructose diet; HOMA-IR, homeostasis model of insulin resistance index; LDL, low-density lipoprotein; TG, triglycerides. $^{*}P \leq 0.05$; $^{**}P \leq 0.01$; $^{***}P \leq 0.001$ versus CD. $^{\#}P \leq 0.05$; $^{\#\#}P \leq 0.01$; $^{\#\#\#}P \leq 0.001$ versus HFGFD-8-week. $^{\dagger}P \leq 0.05$; $^{\dagger\dagger}P \leq 0.01$; $^{\dagger\dagger\dagger}P \leq 0.001$ versus CD-8-week.

The 36-week HFGFD intervention induced increased NASH activity without inducing fibrosis

From a histopathological perspective, both the 8-week and 36-week dietary interventions did result in a consistent reproduction of NASH histological hallmarks, as seen in Figure 11. Overall, the 36w-HFGFD group showed a more intense degree of NASH histological activity (as measured by NAS) (Figure 11D). Although lobular inflammation tended to increase at 36 weeks, reaching maximum scores of 3 in some cases (Figure 11B), most of the increase in activity at 36 weeks was due to a marked increase in steatosis at this time point, with apparent collapse of sinusoidal spaces at light microscopy (Figure 11E). However, despite this increase in activity in the long-term, none of the dietary interventions was able to induce fibrosis (Figure 12A). A non-significant increase in expression of α-SMA was observed in association with the HFGFD at 8 weeks and, interestingly, a significant increase was also observed in the 36w-CD group when compared to both 8w-CD and 36w-HFGFD groups. However, this marker of stellate cell activation was not accompanied by changes in collagen deposition at light microscopy or an increase in expression of COL1A1 in this group, which was even significantly decrease as compared to the 8-week counterparts (Figure 12B).

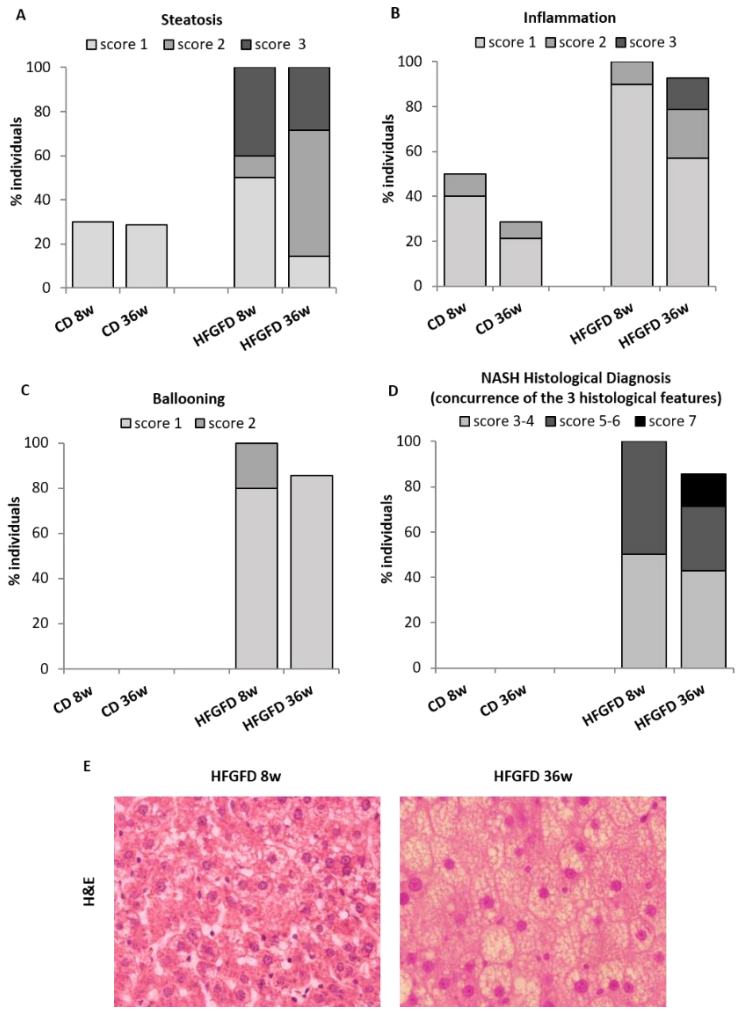

Figure 11. Histological evaluation of the H&E-stained liver sections collected from rats after 8 and 36 weeks of dietary intervention (CD-8w n = 10, HFGFD-8w n = 10, CD-36w n = 14, HFGFD-36w n = 15). Evaluation followed the NASH-Clinical Research Network system. The three first bar diagrams represent the percentage of individuals presenting (A) steatosis, (B) inflammation, and ballooning (C) in the different groups. Each bar includes the percentage of individuals scored with 1 (light gray), 2 (gray), or 3 (dark gray); the last bar diagram (D) represents the percentage of individuals with NASH Histological Diagnosis (defined as NAFLD activity score (NAS) ≥ 3 and concurrence of steatosis, lobular inflammation and hepatocellular ballooning) scored with 3-4 (light gray), 5-6 (dark gray), or 7 (black). (E) Representative images show H&E-stained liver parenchyma of HFGFD rats after 8 and 36 weeks of dietary intervention (40× magnification). CD, control diet; HFGFD, high-fat glucose-fructose diet.

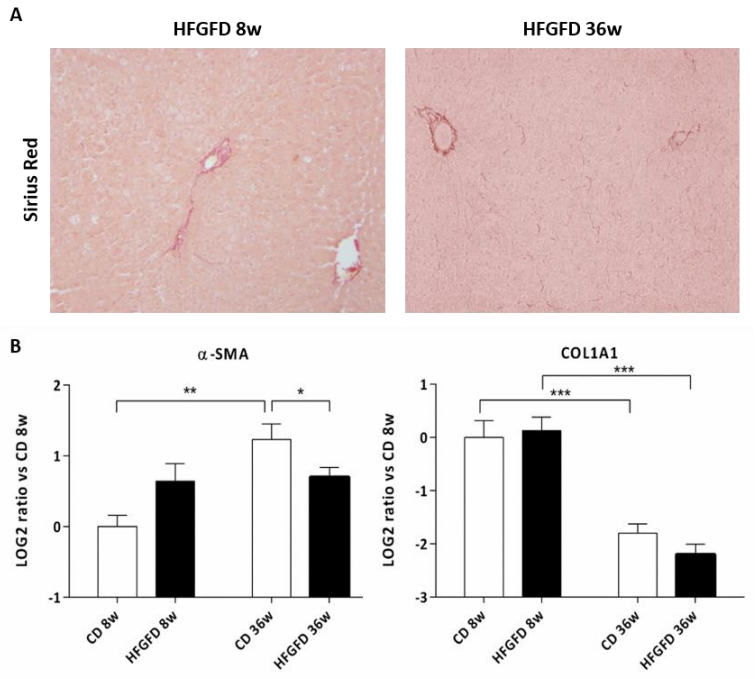

Figure 12. Markers of liver fibrosis. (A) Representative images show Sirius red-stained liver parenchyma of HFGFD rats after 8 and 36 weeks of dietary intervention (10× magnification). (B) Relative mRNA expression of α-SMA and COL1A1 by RT-qPCR and expressed as a log2 ratio. β-Actin was used as an endogenous control, and results were normalized to the control group of 8 weeks. α-SMA, alpha-smooth muscle actin; CD, control diet; COL1A1, collagen type I alpha 1 chain; HFGFD, high-fat glucose-fructose diet. Data represent mean ± SEM. $^{*}P \leq 0.05$; $^{**}P \leq 0.01$; $^{***}P \leq 0.001$.

The 36-week HFGFD intervention significantly worsened portal hypertension and intrahepatic vascular resistance in the NASH rat model

Despite the absence of fibrosis, the HFGFD intervention induced a significant increase in PP at both time points (Table 10). This increase in PP was especially remarkable in the 36-week model: the HFGFD 36-week intervention caused a 40% increase in PP compared to 36w-CD (12.1 versus 8.7 mmHg, $P < 0.001$), being significantly higher than the PP value observed in the 8w-HFGFD model (12.1 versus 10.5 mmHg, $P = 0.006$). This increase in PP was secondary to a significant increase in IHVR at both time points. Aging did not seem to have a relevant effect in portal hemodynamics, since there were no

major differences between CD groups over time, except for the SMAR, which increased in the older group, although this change remained lower than that of the 36w-HFGFD group. No changes in systemic hemodynamics were observed when comparing CD and HFGFD at both time points (Table 10).

Table 10. Hemodynamic measurements in CD and HFGFD rats after 8 and 36 weeks of dietary intervention.

	8 weeks		36 weeks	
	CD (n = 10)	**HFGFD (n = 10)**	**CD (n = 11)**	**HFGFD (n = 8)**
MAP (mmHg)	108.03 ± 4.16	110.03 ± 4.56	118.11 ± 4.38	118.32 ± 6.35
PP (mmHg)	8.43 ± 0.3	10.47 ± 0.31***	8.72 ± 0.31	12.08 ± 0.42$^{***\#\#}$
SMABF (mL/[min · 100 g])	3.60 ± 0.49	3.54 ± 0.36	2.56 ± 0.23	2.06 ± 0.18$^{\#\#}$
SMAR (mmHg/mL · min · 100 g)	31.52 ± 3.62	30.69 ± 4.19	46.87 ± 5.1†	53.14 ± 3.37$^{\#\#}$
IHVR (mmHg/mL · min · 100 g)	3.5 ± 0.23	5.31 ± 0.61**	4.33 ± 0.70	8.90 ± 1.31$^{**\#}$

Values are expressed as mean ± SEM. CD, control diet; HFGFD, high-fat glucose-fructose diet; IHVR, intrahepatic vascular resistance; MAP, mean arterial pressure; PP, portal pressure; SMABF, superior mesenteric artery blood flow; SMAR, superior mesenteric artery resistance. $^{**}P \leq 0.01$; $^{***}P \leq 0.001$ versus CD. $^{\#}P \leq 0.05$; $^{\#\#}P \leq 0.01$ versus HFGFD-8-week. $^{\dagger}P \leq 0.05$ versus CD-8-week.

The marked increase in PP and IHVR in the 36-week model could not be explained by endothelial dysfunction

In order to characterize the intrahepatic mechanisms underlying the increase in IHVR and PP in the absence of fibrosis, endothelial dysfunction was assessed. For this purpose, the expression levels of the phosphorylated proteins Akt and eNOS in total liver were analyzed by Western blot.

In previous works by our group and others (49,50,134), it was shown that at shorter timeframes (8 weeks or less), increased IHVR with different forms of Western-dietary interventions was mainly due to endothelial dysfunction, which was in turn mediated by increased Akt-dependent hepatic IR with those diets. However, in the present study,

for the 36-week HFGFD intervention, molecular features of endothelial dysfunction were similar to those of controls, unlike what was observed in the 8-week model, in which endothelial dysfunction was evidenced by the significant decrease in P-eNOS and P-Akt expression as compared to controls (Figure 13). As seen, the significant decrease in P-Akt and P-eNOS in the 8w-HFGFD versus 8w-CD was lost in the 36-week individuals, for which both P-Akt and P-eNOS were similar to controls, and P-eNOS was significantly higher than that of the 8w-HFGFD model (Figure 13A).

To confirm the absence of endothelial dysfunction in the long-term model, immunohistochemistry of endothelial CD34 in liver tissue was performed, as a molecular marker of LSEC de-differentiation/capillarization. As seen in Figure 13B, expression of CD34 at 36 weeks was significantly decreased, suggesting a reversal to a healthier LSEC phenotype in the long term.

In addition, other molecular pathways relevant in NASH that could lead to the observed changes in histology and portal hemodynamics at 36 weeks were explored. In this line, the link between increased NASH activity and changes in endothelial dysfunction and IHVR was investigated through the quantification of iNOS expression. As seen, there was a significant increase in the hepatic mRNA expression of iNOS in the 36w-HFGFD group compared to controls (Figure 14A). However, iNOS expression in the 8w-HFGFD group (in which the canonic molecular hallmarks of endothelial dysfunction were clearly present) was the same as that of the 8w-CD. In order to study non-LSEC related mechanisms in the NASH models that could go undetected by histology and might be affecting endothelial dysfunction or portal hemodynamics, the protein expression of Shh, a biomarker of hepatocyte lipotoxic injury, was also explored. As seen in Figure 14B, protein expression of Shh seemed to increase in the long term despite the fact that the histological evaluation of ballooning revealed no further deterioration from 8 to 36 weeks (Figure 11C), although these differences in Shh expression did not reach statistical significance.

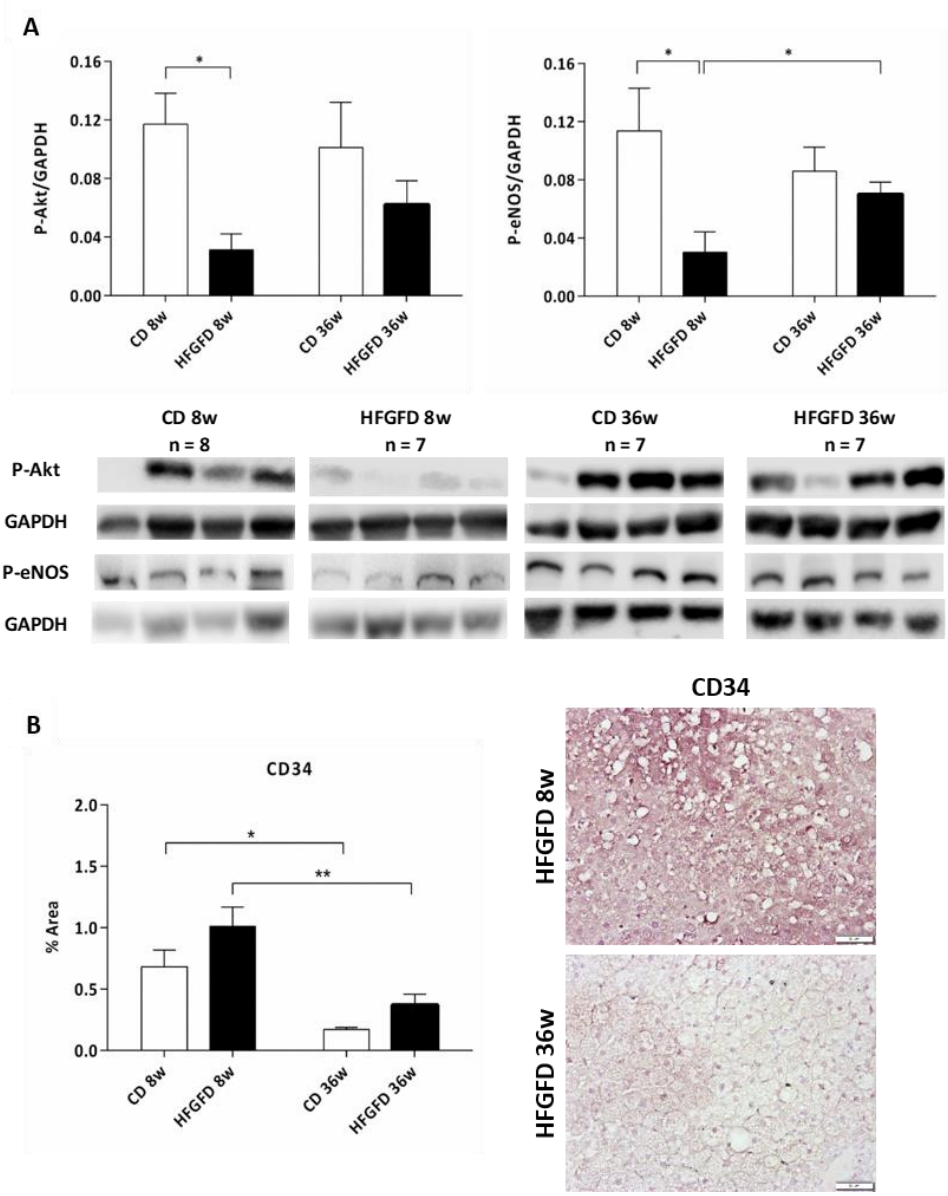

Figure 13. Markers of intrahepatic endothelial dysfunction. (A) The bar graphs show the quantification of the proteins P-Akt and P-eNOS using GAPDH as loading control and normalized to the control group of each time point. Representative Western blots are shown below. (B) The bar graph shows the quantification of CD34, and representative images of immunostained liver parenchyma from 8 and 36-week HFGFD rats (20× magnification). CD, control diet; GAPDH, glyceraldehyde-3-phosphate dehydrogenase; HFGFD, high-fat glucose-fructose diet; P-Akt, phosphorylated protein kinase B; P-eNOS, phosphorylated endothelial nitric oxide synthase. Data represent mean ± SEM. $^{*}P \leq 0.05$; $^{**}P \leq 0.01$.

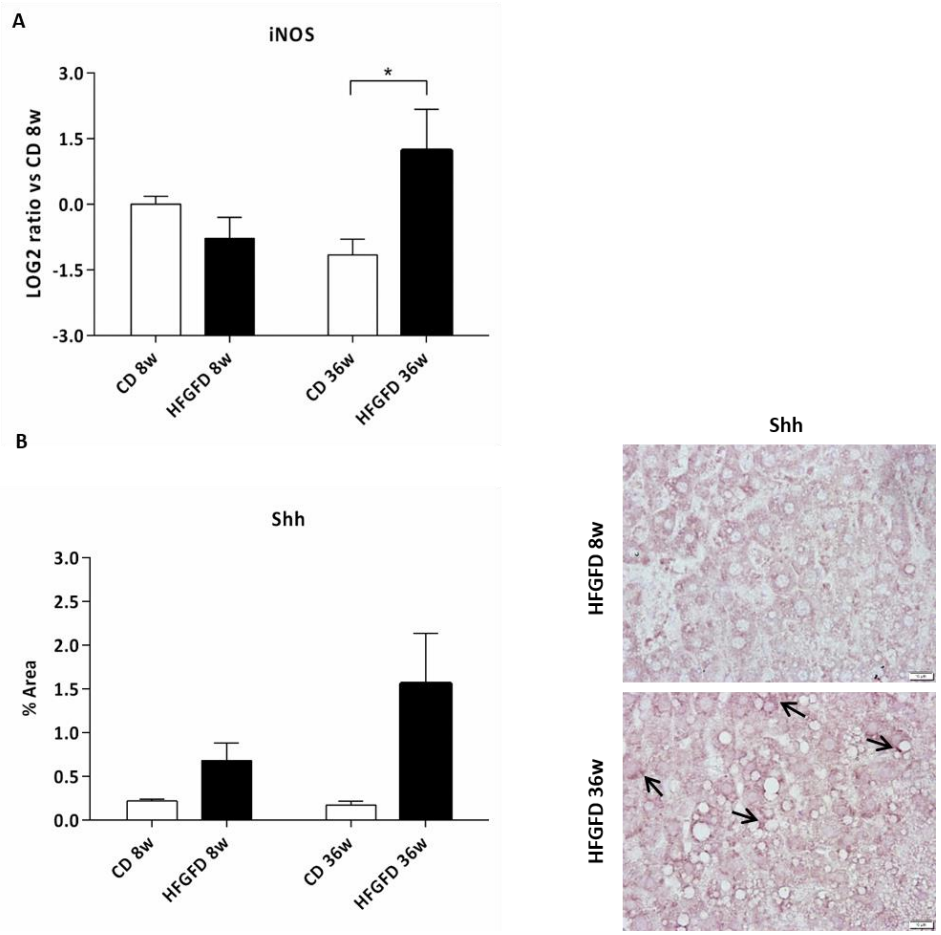

Figure 14. Markers of hepatic inflammation and ballooning. (A) Relative mRNA expression of iNOS by RT-qPCR, expressed as a log2 ratio and normalized with the control group of 8 weeks. (B) Bar graph shows the quantification of Shh, and representative images of immunostained liver parenchyma from 8 and 36-week HFGFD rats (40× magnification). Black arrows indicate more intense areas of Shh expression. CD, control diet; HFGFD, high-fat glucose-fructose diet; iNOS, inducible nitric oxide synthase; Shh, sonic hedgehog. Data represent mean ± SEM. $^{*}P \leq 0.05$.

The marked increase in PP and IHVR in the 36-week model was explained by a structural obstruction associated to increased steatosis

To further explain the increase in IHVR and PP in the absence of endothelial dysfunction in the 36-week model and given the striking histologic increase in steatosis at this time

point, the potential role of a structural component of IHVR as responsible of this increase was evaluated. It was then speculated that the marked increase in lipid content in the hepatocyte at 36 weeks had led to an increase in hepatocyte area at the expense of the sinusoidal area, leading to a structural increase in resistance to the intrahepatic portal blood flow. To that end, a systematic image analysis of hepatocyte fat and sinusoidal areas in histological liver sections at 8 and 36 weeks was conducted according to the theoretical basis and the experimental protocols described in Hall *et al*. (120) (see in Materials and Methods).

Regarding the 8-week model, there was a significant increase in fat area in the HFGFD group compared to controls, but this increase was not marked enough to associate significant differences in terms of intrahepatic sinusoidal area (Figure 15). However, as seen in Figure 15B, the 36w-HFGFD intervention led to a dramatic increase in the total fat area (600% as compared to 36-week controls and 170% as compared to 8-week HFGFD, P = 9.8x10E-7 and 9x10E-4, respectively), and a marked significant increase in both the average area of individual hepatocytes (Figure 15C) and the hepatocyte area/liver weight ratio (Figure 15E). This was associated to a significant decrease in hepatocyte number per field examined (Figure 15D), and, most importantly, a significant decrease in the liver sinusoidal area as compared both to controls and to the 8-week model (Figure 15A).

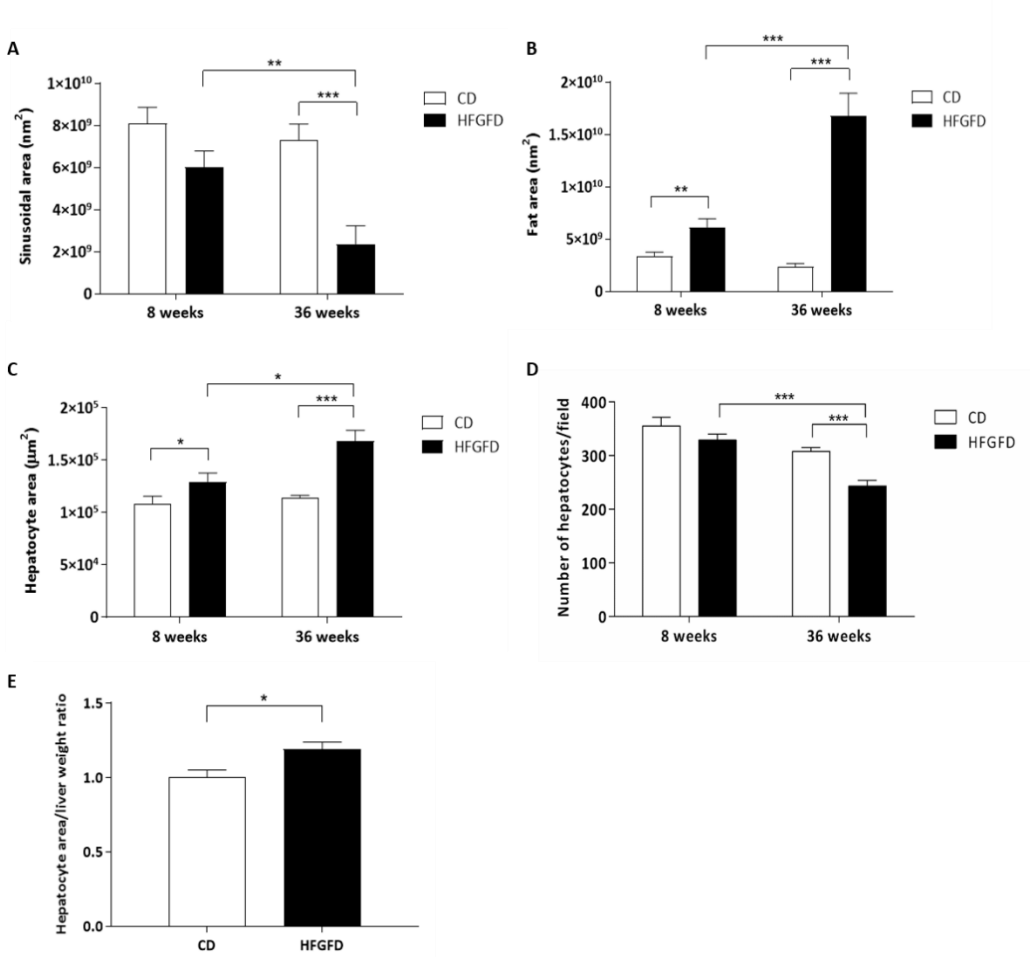

Figure 15. Image analysis of intrahepatic structural changes. Bar graphs show the quantification of the sinusoidal area (A), fat area (B), hepatocyte area (C) and number of hepatocytes per field (D) of CD and HFGFD rats after 8 and 36 weeks of dietary intervention (CD-8w n = 10, HFGFD-8w n = 10, CD-36w n = 14, HFGFD-36w n = 15). The bar graph in E shows the hepatocyte area/liver weight ratio after 36 weeks normalized with the control group. CD, control diet; HFGFD, high-fat glucose-fructose diet. Data represent mean ± SEM. $^{*}P \leq 0.05$; $^{**}P \leq 0.01$; $^{***}P \leq 0.001$.

The compressive effect of steatosis on the hepatic sinusoidal bed at 36 weeks was confirmed by SEM. As seen in Figure 16, control livers from CD-fed rats showed a regular structural pattern with normal-appearing sinusoids, whereas livers from 36w-HFGFD-

fed rats revealed marked intrahepatic structural changes; the sinusoids looked compressed, and the structural pattern was noticeably more disorganized.

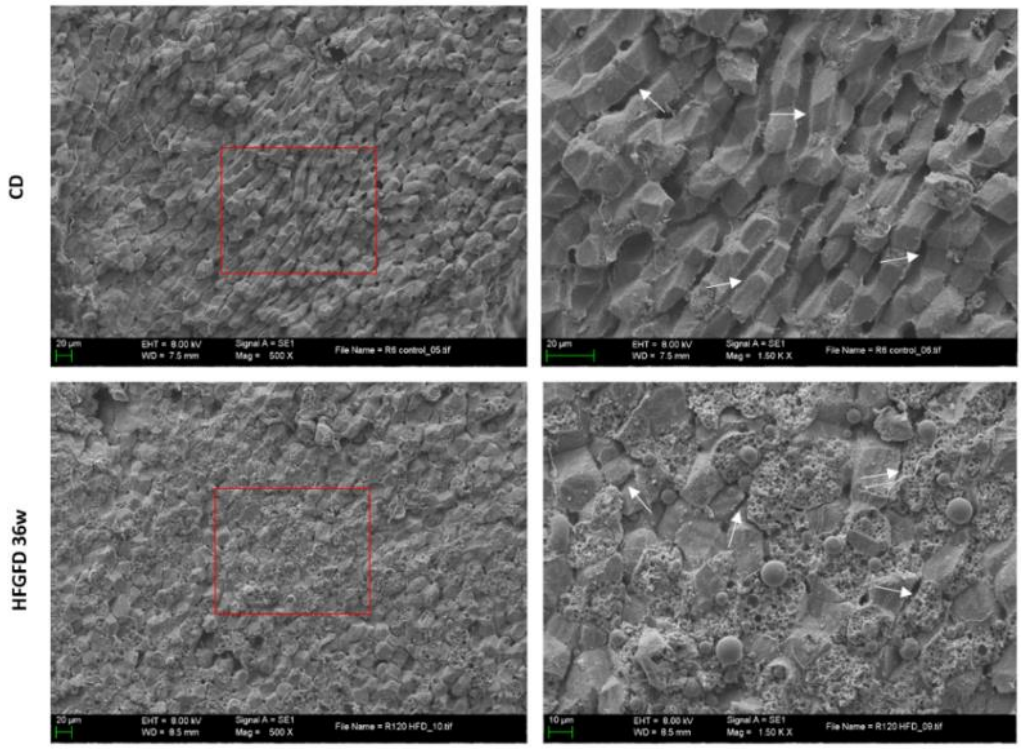

Figure 16. Representative scanning electron microscopic images of the hepatic sinusoidal bed from a normal liver and from a liver after 36 weeks of HFGFD intervention. Images are shown at 500× and 1,500× magnification. White arrows indicate hepatic sinusoids. CD, control diet; HFGFD, high-fat glucose-fructose diet.

To quantify the impact of these structural changes on PP, the correlation between intrahepatic sinusoidal area and PP after 8 and 36 weeks of dietary intervention was examined. Figure 17 Panel A plots the individual sinusoidal areas and PP values of all studied animals at 36 weeks. As seen, all HFGFD individuals had PH (defined statistically as the PP mean of CD group plus 2 times standard deviation, as there is no established PH threshold in animal models) and all individual sinusoidal areas in the HFGFD group were below the minimum values observed in the control group. This suggested that

there could be a critical value of the sinusoidal area (3x10E9 nm^2 as drawn in Figure 17) below which the sinusoidal flux is critically compromised leading to increased IHVR and PP. Figure 17 Panel B shows the plotted individual values of sinusoidal area and PP at 8 weeks. Applying the critical value of sinusoidal area 3x10E9 nm^2, the four HFGFD individuals that presented PH (also statistically defined), only one had a restriction in its sinusoidal area. The sinusoidal area of the rest of the individuals was above the critical value.

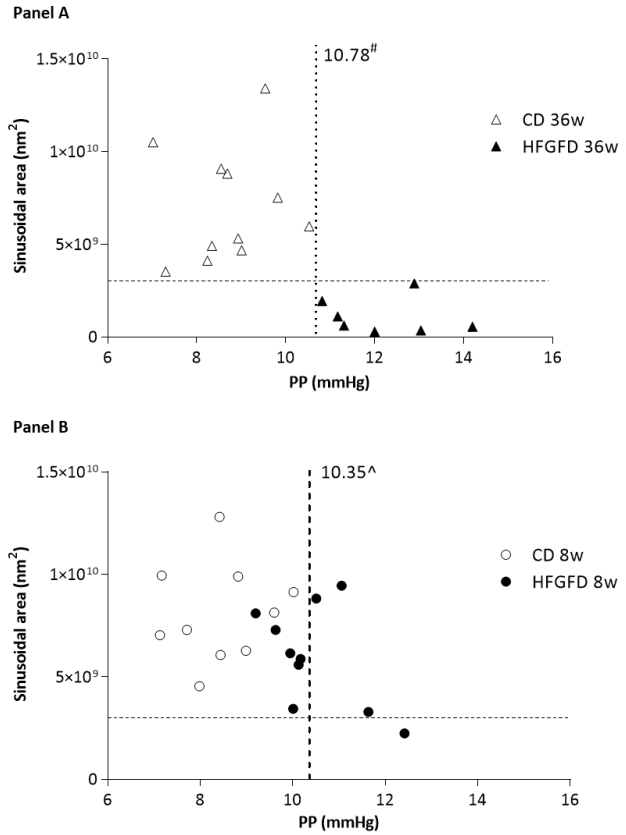

Figure 17. Correlations between intrahepatic sinusoidal area and portal pressure (PP, mmHg) in CD and HFGFD rats after 36 weeks (Panel A) and 8 weeks (Panel B) of dietary intervention. CD, control diet; HFGFD, high-fat glucose-fructose diet. #36-week portal hypertension was defined statistically as the PP mean of CD group plus 2 times standard deviation (>10.78 mmHg). ^8-week portal hypertension was defined statistically as the PP mean of CD group plus 2 times standard deviation (>10.35 mmHg).

The main results obtained in study 1 can be summarized as follows:

1) The long-term (36 weeks) HFGFD intervention was not able to induce fibrosis in the rat model.
2) However, the 36-week dietary intervention led to a marked increase in IHVR and PP compared to the short-term (8 weeks) rat model.
3) This increase in IHVR and PP, contrary to what we expected based on previously published evidence, was mainly associated to a marked reduction of the intrahepatic sinusoidal area (compressed by the enlarged fatty hepatocytes), and not to endothelial dysfunction (which did not have a significant contribution in the long-term model).

5.2. STUDY 2: Evaluation of the effects of microbiota-based treatments in a short-term HFGFD-induced rat model

Once the short-term (8 weeks) HFGFD-induced rat model was developed, and after the 2-week treatment period, body weight, blood biochemistry, NASH histology, and systemic and portal hemodynamics were evaluated to elucidate the effects of the bacterial consortium treatment and FMT on the regulation of PH and endothelial dysfunction in NASH rats. Next, the effects of the bacterial consortium treatment were tested in the STAM^{TM} mouse model at histopathological level.

Microbiota-based treatments significantly improved the metabolic profile

The 8-week HFGFD intervention induced a marked increase in body weight (Table 11). During the 2-week treatment period, animals in the HFGFD-VEH group continued increasing their body weight to a great extent (22.08 ± 3.18 g). However, HFGFD-CON only gained on average 2.91 ± 3.55 g ($P \leq 0.001$), whereas HFGFD-FMT lost on average 5 ± 3.47 g ($P \leq 0.001$). Compared to the HFGFD-VEH, both groups receiving microbiota-based treatments gained significantly less weight during the 2-week treatment. This result was associated with treatment since there were no significant differences in dietary consumption between the vehicle group (112.18 ± 3.66 g/week) and the bacterial consortium (102.18 ± 9.58 g/week) and FMT (103.14 ± 7.39 g/week) groups.

Both microbiota-based treatments displayed an important reduction in fasting blood glucose and insulin levels, and HOMA-IR index with respect to the HFGFD-VEH group, although these differences did not reach statistical significance (Table 11). Both treatments showed a significant but slight increase in TG when compared to the vehicle group. Cholesterol fractions remained unchanged. ALT levels were significantly reduced, and albumin was significantly improved in the HFGFD-FMT group (Table 11).

Table 11. Body weight and biochemical parameters after 2 weeks of intervention in the rat NASH model.

	HFGFD-VEH (n = 13)	**HFGFD-CON (n = 11)**	**HFGFD-FMT (n = 11)**
BW pre-HFGFD (g)	254.46 ± 2.59	256 ± 2.1	256 ± 3.32
BW pre-trt. (g)	531.7 ± 10.3	543.6 ± 10.29	515.1 ± 13.48
BW gain with trt. (g)	22.08 ± 3.18	2.91 ± 3.55***	-5 ± 3.47***
BW post-trt. (g)	552.33 ± 11.77	546.6 ± 11.53	507 ± 12.39*
Glucose (mg/dL)	182.45 ± 14.94	166.9 ± 14.89	171.36 ± 10.47
Insulin (ng/mL)	15.36 ± 3.6	9.24 ± 1.17	11.21 ± 1.13
HOMA-IR	7.89 ± 2.3	3.7 ± 0.54	4.68 ± 0.45
Albumin (g/dL)	2.9 ± 0.04	3.03 ± 0.05	3.13 ± 0.06**
Bilirubin (mg/dL)	0.09 ± 0.01	0.09 ± 0.02	0.11 ± 0.01
AST (IU/L)	205.56 ± 34.05	234.29 ± 45.72	172 ± 63.52
ALT (IU/L)	66.15 ± 4.36	67.1 ± 9.29	47.5 ± 31.31*
TG (mg/dL)	27.92 ± 1.35	33 ± 1.91**	33.54 ± 2.96*
Cholesterol (mg/dL)	75.54 ± 4.75	86.78 ± 3.89	78.91 ± 2.99
Cholesterol HDL (mg/dL)	41.93 ± 2.43	46.78 ± 1.97	45.54 ± 2.48
Cholesterol LDL (mg/dL)	25.27 ± 2.52	34.75 ± 3.4	27 ± 1.96

Values are expressed as mean ± SEM. HFGFD-VEH: group of NASH rats receiving sham gavage (vehicle); HFGFD-CON: group of NASH rats receiving the 9-strain bacterial consortium daily; HFGFD-FMT: group of NASH rats receiving fecal microbiota transplantation from control lean rats (1x transplantation followed by sham gavage). ALT, alanine aminotransferase; AST, aspartate aminotransferase; BW; body weight; HDL, high-density lipoprotein; HFGFD, high-fat glucose-fructose diet; HOMA-IR, homeostasis model of insulin resistance index; LDL, low-density lipoprotein; TG, triglycerides. *P ≤ 0.05; **P ≤ 0.01; ***P ≤ 0.001 versus HFGFD-VEH.

No treatment group significantly reversed the NASH histological pattern

The 10-week HFGFD intervention resulted in a consistent reproduction of NASH histological hallmarks, as seen in Figure 18. However, none of the 2-week microbiota-based treatments were associated with significant improvements in overall NASH histological diagnosis or its individual features. This is in line with previously obtained results following FMT in this particular NASH model (50). Interestingly, no animals receiving HFGFD-CON presented inflammation or ballooning scores above 1 (Figure 18B, C). Finally, as shown in the Sirius red-stained liver sections in Figure 19A, none of the groups developed histological fibrosis. This is also in agreement with previous results (50). However, expression of the pro-fibrotic hepatic marker COL1A1 was significantly reduced in the microbiota-based treatment groups when compared with the vehicle group; in contrast, α-SMA was only reduced by the bacterial consortium treatment (Figure 19B).

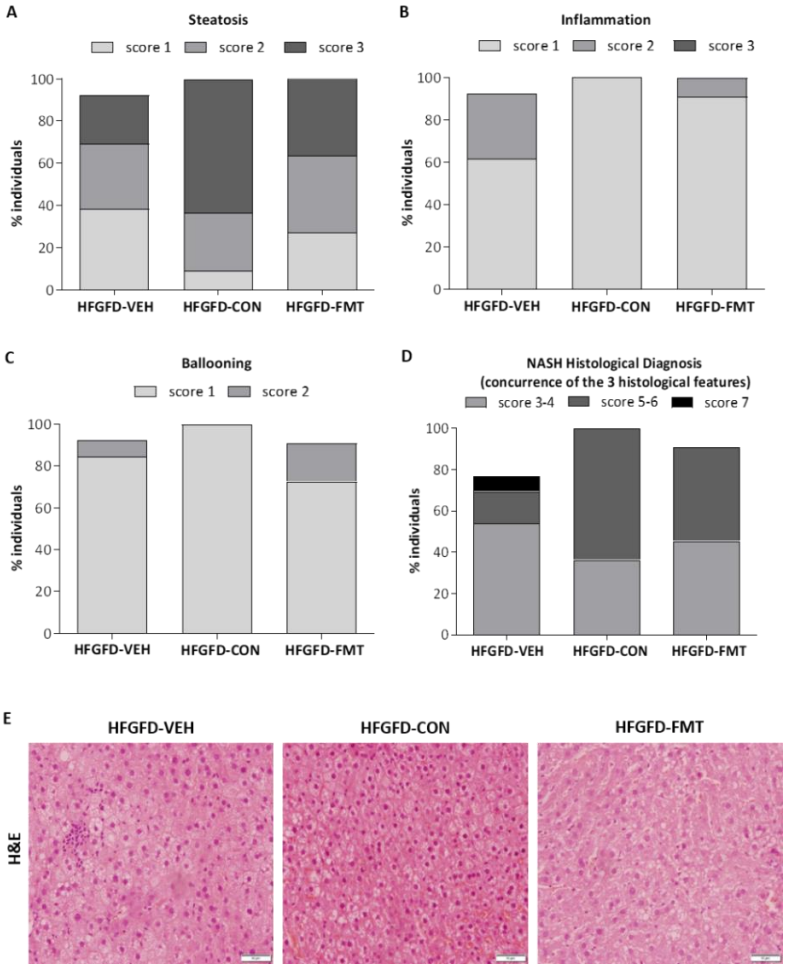

Figure 18. Histological evaluation of the H&E-stained liver sections collected from the NASH rats (HFGFD-VEH n= 13, HFGFD-CON n = 11, HFGFD-FMT n = 11). Evaluation followed the NASH-Clinical Research Network system. The three first bar diagrams represent the percentage of individuals presenting (A) steatosis, (B) inflammation, and (C) ballooning in the different groups. Each bar includes the percentage of individuals scored with 1 (light gray), 2 (gray), or 3 (dark gray); the last bar diagram (D) represents the percentage of individuals with NASH Histological Diagnosis (defined as NAFLD activity score (NAS) ≥ 3 and concurrence of steatosis, lobular inflammation and hepatocellular ballooning) scored with 3-4 (light gray), 5-6 (dark gray), or 7 (black). (E) Representative images show H&E-stained liver parenchyma in sections collected from the NASH rats (20× magnification). HFGFD-VEH: group of NASH rats receiving sham gavage (vehicle); HFGFD-CON: group of NASH rats receiving the 9-strain bacterial consortium daily; HFGFD-FMT: group of NASH rats receiving fecal microbiota transplantation from control lean rats (1x transplantation followed by sham gavage).

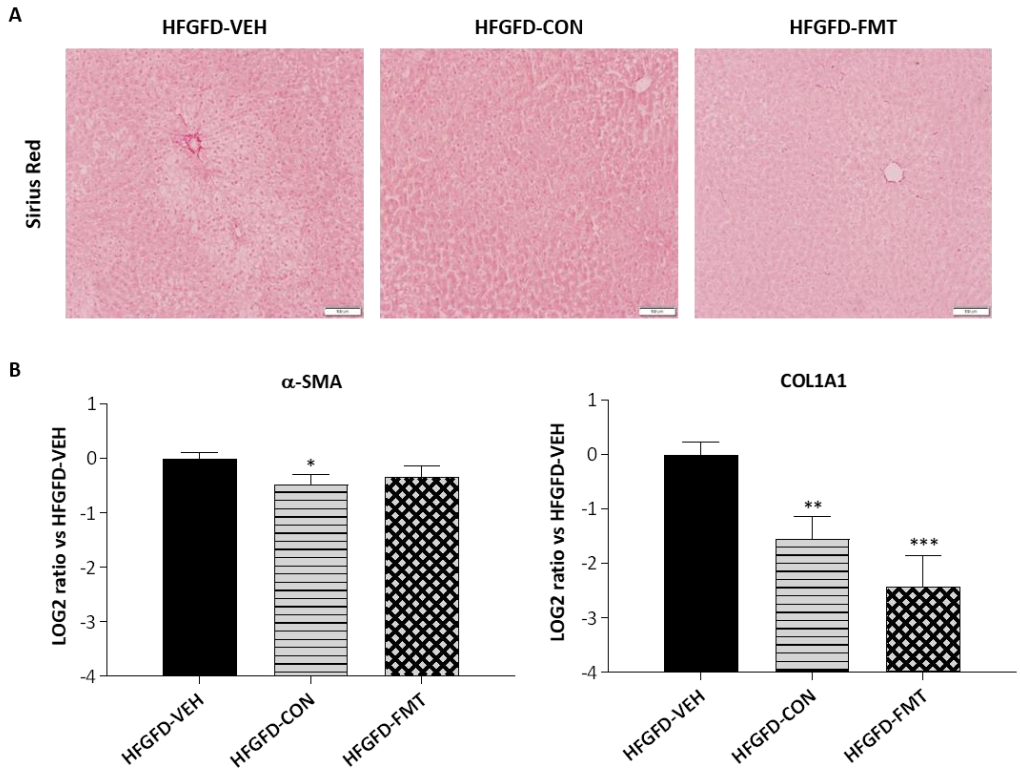

Figure 19. Markers of liver fibrosis. (A) Representative images show Sirius red-stained liver parenchyma in sections collected from the NASH rats (10× magnification). (B) Relative mRNA expression of α-SMA and COL1A1 by RT-qPCR in the liver of NASH rats and expressed as log2 ratio. β-Actin was used as endogenous control, and results were normalized to the HFGFD-VEH group. HFGFD-VEH: group of NASH rats receiving sham gavage (vehicle); HFGFD-CON: group of NASH rats receiving the 9-strain bacterial consortium daily; HFGFD-FMT: group of NASH rats receiving fecal microbiota transplantation from control lean rats (1x transplantation followed by sham gavage). α-SMA, alpha-smooth muscle actin; COL1A1, collagen type I alpha 1 chain. Data represent mean ± SEM. $^{*}P \leq 0.05$; $^{**}P \leq 0.01$; $^{***}P \leq 0.001$ versus HFGFD-VEH.

Microbiota-based treatments significantly improved liver hemodynamics

Consistent with previous findings (50,135), and despite the absence of histological fibrosis, animals in the 10-week HFGFD intervention showed values of PP of 10.32 mmHg on average (Table 12). Importantly, both the bacterial consortium treatment and FMT significantly reduced PP when compared to the vehicle-treated group, even while

maintaining the HFGFD during the 2-week treatment period (Table 12). This decrease in PP observed in the HFGFD-CON group was secondary to a significant decrease (80% reduction) in IHVR as compared to HFGFD-VEH, in a similar degree as measured in the HFGFD-FMT group (104% reduction) (Table 12). Regarding systemic hemodynamics, no relevant differences were observed between groups (Table 12).

Table 12. Hemodynamic measurements after 2 weeks of intervention in the rat NASH model.

	HFGFD-VEH (n = 13)	**HFGFD-CON (n = 11)**	**HFGFD-FMT (n = 11)**
MAP (mmHg)	113.05 ± 4.53	119.95 ± 4.21	117.34 ± 5.14
PP (mmHg)	10.32 ± 0.22	9.58 ± 0.19*	9.21 ± 0.12***
SMABF (mL/[min · 100 g])	2.73 ± 0.24	2.71 ± 0.21	2.82 ± 0.17
SMAR (mmHg/mL · min · 100 g)	40.78 ± 3.25	40.79 ± 4.36	39.35 ± 2.36
IHVR (mmHg/mL · min · 100 g)	7.58 ± 1.27	4.20 ± 0.35*	3.71 ± 0.21*

Values are expressed as mean ± SEM. HFGFD-VEH: group of NASH rats receiving sham gavage (vehicle); HFGFD-CON: group of NASH rats receiving the 9-strain bacterial consortium daily; HFGFD-FMT: group of NASH rats receiving fecal microbiota transplantation from control lean rats (1x transplantation followed by sham gavage). HFGFD, high-fat glucose-fructose diet; IHVR, intrahepatic vascular resistance; MAP, mean arterial pressure; PP, portal pressure; SMABF, superior mesenteric artery blood flow; SMAR, superior mesenteric artery resistance. $^{*}P \leq 0.05$; $^{***}P \leq 0.001$ versus HFGFD-VEH.

Features of endothelial dysfunction were improved in animals after receiving microbiota-based treatments

Endothelial dysfunction molecular hallmarks were assessed to further characterize the changes observed in IHVR and PP induced by the microbiota-based treatments with respect to the vehicle-treated group. As seen in Figure 20, microbiota-based treatments induced a significant increase in P-Akt. P-eNOS showed a tendency to increase in both HFGFD-CON and HFGFD-FMT when compared to HFGFD-VEH, although it did not reach

statistical significance. Interestingly, only the consortium-treated group showed a marked significant increase in KLF2 (Figure 20).

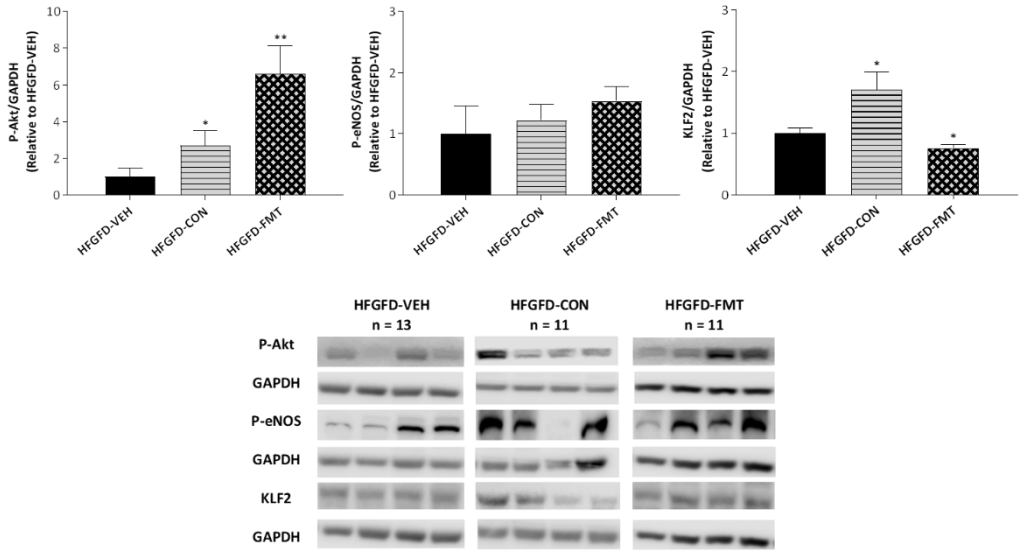

Figure 20. Markers of intrahepatic endothelial dysfunction. The bar graphs show the quantification of the proteins P-Akt, P-eNOS and KLF2 using GAPDH as loading control and normalized to the HGFGD-VEH group. Representative Western blots are shown below. HFGFD-VEH: group of NASH rats receiving sham gavage (vehicle); HFGFD-CON: group of NASH rats receiving the 9-strain bacterial consortium daily; HFGFD-FMT: group of NASH rats receiving fecal microbiota transplantation from control lean rats (1x transplantation followed by sham gavage). GAPDH, glyceraldehyde-3-phosphate dehydrogenase; HFGFD, high-fat glucose-fructose diet; KLF2, Kruppel Like Factor 2; P-Akt, phosphorylated protein kinase B; P-eNOS, phosphorylated endothelial nitric oxide synthase. Data represent mean ± SEM. $^{*}P \leq 0.05$; $^{**}P \leq 0.01$ versus HFGFD-VEH.

Microbiota-based treatments improved cecal species diversity and induced composition shifts

To verify the effect of both microbiota-based treatments on (bacterial) species diversity and taxonomic composition, the cecum content of rats was collected at sacrifice, and microbial DNA was extracted and sequenced. The Inverse Simpson diversity index revealed that, although not reaching the microbial diversity levels of a CD group,

diversity improved over vehicle (HFGFD-VEH) in both treatment groups; this was nearly statistically significant in the bacterial consortium (HFGFD-CON) treatment group (Figure 21).

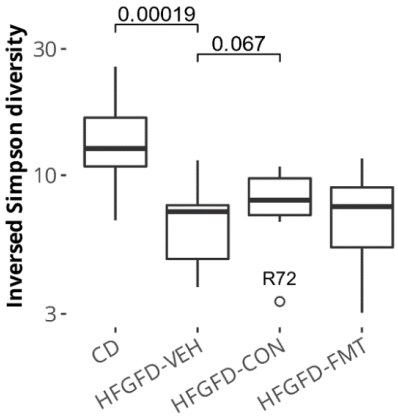

Figure 21. Microbial diversity in the cecum of NASH rats. Statistically significant differences are depicted above boxplots; these represent Wilcoxon signed-rank test P-values computed without the outlier R72. HFGFD-VEH: group of NASH rats receiving sham gavage (vehicle); HFGFD-CON: group of NASH rats receiving the 9-strain bacterial consortium daily; HFGFD-FMT: group of NASH rats receiving fecal microbiota transplantation from control lean rats (1x transplantation followed by sham gavage). CD, control diet; HFGFD, high-fat glucose-fructose diet.

Classifier performance as analyzed through balanced error rate (BER) suggested that HFGFD-CON induced a more defined change than HFGFD-FMT (Figure 22). In addition, the corresponding feature selection (VIP > 1, n = 123) showed that the bacterial consortium treatment induced suppression of 72 (58.5% of observable change) vehicle-associated taxa and promoted the emergence of 48 (41.5%) non-product treatment associated taxa, whereas FMT, according to feature selection (n = 0) induced suppression of 135 (75.8%) taxa, and replacement with 43 (24.2%) taxa. Hence, both treatments operated an important replacement of the HFGFD-VEH associated microbial community, but the bacterial consortium achieved a more defined and richer replacement than FMT. Figure 22B provides the top 10 discriminant taxa according to classifier estimated variable importance (VIP) and their associations, whereas Figure

22C combines the three VEH/CON, VEH/FMT and CON/FMT contrasts into a single Euler plot proportional to the numbers of features selected for each contrast.

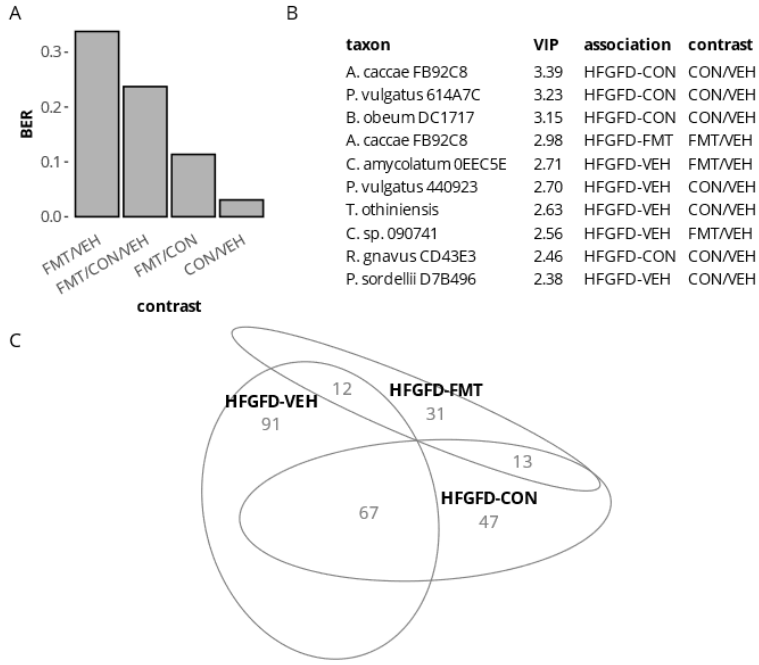

Figure 22. Microbial taxonomic composition in the cecum of NASH rats (sPLS-DA classifier). (A) Per-contrast balanced error rate (BER). (B) Top 10 HFGFD-VEH discriminant taxa according to classifier estimated variable importance (VIP). (C) Euler diagram of contrast specific taxa. HFGFD-VEH: group of NASH rats receiving sham gavage (vehicle); HFGFD-CON: group of NASH rats receiving the 9-strain bacterial consortium daily; HFGFD-FMT: group of NASH rats receiving fecal microbiota transplantation from control lean rats (1x transplantation followed by sham gavage). HFGFD, high-fat glucose-fructose diet.

The 9-strain bacterial consortium induced functional microbiome shifts

Changes in microbial composition, as evaluated by WMS sequencing, were used to conduct predictive pathway analysis to unravel putative biosynthetic pathways that could be modulated by treatment. The bacterial consortium treatment was predicted to drive an increase in microbial branched-chain amino acids (BCAA) such as valine and isoleucine (Figure 23A and B) and a decrease in aromatic amino acids (AAA) biosynthesis

capacities (Figure 23C). In addition, methionine biosynthesis was also predicted to decrease (Figure 23D). These changes over HFGFD-VEH were significant in the HFGFD-CON but not in the HFGFD-FMT group (Figure 23).

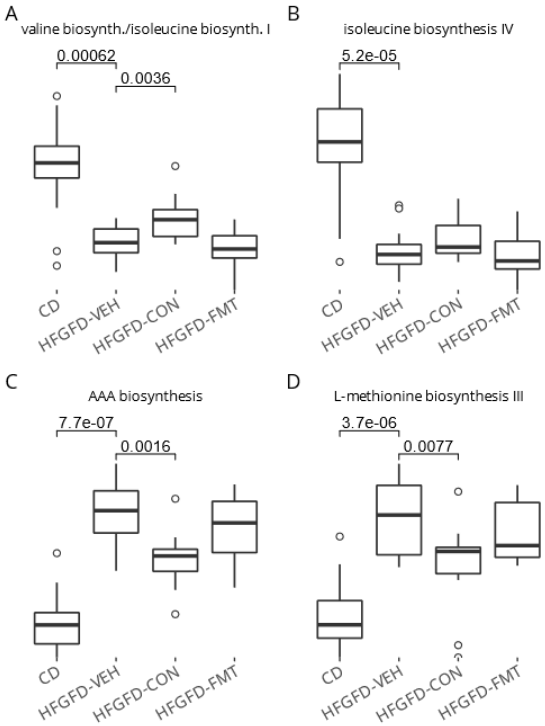

Figure 23. Predicted BCAA (A and B), AAA (C), and Methionine (D) biosynthesis pathways in the cecum of NASH rats. Statistically significant differences are depicted above boxplots. HFGFD-VEH: group of NASH rats receiving sham gavage (vehicle); HFGFD-CON: group of NASH rats receiving the 9-strain bacterial consortium daily; HFGFD-FMT: group of NASH rats receiving fecal microbiota transplantation from control lean rats (1x transplantation followed by sham gavage). AAA, aromatic amino acids; BCAA, branched-chain amino acids; CD, control diet; HFGFD, high-fat glucose-fructose diet.

Microbiota-based treatments induced differential hepatic gene expression

The expression of 20,359 liver genes was documented through RNA-Seq analysis of the three HFGFD groups. Of these, 444 (2.2%) were considered discriminant by sPLS-DA analysis for one or more of the CON/VEH, FMT/VEH or CON/FMT contrasts, with most

genes being induced by treatment. Figure 24C depicts the breakdown on up- versus down-regulated discriminant genes.

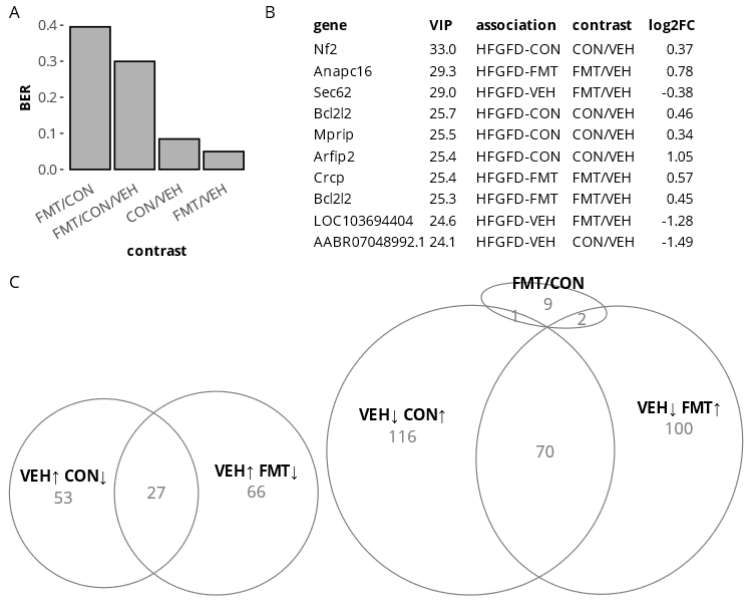

Figure 24. Liver gene expression in NASH rats (sPLS-DA classifier). (A) Per-contrast balanced error rate (BER). (B) Top 10 discriminant genes. (C) Euler diagram of the 444 contrast specific genes. HFGFD-VEH: group of NASH rats receiving sham gavage (vehicle); HFGFD-CON: group of NASH rats receiving the 9-strain bacterial consortium daily; HFGFD-FMT: group of NASH rats receiving fecal microbiota transplantation from control lean rats (1x transplantation followed by sham gavage).

Table 13 provides details on gene expression modulation by the microbiota consortium of the top 1,000 fatty liver associated genes according to the Harmonizome database, and eventual FMT equivalent. Molecular chaperones were found to be predominantly modulated by both microbiota-based treatments. Among all modulated chaperones, the heat shock protein (Hsp) family members *Hspa1a*, *Hspa1b*, and *Hspa8* stand out, as these were strongly downregulated by both treatments. Microbiota treatments also induced the downregulation of the ER chaperone BiP (*Hspa5*), as well as of its co-chaperone *Dnajb9*. Additional key genes downregulated by treatment were the cell division cycle *(Cdc)42* and the Rac family small GTPase *(Rac)1* (Table 13). The RNA-seq

analysis also revealed that both microbial treatments enhanced the expression of several putative tumor suppressor genes (Table 14).

Among the upregulated genes, the thyroid hormone responsive *Spot14* (*Thrsp*) gene was found to be one of the main modulated genes, as both treatments considerably increased its expression. In addition, the AKT Serine/Threonine Kinase 1 (*Akt1*) was found to be only upregulated by the microbiota consortium treatment (Table 13).

Table 13. Modulation of the top 1,000 fatty liver disease genes in the liver of NASH rats.

Rat Gene	Human Ortholog	CON/VEH	CON/VEH	FMT/VEH	FMT/VEH	Protein
		Log2FC	pFDR	Log2FC	pFDR	
Hspa1b	HSPA1B, HSPA1A	−3.48	0.002	−4.36	0.000	Heat shock 70 kDa protein 1B, and 1A
AABR07048992.1	HSPA8	−1.49	0.000	−1.50	0.000	Heat shock cognate 71 kDa protein
Hsph1	HSPH1	−0.74	0.060	−0.93	0.005	Heat shock protein 105 kDa
Pir	PIR	−0.74	0.084	-	-	Pirin
Sdf2l1	SDF2L1	−0.71	0.066	-	-	Stromal cell-derived factor 2-like protein 1
Dnajb9	DNAJB9	−0.71	0.016	−0.69	0.012	DNAJ homolog subfamily B member 9
LOC680121	HSPA8	−0.64	0.003	−0.48	0.024	Heat shock cognate 71 kDa protein
AABR07012795.1	PRDX1	−0.62	0.067	-	-	Peroxiredoxin−1
Hspa5	HSPA5	−0.61	0.058	−0.62	0.031	Endoplasmic reticulum chaperone BiP
Sult2a1	SULT2A1	−0.55	0.073	-	-	Sulfotransferase 2A1
Dusp6	DUSP6	−0.51	0.084	-	-	Dual specificity protein phosphatase 6
Calr	CALR	−0.40	0.030	−0.38	0.022	Calreticulin
Pnrc1	PNRC1	−0.40	0.081	-	-	Proline-rich nuclear receptor coactivator 1

Cdc42	CDC42	−0.36	0.000	−0.21	0.013	Cell division control protein 42 homolog
NEWGENE_620180	SLC40A1	−0.35	0.021	−0.43	0.002	Solute carrier family 40 member 1
Prdx1	PRDX1	−0.35	0.001	-	-	Peroxiredoxin-1
Litaf	LITAF	−0.34	0.000	-	-	Lipopolysaccharide-induced tumor necrosis factor-alpha factor
Atp2a2	ATP2A2	−0.32	0.065	−0.40	0.007	Sarcoplasmic/endoplasmic reticulum calcium ATPase 2
Slc10a1	SLC10A1	−0.30	0.081	−0.28	0.074	Sodium/bile acid cotransporter
Pdia3	PDIA3	−0.29	0.084	−0.29	0.051	Protein disulfide isomerase A3
Idh1	IDH1	−0.28	0.050	−0.32	0.008	Isocitrate dehydrogenase
Slc39a8	SLC39A8	−0.27	0.017	−0.19	0.093	Metal cation symporter ZIP8
Apoe	APOE	−0.26	0.067	−0.23	0.067	Apolipoprotein E
Maoa	MAOA	−0.25	0.049	−0.24	0.042	Amine oxidase
Ctsb	CTSB	−0.25	0.048	−0.34	0.001	Cathepsin B
Psmb4	PSMB4	−0.24	0.040	-	-	Proteasome subunit beta type-4
Ccnd3	CCND3	−0.24	0.051	-	-	G1/S-specific cyclin-D3
Dpp4	DPP4	−0.23	0.050	−0.35	0.000	Dipeptidyl peptidase 4
Aldoa	ALDOA	−0.23	0.067	-	-	Fructose bisphosphate aldolase A
Ctsd	CTSD	−0.22	0.069	−0.29	0.005	Cathepsin D
Rac1	RAC1	−0.21	0.000	−0.24	0.000	Ras-related C3 botulinum toxin substrate 1
Enpp1	ENPP1	−0.20	0.057	−0.26	0.004	Ectonucleotide pyrophosphatase/phosphodiesterase 1
Calm1	CALM1	−0.19	0.064	-	-	Calmodulin−1
Sdc2	SDC2	−0.19	0.064	−0.33	0.000	Syndecan-2

Akt1	AKT1	0.20	0.056	-	-	RAC-alpha serine/threonine-protein kinase
Abcg3l3	ABCG2	0.36	0.078	-	-	Broad substrate specificity ATP-binding cassette transporter ABCG2
Atm	ATM	0.39	0.006	-	-	Serine-protein kinase ATM
Abcg3l1	ABCG2	0.42	0.019	-	-	Broad substrate specificity ATP-binding cassette transporter ABCG2
Inhba	INHBA	0.48	0.099	-	-	Inhibin beta A chain
Abcc5	ABCC5	0.49	0.097	-	-	ATP-binding cassette sub-family C member 5
VEGFA	VEGFA	0.57	0.003	0.50	0.007	Vascular endothelial growth factor A
Egf	EGF	0.64	0.030	0.56	0.042	Pro-epidermal growth factor
LOC108348190	EGF	0.72	0.046	-	-	Pro-epidermal growth factor
Thrsp	THRSP	1.07	0.049	0.93	0.067	Thyroid hormone-inducible hepatic protein

VEH: group of NASH rats receiving sham gavage (vehicle); CON: group of NASH rats receiving the 9-strain bacterial consortium daily; FMT: group of NASH rats receiving fecal microbiota transplantation from control lean rats (1x transplantation followed by sham gavage).

Table 14. Modulation of putative tumor suppressors.

Gene	CON/VEH log2FC	CON/VEH pFDR	FMT/VEH log2FC	FMT/VEH pFDR	Protein
ATM	0.39	0.006			Serine-protein kinase ATM
NRBP2	0.66	0.008	0.76	0.001	Nuclear receptor-binding protein 2
SETD2	0.32	0.063			Histone-lysine N-methyltransferase SETD2
SLC26A6	0.66	0.002	0.58	0.005	Solute carrier family 26 member 6
WWC1	0.41	0.016	0.58	0.000	Protein KIBRA

VEH: group of NASH rats receiving sham gavage (vehicle); CON: group of NASH rats receiving the 9-strain bacterial consortium daily; FMT: group of NASH rats receiving fecal microbiota transplantation from control lean rats (1x transplantation followed by sham gavage).

Finally, over-representation analysis of differentially expressed genes induced by the microbiota consortium treatment was performed. Up- and down-regulated genes were considered separately and both a restrictive (VIP > 1, pFDR < 0.1) and a relaxed (pFDR < 0.1) conditions were used as input, generating respectively, 281 up- and 191 down-regulated genes, and 489 up- and 326 down-regulated genes. Consistent with the observed amelioration of the hepatic pro-fibrotic marker COL1A1 (Figure 19B), liver transcriptomics identified numerous pro-fibrotic pathways being positively modulated by the two microbiome-based treatments. In this regard, the pro-fibrotic signaling pathways VEGFA-VEGFR2 (WP3888), Wnt signaling (WP428), and the Cytoskeletal regulation by Rho GTPases (P00016) stand out, all found to be putatively downregulated by the microbiota consortium treatment (Table 15).

Table 15. Putatively down-regulated pro-fibrotic signaling pathways in the liver of NASH rats treated with the 9-strain bacterial consortium.

Pathway ID	N	q-value	Human orthologs	Description
WP3888↓	21	0.090	RPS11, TPP1, ALDOA, PPP1CA, CTNND1, SDCBP, DNAJA1, CDC42, SSR4, DNAJB9, RAP1B, RHOA, PFN1, YWHAE, PSMD11, PAK2, SDF2L1, CALR, ATP6V0D1, HSPA1A, RAC1	VEGFA-VEGFR2 Signaling pathway
WP4656↑	8	0.067	CSPP1, CEP104, DVL1, OFD1, ATM, BBS4, PCM1, CEP120	Joubert Syndrome
WP428↓	7	0.091	RHOA, RAC1, WNT11, CCND3, PPP3R1, GPC4, NLK	Wnt Signaling
P00016↓	6	0.031	ARPC4, CDC42, ARPC5, PFN1, PAK2, RAC1	Cytoskeletal regulation by Rho GTPase
pid_21478↓	5	0.007	ARPC4, CDC42, PIR, ACTR3, RAC1	y branching of actin filaments
pid_5967↓	5	0.007	ARPC4, CDC42, RHOA, ACTR3, RAC1	Role of pi3k subunit p85 in regulation of actin organization and cell migration
R-HSA-390450↓	3	0.030	TCP1, CCT4, CCT8	Folding of actin by CCT/TriC
R-HSA-5625970↓	3	0.030	CDC42, RHOA, RAC1	RHO GTPases activate KTN1
R-HSA-389960↓	3	0.053	TCP1, CCT4, CCT8	Formation of tubulin folding intermediates by CCT/TriC

The 9-strain bacterial consortium delays disease progression and improves NAFLD disease markers in the STAM™ mouse model

Because liver transcriptomics performed in the NASH rats suggested that the tested bacterial consortium could be favorably modulating pro-fibrogenic pathways (Table 15), the same consortium was tested on a rodent model that displays notable signs of fibrosis at histopathology. For that, the STAM™ mouse model was used. The therapeutic effect of the 9-strain bacterial consortium was evaluated and compared to the benchmark Telmisartan. The effects were evaluated at histopathological level and blood was collected for biochemical analysis.

Because STAM animals are lean (136), as expected, the bacterial consortium did not improve body weight. As observed in the NASH rats, no significant alterations were detected in blood parameters, namely ALT and cholesterol levels (Table 16). However, a trend to decrease whole blood levels of HbA1c, a marker that indicates the presence of excessive glucose in the bloodstream, was observed by the end of the study (Figure 25).

Table 16. Biochemical characteristics after 4 weeks of intervention in the STAM™ mouse model.

	CD+VEH 9 weeks (n = 8)	STAM+VEH 9 weeks (n = 8)	STAM+CON 9 weeks (n = 10)	STAM+TLM 9 weeks (n = 8)	STAM+VEH 12 weeks (n = 8)	STAM+CON 12 weeks (n = 8)
ALT (IU/L)	24.00*** ± 1.27	39.38 ± 2.41	43.5 ± 3.28	35.00 ± 2.39	65.13 ± 14.04	60.63 ± 12.81
TG (mg/dL)	79.63* ± 10.46	500.9 ± 152.5	679.9 ± 91.35	465.6 ± 107.6	926.4 ± 251.6	1017 ± 248.8
Cholesterol (mg/dL)	76.92**** ± 3.51	125.7 ± 8.11	124.8 ± 4.32	132.7 ± 2.71	187.3 ± 41.99	186.9 ± 38.81
Cholesterol HDL (mg/dL)	57.84** ± 2.75	83.69 ± 7.13	75.55 ± 3.31	97.21 ± 4.73	72.24 ± 7.46	70.21 ± 6.84
Cholesterol LDL (mg/dL)	13.1 ± 0.66	14.68 ± 1.20	13.64 ± 0.74	18.78* ± 1.10	24.35 ± 6.12	23.76 ± 5.16

Values are expressed as mean ± SEM. CD+VEH: group of control diet mice receiving sham gavage (vehicle); STAM+VEH: group of STAM mice receiving sham gavage (vehicle); STAM+CON: group of STAM mice receiving the 9-strain bacterial consortium daily; STAM+TLM: group of STAM mice receiving Telmisartan daily. ALT, alanine aminotransferase; HDL, high-density lipoprotein; LDL, low-density lipoprotein; n, number of mice; TG, triglycerides. $^{*}P \leq 0.05$; $^{**}P \leq 0.01$; $^{***}P \leq 0.001$; $^{****}P \leq 0.0001$ versus STAM+VEH.

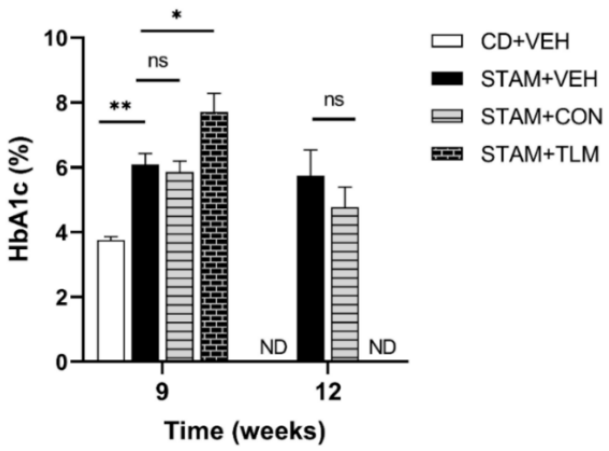

Figure 25. Whole blood HbA1c (%) measured in the STAM mice at 9 and 12 weeks of age (euthanasia 1 and 2, respectively). CD+VEH: group of control diet mice receiving sham gavage (vehicle); STAM+VEH: group of STAM mice receiving sham gavage (vehicle); STAM+CON: group of STAM mice receiving the 9-strain bacterial consortium daily; STAM+TLM: group of STAM mice receiving Telmisartan daily. CD, control diet; HbA1c, glycated hemoglobin; ND: not determined for the CD+VEH and STAM+TLM groups at 12 weeks; ns: not significant. $^{*}P \leq 0.05$; $^{**}P \leq 0.01$ versus STAM+VEH.

The consortium of 9 gut commensals improved NAS at histopathology at 9 weeks of age

As expected (106), liver sections from vehicle-treated STAM group exhibited micro- and macrovesicular fat deposition, hepatocellular ballooning and inflammatory cell infiltration (Figure 26). The bacterial consortium-treated STAM mice (STAM-CON) displayed significantly reduced NAS scores when compared to the disease group at 9 weeks of age (Figure 26D). This was a result from reduced steatosis and ballooning scores (Figure 26B and C). At 12 weeks of age this was no longer observed.

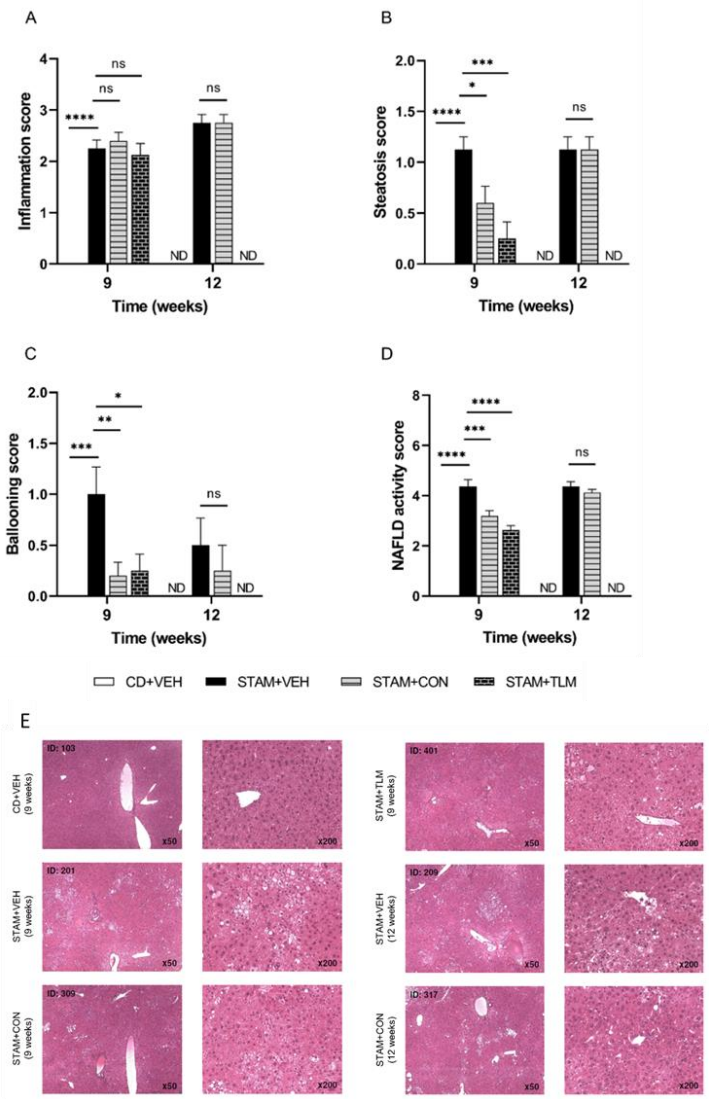

Figure 26. Histological evaluation of the H&E-stained liver sections collected from the STAM mice. The components (A) inflammation, (B) steatosis, (C) ballooning, and (D) the composite score, were evaluated at both 9 and 12 weeks of age (euthanasia 1 and 2, respectively). (E) Representative images show H&E-stained liver parenchyma in sections collected from the STAM mice (50× and 200× magnification). CD+VEH: group of control diet mice receiving sham gavage (vehicle); STAM+VEH: group of STAM mice receiving sham gavage (vehicle); STAM+CON: group of STAM mice receiving the 9-strain bacterial consortium daily; STAM+TLM: group of STAM mice receiving Telmisartan daily. ND: not determined for the CD+VEH and STAM+TLM groups at 12 weeks; ns: not significant. Data represent mean ± SEM. $^{*}P \leq 0.05$; $^{**}P \leq 0.01$; $^{***}P \leq 0.001$; $^{****}P \leq 0.0001$ versus STAM+VEH.

The consortium of 9 gut commensals improved fibrosis, and showed reduced hepatic expression of F4/80 and serum CK-18 levels

To evaluate collagen deposition, mice liver sections were stained with Sirius red (Figure 27A and D). As expected, liver sections from the vehicle-treated STAM group (STAM-VEH) displayed increased collagen deposition in the pericentral region of the liver lobule when compared to the CD group. The bacterial consortium-treated group (STAM-CON) showed a significant decrease in the hepatic fibrosis (Sirius red-positive) area when compared to the disease group at 12 weeks of age but not at 9 weeks of age, when the amount of fibrosis is lesser. This therapeutic effect on fibrosis was also confirmed on fibronectin immunostained liver sections (Figure 28).

To further evaluate inflammation, the macrophage F4/80 immunostaining was used in liver sections. Even though no significantly reduced general inflammation was observed in H&E-stained liver sections (Figure 26A and E), the F4/80 immunostained liver sections showed a significant reduction in macrophage inflammatory infiltration in the consortium-treated group at 9 weeks of age, and a trend to decrease at 12 weeks of age (Figure 27B and E). Finally, serum CK-18 levels were also significantly reduced in the consortium-treated group at 9 weeks of age, and a trend to decrease was observed by 12 weeks of age (Figure 27C), a result that correlates with reduced hepatocyte apoptosis and improved histological activity.

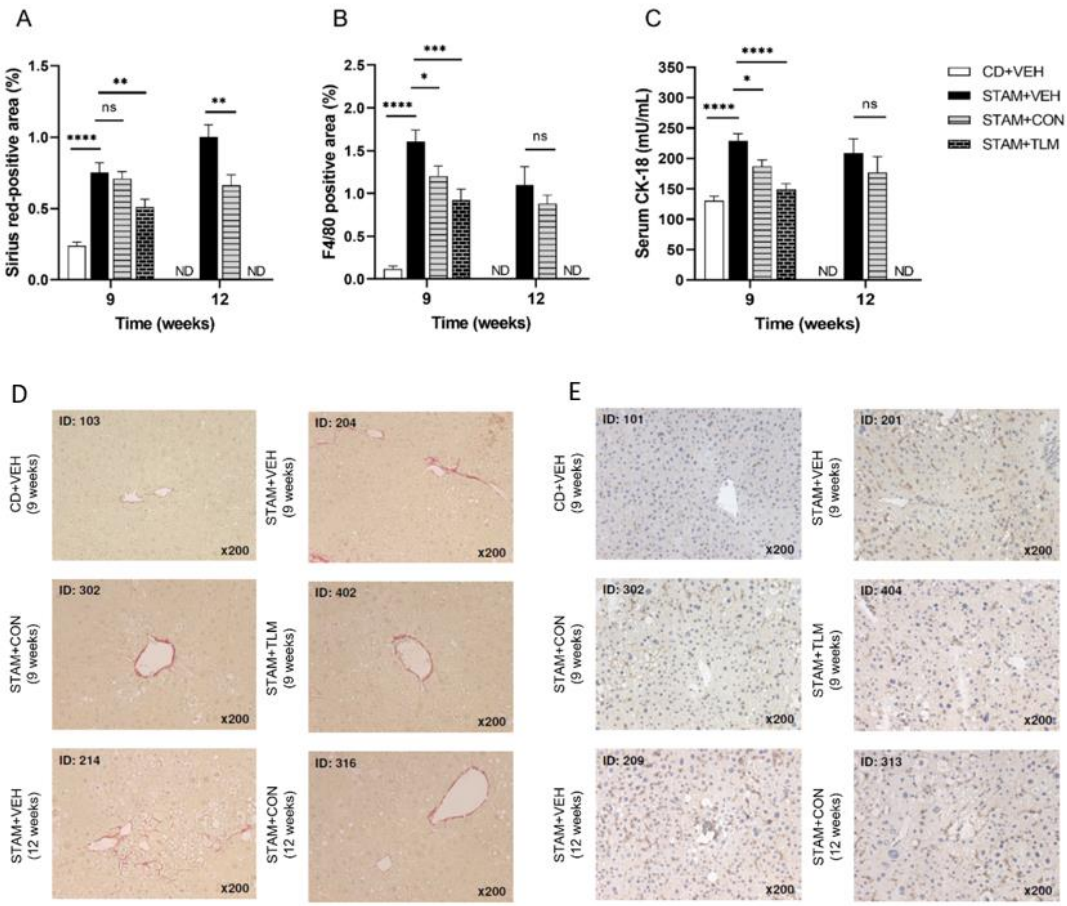

Figure 27. Hepatic fibrosis area, F4/80 positive area, and serum CK-18 levels in the STAM™ mouse model. (A) Fibrosis assessed in Sirius red-stained liver sections. (B) Immunohistochemistry of macrophages evaluated in F4/80-immunostained sections. (C) Serum levels of CK-18, a marker for apoptotic hepatocytes. All markers were evaluated at both 9 and 12 weeks of age (euthanasia 1 and 2, respectively). Representative images of (D) Sirius red-stained, and (E) F4/80 immunostained liver sections collected from the STAM™ mouse model at both 9 and 12 weeks of age (200× magnification). CD+VEH: group of control diet mice receiving sham gavage (vehicle); STAM+VEH: group of STAM mice receiving sham gavage (vehicle); STAM+CON: group of STAM mice receiving the 9-strain bacterial consortium daily; STAM+TLM: group of STAM mice receiving Telmisartan daily. ND: not determined for the CD+VEH and STAM+TLM groups at 12 weeks. ns: not significant. Data represent mean ± SEM. $^{*}P \leq 0.05$; $^{**}P \leq 0.01$; $^{***}P \leq 0.001$; $^{****}P \leq 0.0001$ versus STAM+VEH.

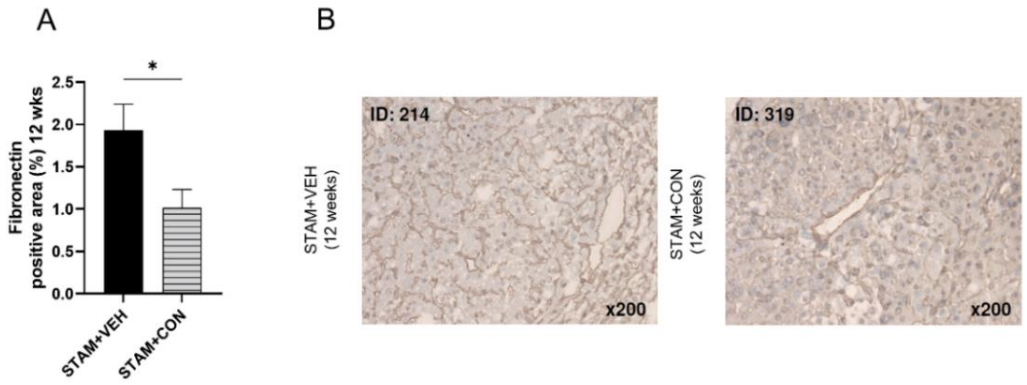

Figure 28. Immunohistochemistry of (A) fibronectin at 12 weeks, and (B) representative images of fibronectin immunostained liver sections collected from the STAM mice at 12 weeks of age (euthanasia 2) (200× magnification). CD+VEH: group of control diet mice receiving sham gavage (vehicle); STAM+VEH: group of STAM mice receiving sham gavage (vehicle); STAM+CON: group of STAM mice receiving the 9-strain bacterial consortium daily; STAM+TLM: group of STAM mice receiving Telmisartan daily. Data represent mean ± SEM. $^{*}P \leq 0.05$.

The main results obtained in study 2 can be summarized as follows:

1) In the 8-week HFGFD-induced rat model, the 9-strain bacterial consortium showed a protective effect on body weight, a trend to improve fasting blood insulin levels and HOMA-IR, and a marked protective effect on PH, namely a significant reduction in PP and IHVR.
2) An improvement in all features of endothelial function and gene expression of liver fibrosis markers was also observed.
3) Gut microbial compositional changes revealed that the consortium achieved a more defined and richer replacement of the gut microbiome than FMT.
4) Liver transcriptomics suggested that the bacterial consortium beneficially modulates pro-fibrogenic pathways in the rat model.
5) In the STAM^{TM} mouse model, the bacterial consortium improved histological liver fibrosis and the NASH activity score. The consortium also significantly reduced F4/80 positive area and serum CK-18 levels.

5.3. STUDY 3: Characterization of a 16-week HFHC/GF-induced rat model (FIBRO-SH rat model)

To confirm the presence of fibrosis in the FIBRO-SH rat model, liver biopsies were performed in some individuals at week 12. By the end of week 16, liver hemodynamics and blood biochemistry were performed, and liver tissue was collected for histopathology and molecular pathway analyses.

Liver biopsies from HFHC/GF animals showed fibrosis at week 12

Light-microscopic examination of Sirius red-stained liver sections revealed the presence of fibrosis in the HFHC/GF group after 12 weeks of dietary intervention. HFHC/GF livers also showed severe steatosis and inflammatory infiltrates confirmed by H&E staining (Figure 29).

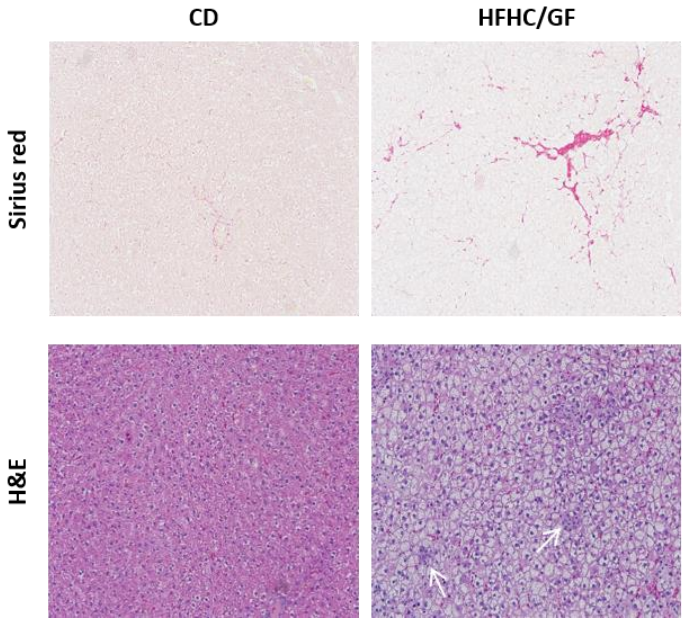

Figure 29. Illustrative Sirius red and H&E-stained sections of biopsied livers from each group after 12 weeks of diet intervention (10× magnification). White arrows indicate inflammatory infiltrates. CD, control diet; HFHC/GF, high-fat high-cholesterol glucose-fructose diet.

The HFHC/GF intervention induced an altered hepatic function at 16 weeks

Animals fed with HFHC/GF during 16 weeks had enlarged livers, which were pale and yellowish in color, indicating lipid accumulation (Figure 30). Accordingly, the liver weight, as well as the liver to body weight ratio, were significantly increased compared to CD animals ($P \leq 0.001$). Animals in the HFHC/GF group showed an increase in body weight compared to controls, although it did not reach statistical significance. This was consistent with the significant increase in total calories consumed from food and drink by HFHC/GF-fed animals (Table 17).

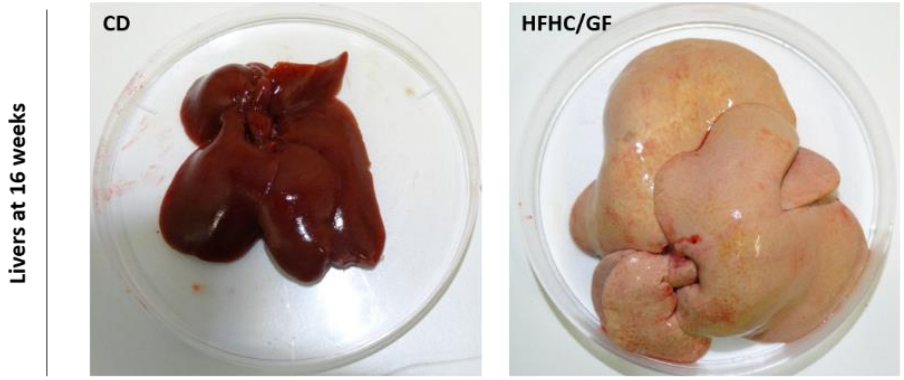

Figure 30. Representative images of liver morphology after 16 weeks of feeding with CD and HFHC/GF. Plates are 100 mm. CD, control diet; HFHC/GF, high-fat high-cholesterol glucose-fructose diet.

Table 17. Calorie intake, body weight and liver weight after 16 weeks of dietary intervention.

	CD (n = 6)	HFHC/GF (n = 12)
Calorie intake		
Food (kcal/day)	81.54 ± 0.89	93.18 ± 0.83***
Drink (kcal/day)	0 ± 0	32.79 ± 0.7***
Total (kcal/day)	81.54 ± 0.89	125.97 ± 0.86***
BW		
Final (g)	651 ± 24.2	713 ± 32.9
BW gain (g)	386 ± 22.35	446 ± 29.4
Liver weight		
(g)	15.08 ± 0.99	49.3 ± 4.19***
Liver to BW ratio (g)	1 ± 0.04	3.02 ± 0.11***

Values are expressed as mean ± SEM. BW, body weight; CD, control diet; HFHC/GF, high-fat high-cholesterol glucose-fructose diet; n, number of rats. ***P ≤ 0.001 versus CD.

As shown in Table 18, HFHC/GF was associated with significant increases in fasting blood concentrations of transaminases (ALT and AST), alkaline phosphatase (AP) and total cholesterol. Surprisingly, a significant increase in albumin and a decrease in TG compared to CD was also observed. Moreover, the 16-week HFHC/GF intervention did not induce changes in fasting serum glucose and insulin levels, and thus in HOMA-IR, indicating the absence of systemic IR in the FIBRO-SH rat model.

Table 18. Blood biochemistry after 16 weeks of dietary intervention.

	CD (n = 6)	HFHC/GF (n = 12)
Glucose (mg/dL)	187.67 ± 31.35	190.17 ± 12.22
Insulin (ng/mL)	3.72 ± 0.53	2.77 ± 0.16
HOMA-IR	1.83 ± 0.51	1.31 ± 0.12
Albumin (g/dL)	3.58 ± 0.08	4.08 ± 0.06***
AST (IU/L)	95.5 ± 26.5	371 ± 33.15**
ALT (IU/L)	39.2 ± 3.61	157.42 ± 19.68**
TG (mg/dL)	35.33 ± 3.6	24.17 ± 2.53*
AP (IU/L)	61.6 ± 5.66	162.09 ± 9.77***
Cholesterol (mg/dL)	62.33 ± 5.09	129.17 ± 5.74***

Values are expressed as mean ± SEM. ALT, alanine aminotransferase; AP, alkaline phosphatase; AST, aspartate aminotransferase; CD, control diet; HFHC/GF, high-fat high-cholesterol glucose-fructose diet; HOMA-IR, homeostasis model of insulin resistance index; n, number of rats; TG, triglycerides. *P ≤ 0.05; **P ≤ 0.01; ***P ≤ 0.001 versus CD.

The 16-week HFHC/GF intervention induced increased NASH histological activity with liver fibrosis

Regarding histopathological findings, the 16-week HFHC/GF intervention resulted in a consistent reproduction of NASH histological hallmarks, as seen in Figure 31. The HFHC/GF-fed animals showed an intense degree of NASH histological activity (as measured by NAS), whereas no individual in the control group developed NASH (Figure 31D). All individuals in the HFHC/GF group had a NAS of 5 or greater, within nearly 45% of individuals achieving a NAS of 7. This was accompanied by steatosis score 3 in all individuals (Figure 31A) and high percentages of individuals with score 2 in inflammation (70%) (Figure 31B) and ballooning (44%) (Figure 31C).

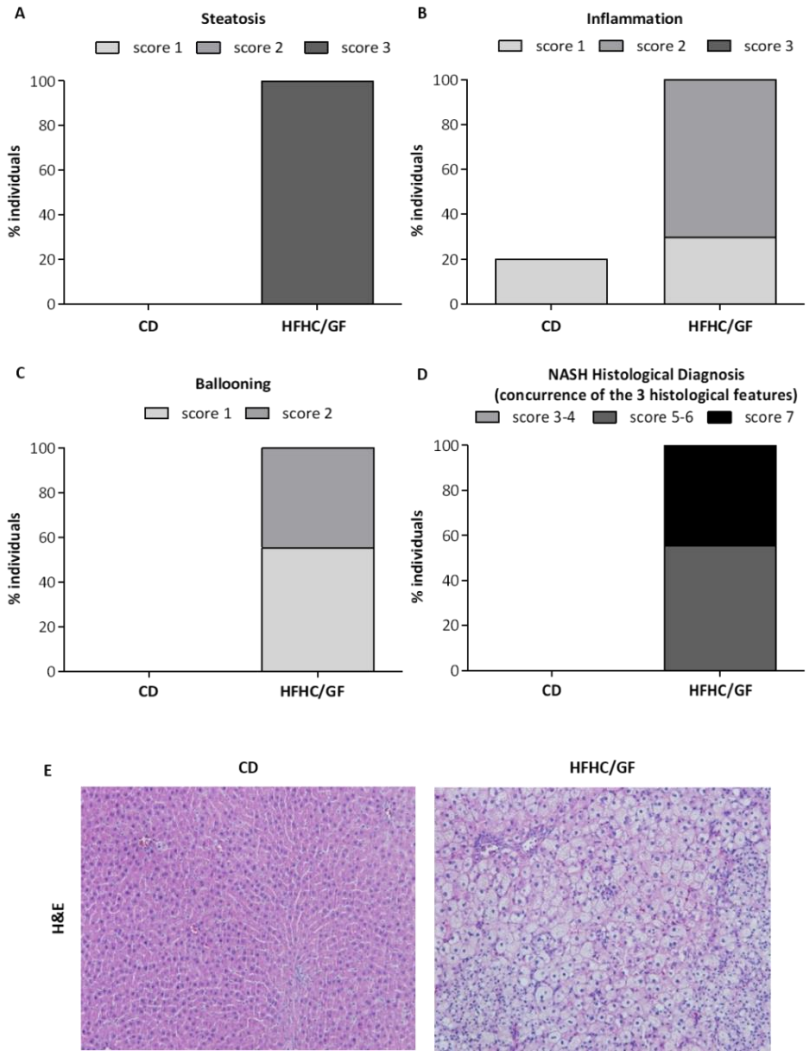

Figure 31. Histological evaluation of the H&E-stained liver sections collected from rats after 16 weeks of dietary intervention (CD n= 5, HFHC/GF n = 9). Evaluation followed the NASH-Clinical Research Network system. The three first bar diagrams represent the percentage of individuals presenting (A) steatosis, (B) inflammation, and (C) ballooning in the different groups. Each bar includes the percentage of individuals scored with 1 (light gray), 2 (gray), or 3 (dark gray); (D) the last bar diagram represents the percentage of individuals with NASH Histological Diagnosis (defined as NAFLD activity score (NAS) ≥ 3 and concurrence of steatosis, lobular inflammation and hepatocellular ballooning) scored with 3-4 (light gray), 5-6 (dark gray), or 7 (black). (E) Representative images show H&E-stained liver parenchyma of rats from each group after 16 weeks of dietary intervention (10× magnification). CD, control diet; HFHC/GF, high-fat high-cholesterol glucose-fructose diet.

Liver fibrosis was also assessed quantitatively by image analysis and graded histologically following the NASH-CRN system. As expected, collagen deposition, confirmed by Sirius red staining, was observed in the liver parenchyma of HFHC/GF rats after 16 weeks of feeding. No histological signs of fibrosis were observed in the liver parenchyma of CD-fed rats (Figure 32).

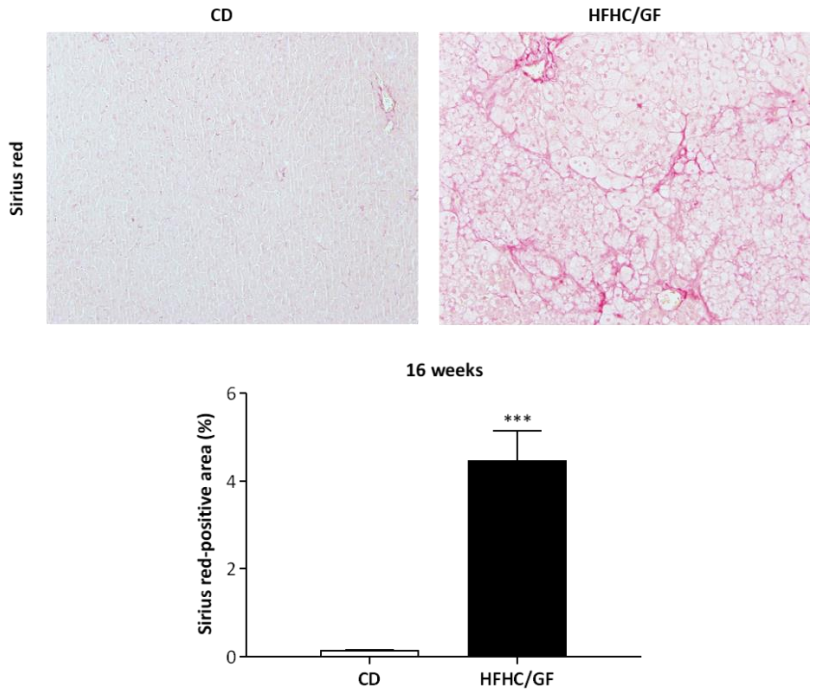

Figure 32. Evaluation of histological liver fibrosis after 16 weeks of dietary intervention. Representative images show Sirius red-stained liver parenchyma of rats from each group (10× magnification). The bar diagram shows the quantification of the hepatic fibrosis area (%).CD, control diet; HFHC/GF, high-fat high-cholesterol glucose-fructose diet. Data represent mean ± SEM. $^{***}P \leq 0.001$ versus CD.

Histological fibrosis assessment following the NASH-CRN system, as shown in Table 19, revealed that all individuals in the control group had F0 stage (no fibrosis). By contrast, all individuals in the HFHC/GF group developed fibrosis, with 7 out of 9 (78%) having F2 stage or greater. In addition, cirrhosis (F4 stage) was present in one individual in the group (Table 19).

Table 19. Number of individuals according to fibrosis staging following the NASH-CRN system (119).

Group	Fibrosis stage (n)					
	0	**1A**	**1B**	**2**	**3**	**4**
CD	5	0	0	0	0	0
HFHC/GF	0	2	0	3	3	1

In CD and HFHC/GF groups at 16 weeks, n = 5 and n = 9, respectively. CD, control diet; HFHC/GF, high-fat high-cholesterol glucose-fructose diet.

The 16-week HFHC/GF intervention significantly worsened liver hemodynamics

As seen in Table 20, rats in the HFHC/GF group had significantly higher PP (+52%) compared to those in the CD group at 16 weeks. The presence of PH in these animals was a consequence of a significant increase in IHVR. Regarding systemic hemodynamic parameters, no notable changes were observed between groups (Table 20).

Table 20. Hemodynamic measurements after 16 weeks of dietary intervention.

	CD (n = 5)	**HFHC/GF (n = 10)**
MAP (mmHg)	100.75 ± 2.96	99.1 ± 4.36
PP (mmHg)	8.74 ± 0.31	13.29 ± 0.7***
SMABF (mL/[min · 100 g])	2.22 ± 0.22	2.4 ± 0.34
SMAR (mmHg/mL · min · 100 g)	43.01 ± 4.29	41.1 ± 5.04
IHVR (mmHg/mL · min · 100 g)	3.5 ± 0.34	6.88 ± 0.78*

Values are expressed as mean ± SEM. CD, control diet; HFHC/GF, high-fat high-cholesterol glucose-fructose diet; IHVR, intrahepatic vascular resistance; MAP, mean arterial pressure; n, number of rats PP, portal pressure; SMABF, superior mesenteric artery blood flow; SMAR, superior mesenteric artery resistance. *P ≤ 0.05; ***P ≤ 0.001 versus CD.

As seen in Figure 33, the percentage of fibrotic area stained with Sirius red was positively and strongly correlated with PP (R = 0.4787; P = 0.0043), showing that individuals with a higher PP were those who showed a greater deposition of collagen in the liver and suggesting that liver fibrosis might be determinant of the marked increase in IHVR and PP observed in the FIBRO-SH rat model.

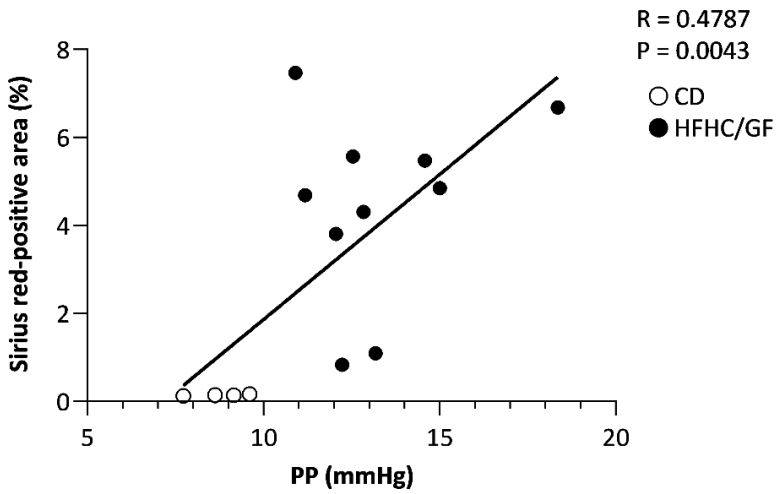

Figure 33. Correlation between hepatic fibrosis area (%) and portal pressure (PP, mmHg) in the CD and HFHC/GF groups. CD, control diet; HFHC/GF, high-fat high-cholesterol glucose-fructose diet.

Hepatic endothelial dysfunction contributed to the development of portal hypertension in the FIBRO-SH rat model

Apart from fibrosis, the features of endothelial dysfunction were also evaluated as other possible factors contributing to the presence of PH in the FIBRO-SH rat model. Western blot analysis revealed a significant reduction in the hepatic P-eNOS and KLF2 levels and a trend towards decreased P-Akt levels in HFHC/GF-fed rats compared to CD-fed rats (Figure 34). These results suggest that endothelial dysfunction is another underlying mechanism of increased IHVR and PP in the FIBRO-SH model.

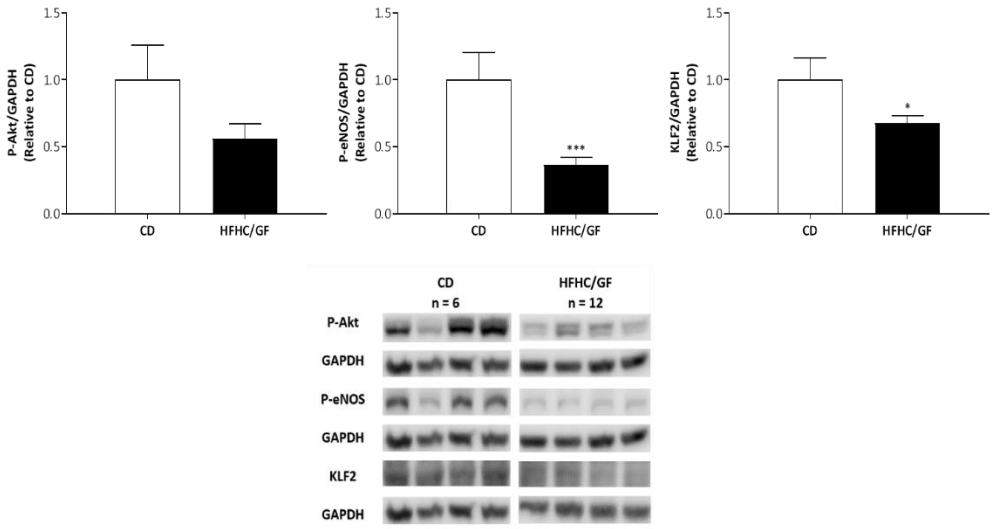

Figure 34. Markers of intrahepatic endothelial dysfunction. The bar graphs show the quantification of the proteins P-Akt, P-eNOS and KLF2 using GAPDH as loading control and normalized to CD group. Representative Western blots are shown below. CD, control diet; GAPDH, glyceraldehyde-3-phosphate dehydrogenase; HFHC/GF, high-fat high-cholesterol glucose-fructose diet; KLF2, Kruppel Like Factor 2; n, number of rats; P-Akt, phosphorylated protein kinase B; P-eNOS, phosphorylated endothelial nitric oxide synthase. Data represent mean ± SEM. $^{*}P \leq 0.05$; $^{***}P \leq 0.001$ versus CD.

HFHC/GF-fed animals developed hepatic insulin resistance

Although the HFHC/GF animals did not exhibit features associated to systemic IR, namely fasting hyperglycemia and hyperinsulinemia, we continued to address the role of the hepatic insulin signaling pathway (IRS/PI3K/Akt) associated to endothelial dysfunction, through the evaluation of the expression of genes encoding the insulin receptor substrates IRS-1 and IRS-2. In this regard, we found a significant repression of both genes in the liver of HFHC/GF-fed rats compared to controls (Figure 35). Thus, the impairment of the IRS/PI3K/Akt pathway indicates the presence of hepatic IR in the FIBRO-SH rat model.

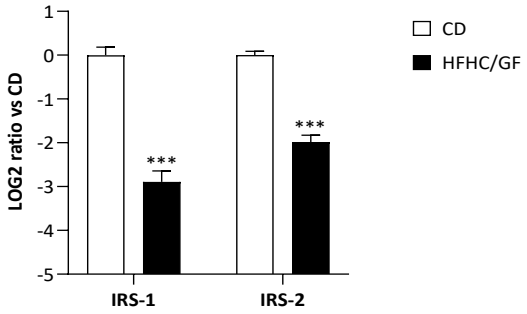

Figure 35. Relative quantification of hepatic IRS-1 and IRS-2 mRNA expression, expressed as a log2 ratio. β-Actin was used as an endogenous control, and results were normalized to the control group. CD, control diet; HFHC/GF, high-fat high-cholesterol glucose-fructose diet; IRS, insulin receptor substrate. Data represent mean ± SEM. $^{***}P \leq 0.001$ versus CD.

Furthermore, we examined the possible contribution of adipokines to the development of hepatic IR in the FIBRO-SH rat model. For this purpose, we analyzed the hepatic expression of the adiponectin receptor 2 (AdipoR2) and the leptin receptor (LepR). The RT-qPCR analysis revealed a significant decrease in the hepatic mRNA expression of both receptors in the HFHC/GF group compared to controls (Figure 36). These data also appear to indicate an altered hepatic insulin sensitivity in the model.

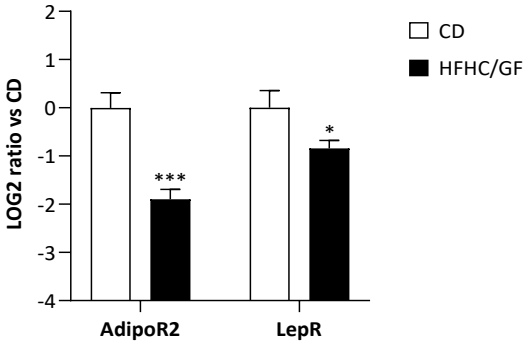

Figure 36. Relative quantification of hepatic AdipoR2 and LepR mRNA expression, expressed as a log2 ratio. β-Actin was used as an endogenous control, and results were normalized to the control group. AdipoR2, adiponectin receptor 2; CD, control diet; HFHC/GF, high-fat high-cholesterol glucose-fructose diet; LepR, leptin receptor. Data represent mean ± SEM. $^{*}P \leq 0.05$; $^{***}P \leq 0.001$ versus CD.

The main results observed in study 3 can be summarized as follows:

1) The 16-week HFHC/GF-induced rat model, termed FIBRO-SH rat model, showed a non-significant increase in body weight and a marked increase in serum transaminases, cholesterol and AP. However, fasting blood glucose and insulin levels and thus HOMA-IR remained unchanged.
2) The FIBRO-SH rat model also exhibited an intense degree of NASH activity with histological liver fibrosis.
3) The presence of significant PH in the FIBRO-SH rat model was explained by both structural (liver fibrosis) as well as functional (hepatic endothelial dysfunction) factors.
4) Although HFHC/GF-fed rats lacked systemic IR, we found evidence of hepatic IR through exploration of the hepatic IRS/PI3K/Akt signaling pathway and also through significantly reduced gene expression of adipokine receptors in the liver.

6. DISCUSSION

6. DISCUSSION

NAFLD represents a worldwide clinical problem, and its increasing prevalence parallels the global rise in obesity and type 2 diabetes (137). NAFLD, considered the hepatic manifestation of metabolic syndrome, is characterized by fat accumulation in the liver evolving to NASH, an inflammatory subtype that can lead to liver fibrosis, cirrhosis, and eventually HCC (12). To date, there is no approved treatment for NAFLD. Treatment is therefore based on lifestyle interventions aimed at weight loss. However, its common low adherence makes it urgent to develop complementary or alternative therapeutic approaches that can halt or reverse NASH progression.

Study 1

Most of the clinical consequences associated to NASH are linked directly to the progression of PH. Interestingly, it has been shown both in humans and experimental models, that NASH can induce PH in pre-cirrhotic stages, even in complete absence of fibrosis (44,46,49,50,134,138). However, the exact mechanisms driving these observations are incompletely understood. It has been previously shown by our group and others that liver endothelial dysfunction might represent a potent driver of PH in NASH, at least in short-term models of the disease, in which PH is observed in absence of liver fibrosis (46,49,50,134). As a follow-up to previous work by our group (50), in study 1 we assessed whether a long-term (36 weeks) extension of a HFGFD intervention was able to induce liver fibrosis, on one hand, and to evaluate whether it was also capable of perpetuating or aggravating the endothelial dysfunction and PH observed in the short-term (8 weeks) model, on the other hand.

To the best of our knowledge, this is the first study showing that steatosis *per se* can induce PH in NASH in the absence of all other accepted mechanisms that can associate increases in PP, namely liver fibrosis or hepatic endothelial dysfunction. There is some

previous evidence suggesting that steatosis is an important contributor of PH in ALD. Human and experimental studies performed in the 1980's clearly showed that PH was present in ALD patients and animal models even in absence of fibrosis, as long as a critical hepatocyte area was surpassed due to lipid and water accumulation inside the hepatocytes (138–141). However, those observations could not rule out other important potential contributors to the effect, such as endothelial dysfunction. Besides, transferability of these observations to NASH is unclear, given the differences in terms of mechanisms and dynamics of hepatocyte enlargement between the two conditions; the unclear and striking differences in the development of hepatomegaly in ALD but not in NASH represent a puzzling example (141). More recent studies, focused in NAFLD, also suggested that steatosis might be contributing to the development of PH in non-alcoholic fatty livers, even in the absence of fibrosis. Works of Francque and collaborators (44), validated more recently by Rodrigues *et al*. (138), clearly showed that PH is not uncommon in pre-cirrhotic NAFLD. Francque *et al*. also conducted elegant translational studies exploring the underlying mechanisms for this observation in animal models (44,46,142). However, in those studies, the precise contribution of the mechanical compressive effect of enlarged fatty hepatocytes could not be dissected from the relative contribution of endothelial dysfunction, which seemed to have more of a leading role, at least in short-term models of the disease.

In our study, the extension of the dietary intervention provides a unique model to isolate the contribution of the mechanical compression by steatosis as the main determinant to the increase in PP in non-cirrhotic NASH. Contrary to our initial hypotheses, the dietary extension was not able to either induce fibrosis or perpetuate endothelial dysfunction. Regarding the former, we showed that in Sprague-Dawley rats, the sole extension in time of the HFGFD was unable to elicit a fibrotic response. This is in line with all efforts trying to induce fibrosis with interventions as similar as possible to what is seen in patients with NASH (72,139,140). We did find signals of stellate cell

activation in the long term, but these did not translate into either histological fibrosis or even an increase in expression of COL1A1. Thus, the marked increase in PP at 36 weeks cannot be attributed to the architectural disruption usually seen in cirrhosis.

In previous work from our group and others, it was shown that short-term HFGFD interventions were able to induce endothelial dysfunction through insulin-dependent mechanisms, which translated into increased IHVR and PP (49,50,134,142). Thus, we hypothesized that endothelial dysfunction might be the main determinant of the marked increase in IHVR and PP observed at 36-weeks. However, this also seemed not to be the case. The significant increase in P-eNOS and decrease in CD34 in the 36w-HFGFD group suggested a reversal to a healthier LSEC phenotype in the long term. In this line, we explored other potential biological processes that could underlie the observed deterioration of portal hemodynamics and the increase in NASH activity.

Regarding a more in-depth molecular characterization of other biological processes that could account for this increase in IHVR and PP, we chose to analyze iNOS expression as a potential direct link between intrahepatic inflammation and endothelial dysfunction. Upregulation of iNOS has been linked to LSEC capillarization both in vitro and in BDL models (143,144). We observed an increase of iNOS expression in the 36w-HFGFD group. However, since iNOS was not elevated in the NASH model at 8 weeks (in which endothelial dysfunction was more obvious), it is hard to assume that the increase of iNOS at 36 weeks might be a reflection of an underlying endothelial dysfunction at this time point. Thus, the iNOS elevation might be interpreted to be a molecular reflection of the increase in histological NASH activity at this time point, although this interpretation remains purely speculative. In the same line, we evaluated activation of the Shh pathway in the liver in the 4 groups (Figure 14B). We observed a marked increase in Shh ligand expression in HFGFD versus CD, which was more intense at 36 weeks, suggesting an increase in the amount of lipotoxic injury (145) and/or in hepatocyte ballooning (146) with the HFGFD intervention which was aggravated in the

long term. However, these changes did not reach statistical significance. Although the increase in Shh expression goes in line with the increase in NASH histological activity observed in the 36w-HFGFD group (147), it is worth noting that ballooning did not change over time in our model. Thus, it is indeed hard to discern whether this increase in Shh expression was related to subclinical changes (i.e., not obvious as ballooning at light microscopy) in lipotoxic hepatocytes or to other potential cellular sources (HSC, LSEC, inflammatory cells), or how this might be related or not with endothelial dysfunction.

Finally, it is worth remarking the changes observed in the 36w-CD group. This group showed an altered metabolic biochemical profile as compared to the 8w-CD, as well as increased α-SMA expression and an increase in SMAR, without apparent changes in liver histology or hemodynamics. These data suggest a potential role of aging and sedentarism in the long-term animals, placing the 36w-CD group as an intermediate step in between the healthy 8w-CD phenotype and the full-NASH phenotype of the aged 36w-HFGFD group.

In all, although the exact mechanisms for these molecular adaptations remain unclear, this should at least serve as a reminder that, sometimes, apparently relevant pathways in short-term animal models might be lost in the long-term probably due to the emergence of compensatory mechanisms and the effects of aging and sedentarism with these long-term interventions.

Finally, through a systematic image analysis, we were able to show that the sinusoidal space is severely restricted at 36 weeks, in correlation with a marked increase in liver fat and hepatocyte area, pointing to a direct compressive effect of fat-laden hepatocytes. The direct compressive effect of fatty hepatocytes was already described for ALD in the 1980's (139). However, the relative contribution of this compressive effect could not be isolated from other confounding contributors, such as liver fibrosis

or endothelial dysfunction. Besides, the sinusoidal area was not directly quantified in those studies, and the compressive effect was deduced from an indirect observation (e.g., the increase in hepatocyte area). In our study, and following previous work by Hall *et al*. (120), we take advantage of currently available image analysis tools to provide a direct quantification of both the hepatocyte area and number, and of the sinusoidal area. Through this approach, we observed that IHVR and PP in the 36-week model only started to increase when the sinusoidal area went below a certain critical threshold. Given the absence of liver fibrosis or endothelial dysfunction in the long-term model, we were able to show in a quantifiable manner the individual contribution of steatosis in this model on NASH. In addition, a non-quantitative approach was considered for an in-depth exploration of this structural effect. Previous studies have elegantly used micro-CT and/or SEM of vascular corrosion casts to characterize the vascular changes induced by steatosis in NASH models (142,148). In our long-term HFGFD rat model, we confirmed by SEM the disturbances in liver structure characterized by narrow and irregular sinusoids, suggesting that morphologically the hepatic microcirculation was impaired as a result of compression by fat-laden hepatocytes.

The implications of these findings could go beyond the abstract proof-of-concept on the contribution of steatosis to the development of PH in NASH. The dynamics of steatosis in NASH are markedly faster than that of fibrosis, and the decreases in PP observed in patients with NASH with non-controlled lifestyle interventions (149) or in the placebo arm of randomized controlled trials (150,151) could be due to rapid changes in steatosis leading to increased sinusoidal area and decreased IHVR. Unfortunately, in all these studies steatosis has been addressed in a semi-quantitative manner, and the structural influence of the effect has not been systematically addressed. The image analysis proposed in this study can be easily standardized and could help at quantifying the effect of changes in steatosis on PH.

Summarizing study 1, we have provided evidence that steatosis *per se* is able to induce a marked increase in IHVR and PP through a direct structural compression of the sinusoidal area, in the absence of other potential contributors to the effect (endothelial dysfunction or liver fibrosis) in a long-term animal model of diet-induced NASH. We have also provided a systematic histologic image approach that could be used to quantify this effect in animal models and patients with NASH.

Study 2

In study 2 of this thesis, and following previous results of the beneficial effects of healthy FMT on a rat model of early stage of NASH, we wanted to try the protective effect of a selected bacterial consortium on liver endothelial function and progression of PH in NASH.

The gut–liver axis has a recognized role in NASH onset and progression. It is well described that intestinal dysbiosis and consequent disruption of intestinal barrier integrity are frequently observed in NAFLD patients, and that the ensuing endotoxemia, correlates with disease severity (152). However, the effects of bacterial-derived molecules go beyond the translocation of PAMPs such as LPS, and numerous metabolites resulting from bacterial fermentation have been described to contribute to pathology (153). Therefore, therapeutic approaches aimed to restore and balance gut microbiota are considered a promising strategy to treat NASH and other liver diseases (40,154). As already said, FMT from control lean rats has been shown to improve disease, by restoring the sensitivity to insulin through the hepatic IRS/PI3K/Akt pathway, thereby improving IHVR and PP (50). In humans, this treatment modality is also being explored (154,155), and although so far, no severe adverse events have been reported in NAFLD-FMT trials, several factors may hamper its clinical applicability such as the amount and frequency of stool transplantation, the need for bowel preparation prior to treatment, heterogeneity of fecal donors, and long-term expected effects (153).

Therefore, consortia of defined bacterial composition are a valuable alternative (40,153,154).

Relevant research, conducted in different animal models as well as in clinical studies, has been previously performed using combinations of defined bacterial strains as therapeutic strategies in the management of NASH (40,156–158). The combined administration of several bacterial strains may be more effective than a single one because of the multiple pathologic mechanisms of NAFLD (159,160). Therefore, in study 2, we sought to test the efficacy of a 9-strain consortium of gut commensals of defined composition and amount. Among others, the tested bacterial consortium was composed of four butyrate producers (*Faecalibacterium prausnitzii*, *Butyricicocccus pullicaecorum*, *Roseburia inulinivorans*, and *Anaerostipes caccae*) and five propionate producers (*Roseburia inulinivorans*, *Akkermansia muciniphila*, *Phocaeicola vulgatus*, *Veillonella parvula*, and *Blautia obeum*). We tested this consortium in a therapeutic setting in two well-established rodent models of NASH: the 8-week HFGFD-induced rat model previously reported by our group (50) (the same used in study 1), and the STAM™ mouse model. In rats, the bacterial consortium showed a protective effect on body weight, a trend to improve fasting blood insulin levels and HOMA-IR, and a significant protective effect on PH, namely a significant reduction in IHVR and PP. Similar to the FMT group, included in study 2 as a positive control group, protection occurred through the restoration of the sensitivity to insulin of the hepatic IRS/PI3K/Akt signaling pathway. In addition, an upregulation of KLF2 was observed in the liver of consortium-treated rats. This is also relevant, as the upregulation of hepatic KLF2 has been shown to ameliorate PH in cirrhotic rats, via inactivation and apoptosis of HSC, together with a reduction in oxidative stress and improvement in endothelial function (161,162). Despite these results, we did not observe improvement in NASH at histopathology. Nevertheless, this is also in accordance to our previous study testing the efficacy of FMT

in this model, specifically developed to evaluate diet-induced endothelial dysfunction and PH in NASH, rather than NASH histopathology (50).

Previously, FMT has been shown to significantly alter the gut microbial composition of NASH rats (50). However, FMT is preceded by intestinal emptying before stool transplant, which, in this study, resulted in the suppression of numerous microbial taxa as opposed to the consortium treatment. Thus, we observed that the bacterial consortium induced more defined and richer changes in gut microbiota than FMT. When translating these taxonomic shifts into predictive metabolic alterations, namely putative changes on microbial metabolic pathways, results suggested that the consortium was predicted to increase the biosynthesis of BCAA, and to decrease the biosynthesis of AAA and methionine. This is an interesting result, because a decreased BCAA/AAA ratio has been shown to correlate with liver dysfunction in cirrhotic patients (163). Whether an altered fecal amino acid profile contributes to NAFLD disease progression in this study remains to be determined. Nonetheless, BCAA treatment was shown to ameliorate liver fat accumulation in experimental animal models via increased production of acetic acid by gut microbes (164). Therefore, this warrants further investigation, to determine whether the 9-strain bacterial consortium can effectively increase the levels of BCAA and decrease those of AAA as predicted, and thereby ameliorate disease.

The administration of the 9-strain consortium also altered the hepatic gene expression. Several disease-associated genes were downregulated by this treatment. Among these, several members of the heat shock family of proteins (HSP) were strongly downregulated by both the consortium and FMT treatments, including Hspa1a, Hspa1b, Hspa8, and Hspa5, all members of the Hsp70 family of proteins, and the Hsp40 co-chaperone Dnajb9. HSP are produced in response to stress and play an important role in assisting protein synthesis from the secretory pathways of the ER, to ensure correct protein folding (165). ER stress is involved in the progression of NAFLD to NASH and abnormal ER stress responses have direct pathological consequences, including fat

accumulation, IR, inflammation, apoptosis, and, consequently, fibrosis (166). Of importance, drugs targeting HSP as anti-fibrotics in NASH are currently in Phase II of clinical development (ClinicalTrials.gov NCT04267393). It is therefore conceivable that the observed downregulation of HSP by the microbiota-based treatments in our study reflects a diminished ER stress response. Among the upregulated genes, Spot14 (S14) found to be induced by both treatments. S14 was originally identified as a mRNA from rat liver that responded rapidly to thyroid hormone (167). Recently, it has been described to play a key role in the tissue-specific regulation of lipid metabolism in response not only to thyroid hormone but also to dietary substrates such as glucose and polyunsaturated fatty acids, and also to other hormones such as insulin and glucagon (168). S14 is involved in *de novo* synthesis of fatty acids, and in the export of lipids from the liver as VLDL particles (168). Why the currently tested microbiota-based treatments would induce S14 transcription is not clear, but it may reflect the increased hepatic responsiveness to insulin, as suggested by studies performed both in rodents and obese patients (169–171).

Even though histological changes in fibrosis cannot be addressed in the NASH rat model, some pro-fibrotic markers such as α-SMA and COL1A1 were found to be down-regulated upon treatment with the 9-strain consortium. In addition, liver transcriptomics analysis suggested that a few fibrogenic pathways were downregulated by the treatment, such as the VEGFA-VEGFR2, the Wnt signaling, and the Cytoskeletal regulation by Rho GTPases pathways (172). However, because histological fibrosis cannot be adequately tested in the NASH rat model, we tested the same 9-strain consortium in a rodent model with well-established histological liver fibrosis: the STAM™ mouse model (105,106). The therapeutic effect of the bacterial consortium was evaluated and compared to the benchmark Telmisartan, a drug that has been shown to have clear benefits in this model (118). In this study, the consortium-treated mice showed anti-fibrotic effects, and significantly reduced collagen- and fibronectin-positive areas in the liver sections at 12

weeks. Although a trend to decrease at 9 weeks was also observed, this did not reach statistical significance, possibly because of the lower fibrosis levels developed at that time point. In addition, consortium-treated animals also displayed a reduced F4/80 positive area, a marker for mouse macrophages, as well as lower serum CK-18 levels, a marker of hepatocyte apoptosis, thereby suggesting an overall beneficial effect on all key aspects of NASH pathology (173). Of further relevance is that the consortium dosage stopped at 9 weeks of age. This may explain, in part, the lesser protective effects observed at 12 weeks in histological steatosis, ballooning, and inflammation, especially when compared with the clear beneficial effects at 9 weeks, thus suggesting a reversal of these more dynamic readouts upon treatment withdrawal. However, it also showed that the protective effect observed at the level of fibrosis at 12 weeks of age was long-lasting, and still apparent 3 weeks after the cessation of treatment. It is still to be evaluated whether these therapeutic effects would be even more pronounced if the consortium had been administered until sacrifice at 12 weeks.

The currently tested consortium is composed, among others, of several butyrate and propionate producers. A non-significant increase in cecal butyrate and propionate levels was measured in the consortium-treated rats (see in Appendix 2). Whether these account for the observed benefits in this study is not known. However, both direct supplementation of sodium butyrate and butyrate-producing gut bacteria have been shown to have beneficial effects in the prevention of NAFLD progression in rodent models, most likely by restoring gut dysbiosis and improving gut-barrier functions (174,175). Interestingly, overweight and obese patients also have higher levels of propionate in their stools, suggesting that either propionate is overproduced, or it is mal-absorbed (176). In addition, in overweight adult humans, propionate has been shown to prevent weight gain and IR (177). Although the role of SCFA in liver health is not completely understood, it has been suggested that when the balance between caloric intake and expenditure is maintained, SCFA would benefit liver health (178).

Therefore, it is reasonable to postulate that this consortium may improve disease partially due to increased butyrate and propionate levels in the intestine.

Further work must be performed to recapitulate the findings in the two models, namely in what concerns microbial changes in the gut lumen, as well as liver molecular alterations, to confirm the mode-of-action behind the consortium treatment. Nonetheless, the current results support the use of defined combinations of gut commensal bacteria for the treatment of NASH, so to delay disease progression.

Study 3

As seen in the two previous studies presented in this thesis, animal models are essential to perform proof-of-concept studies to elucidate the mechanisms underlying NASH pathophysiology and to study new therapeutic approaches for the management of NASH. Therefore, there is currently an urgent need to develop an animal model which more closely reflects the full spectrum of human disease, especially in its later fibrotic stages, to allow good translation of the obtained results into the clinics (88).

The HFGFD intervention used so far is not sufficient to induce liver fibrosis, even if extended to 36 weeks, limiting the use of these experimental models to the study of the earliest stages of NASH. This led us to a third study in which we developed a new rat model (termed FIBRO-SH rat model) changing the dietary intervention to HFHC/GF. This diet was also based on a human Western-style diet, but this time with higher amount of dietary cholesterol and supplemented with sodium cholate. Moreover, the total amount of glucose-fructose in the drinking water was also increased to contain 11% (110 g/L) carbohydrate, which better approximates the content of common sugar-sweetened beverages for human consumption (179).

High cholesterol consumption is recognized as a critical factor associated with hepatic inflammation and NAFLD progression in both animal models (95,180) and humans (181).

In our FIBRO-SH rat model, sodium cholate, although it does not resemble a dietary constituent in humans, was supplemented to HFHC/GF to aggravate the effects of dietary cholesterol. By binding to FXR, cholic acid increases the absorption of dietary cholesterol from the intestine and might repress CYP7A1 (a key enzyme in BA biosynthesis), which facilitates cholesterol accumulation in the liver (182). In a recently published study by Ichimura-Shimizu *et al*. (183), it is shown that the addition of dietary cholic acid leads to the development of fibrosis in a dose-dependent severity in a rat NASH model fed with a high-fat high-cholesterol diet. These results are in agreement with a gene expression analysis demonstrating that dietary cholesterol induces the expression of inflammatory genes, while cholic acid enhances the expression of liver fibrosis-related genes, such as those of the collagen family (184).

The main outcome in study 3 was that the HFHC/GF intervention, in contrast to HFGFD, induced the development of NASH with liver fibrosis within the relatively short period of 16 weeks (even sooner), and thus without relying on genetic mutations such as leptin-knockout, toxins such as STZ or a deficiency of nutrients such as methionine and choline.

The 16-week HFHC/GF intervention also resulted in a consistent reproduction of hepatic steatosis, lobular inflammation and hepatocellular ballooning, which are a prerequisite for the diagnosis of NASH. Furthermore, all individuals in the HFHC/GF group developed liver fibrosis, with almost 78% having at least F2 stage. This suggests that the FIBRO-SH model could serve as an experimental model of diet-induced NASH-associated fibrosis.

Another clinically-relevant feature of the FIBRO-SH model is that animals under the HFHC/GF intervention presented significant PH. As previously seen, PH begins to develop in the earliest stages of NAFLD, when fibrosis is far less advanced or absent. However, it is well known that the structural changes associated with fibrosis play a determinant role in the pathogenesis of PH in cirrhosis (43). Here we found a strong and positive correlation between fibrosis and PP, a result that is in line with that observed

in NASH patients (185,186). Therefore, fibrosis might be determinant of liver disease progression leading to significant PH in the FIBRO-SH rat model.

As discussed above, another important factor contributing to the development of PH is the intrahepatic endothelial dysfunction, which has been shown to precede fibrosis in NAFLD (49). HFHC/GF-fed rats showed evidence of endothelial dysfunction, as suggested by the significant reduction in the protein expression of both KLF2 and P-eNOS in the liver. The decrease in eNOS phosphorylation is probably the result of altered vasoprotective capacity of the transcription factor KLF2, which explains the vasodilatory inability of the sinusoidal endothelium due to decreased NO production.

The 16-week HFHC/GF intervention was also associated to an altered metabolic profile with significant increases in fasting blood concentrations of aminotransferases (ALT and AST), total cholesterol and AP. However, contrary to what is frequently found in NAFLD patients, TG levels were significantly reduced in our model. This result is in line with previous studies in which the administration of a diet containing cholesterol and cholate (Ath diet), even with an extremely high fat content, led to a decrease in serum TG levels (95,180). Watanabe *et al*. (187) revealed that BAs such as cholic acid lower serum TG levels by reducing SREBP-1c gene expression, the main regulator of hepatic fatty acid and TG biosynthesis.

Although obesity and IR are considered as common causes of NAFLD/NASH, HFHC/GF-fed rats did not exhibit evident obesity and lacked systemic IR. The latter demonstrated by unchanged serum glucose and insulin levels and HOMA-IR between the HFHC/GF and control groups. These results would reflect what occurs in approximately one-third of patients with NAFLD, especially in the Asian population, who have a non-obese phenotype (188). The reason for the lack of metabolic syndrome in our model is unclear, however, it has been demonstrated that the addition of cholate *per se* to HFD completely prevents HFD-induced hyperglycemia and obesity (189). This effect of

cholate has been attributed to an elevation in energy expenditure resulting in decreased amount of adipose tissue (190).

Although these animals are peripherally insulin sensitive, we wanted to investigate whether they exhibit hepatic IR. Some investigators revealed that hepatic fat accumulation and hepatic IR can occur without the development of peripheral IR (191,192), results later confirmed by Pasarín *et al*. (134). Hepatic IR contributes to steatosis of NAFLD by impairing insulin signaling at the level of the insulin receptor substrates 1/2 (IRS-1/2), thereby affecting the PI3K/Akt pathway (193). In our study, we found a significant suppression in the genes encoding both IRS-1/2 in the liver of HFHC/GF-fed rats, suggesting hepatic IR in the FIBRO-SH model. Perhaps this explains the endothelial dysfunction observed in the model, since IR plays a role in its mediation by the IRS/PI3K/Akt signaling pathway (194).

The adipose tissue plays an important role in the prevention of hepatic IR, at least in part, through the secretion of the adipokines adiponectin and leptin (195). The activation of AdipoR2, the adiponectin receptor mostly found in the liver, induces PPARα, thereby increasing glucose uptake and fatty acid oxidation (196), and so its downregulation has been implicated in the development of IR (197). Leptin, which is also an anti-steatotic hormone, regulates glucose homeostasis and hepatic insulin sensitivity, as well as food intake and energy expenditures by activating its receptor (LepR) (198,199). In this regard, it has been observed that disruption of hepatic leptin signaling induces metabolic abnormalities (200,201). The 16-week HFHC/GF intervention significantly reduced the gene expression of both AdipoR2 and LepR in the liver, supporting the presence of hepatic IR in the FIBRO-SH model.

In summary, the FIBRO-SH rat model is a preclinical model that exhibits liver-related clinical consequences of NASH in a relatively short period of 16 weeks, and therefore could serve to study advanced stages of the disease and to test anti-fibrotic therapies.

7. CONCLUSIONS

7. CONCLUSIONS

- In a long-term diet-induced rat model of NASH, liver steatosis *per se* is able to induce PH through a direct structural compression of the sinusoidal area, in the absence of other potential contributors to the effect, such as endothelial dysfunction or liver fibrosis.

- The systematic histological image approach used to quantify the sinusoidal area might help at predicting the presence of PH in animal models and patients with NASH.

- Administration of a 9-strain bacterial consortium can ameliorate PH and fibrosis in two *in vivo* models of NASH. This approach could represent a more patient-friendly alternative to FMT as potential therapy for NASH.

- The 16-week HFHC/GF-induced rat model, termed FIBRO-SH rat model, is characterized by the presence of histological NASH with significant PH and liver fibrosis, in addition to endothelial dysfunction promoted by hepatic insulin resistance.

- The FIBRO-SH rat model could be a useful tool to study NASH pathophysiology and anti-fibrotic therapies in advanced stages of the disease.

8. LIMITATIONS AND FUTURE PERSPECTIVES

8. LIMITATIONS AND FUTURE PERSPECTIVES

The main weakness in **study 1** is the lack of validation in patients with NASH. Although there is already evidence of the presence of PH in NAFLD even without fibrosis (44), the ideal proof-of-concept validation in humans should include not only the structural histological quantification of steatosis and sinusoidal area, but also molecular and/or functional measurements of endothelial dysfunction in patients with NAFLD or NASH but without fibrosis and, ideally, proof of change of PP with a decrease in steatosis and increase of sinusoidal area above critical thresholds. This would require dedicated collaborative prospective efforts, but would undoubtedly provide clinically relevant insights on the pathophysiology of NASH and PH.

In **study 2**, the 9-strain bacterial consortium was tested in two rodent models of NASH, both lacking some histological or metabolic aspects of human NASH. The absence of fibrosis in the 8-week diet-induced rat model is a major limitation, as fibrosis stage is considered the best prognostic marker in patients and an important endpoint in clinical trials of NASH. Although the STAM^{TM} mouse model helped to elucidate the effect of the bacterial consortium in terms of liver fibrosis, fibrosis is toxin-induced (STZ) and so this model differs considerably from the etiology and pathogenesis of human NASH. Moreover, the STAM^{TM} mouse model lacks the presence of features related to metabolic syndrome such as obesity. For this reason, an interesting line of research would be to test the bacterial consortium in an animal model that more closely mimics the disease progression, while maintaining the relevance to the human condition, in order to increase the predictive validity when testing novel therapeutic approaches. Therefore, the observed anti-fibrotic effect of the bacterial consortium could be examined in the FIBRO-SH rat model, an experimental model of diet-induced NASH with significant liver fibrosis and PH.

The main limitation regarding **study 3** was that the FIBRO-SH rat model lacked features associated with metabolic syndrome, namely obesity and systemic IR. We attributed this to the sodium cholate supplemented in the diet. This remarks the importance of setting the adequate cholate doses to generate a suitable model that fully represents the pathogenesis of human NASH. In this regard, future perspectives will focus on testing different combinations of dietary cholesterol and cholate to achieve a diet-induced NASH model with features of metabolic syndrome and liver fibrosis, more closely resembling the human disease.

9. BIBLIOGRAPHY

9. BIBLIOGRAPHY

1. Schuppan C, Afdhal NH. Liver Cirrhosis. Lancet. 2008;371(9615):838–51.

2. Asrani SK, Devarbhavi H, Eaton J, Kamath PS. Burden of liver diseases in the world. J Hepatol. 2019;70(1):151–71.

3. Marchesini G, Bugianesi E, Forlani G, Cerrelli F, Lenzi M, Manini R, *et al*. Nonalcoholic fatty liver, steatohepatitis, and the metabolic syndrome. Hepatology. 2003;37(4):917–23.

4. Younossi ZM, Koenig AB, Abdelatif D, Fazel Y, Henry L, Wymer M. Global epidemiology of nonalcoholic fatty liver disease—Meta-analytic assessment of prevalence, incidence, and outcomes. Hepatology. 2016;64(1):73–84.

5. Kim D, Kim WR. Nonobese Fatty Liver Disease. Clin Gastroenterol Hepatol. 2017;15(4):474–85.

6. Ye Q, Zou B, Yeo YH, Li J, Huang DQ, Wu Y, *et al*. Global prevalence, incidence, and outcomes of non-obese or lean non-alcoholic fatty liver disease: a systematic review and meta-analysis. Lancet Gastroenterol Hepatol. 2020;5(8):739–52.

7. Loomba R, Friedman SL, Shulman GI. Mechanisms and disease consequences of nonalcoholic fatty liver disease. Cell. 2021;184(10):2537–64.

8. Byrne CD, Targher G. NAFLD: A multisystem disease. J Hepatol. 2015;62(S1):S47–64.

9. Bessone F, Razori MV, Roma MG. Molecular pathways of nonalcoholic fatty liver disease development and progression. Cell Mol Life Sci. 2019;76(1):99–128.

10. Eslam M, Newsome PN, Sarin SK, Anstee QM, Targher G, Romero-Gomez M, *et al*.

A new definition for metabolic dysfunction-associated fatty liver disease: An international expert consensus statement. J Hepatol. 2020;73(1):202–9.

11. Powell EE, Wong VWS, Rinella M. Non-alcoholic fatty liver disease. Lancet. 2021;397(10290):2212–24.

12. De A, Duseja A. Natural History of Simple Steatosis or Nonalcoholic Fatty Liver. J Clin Exp Hepatol. 2020;10(3):255–62.

13. Liu W, Baker RD, Bhatia T, Zhu L, Baker SS. Pathogenesis of nonalcoholic steatohepatitis. Cell Mol Life Sci. 2016;73(10):1969–87.

14. Zhang X, Ji X, Wang Q, Li JZ. New insight into inter-organ crosstalk contributing to the pathogenesis of non-alcoholic fatty liver disease (NAFLD). Protein Cell. 2018;9(2):164–77.

15. Day CP, James OFW. Steatohepatitis: A tale of two “Hits”? Gastroenterology. 1998;114(4):842–5.

16. Buzzetti E, Pinzani M, Tsochatzis EA. The multiple-hit pathogenesis of non-alcoholic fatty liver disease (NAFLD). Metabolism. 2016;65(8):1038–48.

17. Caligiuri A, Gentilini A, Marra F. Molecular pathogenesis of NASH. Int J Mol Sci. 2016;17(9):1575.

18. Than NN, Newsome PN. A concise review of non-alcoholic fatty liver disease. Atherosclerosis. 2015;239(1):192–202.

19. Bugianesi E, Gastaldelli A, Vanni E, Gambino R, Cassader M, Baldi S, *et al*. Insulin resistance in non-diabetic patients with non-alcoholic fatty liver disease: sites and mechanisms. Diabetologia. 2005;48(4):634–42.

20. Alam S, Mustafa G, Alam M, Ahmad N. Insulin resistance in development and progression of nonalcoholic fatty liver disease. World J Gastrointest Pathophysiol. 2016;7(2):211–7.

21. Guilherme A, Virbasius JV., Puri V, Czech MP. Adipocyte dysfunctions linking obesity to insulin resistance and type 2 diabetes. Nat Rev Mol Cell Biol. 2008;9(5):367–77.

22. Bugianesi E, McCullough AJ, Marchesini G. Insulin resistance: A metabolic pathway to chronic liver disease. Hepatology. 2005;42(5):987–1000.

23. Jou J, Choi SS, Diehl AM. Mechanisms of disease progression in nonalcoholic fatty liver disease. Semin Liver Dis. 2008;28(4):370–9.

24. Méndez-Sánchez N, Arrese M, Zamora-Valdés D, Uribe M. Current concepts in the pathogenesis of nonalcoholic fatty liver disease. Liver Int. 2007;27(4):423–33.

25. Donnelly KL, Smith CI, Schwarzenberg SJ, Jessurun J, Boldt MD, Parks EJ. Sources of fatty acids stored in liver and secreted via lipoproteins in patients with nonalcoholic fatty liver disease. J Clin Invest. 2005;115(5):1343–51.

26. Neuschwander-Tetri BA. Hepatic lipotoxicity and the pathogenesis of nonalcoholic steatohepatitis: The central role of nontriglyceride fatty acid metabolites. Hepatology. 2010;52(2):774–88.

27. Marra F, Svegliati-Baroni G. Lipotoxicity and the gut-liver axis in NASH pathogenesis. J Hepatol. 2018;68(2):280–95.

28. Alves-Bezerra M, Cohen DE. Triglyceride metabolism in the liver. Compr Physiol. 2017;8(1):1–8.

29. Malhi H, Gores GJ. Molecular mechanisms of lipotoxicity in nonalcoholic fatty

liver disease. Semin Liver Dis. 2008;28(4):360–9.

30. Singh R, Kaushik S, Wang Y, Xiang Y, Novak I, Komatsu M, *et al*. Autophagy regulates lipid metabolism. Nature. 2009;458(7242):1131–5.

31. Trauner M, Arrese M, Wagner M. Fatty liver and lipotoxicity. Biochim Biophys Acta - Mol Cell Biol Lipids. 2010;1801(3):299–310.

32. Abdul-Hai A, Abdallah A, Malnick SDH. Influence of gut bacteria on development and progression of non-alcoholic fatty liver disease. World J Hepatol. 2015;7(12):1679–84.

33. Arslan N. Obesity, fatty liver disease and intestinal microbiota. World J Gastroenterol. 2014;20(44):16452–63.

34. Leung C, Rivera L, Furness JB, Angus PW. The role of the gut microbiota in NAFLD. Nat Rev Gastroenterol Hepatol. 2016;13(7):412–25.

35. Lu VB, Gribble FM, Reimann F. Nutrient-induced cellular mechanisms of gut hormone secretion. Nutrients. 2021;13(3):883.

36. Ferreira CM, Vieira AT, Vinolo MAR, Oliveira FA, Curi R, Martins FDS. The Central Role of the Gut Microbiota in Chronic Inflammatory Diseases. J Immunol Res. 2014;2014:689492.

37. Aron-Wisnewsky J, Vigliotti C, Witjes J, Le P, Holleboom AG, Verheij J, *et al*. Gut microbiota and human NAFLD: disentangling microbial signatures from metabolic disorders. Nat Rev Gastroenterol Hepatol. 2020;17(5):279–97.

38. Wong VWS, Tse CH, Lam TTY, Wong GLH, Chim AML, Chu WCW, *et al*. Molecular Characterization of the Fecal Microbiota in Patients with Nonalcoholic Steatohepatitis - A Longitudinal Study. PLoS One. 2013;8(4):e62885.

39. Kolodziejczyk AA, Zheng D, Shibolet O, Elinav E. The role of the microbiome in NAFLD and NASH. EMBO Mol Med. 2019;11(2):e9302.

40. Meroni M, Longo M, Dongiovanni P. The role of probiotics in nonalcoholic fatty liver disease: A new insight into therapeutic strategies. Nutrients. 2019;11(11):2642.

41. Sanyal AJ, Bosch J, Blei A, Arroyo V. Portal Hypertension and Its Complications. Gastroenterology. 2008;134(6):1715–28.

42. Bosch J, Berzigotti A, Garcia-Pagan JC, Abraldes JG. The management of portal hypertension: Rational basis, available treatments and future options. J Hepatol. 2008;48(S1):S68–92.

43. Iwakiri Y. Pathophysiology of portal hypertension. Clin Liver Dis. 2014;18(2):281–91.

44. Francque S, Verrijken A, Mertens I, Hubens G, Van Marck E, Pelckmans P, *et al*. Noncirrhotic human nonalcoholic fatty liver disease induces portal hypertension in relation to the histological degree of steatosis. Eur J Gastroenterol Hepatol. 2010;22(12):1449–57.

45. Hirooka M, Koizumi Y, Miyake T, Ochi H, Tokumoto Y, Tada F, *et al*. Nonalcoholic fatty liver disease: Portal hypertension due to outflow block in patients without cirrhosis. Radiology. 2015;274(2):597–604.

46. Francque S, Wamutu S, Chatterjee S, Van Marck E, Herman A, Ramon A, *et al*. Non-alcoholic steatohepatitis induces non-fibrosis-related portal hypertension associated with splanchnic vasodilation and signs of a hyperdynamic circulation in vitro and in vivo in a rat model. Liver Int. 2010;30(3):365–75.

47. Mendes FD, Suzuki A, Sanderson SO, Lindor KD, Angulo P. Prevalence and Indicators of Portal Hypertension in Patients With Nonalcoholic Fatty Liver Disease. Clin Gastroenterol Hepatol. 2012;10(9):1028–33.

48. Bosch J, Abraldes JG, Fernández M, García-Pagán JC. Hepatic endothelial dysfunction and abnormal angiogenesis: New targets in the treatment of portal hypertension. J Hepatol. 2010;53(3):558–67.

49. Pasarín M, La Mura V, Gracia-Sancho J, García-Calderó H, Rodríguez-Vilarrupla A, García-Pagán JC, *et al*. Sinusoidal endothelial dysfunction precedes inflammation and fibrosis in a model of NAFLD. PLoS One. 2012;7(4):e32785.

50. García-Lezana T, Raurell I, Bravo M, Torres-Arauz M, Salcedo MT, Santiago A, *et al*. Restoration of a healthy intestinal microbiota normalizes portal hypertension in a rat model of nonalcoholic steatohepatitis. Hepatology. 2018;67(4):1485–98.

51. Puoti C, Bellis L. Steatosis and portal hypertension. Eur Rev Med Pharmacol Sci. 2005;9(5):285–90.

52. Van der Graaff D, Kwanten WJ, Couturier FJ, Govaerts JS, Verlinden W, Brosius I, *et al*. Severe steatosis induces portal hypertension by systemic arterial hyporeactivity and hepatic vasoconstrictor hyperreactivity in rats. Lab Invest. 2018;98(10):1263–75.

53. Farrell GC, Teoh NC, McCuskey RS. Hepatic microcirculation in fatty liver disease. The Anatomical Record: Adv Integrative Anatomy Evolutionary Biol. 2008;291(6):684–92.

54. Ijaz S, Yang W, Winslet MC, Seifalian AM. Impairment of hepatic microcirculation in fatty liver. Microcirculation. 2003;10(6):447–56.

55. Tsochatzis EA, Bosch J, Burroughs AK. Liver cirrhosis. Lancet. 2014;383(9930):1749–61.

56. García-Pagán JC, Gracia-Sancho J, Bosch J. Functional aspects on the pathophysiology of portal hypertension in cirrhosis. J Hepatol. 2012;57(2):458–61.

57. Hammoutene A, Rautou PE. Role of liver sinusoidal endothelial cells in non-alcoholic fatty liver disease. J Hepatol. 2019;70(6):1278–91.

58. Iwakiri Y, Shah V, Rockey DC. Vascular pathobiology in chronic liver disease and cirrhosis - Current status and future directions. J Hepatol. 2014;61(4):912–24.

59. Fernández-Iglesias A, Gracia-Sancho J. How to face chronic liver disease: The sinusoidal perspective. Front Med. 2017;4:7.

60. Iwakiri Y. Endothelial dysfunction in the regulation of cirrhosis and portal hypertension. Liver Int. 2012;32(2):199–213.

61. Nasiri-Ansari N, Androutsakos T, Flessa CM, Kyrou I, Siasos G, Randeva HS, *et al*. Endothelial Cell Dysfunction and Nonalcoholic Fatty Liver Disease (NAFLD): A Concise Review. Cells. 2022;11(16):2511.

62. Poisson J, Lemoinne S, Boulanger C, Durand F, Moreau R, Valla D, *et al*. Liver sinusoidal endothelial cells: Physiology and role in liver diseases. J Hepatol. 2017;66(1):212–27.

63. Iwakiri Y, Kim MY. Nitric oxide in liver diseases. Trends Pharmacol Sci. 2015;36(8):524–36.

64. DeLeve LD, Wang X, Hu L, McCuskey MK, McCuskey RS. Rat liver sinusoidal endothelial cell phenotype is maintained by paracrine and autocrine regulation.

Am J Physiol - Gastrointest Liver Physiol. 2004;287(4):G757–63.

65. Xie G, Wang X, Wang L, Wang L, Atkinson RD, Kanel GC, *et al*. Role of differentiation of liver sinusoidal endothelial cells in progression and regression of hepatic fibrosis in rats. Gastroenterology. 2012;142(4):918-27.e6.

66. Searles CD. Transcriptional and posttranscriptional regulation of endothelial nitric oxide synthase expression. Am J Physiol - Cell Physiol. 2006;291(5):C803–16.

67. Atkins GB, Jain MK. Role of Krüppel-like transcription factors in endothelial biology. Circ Res. 2007;100(12):1686–95.

68. Iwakiri Y, Tsai MH, McCabe TJ, Gratton JP, Fulton D, Groszmann RJ, *et al*. Phosphorylation of eNOS initiates excessive NO production in early phases of portal hypertension. Am J Physiol - Hear Circ Physiol. 2002;282(6):H2084–90.

69. Dimmeler S, Fleming I, Fisslthaler B, Hermann C, Busse R, Zeiher AM. Activation of nitric oxide synthase in endothelial cells by Akt- dependent phosphorylation. Nature. 1999;399(6736):601–5.

70. Pasarín M, Abraldes JG, Liguori E, Kok B, La Mura V. Intrahepatic vascular changes in non-alcoholic fatty liver disease: Potential role of insulin-resistance and endothelial dysfunction. World J Gastroenterol. 2017;23(37):6777–87.

71. Nevzorova YA, Boyer-Diaz Z, Cubero FJ, Gracia-Sancho J. Animal models for liver disease – A practical approach for translational research. J Hepatol. 2020;73(2):423–40.

72. Santhekadur PK, Kumar DP, Sanyal AJ. Preclinical models of non-alcoholic fatty liver disease. J Hepatol. 2018;68(2):230–7.

73. Hansen HH, Feigh M, Veidal SS, Rigbolt KT, Vrang N, Fosgerau K. Mouse models

of nonalcoholic steatohepatitis in preclinical drug development. Drug Discov Today. 2017;22(11):1707–18.

74. Ahima RS, Flier JS. Leptin. Annu Rev Physiol. 2000;62:413–37.

75. Denk H, Abuja PM, Zatloukal K. Animal models of NAFLD from the pathologist's point of view. Biochim Biophys Acta - Mol Basis Dis. 2019;1865(5):929–42.

76. Trak-Smayra V, Paradis V, Massart J, Nasser S, Jebara V, Fromenty B. Pathology of the liver in obese and diabetic ob/ob and db/db mice fed a standard or high-calorie diet. Int J Exp Pathol. 2011;92(6):413–21.

77. Leclercq IA, Farrell GC, Schriemer R, Robertson GR. Leptin is essential for the hepatic fibrogenic response to chronic liver injury. J Hepatol. 2002;37(2):206–13.

78. Sahai A, Malladi P, Pan X, Paul R, Melin-Aldana H, Green RM, *et al*. Obese and diabetic db/db mice develop marked liver fibrosis in a model of nonalcoholic steatohepatitis: Role of short-form leptin receptors and osteopontin. Am J Physiol - Gastrointest Liver Physiol. 2004;287(5):G1035-43.

79. Carmiel-Haggai M, Cederbaum AI, Nieto N. A high-fat diet leads to the progression of non-alcoholic fatty liver disease in obese rats. FASEB J. 2005;19(1):136–8.

80. Chalasani N, Crabb DW, Cummings OW, Kwo PY, Asghar A, Pandya PK, *et al*. Does leptin play a role in the pathogenesis of human nonalcoholic steatohepatitis? Am J Gastroenterol. 2003;98(12):2771–6.

81. Polyzos SA, Kountouras J, Mantzoros CS. Leptin in nonalcoholic fatty liver disease: A narrative review. Metabolism. 2015;64(1):60–78.

82. Schattenberg JM, Galle PR. Animal models of non-alcoholic steatohepatitis: Of

mice and man. Dig Dis. 2010;28(1):247–54.

83. Carreres L, Jílková ZM, Vial G, Marche PN, Decaens T, Lerat H. Modeling diet-induced NAFLD and NASH in rats: A comprehensive review. Biomedicines. 2021;9(4):378.

84. Veteläinen R, Van Vliet A, Van Gulik TM. Essential pathogenic and metabolic differences in steatosis induced by choline or methione-choline deficient diets in a rat model. J Gastroenterol Hepatol. 2007;22(9):1526–33.

85. Rinella ME, Green RM. The methionine-choline deficient dietary model of steatohepatitis does not exhibit insulin resistance. J Hepatol. 2004;40(1):47–51.

86. Van Herck MA, Vonghia L, Francque SM. Animal models of nonalcoholic fatty liver disease—a starter's guide. Nutrients. 2017;9(10):1072.

87. Matsumoto M, Hada N, Sakamaki Y, Uno A, Shiga T, Tanaka C, *et al*. An improved mouse model that rapidly develops fibrosis in non-alcoholic steatohepatitis. Int J Exp Pathol. 2013;94(2):93–103.

88. Jahn D, Kircher S, Hermanns HM, Geier A. Animal models of NAFLD from a hepatologist's point of view. Biochim Biophys Acta - Mol Basis Dis. 2019;1865(5):943–53.

89. Lieber CS, Leo MA, Mak KM, Xu Y, Cao Q, Ren C, *et al*. Model of nonalcoholic steatohepatitis. Am J Clin Nutr. 2004;79(3):502–9.

90. Rosenstengel S, Stoeppeler S, Bahde R, Spiegel HU, Palmes D. Type of steatosis influences microcirculation and fibrogenesis in different rat strains. J Investig Surg. 2011;24(6):273–82.

91. Stöppeler S, Palmes D, Fehr M, Hölzen JP, Zibert A, Siaj R, *et al*. Gender and strain-

specific differences in the development of steatosis in rats. Lab Anim. 2013 Jan;47(1):43–52.

92. Hewitt KN, Pratis K, Jones MEE, Simpson ER. Estrogen replacement reverses the hepatic steatosis phenotype in the male aromatase knockout mouse. Endocrinology. 2004;145(4):1842–8.

93. Ipsen DH, Lykkesfeldt J, Tveden-Nyborg P. Animal Models of Fibrosis in Nonalcoholic Steatohepatitis: Do They Reflect Human Disease? Adv Nutr. 2020;11(6):1696–711.

94. Jeong WI, Jeong DH, Do SH, Kim YK, Park HY, Kwon OD, *et al*. Mild hepatic fibrosis in cholesterol and sodium cholate diet-fed rats. J Vet Med Sci. 2005;67(3):235–42.

95. Matsuzawa N, Takamura T, Kurita S, Misu H, Ota T, Ando H, *et al*. Lipid-induced oxidative stress causes steatohepatitis in mice fed an atherogenic diet. Hepatology. 2007;46(5):1392–403.

96. Abdelmalek MF, Suzuki A, Guy C, Unalp-Arida A, Colvin R, Johnson RJ, *et al*. Increased fructose consumption is associated with fibrosis severity in patients with nonalcoholic fatty liver disease. Hepatology. 2010;51(6):1961–71.

97. Kohli R, Kirby M, Xanthakos SA, Softic S, Feldstein AE, Saxena V, *et al*. High-fructose, medium chain trans fat diet induces liver fibrosis and elevates plasma coenzyme Q9 in a novel murine model of obesity and nonalcoholic steatohepatitis. Hepatology. 2010;52(3):934–44.

98. Ventura EE, Davis JN, Goran MI. Sugar content of popular sweetened beverages based on objective laboratory analysis: Focus on fructose content. Obesity. 2011;19(4):868–74.

99. Lim JS, Mietus-Snyder M, Valente A, Schwarz JM, Lustig RH. The role of fructose in the pathogenesis of NAFLD and the metabolic syndrome. Nat Rev Gastroenterol Hepatol. 2010;7(5):251–64.

100. Jensen T, Abdelmalek MF, Sullivan S, Nadeau KJ, Green M, Roncal C, *et al*. Fructose and sugar: A major mediator of non-alcoholic fatty liver disease. J Hepatol. 2018;68(5):1063–75.

101. Spruss A, Kanuri G, Wagnerberger S, Haub S, Bischoff SC, Bergheim I. Toll-like receptor 4 is involved in the development of fructose-induced hepatic steatosis in mice. Hepatology. 2009;50(4):1094–104.

102. Lambertz J, Weiskirchen S, Landert S, Weiskirchen R. Fructose: A dietary sugar in crosstalk with microbiota contributing to the development and progression of non-alcoholic liver disease. Front Immunol. 2017;8:1159.

103. Hintze KJ, Benninghoff AD, Cho CE, Ward RE. Modeling the western diet for preclinical investigations. Adv Nutr. 2018;9(3):263–71.

104. Le Chatelier E, Nielsen T, Qin J, Prifti E, Hildebrand F, Falony G, *et al*. Richness of human gut microbiome correlates with metabolic markers. Nature. 2013;500(7464):541–6.

105. Lo L, McLennan SV., Williams PF, Bonner J, Chowdhury S, McCaughan GW, *et al*. Diabetes is a progression factor for hepatic fibrosis in a high fat fed mouse obesity model of non-alcoholic steatohepatitis. J Hepatol. 2011;55(2):435–44.

106. Fujii M, Shibazaki Y, Wakamatsu K, Honda Y, Kawauchi Y, Suzuki K, *et al*. A murine model for non-alcoholic steatohepatitis showing evidence of association between diabetes and hepatocellular carcinoma. Med Mol Morphol. 2013;46(3):141–52.

107. Vilar-Gomez E, Martinez-Perez Y, Calzadilla-Bertot L, Torres-Gonzalez A, Gra-Oramas B, Gonzalez-Fabian L, *et al*. Weight loss through lifestyle modification significantly reduces features of nonalcoholic steatohepatitis. Gastroenterology. 2015;149(2):367-378.e5.

108. Friedman SL, Neuschwander-Tetri BA, Rinella M, Sanyal AJ. Mechanisms of NAFLD development and therapeutic strategies. Nat Med. 2018;24(7):908-22.

109. Sanyal AJ, Chalasani N, Kowdley KV., McCullough A, Diehl AM, Bass NM, *et al*. Pioglitazone, Vitamin E, or Placebo for Nonalcoholic Steatohepatitis. N Engl J Med. 2010;362(18):1675–85.

110. Cusi K, Orsak B, Bril F, Lomonaco R, Hecht J, Ortiz-Lopez C, *et al*. Long-term pioglitazone treatment for patients with nonalcoholic steatohepatitis and prediabetes or type 2 diabetes mellitus a randomized trial. Ann Intern Med. 2016;165(5):305–15.

111. Armstrong MJ, Hull D, Guo K, Barton D, Hazlehurst JM, Gathercole LL, *et al*. Glucagon-like peptide 1 decreases lipotoxicity in non-alcoholic steatohepatitis. J Hepatol. 2016;64(2):399–408.

112. Sinha RA, Bruinstroop E, Singh BK, Yen PM. Nonalcoholic fatty liver disease and hypercholesterolemia: Roles of thyroid hormones, metabolites, and agonists. Thyroid. 2019;29(9):1173–91.

113. Sato K, Gosho M, Yamamoto T, Kobayashi Y, Ishii N, Ohashi T, *et al*. Vitamin E has a beneficial effect on nonalcoholic fatty liver disease: A meta-analysis of randomized controlled trials. Nutrition. 2015;31(7–8):923–30.

114. Wiest R, Albillos A, Trauner M, Bajaj JS, Jalan R. Targeting the gut-liver axis in liver disease. J Hepatol. 2017;67(5):1084–103.

115. Lang S, Schnabl B. Microbiota and Fatty Liver Disease—the Known, the Unknown, and the Future. Cell Host Microbe. 2020;28(2):233–44.

116. Abdel-Razik A, Mousa N, Shabana W, Refaey M, Elzehery R, Elhelaly R, *et al*. Rifaximin in nonalcoholic fatty liver disease: Hit multiple targets with a single shot. Eur J Gastroenterol Hepatol. 2018;30(10):1237–46.

117. Younossi ZM, Ratziu V, Loomba R, Rinella M, Anstee QM, Goodman Z, *et al*. Obeticholic acid for the treatment of non-alcoholic steatohepatitis: interim analysis from a multicentre, randomised, placebo-controlled phase 3 trial. Lancet. 2019;394(10215):2184–96.

118. Park JG, Mok JS, Han YI, Park TS, Kang KW, Choi CS, *et al*. Connectivity mapping of angiotensin-PPAR interactions involved in the amelioration of non-alcoholic steatohepatitis by Telmisartan. Sci Rep. 2019;9(1):4003.

119. Kleiner DE, Brunt EM, Van Natta M, Behling C, Contos MJ, Cummings OW, *et al*. Design and validation of a histological scoring system for nonalcoholic fatty liver disease. Hepatology. 2005;41(6):1313–21.

120. Hall A, Covelli C, Manuguerra R, Luong TV, Buzzetti E, Tsochatzis E, *et al*. Transaminase abnormalities and adaptations of the liver lobule manifest at specific cut-offs of steatosis. Sci Rep. 2017;7(40977):1–9.

121. Thoendel M, Jeraldo P, Greenwood-Quaintance KE, Yao J, Chia N, Hanssen AD, *et al*. Comparison of three commercial tools for metagenomic shotgun sequencing analysis. J Clin Microbiol. 2020;58(3):e00981-19.

122. Franzosa EA, McIver LJ, Rahnavard G, Thompson LR, Schirmer M, Weingart G, *et al*. Species-level functional profiling of metagenomes and metatranscriptomes. Nat Methods. 2018;15(11):962–8.

123. McMurdie PJ, Holmes S. Phyloseq: An R Package for Reproducible Interactive Analysis and Graphics of Microbiome Census Data. PLoS One. 2013;8(4):e61217.

124. Rohart F, Gautier B, Singh A, Lê Cao KA. mixOmics: An R package for 'omics feature selection and multiple data integration. PLoS Comput Biol. 2017;13(11):e1005752.

125. Liao Y, Smyth GK, Shi W. FeatureCounts: An efficient general purpose program for assigning sequence reads to genomic features. Bioinformatics. 2014;30(7):923–30.

126. Anders S, Huber W. Differential expression analysis for sequence count data. Genome Biol. 2010;11(10):R106.

127. Thévenot EA, Roux A, Xu Y, Ezan E, Junot C. Analysis of the Human Adult Urinary Metabolome Variations with Age, Body Mass Index, and Gender by Implementing a Comprehensive Workflow for Univariate and OPLS Statistical Analyses. J Proteome Res. 2015;14(8):3322–35.

128. Wu T, Hu E, Xu S, Chen M, Guo P, Dai Z, *et al*. clusterProfiler 4.0: A universal enrichment tool for interpreting omics data. Innov. 2021;2(3):100141.

129. Martens M, Ammar A, Riutta A, Waagmeester A, Slenter DN, Hanspers K, *et al*. WikiPathways: Connecting communities. Nucleic Acids Res. 2021;49(D1):D613–21.

130. Karp PD, Riley M, Paley SM, Pellegrini-Toole A. The MetaCyc database. Nucleic Acids Res. 2002;30(1):59–61.

131. Jassal B, Matthews L, Viteri G, Gong C, Lorente P, Fabregat A, *et al*. The reactome pathway knowledgebase. Nucleic Acids Res. 2020;48(D1):D498–503.

132. Nishimura D. A view from the web BioCarta. Biotech Softw Internet Rep. 2001;2(3):117–20.

133. Rouillard AD, Gundersen GW, Fernandez NF, Wang Z, Monteiro CD, McDermott MG, *et al*. The harmonizome: a collection of processed datasets gathered to serve and mine knowledge about genes and proteins. Database. 2016;2016:baw100.

134. Pasarín M, Abraldes JG, Rodríguez-Vilarrupla A, La Mura V, García-Pagán JC, Bosch J. Insulin resistance and liver microcirculation in a rat model of early NAFLD. J Hepatol. 2011;55(5):1095–102.

135. Bravo M, Raurell I, Hide D, Fernández-Iglesias A, Gil M, Barberá A, *et al*. Restoration of liver sinusoidal cell phenotypes by statins improves portal hypertension and histology in rats with NASH. Sci Rep. 2019;9(1):20183.

136. Febbraio MA, Reibe S, Shalapour S, Ooi GJ, Watt MJ, Karin M. Perspective Preclinical Models for Studying NASH-Driven HCC : How Useful Are They ? Cell Metab. 2019;29(1):18–26.

137. Younossi ZM. Non-alcoholic fatty liver disease – A global public health perspective. J Hepatol. 2019;70(3):531–44.

138. Rodrigues SG, Montani M, Guixé-Muntet S, De Gottardi A, Berzigotti A, Bosch J. Patients With Signs of Advanced Liver Disease and Clinically Significant Portal Hypertension Do Not Necessarily Have Cirrhosis. Clin Gastroenterol Hepatol. 2019;17(10):2101-2109.e1.

139. Blendis LM. Hepatocyte swelling and portal hypertension. J Hepatol. 1992;15(1–2):4–5.

140. Vidins EI, Britton RS, Medline A, Blendis LM, Israel Y, Orrego H. Sinusoidal caliber

in alcoholic and nonalcoholic liver disease: Diagnostic and pathogenic implications. Hepatology. 1985;5(3):408–14.

141. Israel Y, Orrego H, Colman JC, Britton RS. Alcohol-induced hepatomegaly: pathogenesis and role in the production of portal hypertension. Fed Proc. 1982;41(8):2472–7.

142. Francque S, Laleman W, Verbeke L, Van Steenkiste C, Casteleyn C, Kwanten W, *et al*. Increased intrahepatic resistance in severe steatosis: Endothelial dysfunction, vasoconstrictor overproduction and altered microvascular architecture. Lab Invest. 2012;92(10):1428–39.

143. Witek RP, Yang L, Liu R, Jung Y, Omenetti A, Syn WK, *et al*. Liver Cell-Derived Microparticles Activate Hedgehog Signaling and Alter Gene Expression in Hepatic Endothelial Cells. Gastroenterology. 2009;136(1):320–30.

144. Xie G, Choi SS, Syn WK, Michelotti GA, Swiderska M, Karaca G, *et al*. Hedgehog signalling regulates liver sinusoidal endothelial cell capillarisation. Gut. 2013;62(2):299–309.

145. Guy CD, Suzuki A, Zdanowicz M, Abdelmalek MF, Burchette J, Unalp A, *et al*. Hedgehog pathway activation parallels histologic severity of injury and fibrosis in human nonalcoholic fatty liver disease. Hepatology. 2012;55(6):1711–21.

146. Rangwala F, Guy CD, Lu J, Suzuki A, Burchette JL, Abdelmalek MF, *et al*. Increased production of sonic hedgehog by ballooned hepatocytes. J Pathol. 2011;224(3):401–10.

147. Estep M, Mehta R, Bratthauer G, Alaparthi L, Monge F, Ali S, *et al*. Hepatic sonic hedgehog protein expression measured by computer assisted morphometry significantly correlates with features of non-alcoholic steatohepatitis. BMC

Gastroenterol. 2019;19(1):27.

148. Lefere S, Van de Velde F, Hoorens A, Raevens S, Van Campenhout S, Vandierendonck A, *et al*. Angiopoietin-2 Promotes Pathological Angiogenesis and Is a Therapeutic Target in Murine Nonalcoholic Fatty Liver Disease. Hepatology. 2019;69(3):1087–104.

149. Berzigotti A, Albillos A, Villanueva C, Genescà J, Ardevol A, Augustin S, *et al*. Effects of an Intensive Lifestyle Intervention Program on Portal Hypertension in Patients With Cirrhosis and Obesity: The SportDiet Study. Hepatology. 2017;65(4):1293–1305.

150. Harrison SA, Abdelmalek MF, Caldwell S, Shiffman ML, Diehl AM, Ghalib R, *et al*. Simtuzumab Is Ineffective for Patients With Bridging Fibrosis or Compensated Cirrhosis Caused by Nonalcoholic Steatohepatitis. Gastroenterology. 2018;155(4):1140–53.

151. Garcia-Tsao G, Bosch J, Kayali Z, Harrison SA, Abdelmalek MF, Lawitz E, *et al*. Randomized placebo-controlled trial of emricasan for non-alcoholic steatohepatitis-related cirrhosis with severe portal hypertension. J Hepatol. 2020;72(5):885–95.

152. Miele L, Valenza V, La Torre G, Montalto M, Cammarota G, Ricci R, *et al*. Increased intestinal permeability and tight junction alterations in nonalcoholic fatty liver disease. Hepatology. 2009;49(6):1877–87.

153. Dai X, Hou H, Zhang W, Liu T, Li Y, Wang S, *et al*. Microbial Metabolites: Critical Regulators in NAFLD. Front Microbiol. 2020;11:567654.

154. Ebrahimzadeh Leylabadlo H, Ghotaslou R, Samadi Kafil H, Feizabadi MM, Moaddab SY, Farajnia S, *et al*. Non-alcoholic fatty liver diseases: from role of gut

microbiota to microbial-based therapies. Eur J Clin Microbiol Infect Dis. 2020;39(4):613–27.

155. Philips CA, Pande A, Shasthry SM, Jamwal KD, Khillan V, Chandel SS, *et al*. Healthy Donor Fecal Microbiota Transplantation in Steroid-Ineligible Severe Alcoholic Hepatitis: A Pilot Study. Clin Gastroenterol Hepatol. 2017;15(4):600–2.

156. Li Z, Yang S, Lin H, Huang J, Watkins PA, Moser AB, *et al*. Probiotics and antibodies to TNF inhibit inflammatory activity and improve nonalcoholic fatty liver disease. Hepatology. 2003;37(2):343–50.

157. Xue L, He J, Gao N, Lu X, Li M, Wu X, *et al*. Probiotics may delay the progression of nonalcoholic fatty liver disease by restoring the gut microbiota structure and improving intestinal endotoxemia. Sci Rep. 2017;7(1):45176.

158. Kobyliak N, Abenavoli L, Mykhalchyshyn G, Kononenko L, Boccuto L, Kyriienko D, *et al*. A multi-strain probiotic reduces the fatty liver index, cytokines and aminotransferase levels in NAFLD patients: Evidence from a randomized clinical trial. J Gastrointestin Liver Dis. 2018;27(1):41–9.

159. Hu H, Lin A, Kong M, Yao X, Yin M, Xia H, *et al*. Intestinal microbiome and NAFLD: molecular insights and therapeutic perspectives. J Gastroenterol. 2020;55(2):142–58.

160. Timmerman HM, Koning CJM, Mulder L, Rombouts FM, Beynen AC. Monostrain, multistrain and multispecies probiotics - A comparison of functionality and efficacy. Int J Food Microbiol. 2004;96(3):219–33.

161. Marrone G, Russo L, Rosado E, Hide D, García-Cardeña G, García-Pagán JC, *et al*. The transcription factor KLF2 mediates hepatic endothelial protection and paracrine endothelial-stellate cell deactivation induced by statins. J Hepatol.

2013;58(1):98–103.

162. Marrone G, Maeso-Díaz R, García-Cardena G, Abraldes JG, García-Pagán JC, Bosch J, *et al*. KLF2 exerts antifibrotic and vasoprotective effects in cirrhotic rat livers: Behind the molecular mechanisms of statins. Gut. 2015;64(9):1434–43.

163. Campollo O, Sprengers D, McIntyre N. The BCAA/AAA ratio of plasma amino acids in three different groups of cirrhotics. Rev Invest Clin. 1992;44(4):513–8.

164. Iwao M, Gotoh K, Arakawa M, Endo M, Honda K, Seike M, *et al*. Supplementation of branched-chain amino acids decreases fat accumulation in the liver through intestinal microbiota-mediated production of acetic acid. Sci Rep. 2020;10(1):18768.

165. Raghunath A, Panneerselvam L, Sundarraj K, Perumal E. Heat Shock Proteins and Endoplasmic Reticulum Stress. Heat Shock Proteins and Stress. 2018;15:39–78.

166. Zhang XQ, Xu CF, Yu CH, Chen WX, Li YM. Role of endoplasmic reticulum stress in the pathogenesis of nonalcoholic fatty liver disease. World J Gastroenterol. 2014;20(7):1768–76.

167. Seelig S, Liaw C, Towle HC, Oppenheimer JH. Thyroid hormone attenuates and augments hepatic gene expression at a pretranslational level. Proc Natl Acad Sci U S A. 1981;78(8):4733–7.

168. Cunningham BA, Moncur JT, Huntington JT, Kinlaw WB. "Spot 14" Protein: A Metabolic Integrator in Normal and Neoplastic Cells. Thyroid. 1998;8(9):815–25.

169. Jump DB, Bell A, Lepar G, Hu D. Insulin rapidly induces rat liver S14 gene transcription. Mol Endocrinol. 1990;4(11):1655–60.

170. Chen YT, Tseng PH, Tseng FY, Chi YC, Han DS, Yang WS. The serum level of a novel

lipogenic protein Spot 14 was reduced in metabolic syndrome. PLoS One. 2019;14(2):e0212341.

171. Ortega FJ, Vazquez-Martin A, Moreno-Navarrete JM, Bassols J, Rodriguez-Hermosa J, Gironés J, *et al*. Thyroid hormone responsive Spot 14 increases during differentiation of human adipocytes and its expression is down-regulated in obese subjects. Int J Obes. 2010;34(3):487–99.

172. Cannito S, Novo E, Parola M. Therapeutic pro-fibrogenic signaling pathways in fibroblasts. Adv Drug Deliv Rev. 2017;121:57–84.

173. Tsutsui M, Tanaka N, Kawakubo M, Sheena Y, Horiuchi A, Komatsu M, *et al*. Serum fragmented cytokeratin 18 levels reflect the histologic activity score of nonalcoholic fatty liver disease more accurately than serum alanine aminotransferase levels. J Clin Gastroenterol. 2010;44(6):440–7.

174. Zhou D, Pan Q, Xin FZ, Zhang RN, He CX, Chen GY, *et al*. Sodium butyrate attenuates high-fat diet-induced steatohepatitis in mice by improving gut microbiota and gastrointestinal barrier. World J Gastroenterol. 2017;23(1):60–75.

175. Endo H, Niioka M, Kobayashi N, Tanaka M, Watanabe T. Butyrate-Producing Probiotics Reduce Nonalcoholic Fatty Liver Disease Progression in Rats: New Insight into the Probiotics for the Gut-Liver Axis. PLoS One. 2013;8(5):e63388.

176. Schwiertz A, Taras D, Schäfer K, Beijer S, Bos NA, Donus C, *et al*. Microbiota and SCFA in lean and overweight healthy subjects. Obesity. 2010;18(1):190–5.

177. Chambers ES, Viardot A, Psichas A, Morrison DJ, Murphy KG, Zac-Varghese SEK, *et al*. Effects of targeted delivery of propionate to the human colon on appetite regulation, body weight maintenance and adiposity in overweight adults. Gut.

2015;64(11):1744–54.

178. Sikalidis AK, Maykish A. The Gut Microbiome and Type 2 Diabetes Mellitus: Discussing A Complex Relationship. Biomedicines. 2020;8(1):8.

179. Ackroff K, Sclafani A. Rats' preferences for high fructose corn syrup vs. sucrose and sugar mixtures. Physiol Behav. 2011;102(5):548–52.

180. Ichimura M, Kawase M, Masuzumi M, Sakaki M, Nagata Y, Tanaka K, *et al*. High-fat and high-cholesterol diet rapidly induces non-alcoholic steatohepatitis with advanced fibrosis in Sprague-Dawley rats. Hepatol Res. 2015;45(4):458–69.

181. Ioannou GN, Morrow OB, Connole ML, Lee SP. Association between dietary nutrient composition and the incidence of cirrhosis or liver cancer in the United States population. Hepatology. 2009;50(1):175–84.

182. De Aguiar Vallim TQ, Tarling EJ, Edwards PA. Pleiotropic roles of bile acids in metabolism. Cell Metab. 2013;17(5):657–69.

183. Ichimura-Shimizu M, Watanabe S, Kashirajima Y, Nagatomo A, Wada H, Tsuneyama K, *et al*. Dietary Cholic Acid Exacerbates Liver Fibrosis in NASH Model of Sprague–Dawley Rats Fed a High-Fat and High-Cholesterol Diet. Int J Mol Sci. 2022;23(16):9268.

184. Vergnes L, Phan J, Strauss M, Tafuri S, Reue K. Cholesterol and Cholate Components of an Atherogenic Diet Induce Distinct Stages of Hepatic Inflammatory Gene Expression. J Biol Chem. 2003;278(44):42774–84.

185. Sourianarayanane A, Talluri J, Humar A, McCullough AJ. Stage of fibrosis and portal pressure correlation in nonalcoholic steatohepatitis. Eur J Gastroenterol Hepatol. 2017;29(5):516–23.

186. Sanyal AJ, Harrison SA, Ratziu V, Abdelmalek MF, Diehl AM, Caldwell S, *et al*. The Natural History of Advanced Fibrosis Due to Nonalcoholic Steatohepatitis: Data From the Simtuzumab Trials. Hepatology. 2019;70(6):1913–27.

187. Watanabe M, Houten SM, Wang L, Moschetta A, Mangelsdorf DJ, Heyman RA, *et al*. Bile acids lower triglyceride levels via a pathway involving FXR, SHP, and SREBP-1c. J Clin Invest. 2004;113(10):1408–18.

188. Choudhary NS, Duseja A, Kalra N, Das A, Dhiman RK, Chawla YK. Correlation of adipose tissue with liver histology in Asian Indian patients with nonalcoholic fatty liver disease (NAFLD). Ann Hepatol. 2012;11(4):478–86.

189. Ikemoto S, Takahashi M, Tsunoda N, Maruyama K, Itakura H, Kawanaka K, *et al*. Cholate inhibits high-fat diet-induced hyperglycemia and obesity with acyl-CoA synthetase mRNA decrease. Am J Physiol. 1997;273(1 Pt 1):E37–45.

190. Watanabe M, Houten SM, Mataki C, Christoffolete MA, Kim BW, Sato H, *et al*. Bile acids induce energy expenditure by promoting intracellular thyroid hormone activation. Nature. 2006;439(7075):484–9.

191. Kim JK, Fillmore JJ, Chen Y, Yu C, Moore IK, Pypaert M, *et al*. Tissue-specific overexpression of lipoprotein lipase causes tissue-specific insulin resistance. Proc Natl Acad Sci U S A. 2001;98(13):7522–7.

192. Kraegen EW, Clark PW, Jenkins AB, Daley EA, Chisholm DJ, Storlien LH. Development of muscle insulin resistance after liver insulin resistance in high-fat-fed rats. Diabetes. 1991;40(11):1397–403.

193. Samuel VT, Liu ZX, Qu X, Elder BD, Bilz S, Befroy D, *et al*. Mechanism of hepatic insulin resistance in non-alcoholic fatty liver disease. J Biol Chem. 2004;279(31):32345–53.

194. Muniyappa R, Sowers JR. Role of insulin resistance in endothelial dysfunction. Rev Endocr Metab Disord. 2013;14(1):5–12.

195. Li Y, Ding L, Hassan W, Abdelkader D, Shang J. Adipokines and hepatic insulin resistance. J Diabetes Res. 2013;2013:170532.

196. Kadowaki T, Yamauchi T, Kubota N, Hara K, Ueki K, Tobe K. Adiponectin and adiponectin receptors in insulin resistance, diabetes, and the metabolic syndrome. J Clin Invest. 2006;116(7):1784–92.

197. Yamauchi T, Nio Y, Maki T, Kobayashi M, Takazawa T, Iwabu M, *et al*. Targeted disruption of AdipoR1 and AdipoR2 causes abrogation of adiponectin binding and metabolic actions. Nat Med. 2007;13(3):332–9.

198. Amitani M, Asakawa A, Amitani H, Inui A. The role of leptin in the control of insulin-glucose axis. Front Neurosci. 2013;7:51.

199. Gamarra JR, Haeusler RA. Hepatocentric Leptin Signaling Modulates Gluconeogenesis via MKP-3. Cell Mol Gastroenterol Hepatol. 2022;14(5):1166–7.

200. Levi J, Gray SL, Speck M, Huynh FK, Babich SL, Gibson WT, *et al*. Acute disruption of leptin signaling in vivo leads to increased insulin levels and insulin resistance. Endocrinology. 2011;152(9):3385–95.

201. Huynh FK, Neumann UH, Wang Y, Rodrigues B, Kieffer TJ, Covey SD. A role for hepatic leptin signaling in lipid metabolism via altered very low density lipoprotein composition and liver lipase activity in mice. Hepatology. 2013;57(2):543–54.

10. APPENDIX

10. APPENDIX

10.1. Appendix 1. Buffers and reagents

Sirius red 0.1%

0.36 mM Direct Red 80: 0.5 g

500 mL saturated (1.3% in H_2O) aqueous solution of picric acid

Acidified water (1 L)

5 mL acetic acid glacial

995 mL dH_2O

Triton-lysis buffer (1 mL)

200 µL TBS 5X

50 µL NaPPi 0.2 M (sodium pyrophosphate tetrabasic)

40 µL NaF 0.5 M (sodium fluoride)

100 µL Tritox™ 10%

10 µL SOV 200 mM (sodium orthovanadate)

10 µL A Ok (okadaic acid)

12 µL PIM 1 µM (protein inhibitors mix)

4 µL PMSF (phenylmethylsulfonyl fluoride)

574 µL dH_2O

Tris-EDTA 1X (1 L)

10 mM Tris base: 1.21 g

1 mM EDTA: 0.37 g

dH_2O to 1 L

Adjust pH to 9

0.5 mL Tween 20

Tris-buffered saline (TBS) 10X (1 L)

1.4 M NaCl: 80 g

27 mM KCl: 2 g

254 mM Tris-HCl: 40 g

dH_2O to 1 L

Adjust pH to 7.4

TTBS 1X (1 L)

100 mL TBS 10X

900 mL dH_2O

1 mL Tween-20 +

10.2. Appendix 2. Figure

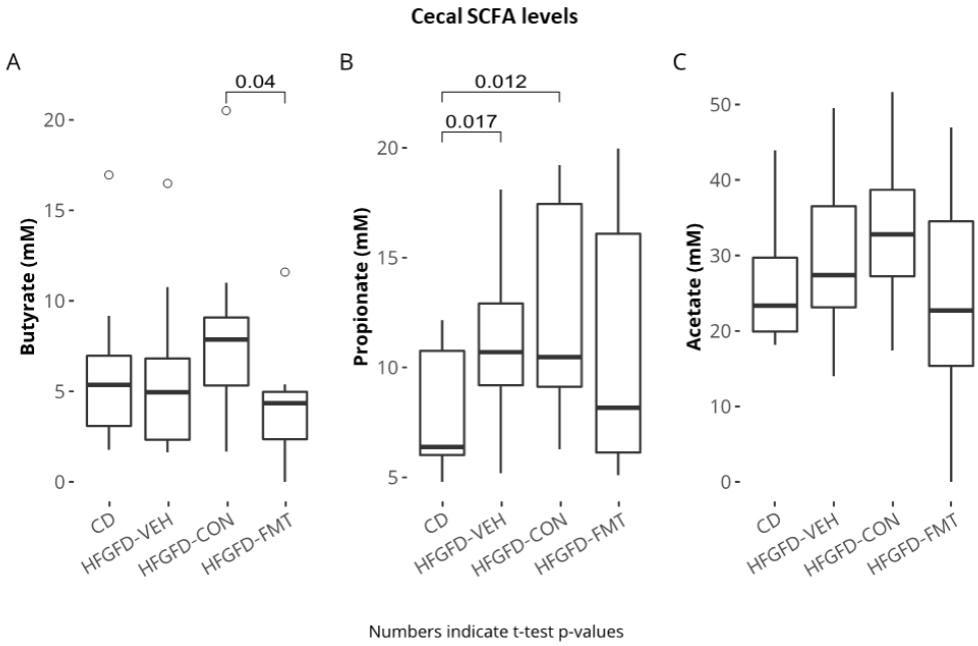

10.3. Appendix 3. Publications resulting from this thesis

10.3.1. Publication 1

Barberá A, Raurell I, García-Lezana T, Torres-Arauz M, Bravo M, Hide D, Gil M, Salcedo MT, Genescà J, Martell M, Augustin S. Steatosis as main determinant of portal hypertension through a restriction of hepatic sinusoidal area in a dietary rat nash model. Liver Int. 2020;40(11):2732-43.

DOI: 10.1111/liv.14632

Received: 17 April 2020 | Revised: 10 July 2020 | Accepted: 2 August 2020

DOI: 10.1111/liv.14632

ORIGINAL ARTICLE

Liver INTERNATIONAL WILEY

Steatosis as main determinant of portal hypertension through a restriction of hepatic sinusoidal area in a dietary rat nash model

Aurora Barberá[1] | Imma Raurell[1] | Teresa García-Lezana[2] | Manuel Torres-Arauz[1] | Miren Bravo[1] | Diana Hide[1] | Mar Gil[1] | María Teresa Salcedo[3] | Joan Genescà[1,4] | María Martell[1,4] | Salvador Augustin[1,4]

[1]Liver Unit, Vall d'Hebron Hospital Universitari, Vall d'Hebron Institut de Recerca (VHIR), Vall d'Hebron Barcelona Hospital Campus, Universitat Autònoma de Barcelona, Barcelona, Spain, Barcelona, Spain

[2]Icahn School of Medicine at Mount Sinai, New York, NY, USA

[3]Pathology Department, Hospital Universitari Vall d´Hebron, Universitat Autònoma de Barcelona, Barcelona, Spain

[4]Centro De Investigación Biomédica En Red De Enfermedades Hepáticas y Digestivas, Instituto De Salud Carlos III, Madrid, Spain

Correspondence
Joan Genescà and Salvador Augustin, Hospital Universitari Vall d'Hebron, Passeig Vall d'Hebron 119-129, 08035 Barcelona, Spain.
Email: jgenesca@vhebron.net (J. G.); salva.augustin@gmail.com (S. A.)

Funding information
SA was a recipient of a PERIS intensification grant (267/G60594009) by Departament de Salut de la Generalitat de Catalunya. JG is a recipient of a Research Intensification grant and DH is a recipient of a post-doctoral Sara Borrell from the Instituto de Salud Carlos III (ISCIII). MG and AB are recipients of a predoctoral fellowship grant AGAUR and ISCIII respectively. SA was a recipient of Gilead Sciences International Research Scholars Grant 2017. The work was partially funded by grants PI17/00310, PI17/00754, PI18/00947 and AC18/00033 (ENM3 2018) from ISCIII and co-funded by

Abstract

Background & Aims: Portal hypertension (PH) can be present in pre-cirrhotic stages, even in absence of fibrosis in non-alcoholic steatohepatitis (NASH) patients. Liver endothelial dysfunction (ED) has been shown as responsible for this effect in short-term dietary animal models. We evaluated the persistence of PH and underlying mechanisms in a long-term rat model of NASH.

Methods: Sprague-Dawley rats were fed 8 or 36 weeks with control diet or high-fat high-glucose/fructose diet. Metabolic parameters, histology, ED and haemodynamics were characterized. Structural characteristics of liver sections were analysed using image analysis.

Results: Both interventions reproduced NASH histological hallmarks (with steatosis being particularly increased at 36 weeks), but neither induced fibrosis. The 36-week intervention induced a significant increase in portal pressure (PP) compared to controls (12.1 vs 8.7 mmHg, $P < .001$) and the 8-week model (10.7 mmHg, $P = .006$), but all features of ED were normalized at 36 weeks. Image analysis revealed that the increased steatosis at 36-week was associated to an increase in hepatocyte area and a significant decrease in the sinusoidal area, which was inversely correlated with PP. The analysis provided a critical sinusoidal area above which animals were protected from developing PH and below which sinusoidal flux was compromised and PP started to increase.

Conclusion: Liver steatosis per se (in absence of fibrosis) can induce PH through a decrease in the sinusoidal area secondary to the increase in hepatocyte area in a long-term diet-induced rat model of NASH. Image analysis of the sinusoidal area might predict the presence of PH.

Abbreviations: ALT, alanine aminotransferase; AST, aspartate aminotransferase; CD, control diet; COL1A1, collagen-a1; ED, liver endothelial dysfunction; H&E, haematoxylin and eosin; HFGFD, high-fat-high-glucose/fructose diet; HOMA-IR, homeostasis model assessment of insulin resistance; IHVR, intrahepatic vascular resistance; iNOS, inducible nitric oxide synthase; IR, insulin resistance; NAFLD, non-alcoholic fatty liver disease; NAS, NASH activity score; NASH, non-alcoholic steatohepatitis; P-Akt, phosphorylated protein kinase B; P-eNOS, phosphorylated endothelial nitric oxide synthase; PH, portal hypertension;; PP, portal pressure; Shh, sonic hedgehog; α-SMA, alpha smooth muscle actin.

Maria Martell and Salvador Augustin share senior authorship.

© 2020 John Wiley & Sons A/S. Published by John Wiley & Sons Ltd

Appendix

European Union (ERDF/ESF, "Investing in your future"). CIBERehd is supported by Instituto de Salud Carlos III. AB, MG and MB are PhD students at Universitat Autònoma de Barcelona.

Handling Editor: Utpal Pajvani

KEYWORDS

endothelial dysfunction, hepatocyte area, non-alcoholic steatohepatitis, portal hypertension, sinusoidal area, steatosis

1 | INTRODUCTION

Non-alcoholic fatty liver disease (NAFLD) is currently the most common type of chronic liver disease in developed countries. The hallmark of NAFLD is the accumulation of fat in the hepatocytes (steatosis), in the form of lipid droplets containing triglycerides.[1] NAFLD is considered the hepatic manifestation of the metabolic syndrome as it is strongly associated with obesity and insulin resistance (IR).[2] The term NAFLD encompasses a broad spectrum of liver disorders, ranging from isolated steatosis to non-alcoholic steatohepatitis (NASH), which is the result of the coexistence of steatosis, lobular inflammation and hepatocellular injury (ballooning). NASH may lead to progressive fibrosis and cirrhosis with an increased risk of developing portal hypertension (PH), liver failure and hepatocellular carcinoma.[3] The mechanisms regulating this progression are incompletely understood.

PH is responsible for most of the complications associated with advanced NAFLD, and it is defined as a complex syndrome, consequence of haemodynamic abnormalities of the portal venous system, linked to increased intrahepatic vascular resistance (IHVR) and altered splanchnic blood flow.[4] Several studies demonstrated that PH can be present at very early stages of NASH both in humans and in animal models, even when fibrosis is far less advanced or even absent.[5-7] One of the factors contributing to the early development of PH is the presence of endothelial dysfunction (ED), with decreased nitric oxide production resulting in sinusoidal vasoconstriction.[8,9] Furthermore, experiments have shown that severe steatosis by itself may also be associated with the induction of significant PH.[10,11] This induced increase in PH could result from pure structural changes such as sinusoidal narrowing by enlarged steatotic hepatocytes.[12,13]

Vital insights into the pathogenesis and underlying mechanisms of NAFLD have been gained from the study of existing animal models. However, none of the current available NAFLD models recapitulates adequately all the key elements of human disease. Thus, the recognition of the limitations from the different animal models is necessary to most effectively translate findings from such models to improved therapeutics in humans.[14] In a previous study from our group,[9] we developed and characterized a dietary model of NASH in rat that was able to reproduce the key phenotypic features of the early stages of NASH: obesity, IR, intestinal dysbiosis, ED and PH. Although this model failed to induce fibrosis, it helped at characterizing the link between IR, ED and the gut microbiome in the development of PH in NASH.

LAY SUMMARY

In this translational study we found that, in a long-term diet-induced rat model of NASH, liver fat per se (in the absence of other mechanisms such as endothelial dysfunction or fibrosis), is able to induce portal hypertension through a marked increase in the hepatocyte area that promotes a mechanical reduction of the hepatic sinusoidal area. Image analysis of the sinusoidal area might help at predicting the presence of portal hypertension in NASH.

The aim of this experimental study was to develop and characterize the long-term effects of the same dietary intervention on NASH histology and PH in rat, and to elucidate the specific mechanistic contributions of ED and/or intrahepatic structural changes in the progression of PH over time in the NASH model.

2 | MATERIAL AND METHODS

2.1 | Animal model and diet

The experimental models were developed in male Sprague-Dawley rats (Charles River Laboratories) weighting 200-220 g at the beginning of the experiments. Animals were housed under a 12-hour light/dark cycle at constant temperature (24 ± 1°C) and relative humidity (55 ± 10%). Animals had ad libitum access to a high-fat high-glucose/fructose diet (HFGFD) or a control diet (CD). The HFGFD consisted of 30% fat (butter, coconut oil, palm oil, beef tallow) with mainly saturated fatty acids (5.73 kcal/g; Ssniff Spezialdiäten GmbH), supplemented with cholesterol (1 g/kg) and a beverage of glucose/fructose (42 g/L, 45% glucose and 55% fructose). The CD consisted of a grain-based chow with 4% fat (2.89 kcal/g; Teklad 2014; Harlan laboratories, Indianapolis, IN) and tap water. Body weight and food consumption were monitored once a week.

All procedures were conducted in accordance with European Union Guidelines for Ethical Care of Experimental Animals (EC Directive

86/609/EEC for animal experiments), approved by the Animal Care Committee of the Vall d'Hebron Institut de Recerca (Barcelona, Spain), and conducted in the animal facilities of Vall d'Hebron Institut de Recerca.

2.2 | Model development and characterization

For model development and characterization, rats were fed with CD or HFGFD for 8 and 36 weeks. After diet intervention, blood biochemistry, liver haemodynamics, liver histology and molecular pathways related to ED were analysed. In addition, structural characteristics of all 8- and 36-weeks' rat liver sections were systematically analysed using digital image analysis. The methods followed to perform the blood biochemistry measurements, immunohistochemistry, as well as for Western blot and real-time PCR analyses are described in detail in the Supplementary Material.

2.3 | Haemodynamic measurements

The haemodynamic measurements were made under intraperitoneal anaesthesia with ketamine (100 mg/kg) plus midazolam (5 mg/kg) and body temperature maintained at 37°C. Mean arterial pressure (MAP) was measured by catheterization of the femoral artery and portal pressure (PP) assessed by ileocolic vein catheterization using highly sensitive pressure transducers (Harvard apparatus). Superior mesenteric artery (SMA) blood flow (SMABF, mL/ [min*100 g]) and portal blood flow (PBF, mL/ [min*100g]) were measured with a perivascular ultrasonic transit-time flow probe (1 mm diameter, Transonic systems Inc). SMA resistance (SMAR) and intrahepatic vascular resistance (IHVR, mmHg/mL*min*100g) were calculated as ([MAP-PP]/SMABF) and (PP/PBF) respectively.[9]

2.4 | Histological analyses

For histological analyses, liver samples were extracted, fixed in 4% formalin, embedded in liquid paraffin at 65°C and sectioned in 4μm thick slides. Samples were then stained with haematoxylin and eosin (H&E) to assess liver parenchyma and picrosirius red to detect collagen fibres. All stained liver samples were examined by an expert liver pathologist blinded to the interventions performed on the animals. The diagnosis of NASH was established based on the presence of all three characteristic patterns of the disease, which include the coexistence of steatosis, lobular inflammation and hepatocellular ballooning. The NASH-CRN Activity Score (NAS) was used to quantify NASH activity. NAS was the unweighted sum of the histological components: steatosis (0-3), lobular inflammation (0-3) and hepatocellular ballooning (0-2). Fibrosis was also classified in five stages according to the NASH-CRN system, ranging from F0 (no fibrosis) to F4 (cirrhosis). Histological analyses were performed in all animals: 20 liver specimens from the 8-week model (10 CD and 10 HFGFD) and 29 samples of the 36-week model (14 CD and 15 HFGFD).

2.5 | Digital image analyses

Digital image analysis was performed to measure sinusoidal area, fat area, hepatocyte area and number of hepatocytes from 8- and 36-week rat liver H&E sections by using ImageJ. The same number of liver samples as in the histological analyses were analysed. All digital analyses were performed through two rounds of measurements by AB who was blinded to the group origin of the samples and the haemodynamic results and verified by MM and IR in an additional round of measurements.

2.6 | Sinusoidal and fat area

For each H&E sample, 21 randomly selected non-overlapping areas were imaged at x20 magnification. The measurement of the areas was calculated using the ImageJ program in which we assigned a threshold in order to mark on the one hand the hepatic sinusoids and on the other hand the liver fat (see images in the Supplementary Material). The result was reported as the median of all measurements for each sample and finally for each group.

2.7 | Hepatocyte area

From the same samples, 10 randomly selected non-overlapping areas per sample were imaged at x40 magnification. For each image, we randomly selected 20 hepatocytes. The areas of the hepatocytes were measured (as already described by Andrew Hall et al[15]) in two perpendicular dimensions and were then calculated as an oval (see the formula below). The result was first reported as the median of all hepatocyte areas for each sample and finally as the median for each group.

$$\text{Cell area}\ (\mu m^2) = \pi \times \left(\frac{\text{max lobule diameter}}{2}\right) \times \left(\frac{\text{perpendicular lobule diameter}}{2}\right)$$

2.8 | Number of hepatocytes

As in the case of the sinusoidal and the fat area, 21 randomly selected non-overlapping areas per sample were imaged at ×20 magnification to then calculate the number of hepatocytes by counting their nucleus. The result was reported as the median of the number of hepatocytes for each sample and finally for each group.

2.9 | Statistical analyses

Statistical analyses were performed with Sigmastat 3.0 package. Continuous variables were described as mean ± error or standard

Appendix

deviation of the mean (SEM) and a *P*-value < .05 was considered as statistically significant. The comparisons between continuous variables were made with a Student´s *t* test or paired samples *t* tests (or their non-parametric alternatives) as appropriate.

For the statistical analysis of the RT-qPCR, the log2 (−ΔΔCT) values were used (that is, a mathematical transformation of ΔΔCT that does not modify the absolute value, but that causes the under expression to be represented from 0 to −∞ and overexpression from 0 to +∞).

3 | RESULTS

3.1 | The 36-week HFGFD intervention further worsened the altered metabolic profile of the 8-week NASH model

Metabolic, histological and haemodynamic features were evaluated in order to characterize the short- and long-term models after the dietary intervention. HFGFD administration significantly increased the body weight of rats compared to CD at both time points (Table 1). The 36-week HFGFD (36w-HFGFD) intervention was associated with a significant increase in fasting glucose levels as compared to 36-week controls and 8-week groups. This intervention also associated a significant increase in fasting insulin as well as in insulin resistance (HOMA-IR) as compared to the 8-week intervention. These changes did not reach statistical significance when compared to 36-week controls (36w-CD) because of the marked raise in insulin plasma levels in these sedentary 36w-CD individuals. Serum transaminases (ALT and AST) were also significantly increased in the 36w-HFGFD group compared to 36w-CD and 8-week groups. The same significant differences between the 8- and 36-week HFGFD interventions were observed with fasting blood concentrations of cholesterol and high-density lipoprotein (HDL). Overall, the expected disturbed metabolic profile of the model was further worsened with the long-term time extension of the HFGFD intervention.

3.2 | The 36-week HFGFD administration induced increased NASH activity without inducing fibrosis

From a histopathological perspective, both the 8-week and 36-week dietary interventions did result in a consistent reproduction of NASH histological hallmarks, as seen in Figure 1. Overall, the 36w-HFGFD group showed a more intense degree of NASH histological activity (as measured by the NASH Activity Score, NAS) (Figure 1D). Although lobular inflammation tended to increase at 36 weeks, reaching maximum scores of 3 in some cases (Figure 1C), most of the increase in activity at 36 weeks was because of a marked increase in steatosis at this time point, with apparent collapse of sinusoidal spaces at light microscopy (Figure 1E). However, despite this increase in activity in the long-term, none of the dietary interventions was able to induce fibrosis. We did

TABLE 1 Body weight and biochemical parameters in CD and HFGFD rats after 8 and 36 wks of diet intervention

	8 wks		36 wks	
	CD (n = 10)	HFGFD (n = 10)	CD (n = 14)	HFGFD (n = 15)
Body weight (g)	461 ± 12.83	492.8 ± 16.61	654 ± 21.9†	798 ± 29.46$^{*,\#}$
Glucose (mg/dL)	140.88 ± 8.72	181.22 ± 27.78	179 ± 11.87†	227.53 ± 10.67$^{*,\#}$
Insulin (ng/mL)	4.23 ± 7.05	7.96 ± 7.25	15.44 ± 2.76†	25.98 ± 6.38$^{\#}$
HOMA-IR	1.97 ± 3.4	3.83 ± 4.1	8.35 ± 1.2†	13.75 ± 3.82$^{\#}$
Albumin (g/dL)	2.55 ± 0.09	2.87 ± 0.05*	2.8 ± 0.04†	2.8 ± 0.05
Bilirubin (mg/dL)	0.09 ± 0.01	0.1 ± 0.02	0.14 ± 0.02†	0.125 ± 0.02
AST (IU/L)	117.29 ± 6.36	170.14 ± 21.3*	206 ± 30.87†	447 ± 193.09$^{*,\#}$
ALT (IU/L)	33.22 ± 6.3	45.67 ± 3.57	66.5 ± 7.99†	206 ± 75.69$^{*,\#}$
TG (mg/dL)	37.11 ± 3.23	45.33 ± 5.1	42.21 ± 3.63	52 ± 16.121
Cholesterol (mg/dL)	85 ± 5.45	80.22 ± 4.13	119.5 ± 10.14†	104 ± 9.37$^{\#}$
Cholesterol HDL (mg/dL)	47.21 ± 2.59	45.56 ± 1.76	67 ± 5.89†	58 ± 4.83$^{\#}$
Cholesterol LDL (mg/dL)	27.2 ± 1.22	25.6 ± 4.07	41.5 ± 4.32†	35 ± 3.76

Note: Values are expressed as mean ± SEM.

Abbreviations: ALT, alanine aminotransferase; AST, aspartate aminotransferase; HDL, high density lipoprotein; HOMA-IR, index of homeostasis model assessment insulin resistance; LDL, low density lipoprotein; n, number of rats; TG, triglycerides.

$^{*}P \leq .05$ vs CD.

$^{\#}P \leq .05$ vs HFGFD-8-wk.

$^{\dagger}P \leq .05$ vs CD-8-wk.

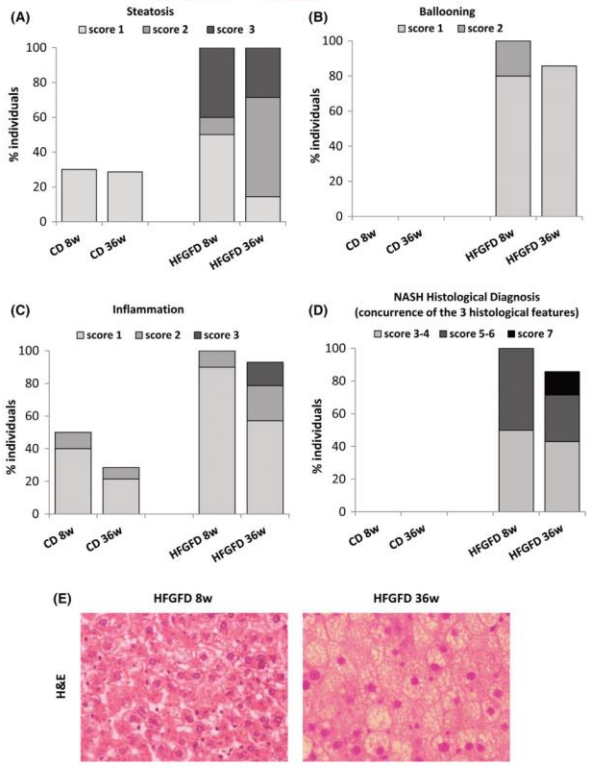

FIGURE 1 Histological evaluation of NASH activity following the NASH-Clinical Research Network system. Bar graphs representing the percentage of individuals presenting steatosis (A), ballooning (B) and inflammation (C) in the CD and HFGFD groups after 8 and 36 wks of diet intervention. Each colour represents the percentage of individuals with the corresponding score (score 1: light grey, score 2: grey or score 3: dark grey). The bar graph in D shows the percentage of individuals with histological NASH represented with different NAS scores (score 3-4: light grey, score 5-6: dark grey or score 7: black). (E) Representative images show liver parenchyma stained with haematoxylin and eosin of HFGFD rats after 8 and 36 wks of diet intervention (×40) used to perform the histological evaluation

observe a non-significant increase in expression of α-SMA in association with the HFGFD at 8 weeks and, interestingly, a significant increase in the 36w-CD group when compared to both 8w-CD and 36w-HFGFD groups. However, this marker of stellate cell activation was not accompanied by changes in collagen deposition at light microscopy or an increase in expression of COL1A1 in this group, which was even significantly decrease as compared to the 8-week counterparts (Figure 2).

3.3 | The 36-week HFGFD intervention significantly worsened portal hypertension and intrahepatic vascular resistance in the NASH model

Despite the absence of fibrosis, the HFGFD intervention induced a significant increase in portal pressure (PP) at both time-points (Table 2). This increase in PP was especially remarkable in the 36-week model: the HFGFD 36-week intervention caused a 40% increase in PP compared to 36w-CD (12.1 vs 8.7 mmHg, $P < .001$), being significantly higher than the PP value observed in the 8w-HFGFD model (12.1 vs 10.5 mmHg, $P = .006$). This increase in PP was secondary to a significant increase in IHVR at both time-points. Ageing did not seem to have a relevant effect in portal haemodynamics, since there were no major differences between CD groups over time, except for the resistance at the superior mesenteric artery resistance (SMAR), which increased in the older group, although this change remained significantly lower than that of the 36w-HFGFD group. No changes in systemic haemodynamics were observed when comparing CD and HFGFD at both time-points (Table 2).

3.4 | The marked increase in portal pressure and IHVR in the 36-week model could not be explained by endothelial dysfunction

In order to characterize the intrahepatic mechanisms underlying the increase in IHVR and PP in the absence of fibrosis, ED was assessed.

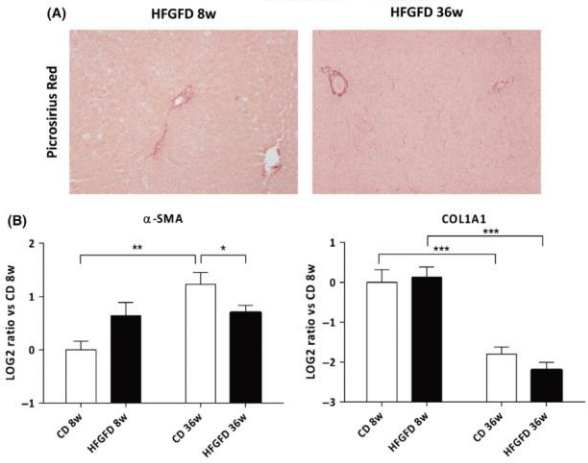

FIGURE 2 Markers of hepatic fibrosis. A, Representative images show liver fibrosis stained by picrosirius red of HFGFD rats after 8 and 36 wks of diet intervention (×10). B, Relative mRNA expression of COL1a1 and α-SMA by quantitative RT-PCR, expressed as a log2 ratio and normalized with the control group of 8 wks. Data represent mean ± SEM. $^{*}P \leq .05$; $^{**}P \leq .01$; $^{***}P \leq .001$

TABLE 2 Haemodynamic measurements in CD and HFGFD rats after 8 and 36 wks of diet intervention

	8 wks		36 wks	
	CD (n = 10)	HFGFD (n = 10)	CD (n = 11)	HFGFD (n = 8)
MAP (mmHg)	108.03 ± 4.16	110.03 ± 4.56	118.11 ± 4.38	118.32 ± 6.35
PP (mmHg)	8.43 ± 0.3	10.47 ± 0.31*	8.72 ± 0.31	12.08 ± 0.42$^{*,\#}$
SMABF (mL/[min*100 g])	3.60 ± 0.49	3.54 ± 0.36	2.56 ± 0.23	2.06 ± 0.18$^{\#}$
SMAR (mmHg/mL*min*100 g)	31.52 ± 3.62	30.69 ± 4.19	46.87 ± 5.1†	53.14 ± 3.37$^{\#}$
IHVR (mmHg/mL*min*100g)	3.5 ± 0.23	5.31 ± 0.61*	4.33 ± 0.70	8.90 ± 1.31$^{*,\#}$

Note: Values are expressed as mean ± SEM.

Abbreviations: IHVR, intrahepatic vascular resistance; MAP, mean arterial pressure; n, number of rats; PP, portal pressure; SMABF, superior mesenteric artery blood flow; SMAR, superior mesenteric artery resistance.

$^{*}P \leq .05$ vs CD.

$^{\#}P \leq .05$ vs HFGFD-8-wk.

$^{\dagger}P \leq .05$ vs CD-8-wk.

For this purpose, we analysed the phosphorylated proteins kinase B (Akt) and endothelial nitric oxide synthase (eNOS). In previous work by our group and others,[8,9,16] we showed that at shorter timeframes (8 weeks or less), increased IHVR with different forms of Western-diet interventions was mainly because of ED, which was in turn mediated by increased Akt-dependent hepatic IR with those diets. However, in the present study, for the 36-week HFGFD intervention, molecular features of ED were similar to those of controls, unlike what was observed in the 8-week model (in which ED was evidenced by the significant decrease in P-eNOS and P-Akt expression as compared to controls) (Figure 3). As seen, the significant decrease in P-Akt and P-eNOS in the 8w-HFGFD *vs*. 8w-CD confirmed in the 8-week model was lost in the 36-week individuals, for which both P-Akt and P-eNOS were similar to controls, and P-eNOS was significantly higher than that of the 8w-HFGFD model (Figure 3A). To a more in-depth assessment of the absence of ED in the long-term model, we analysed other candidate biomarkers in endothelial cells, which could explain the significant increase in IHVR and PP. We thus performed immunohistochemical staining for CD34. De novo expression of CD34 in liver sinusoidal endothelial cells (LSEC) has been consistently proven as a reliable molecular marker of loss of a healthy LSEC phenotype in different models of liver disease,[17-20] including NASH.[8] As seen in Figure 3B, expression of CD34 at 36 weeks was significantly decreased, suggesting a reversal to a healthier LSEC phenotype in the long-term. We also explored other molecular pathways relevant in NASH that

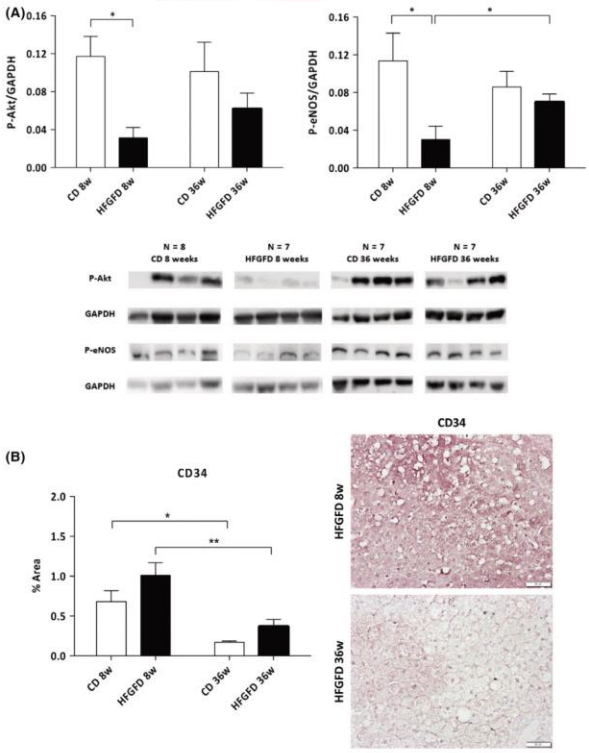

FIGURE 3 Western blot analyses of intrahepatic markers of endothelial dysfunction. A, The bar graphs show the quantification of P-Akt and P-eNOS using GAPDH as loading control and normalized with the control group of each time-point. Representative Western blots are shown below. B, Bar graphs showing immunohistochemical quantification of CD34, and representative images of 8 and 36-wk HFGFD rats (x20). Data represent mean ± SEM. $^{*}P \leq .05$; $^{**}P \leq .01$. Abbreviations: n, number of rats; P-Akt, phosphorylated protein kinase B; P-eNOS, phosphorylated endothelial nitric oxide synthase; GAPDH, glyceraldehyde-3-phosphate dehydrogenase

could lead to the observed changes in histology and portal haemodynamics at 36 weeks. In this line, we explored the link between increased NASH activity and changes in ED and IHVR through the quantification of the inducible nitric oxide synthase (iNOS) expression. As seen, there was a significant increase in the hepatic mRNA expression of iNOS in the 36w-HFGFD group compared to controls (Figure 4A). However, iNOS expression in the 8w-HFGFD group (in which the canonic molecular hallmarks of ED were clearly present) was the same as that of the 8w-CD. In order to study non-LSEC related mechanisms in the NASH models that could go undetected by histology and might be affecting ED or portal haemodynamics, we also explored the protein expression of sonic hedgehog (Shh) as biomarker of hepatocyte lipotoxic injury. As seen in Figure 4B, protein expression of Shh seemed to increase in the long-term despite the fact that the histological evaluation of ballooning revealed no further deterioration from 8 to 36 weeks (Figure 1B), although these differences in Shh expression did not reach statistical significance.

3.5 | The marked increase in portal pressure and IHVR in the 36-week model was explained by a structural obstruction associated to increased steatosis

To further explain the increase in IHVR and PP in the absence of ED in the 36-week model and given the striking histological increase in steatosis at this time point, we evaluated the potential role of a structural component of IHVR as responsible of this increase. We speculated that the marked increase in lipid content in the hepatocyte at 36 weeks had led to an increase in hepatocyte area at the expense of the sinusoidal area, leading to a structural increase in resistance to the intrahepatic portal blood flow. To that end we conducted a systematic image analysis of hepatocyte fat and sinusoidal areas in the histological liver sections at 8- and 36-week according to the theoretical basis and the experimental protocols described in Andrew Hall et al[15] (see in Methods).

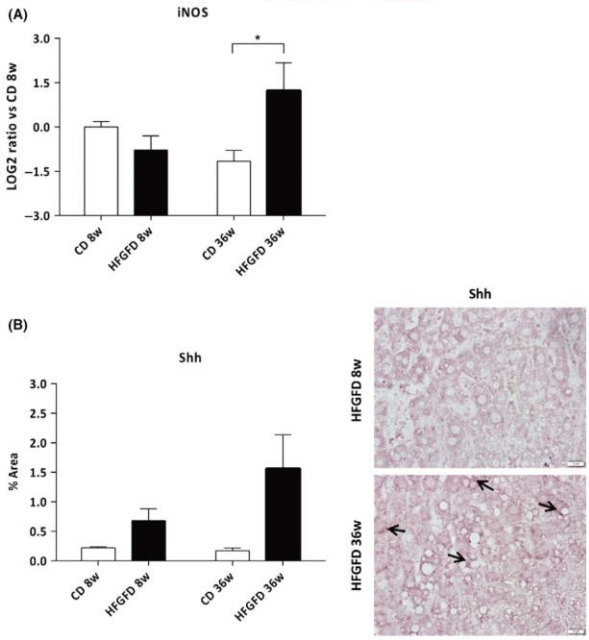

FIGURE 4 Markers of hepatic inflammation and ballooning. A, Relative mRNA expression of iNOS by quantitative RT-PCR, expressed as a log2 ratio and normalized with the control group of 8 wks. B, Bar graphs showing immunohistochemical quantification of Shh, and representative images of 8 and 36-wk HFGFD rats (×40). Black arrows indicate more intense areas of Shh expression. Data represent mean ± SEM. $^{*}P \leq .05$

Regarding the 8-week model, there was a significant increase in fat area in the HFGFD group compared to controls, but this increase was not marked enough to associate significant differences in terms of hepatocyte area or sinusoidal area (Figure 5). However, as seen in Figure 5B, the 36w- HFGFD intervention led to a dramatic increase in the total fat area (600% as compared to 36-week controls and 170% as compared to 8-week HFGFD, $P = 9.8 \times 10E\text{-}7$ and $9 \times 10E\text{-}4$, respectively), and a marked significant increase in both the average area of individual hepatocytes (Figure 5C) and the hepatocyte area/liver weight ratio (Figure 5E). This was associated to a significant decrease in hepatocyte number per field examined (Figure 5D), and, most importantly, a significant decrease in the liver sinusoidal area as compared both to controls and to the 8-week model (Figure 5A).

In order to quantify the impact of these structural changes on PP, we proceeded to study the correlation between intrahepatic sinusoidal area and PP after 8 and 36 weeks of diet intervention. Figure 6 panel A plots the individual sinusoidal areas and PP values of all studied animals at 36 weeks. As seen, all HFGFD individuals had PH (defined statistically as the PP mean of CD group plus $2 \times$ SD, as there is no established PH threshold in animal models) and all individual sinusoidal areas in the HFGFD group were below the minimum values observed in the control group. This suggested that there could be a critical value of the sinusoidal area) ($3 \times 10E9$ nm^2 as drawn in Figure 6) below which the sinusoidal flux is critically compromised leading to increased IHVR and PH. Figure 6 panel B shows the plotted individual values of sinusoidal area and PP at 8 weeks. Applying the critical value of sinusoidal area 3x10E9nm^2, we observed that of the 4 HFGFD individuals who presented PH (also statistically defined), only one had a restriction in its sinusoidal area. The sinusoidal area of the rest of the individuals was above the critical value.

4 | DISCUSSION

In the present experimental study, we have shown that steatosis per se is able to induce PH in the absence of liver fibrosis or ED, because of a mechanical restriction of the sinusoidal area, in a long-term diet-induced NASH model in rat. We also provide an imaging approach to evaluate the sinusoidal area in liver slides to estimate the relative weight of the mechanical obstruction associated to increased steatosis on the development of PP in NASH.

Most of the clinical consequences associated to NASH are linked directly to the progression of PH. Interestingly, it has been shown both in humans and experimental models, that NASH can induce PH in pre-cirrhotic stages, even in complete absence of cirrhosis.[5,7-9,16,21] However, the exact mechanisms driving these observations are incompletely understood. It has been previously shown by our group and others that liver ED might represent a potent driver

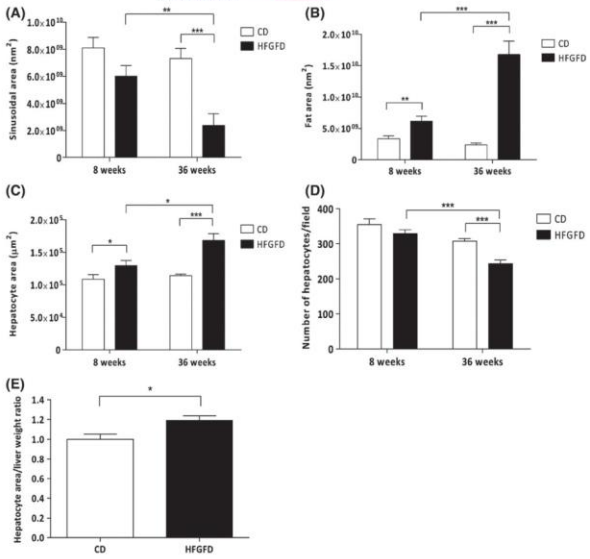

FIGURE 5 Image analysis of intrahepatic structural changes. Bar graphs show the quantification of the sinusoidal area (A), fat area (B), hepatocyte area (C) and number of hepatocytes (D) of CD and HFGFD rats after 8 and 36 wks of diet intervention. The bar graph in E shows the hepatocyte area/liver weight ratio after 36 wks normalized with the control group. Data represent mean ± SEM. $^{*}P \leq .05$; $^{**}P \leq .01$; $^{***}P \leq .001$

of PH in NASH, at least in short-term models of the disease, in which PH is observed in absence of liver fibrosis.[7-9,16] As a follow-up to previous work by our group, in the present project we wanted to study whether a long-term extension of a HFGFD intervention was able to induce liver fibrosis, on one hand, and to evaluate whether it was also capable of perpetuating or aggravating the ED and PH observed in the short-term model, on the other hand.

The main results of the study can be summarized as follows: (a) the long-term dietary intervention was not able to induce fibrosis in the rat model; (b) however, the intervention led to a marked increase in IHVR and PH; and (c) this increase in IHVR and PP, contrary with what we expected based on previously published evidence, was mainly associated to a marked reduction of the intrahepatic sinusoidal area (compressed by the enlarged steatotic hepatocytes), and not to ED (which did not have a significant contribution in the long-term model).

4.1 | Context

To the best of our knowledge, this is the first study showing that steatosis per se can induce PH in NASH in the absence of all other accepted mechanisms that can associate increases in PP. There is some previous evidence suggesting that steatosis is an important contributor of PH in alcoholic liver disease. Human and experimental studies performed in the 1980's clearly showed that PH was present in alcoholic liver disease patients and animal models even in absence of fibrosis, as long as a critical hepatocyte area was surpassed because of lipid and water accumulation inside the hepatocytes.[21-24] However, those observations could not rule out other important potential contributors to the effect, such as ED. Besides, transferability of these observations to NASH is unclear, given the differences in terms of mechanisms and dynamics of hepatocyte enlargement between the two conditions; the unclear and striking differences in the development of hepatomegaly in alcoholic liver disease but not in NASH represent a puzzling example.[24] More recent studies, focused in NAFLD, also suggested that steatosis might be contributing to the development of PH in non-alcoholic fatty livers, even in the absence of fibrosis. Works of Francque and collaborators,[5] validated more recently by Rodrigues et al,[21] clearly showed that PH is not uncommon in pre-cirrhotic NAFLD. Francque et al, also conducted elegant translational studies exploring the underlying mechanisms for this observation in animal models.[5,7,25] However, in those studies, the precise contribution of the mechanical compressive effect of enlarged fatty hepatocytes could not be dissected from the relative contribution of ED, which seemed to have more of a leading role, at least in short-term models of the disease.

In our study, the extension of the dietary intervention provides a unique model to isolate the contribution of the mechanical compression by steatosis as the main determinant to the increase in PP in non-cirrhotic NASH. Contrary with our initial hypotheses, the dietary extension was not able to either induce fibrosis or perpetuate ED. Regarding the former, we showed that in Sprague-Dawley rats, the sole extension in time of the HFGFD was unable to elicit a

Appendix

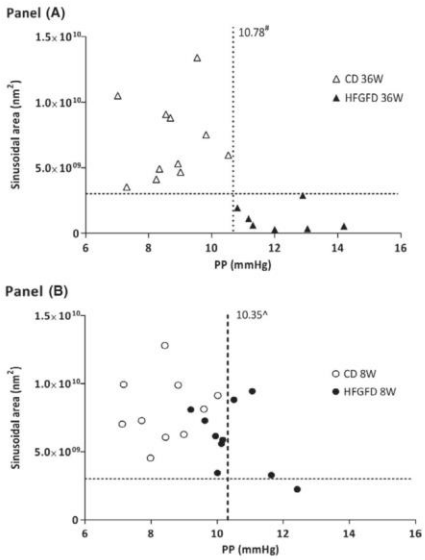

FIGURE 6 Correlations between sinusoidal area and portal pressure (PP) in CD and HFGFD rats after 36 wks (Panel A) and 8 wks (Panel B) of diet intervention. #36-wk portal hypertension was defined statistically as the PP mean of CD group plus two times SD (>10.78 mmHg). ^8-wk portal hypertension was defined statistically as the PP mean of CD group plus two times SD (>10.35 mmHg)

fibrotic response. This is in line with all efforts trying to induce fibrosis with interventions as similar as possible to what is seen in patients with NASH.[14,22,23] We did find signals of stellate cell activation in the long-term, but these did not translate into either histological fibrosis or even an increase in expression of COL1A1. Thus, the marked increase in PP at 36 weeks cannot be attributed to the architectural disruption usually seen in cirrhosis.

4.2 | Liver endothelial dysfunction and other intrahepatic biological processes

Regarding liver ED, in previous work from our group and others it was shown that short-term HFGFD interventions were able to induce ED through insulin-dependent mechanisms, which translated into increased IHVR and PP.[8,9,16,25] Thus, we hypothesized that ED might be the main determinant of the marked increase in IHVR and PP observed at 36-weeks. However, this also seemed not to be the case. The significant increase in P-eNOS and decrease in CD34 in the 36w-HFGFD group suggested a reversal to a healthier LSEC phenotype in the long-term. In this line, we explored other potential biological processes that could underlie the observed deterioration of portal haemodynamics and the increase in NASH activity.

Regarding a more in-depth molecular characterization of other biological processes that could account for this increase in IHVR and PP, we chose to analyse iNOS expression as a potential direct link between intrahepatic inflammation and ED. Upregulation of iNOS has been linked to capillarization of LSECs both in vitro and in BDL models.[19,26] We observed an increase of iNOS expression in the 36w-HFGFD group. However, since iNOS was not elevated in the NASH model at 8 weeks (in which ED was more obvious), it is hard to assume that the increase of iNOS at 36 weeks might be a reflection of an underlying ED at this time point. Thus, the iNOS elevation might be interpreted to be a molecular reflection of the increase in histological NASH activity at this time point, although this interpretation remains purely speculative. In the same line, we evaluated activation of the Sonic hedgehog (Shh) pathway in the liver in the four groups (Figure 4B). We observed a marked increase in Shh ligand expression in HFGFD vs CD, which was more intense at 36 weeks, suggesting an increase in the amount of lipotoxic injury[27] and/or in hepatocyte ballooning[28] with the dietary intervention which were aggravated in the long-term. However, these changes did not reach statistical significance. Although the increase in Shh expression goes in line with the increase in NASH histological activity observed in the 36w-HFGFD group,[29] it is worth noting that ballooning did not change over time in our model. Thus, it is indeed hard to discern in our model whether this increase in Shh expression was related to subclinical changes (ie not obvious as ballooning at light microscopy) in lipotoxic hepatocytes or to other potential cellular sources (HSC, LSECs, inflammatory cells), or how this might be related or not with ED.

Finally, it is worth remarking the changes observed in the 36w-CD group. This group showed an altered metabolic biochemical profile as compared to the 8w-CD, as well as increased alpha-SMA expression and an increase in SMAR, without apparent changes in liver histology or haemodynamics. These data suggest a potential role of ageing and sedentarism in the long-term animals, placing the 36w-CD group as an intermediate step in between the healthy 8w-CD phenotype and the full-NASH phenotype of the aged 36w-HFGFD group.

In all, although the exact mechanisms for these molecular adaptations remain unclear, this should at least serve as a reminder that, sometimes, apparently relevant pathways in short-term animal models might be lost in the long-term probably because of the emergence of compensatory mechanisms and the effects of ageing and sedentarism with these long-term interventions.

4.3 | Steatosis as determinant of PH in the model

Finally, through a systematic image analysis, we were able to show that the sinusoidal space is severely restricted at 36 weeks, in correlation with a marked increase in liver fat and hepatocyte area, pointing to a direct compressive effect of fat-laden hepatocytes. The direct compressive effect of steatotic hepatocytes was already described

for alcoholic liver disease in the 1980's.[19,22] However, the relative contribution of this compressive effect could not be isolated from other confounding contributors, such as liver fibrosis or ED. Besides, the sinusoidal area was not directly quantified in those studies, and the compressive effect was deduced from an indirect observation (eg the increase in hepatocyte area). In our study, and following previous work by Hall et al,[15] we take advantage of the currently available image analysis tools to provide a direct quantification of both the hepatocyte area and number and of the sinusoidal area. Through this approach, we observed that IHVR and PP in the 36-week model only started to increase when the sinusoidal area went below a certain critical threshold. Given the absence of liver fibrosis or ED in the long-term model, we were able to show in a quantifiable manner the individual contribution of steatosis in this model on NASH.

4.4 | Implications

The implications of these findings could go beyond the abstract proof-of-concept on the contribution of steatosis to the development of PH in NASH. The dynamics of steatosis in NASH are markedly faster than that of fibrosis, and the decreases in PP observed in patients with NASH with non-controlled lifestyle interventions[30] or in the placebo arm of randomized controlled trials[31,32] could be because of rapid changes in steatosis leading to increased sinusoidal area and decreased IHVR. Unfortunately, in all these studies steatosis has been addressed in a semi-quantitative manner, and the structural influence of the effect has not been systematically addressed. The image analysis proposed in the present study can be easily standardized and could help at quantifying the effect of changes in steatosis on PH.

4.5 | Limitations

The main weakness of the present study is the lack of validation in patients with NASH. Although there is already evidence of the presence of PH in NAFLD even without fibrosis,[5] the ideal proof-of-concept validation in humans should include not only the structural histological quantification of steatosis and sinusoidal area, but also molecular and/or functional measurements of ED in patients with NAFLD or NASH but without fibrosis and, ideally, proof of change of PP with a decrease in steatosis and increase of sinusoidal area above critical thresholds. This would require dedicated collaborative prospective efforts, but would undoubtedly provide clinically relevant insights on the pathophysiology of NASH and PH. Another limitation of our study is the use of a single approach to evaluate the compressive effect of steatosis on the hepatic sinusoidal bed. Previous studies have elegantly used micro-CT and/or electronic microscope scanning of vascular corrosion casts to characterize the vascular changes induced by steatosis in NASH models.[25,33] These non-quantitative should be considered in subsequent experiments for an in-depth exploration of this structural effect.

In summary, in this proof-of-concept experimental study, we provide evidence that steatosis per se is able to induce a marked increase in IHVR and PP through a direct structural compression of the sinusoidal area, in the absence of other potential contributors to the effect (ED or liver fibrosis) in a long-term animal model of diet-induced NASH. We also provide a systematic histological image approach that could be used to quantify this effect in animal models and patients with NASH.

DISCLOSURES

SA has received Consulting fees from Gilead, IQVIA, Intercept, Novartis, Pfizer; speaking fees from Allergan, Gilead, MSD, Menarini, Novartis; and research grants from Gilead.

ORCID

Aurora Barberá https://orcid.org/0000-0002-6201-2643
Miren Bravo https://orcid.org/0000-0001-5889-9125
Joan Genescà https://orcid.org/0000-0002-0831-8422
María Martell https://orcid.org/0000-0002-0935-0029
Salvador Augustin https://orcid.org/0000-0002-3515-9033

REFERENCES

1. Liu Q, Bengmark S, Qu S. The role of hepatic fat accumulation in pathogenesis of non-alcoholic fatty liver disease (NAFLD). *Lipids Health Dis*. 2010;9:42.
2. Paschos P, Paletas K. Nonalcoholic fatty liver disease and metabolic syndrome. *Hippokratia*. 2009;13(1):9-19.
3. Benedict M, Zhang X. Non-alcoholic fatty liver disease: an expanded review. *World J Hepatol*. 2017;9(16):715-732.
4. Baffy G. Origins of portal hypertension in nonalcoholic fatty liver disease. *Dig Dis Sci*. 2018;63(3):563-576.
5. Francque S, Verrijken A, Mertens I, et al. Noncirrhotic human non-alcoholic fatty liver disease induces portal hypertension in relation to the histological degree of steatosis. *Eur J Gastroenterol Hepatol*. 2010;1:1449-1457.
6. Hirooka M, Koizumi Y, Miyake T, et al. Nonalcoholic fatty liver disease: portal hypertension due to outflow block in patients without cirrhosis. *Radiology*. 2015;274(2):597-604.
7. Francque S, Wamutu S, Chatterjee S, et al. Non-alcoholic steatohepatitis induces non-fibrosis-related portal hypertension associated with splanchnic vasodilation and signs of a hyperdynamic circulation in vitro and in vivo in a rat model. *Liver International*. 2010;30(3):365-375.
8. Pasarín M, La Mura V, Gracia-Sancho J, et al. Sinusoidal endothelial dysfunction precedes inflammation and fibrosis in a model of NAFLD. *PLoS One*. 2012;7(4):e32785.
9. García-Lezana T, Raurell I, Bravo M, et al. Restoration of a healthy intestinal microbiota normalizes portal hypertension in a rat model of nonalcoholic steatohepatitis. *Hepatology*. 2018;67(4):1485-1498.
10. Puoti C, Bellis L. Steatosis and portal hypertension. *Eur Rev Med Pharmacol Sci*. 2005;9(5):285-290.
11. Van der Graaff D, Kwanten W, Couturier F, et al. Severe steatosis induces portal hypertension by systemic arterial hyporeactivity and hepatic vasoconstrictor hyperreactivity in rats. *Lab Invest*. 2018;98(10):1263-1275.
12. Farrell G, Teoh N, Mccuskey R. Hepatic microcirculation in fatty liver disease. *The Anatomical Record: Adv Integrative Anatomy Evolutionary Biol*. 2008;291(6):684-692.
13. Ijaz S, Yang W, Winslet M, Seifalian A. Impairment of hepatic microcirculation in fatty liver. *Microcirculation*. 2003;10(6):447-456.

Appendix

14. Santhekadur PK, Kumar DP, Sanyal AJ. Preclinical models of non-alcoholic fatty liver disease. *J Hepatol*. 2018;68(2):230-237.
15. Hall A, Covelli C, Manuguerra R, et al. Transaminase abnormalities and adaptations of the liver lobule manifest at specific cut-offs of steatosis. *Sci Rep*. 2017;7(40977):1-9.
16. Pasarín M, Abraldes J, Rodríguez-Vilarrupla A, La Mura V, García-Pagán J, Bosch J. Insulin resistance and liver microcirculation in a rat model of early NAFLD. *J Hepatol*. 2011;55(5):1095-1102.
17. Ohmori S, Shiraki K, Sugimoto K, et al. High expression of CD34-positive sinusoidal endothelial cells is a risk factor for hepatocellular carcinoma in patients with HCV-associated chronic liver diseases. *Hum Pathol*. 2001;32(12):1363-1370.
18. Couvelard A, Scoazec JY, Feldmann G. Expression of cell-cell and cell-matrix adhesion proteins by sinusoidal endothelial cells in the normal and cirrhotic human liver. *Am J Pathol*. 1993;143(3):738-752.
19. Witek RP, Yang L, Liu R, et al. Liver cell-derived microparticles activate hedgehog signaling and alter gene expression in hepatic endothelial cells. *Gastroenterology*. 2009;136(1):320-330.
20. DeLeve LD, Wang X, Hu L, McCuskey MK, McCuskey RS. Rat liver sinusoidal endothelial cell phenotype is maintained by paracrine and autocrine regulation. *Am J Physiol Gastrointest Liver Physiol*. 2004;287(4):G757-G763.
21. Rodrigues S, Montani M, Guixé-Muntet S, De Gottardi A, Berzigotti A, Bosch J. Patients with signs of advanced liver disease and clinically significant portal hypertension do not necessarily have cirrhosis. *Clin Gastroenterol Hepatol*. 2019;17(10):2101-2109.e1.
22. Blendis L. Hepatocyte swelling and portal hypertension. *J Hepatol*. 1992;15(1–2):4-5.
23. Vidins E, Britton R, Medline A, Blendis L, Israel Y, Orrego H. Sinusoidal caliber in alcoholic and nonalcoholic liver disease: diagnostic and pathogenic implications. *Hepatology*. 1985;5(3):408-414.
24. Israel Y, Orrego H, Colman JC, Britton RS. Alcohol-induced hepatomegaly: pathogenesis and role in the production of portal hypertension. *Fed Proc*. 1982;41(8):2472-2477.
25. Francque S, Laleman W, Verbeke L, et al. Increased intrahepatic resistance in severe steatosis: endothelial dysfunction, vasoconstrictor overproduction and altered microvascular architecture. *Lab Invest*. 2012;92(10):1428-1439.
26. Xie G, Choi SS, Syn W-K, et al. Hedgehog signalling regulates liver sinusoidal endothelial cell capillarisation. *Gut*. 2013;62(2):299-309.
27. Guy CD, Suzuki A, Zdanowicz M, et al. Hedgehog pathway activation parallels histologic severity of injury and fibrosis in human nonalcoholic fatty liver disease. *Hepatology*. 2012;55(6):1711-1721.
28. Rangwala F, Guy CD, Lu J, et al. Increased production of sonic hedgehog by ballooned hepatocytes. *J Pathol*. 2011;224(3):401-410.
29. Estep M, Mehta R, Bratthauer G, et al. Hepatic sonic hedgehog protein expression measured by computer assisted morphometry significantly correlates with features of non-alcoholic steatohepatitis. *BMC Gastroenterol*. 2019;19(1):27.
30. Berzigotti A, Albillos A, Villanueva C, et al. Effects of an intensive lifestyle intervention program on portal hypertension in patients with cirrhosis and obesity: the SportDiet study. *Hepatology*. 2017;65(4):1293-1305.
31. Harrison S, Abdelmalek M, Caldwell S, et al. Simtuzumab is ineffective for patients with bridging fibrosis or compensated cirrhosis caused by nonalcoholic steatohepatitis. *Gastroenterology*. 2018;155(4):1140-1153.
32. Garcia-Tsao G, Bosch J, Kayali Z, et al. Randomized placebo-controlled trial of emricasan in Non-alcoholic Steatohepatitis (NASH) cirrhosis with severe portal hypertension. *J Hepatol*. 2020;72(5):885-895.
33. Lefere S, Van de Velde F, Hoorens A, et al. Angiopoietin-2 promotes pathological angiogenesis and is a therapeutic target in murine nonalcoholic fatty liver disease. *Hepatology*. 2019;69(3):1087-1104.

SUPPORTING INFORMATION

Additional supporting information may be found online in the Supporting Information section.

How to cite this article: Barberá A, Raurell I, García-Lezana T, et al. Steatosis as main determinant of portal hypertension through a restriction of hepatic sinusoidal area in a dietary rat nash model. *Liver Int*. 2020;40:2732–2743. https://doi.org/10.1111/liv.14632

10.3.2. Publication 2

Pinheiro I, Barberá A, Raurell I, Estrella F, de Leeuw M, Bolca S, Gottardi D, Horscroft N, Possemiers S, Salcedo MT, Genescà J, Martell M, Augustin S. A Nine-Strain Bacterial Consortium Improves Portal Hypertension and Insulin Signaling and Delays NAFLD Progression In Vivo. Biomedicines. 2022;10(5):1191.

DOI: 10.3390/biomedicines10051191

biomedicines

MDPI

Article

A Nine-Strain Bacterial Consortium Improves Portal Hypertension and Insulin Signaling and Delays NAFLD Progression In Vivo

Iris Pinheiro [1,*,†], Aurora Barberá [2,†], Imma Raurell [2,3], Federico Estrella [2], Marcel de Leeuw [1], Selin Bolca [1], Davide Gottardi [1], Nigel Horscroft [1], Sam Possemiers [1], María Teresa Salcedo [4], Joan Genescà [2,3], María Martell [2,3] and Salvador Augustin [2,3,*]

[1] MRM Health NV, 9052 Ghent, Belgium; marcel.deleeuw@mrmhealth.com (M.d.L.); selin.bolca@mrmhealth.com (S.B.); davide.gottardi2@unibo.it (D.G.); nigel.horscroft@mrmhealth.com (N.H.); sam.possemiers@mrmhealth.com (S.P.)
[2] Liver Unit, Department of Internal Medicine, Hospital Universitari Vall d'Hebron, Institut de Recerca Vall d'Hebron, Universitat Autònoma de Barcelona, 08035 Barcelona, Spain; aurora.barbera@vhir.org (A.B.); imma.raurell@vhir.org (I.R.); dr.estrella1@gmail.com (F.E.); jgenesca@vhebron.net (J.G.); maria.martell@vhir.org (M.M.)
[3] Centro De Investigación Biomédica en Red de Enfermedades Hepáticas y Digestivas, Instituto De Salud Carlos III, 28029 Madrid, Spain
[4] Pathology Department, Hospital Universitari Vall d'Hebron, Universitat Autònoma de Barcelona, 08035 Barcelona, Spain; mtsalcedo@vhebron.net
* Correspondence: iris.pinheiro@mrmhealth.com (I.P.); salva.augustin@gmail.com (S.A.); Tel.: +32-92770864 (I.P.)
† These authors contributed equally to this work.

check for updates

Citation: Pinheiro, I.; Barberá, A.; Raurell, I.; Estrella, F.; de Leeuw, M.; Bolca, S.; Gottardi, D.; Horscroft, N.; Possemiers, S.; Salcedo, M.T.; et al. A Nine-Strain Bacterial Consortium Improves Portal Hypertension and Insulin Signaling and Delays NAFLD Progression In Vivo. *Biomedicines* **2022**, *10*, 1191. https://doi.org/10.3390/biomedicines10051191

Academic Editors: Juan Manuel Pericas, Andreea Ciudin and Francisco Javier Cubero

Received: 20 April 2022
Accepted: 19 May 2022
Published: 20 May 2022

Publisher's Note: MDPI stays neutral with regard to jurisdictional claims in published maps and institutional affiliations.

Copyright: © 2022 by the authors. Licensee MDPI, Basel, Switzerland. This article is an open access article distributed under the terms and conditions of the Creative Commons Attribution (CC BY) license (https://creativecommons.org/licenses/by/4.0/).

Abstract: The gut microbiome has a recognized role in Non-alcoholic fatty liver disease (NAFLD) and associated comorbidities such as Type-2 diabetes and obesity. Stool transplantation has been shown to improve disease by restoring endothelial function and insulin signaling. However, more patient-friendly treatments are required. The present study aimed to test the effect of a defined bacterial consortium of nine gut commensal strains in two in vivo rodent models of Non-alcoholic steatohepatitis (NASH): a rat model of NASH and portal hypertension (PHT), and the Stelic animal (mouse) model (STAM™). In both studies the consortium was administered orally q.d. after disease induction. In the NASH rats, the consortium was administered for 2 weeks and compared to stool transplant. In the STAM™ study administration was performed for 4 weeks, and the effects compared to vehicle or Telmisartan at the stage of NASH/early fibrosis. A second group of animals was followed for another 3 weeks to assess later-stage fibrosis. In the NASH rats, an improvement in PHT and endothelial function was observed. Gut microbial compositional changes also revealed that the consortium achieved a more defined and richer replacement of the gut microbiome than stool transplantation. Moreover, liver transcriptomics suggested a beneficial modulation of pro-fibrogenic pathways. An improvement in liver fibrosis was then confirmed in the STAM™ study. In this study, the bacterial consortium improved the NAFLD activity score, consistent with a decrease in steatosis and ballooning. Serum cytokeratin-18 levels were also reduced. Therefore, administration of a specific bacterial consortium of defined composition can ameliorate NASH, PHT, and fibrosis, and delay disease progression.

Keywords: NAFLD; gut microbiome; bacterial consortium; portal hypertension; fibrosis

1. Introduction

Non-alcoholic fatty liver disease (NAFLD), and its progressive form non-alcoholic steatohepatitis (NASH), is the hepatic manifestation of metabolic syndrome, and common

comorbidities include obesity, type 2 diabetes mellitus (T2DM), hyperlipidemia, and hypertension [1]. Metabolic dysregulation is a hallmark of NAFLD, and insulin resistance (IR), hyperlipidemia, or dyslipidemia are common features. The gut microbiome has gained much attention in the past few years and its association with metabolic syndrome-related disorders, namely NAFLD, is well documented [2–4]. In this regard, numerous gut-born metabolites, synthetized by microbes, have been implicated in disease progression [4,5]. However, some gut-born metabolites may be of benefit to metabolic diseases. For instance, short-chain fatty acids (SCFAs), such as butyrate and propionate, have demonstrated positive effects, such as promoting the production of the anorexigenic peptides Peptide YY (PYY) and Glucagon-like peptide 1 (GLP1) [6]. Moreover, butyrate and propionate have well-established barrier protective and anti-inflammatory roles in the intestine [7]. Conversely, colonic inflammation lowers the abundance of SCFA-producing bacteria: a reduction in the genus *Faecalibacterium*, containing butyrate producers, has been observed in NASH patients [8]. Therefore, the growing interest in the gut–liver axis has opened avenues for the treatment or prevention of NAFLD using gut microbial approaches [9,10]. Previous studies have shown that the transfer of fecal microbiota collected from lean rats into NASH rats fed a high-fat glucose/fructose diet (HFGFD) restored the sensitivity to insulin of the hepatic protein kinase B (Akt)-dependent endothelial nitric oxide synthase (eNOS) signaling pathway, and thereby led to an improvement in intrahepatic vascular resistance (IHVR) and portal pressure (PP) [11]. Despite the observed protective effects on liver endothelial function, fecal transfer is unlikely to become a long-term therapeutic option, especially considering the chronic and progressive nature of this disease. Consequently, microbial-based therapies of defined composition would represent a more patient-friendly approach.

Therefore, in the current study we tested the efficacy of a bacterial consortium composed of nine human gut commensal strains capable of producing both butyrate and propionate, on a rat NASH model of portal hypertension (PHT) and compared it to that of fecal microbiota transplantation (FMT) from lean rats. We also tested the same nine-strain bacterial consortium in a rodent model described to develop liver fibrosis at histopathology: the STAM™ mouse model.

2. Materials and Methods

2.1. Rat NASH Model of Portal Hypertension (PHT)

Male Sprague-Dawley OFA rats (Charles River Laboratories, l'Arbresle, France), weighting 200–220 g were used for the diet-induced NASH model, as previously described [11]. Briefly, animals had ad libitum access to a high-fat high-glucose/fructose diet (HFGFD) for 8 weeks (Figure 1A and Supplementary Materials), during which body weight and food and drink consumption were monitored weekly. After that, they were randomized into three groups: HFGFD-vehicle (HFGFD-VEH, n = 13), HFGFD-consortium of nine human commensal bacterial strains (HFGFD-CON, n = 11), and HFGFD-transplanted with fecal microbiota from lean rats (HFGFD-FMT, n = 11). HFGFD-VEH individuals received oral probing vehicle (sterile PBS), while individuals in HFGFD-CON and HFGFD-FMT groups were subjected to different microbiota-based treatments, which consisted of oral administration of a bacterial consortium of defined composition and fecal microbiota transplantation (FMT), respectively (see further). The consortium treatment started after 8 weeks of HFGFD intervention, and it consisted of the administration of the following nine human gut commensal strains: *Faecalibacterium prausnitzii*, *Butyricicocccus pullicaecorum*, *Roseburia inulinivorans*, *Akkermansia muciniphila*, *Lactiplantibacillus plantarum* (former *Lactobacillus plantarum*), *Anaerostipes caccae*, *Phocaeicola vulgatus* (former *Bacteroides vulgatus*), *Veillonella parvula*, and *Blautia obeum*. On each dosing day, lyophilized consortium was washed and reconstituted in anaerobic DPBS (5340 g, 10 min, ambient), in an anaerobic hood (N2:CO2:H2; 80:10:10). As a result, a concentrated liquid, ready-to-use formulation in air-tight vials, was obtained. This suspension was administered immediately. Animals were dosed daily with 2×10^9 CFU (total counts of the 9 strains), using a disposable oral probe (Biochrom Ltd., Cambridge, UK); this procedure was repeated every 24 h for 2 weeks. For individuals

belonging to the vehicle group, the same procedure was followed, but sterile DPBS was administered instead. Rats receiving the bacterial consortium were housed individually throughout the treatment period to avoid cross-contamination.

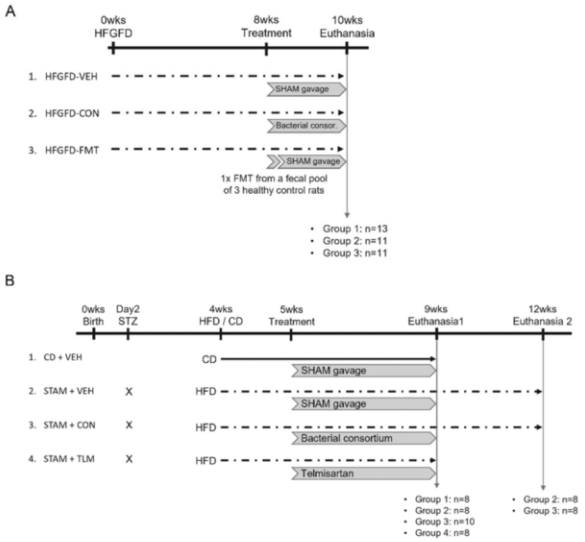

Figure 1. Experimental design. (**A**) Rat NASH model of PHT. Rats were fed a high-fat, high-glucose/fructose diet (HFGFD) for 8 weeks, after which they received either sham or bacterial consortium treatment for 2 additional weeks. HFGFD-VEH: group of NASH rats receiving sham gavage (vehicle); HFGFD-CON: group of NASH rats receiving the 9-strain bacterial consortium daily (2×10^9 CFU/d, total counts); HFGFD-FMT: group of NASH rats receiving fecal microbiota transplantation from control lean rats ($1\times$ transplantation followed by sham gavage). (**B**) STAM™ mouse study. C57BL/6J male mice were subcutaneously injected with 200 µg STZ, a β-cell toxin, two days after birth. At 4 weeks of age animals received a high-fat diet (HFD) or regular control diet (CD). At 5 weeks of age treatment was initiated: control diet animals and STAM mice received sham gavage (CD + VEH and STAM + VEH, respectively) for a total of 4 weeks. In the two test groups, STAM animals received either the 9-strain consortium (10^9 CFU/d, total counts) (STAM + CON) or Telmisartan (10 mg/kg/d) (STAM + TLM) also for a total of 4 weeks. At 9 weeks of age, the animals were sacrificed (euthanasia 1). Two groups of STAM animals belonging to the vehicle control or the consortium groups were followed for an additional three weeks until sacrifice at 12 weeks of age (euthanasia 2).

Fecal microbiota transplantation (FMT) was also performed after 8 weeks of HFGFD intervention. To achieve higher homogeneity in the transplantation procedure, feces from three control (lean) rat donors were pooled to be used for transplantation. With the aim of reducing gastric acidity and thus increasing the survival of the microorganisms, omeprazole was administered orally at a dose of 50 kg/day during the 3 days prior to intestinal decontamination. To proceed with intestinal emptying, rats were maintained in isolation in fast grills, and two oral doses of CitraFleet (sodium picosulfate, 0.16 mg/mL and magnesium oxide 51.2 mg/mL) of 1 mL and 2 mL were administered 24 h and 12 h, respectively, before the transplant. These administrations were accompanied by 2 mL of

water each. Recolonization was performed by a single oral gavage, for which 100 mg of the fecal pool were dissolved in 2 mL of sterile DPBS. In both the consortium and FMT groups, the treatment period lasted 2 weeks during which animals were maintained on the original diet (Figure 1A). Rats were housed under a 12 h light/dark cycle at constant temperature (24 ± 1 °C) and relative humidity ($55 \pm 10\%$). At week 10, liver hemodynamics and blood biochemistry were performed, and liver tissue samples were collected for histological and molecular analyses. In addition, the cecum content was collected for shotgun sequencing of gut microbes (Supplementary Materials). For metagenomics analysis, fecal samples were also obtained from a group of rats receiving a regular diet to compare HFGFD-induced changes on microbial composition with those of rats fed a control diet (CD).

2.2. STAM™ Mouse Model of NASH

The STAM™ study was conducted by SMC Laboratories in Japan, following previously reported protocols [12,13]. Briefly, NASH was induced in C57 BL/6J male mice by a single subcutaneous injection of 200 µg streptozotocin (STZ, Sigma-Aldrich, St. Louis, MO, USA) 2 days after birth, to induce mild pancreatic islet inflammation and destruction (Figure 1B). At 4 weeks of age, the animals initiated a high-fat diet (HFD, 57 kcal% fat, Cat# HFD32, CLEA Japan, Inc., Tokyo, Japan). Animals were randomized into three treatment groups based on their body weight the day before initiating the HFD. At 5 weeks of age (after one week on HFD), the animals received either sham gavage (STAM + VEH, $n = 16$), the nine-strain bacterial consortium (STAM + CON, $n = 18$), or Telmisartan (STAM + TLM, $n = 8$), an angiotensin II receptor blocker that decreases hepatic fat accumulation and inhibits hepatic stellate cell activation and thus suppresses hepatic fibrogenesis [14]. Vehicle (sterile PBS) and bacterial consortium were administered orally in a volume of 200 µL/mouse; the consortium was administered at the dose of 10^9 CFU/day (total counts of the 9 strains) for a total of 4 weeks. Product suspensions were prepared as described above. Telmisartan was used as benchmark and administered orally at the daily dose of 10 mg/kg in a volume of 10 mL/kg for 4 weeks. For that, one tablet of Telmisartan was transferred into a mortar and triturated with pestle by adding pure water until obtaining a homogenous suspension of 1 mg/mL. All treatments were prepared freshly prior to administration. A control group fed a regular diet and receiving sham gavage was also included in this study (CD + VEH, $n = 8$) (Figure 1B). Body weight was recorded daily during the experimental period. Animals were maintained in a SPF facility under controlled conditions of temperature (23 ± 3 °C), humidity ($50 \pm 20\%$), lighting (12 h artificial light and dark cycles; light from 8:00 to 20:00), and air exchange.

Animals belonging to the control (CD + VEH, $n = 8$) and STAM groups (STAM + VEH, STAM + CON, and STAM + TLM, $n = 8$, $n = 10$, or $n = 8$, respectively) were sacrificed after 4 weeks of treatment, i.e., at 9 weeks of age, which corresponds to a steatohepatitis/early fibrosis stage. In addition, two groups of STAM animals belonging to the vehicle ($n = 8$) and consortium ($n = 8$) groups were followed for three additional weeks and were sacrificed at 12 weeks of age, which corresponds to a stage of late fibrosis. This was performed to investigate the potential of the bacterial consortium to delay disease progression upon cessation of treatment (Figure 1B). Animals were sacrificed by exsanguination through direct cardiac puncture under isoflurane anesthesia (Pfizer Inc., Tokyo, Japan). Blood was collected for biochemistry, and the whole liver for immunohistochemistry and histopathology.

2.3. Blood Biochemistry

Blood samples from fasting rats were collected from the cava vein at sacrifice. Glucose, bilirubin, alanine aminotransferase (ALT), aspartate aminotransferase (AST), cholesterol, high-density lipoprotein (HDL), low-density lipoprotein (LDL), triglycerides, and albumin were measured with standard methods at the Hospital Vall d'Hebron CORE lab. Insulin was measured using an ELISA kit following the manufacturer's instructions (EMD Millipore, Billerica, MA, USA). Insulin resistance was estimated by applying the homeostasis

model of insulin resistance index (HOMA-IR): (fasting insulin (ng/mL) × fasting glucose (mg/dL))/405.

In the STAM™ mice, non-fasting blood was drawn from the facial vein for the quantification of glycated hemoglobin (HbA1c), cytokeratin (CK)-18, and biochemistry. HbA1c levels were quantified in whole blood by DCN2000 + (Siemens Healthcare Diagnostics, USA). Serum CK-18 levels were measured by using the Mouse Cytokeratin 18-M30 ELISA kit (Cusabio Biotech Co., Ltd., Wuhan, China). Serum alanine aminotransferase (ALT) and triglyceride levels were measured by FUJI DRI-CHEM 7000 (Fujifilm Corporation, Tokyo, Japan). Serum total cholesterol, high-density lipoprotein (HDL)-cholesterol, and low-density lipoprotein (LDL)-cholesterol levels were quantified by HPLC at Skylight Biotech Inc. (Akita, Japan).

2.4. Histological Analyses

Animal liver samples were extracted, fixed in 4% formalin, embedded in liquid paraffin at 65 °C, and sectioned in 4 µm thick slices (rats) or fixed in Bouin´s solution (Sigma-Aldrich Japan, Tokyo, Japan) (mice). Samples were then stained with hematoxylin and eosin (H&E) to assess liver parenchyma, or with Sirius red to detect collagen fibers. All stained liver samples were examined by an expert liver pathologist blinded to the interventions.

The diagnosis of NASH in rats was established based on the presence of all three characteristic patterns of the disease, which include the coexistence of steatosis, lobular inflammation, and hepatocellular ballooning. The NASH-CRN Activity Score (NAS) was used to quantify NASH activity. NAS comprises the unweighted sum of the histological components: steatosis (0–3), lobular inflammation (0–3), and hepatocellular ballooning (0–2). Fibrosis was also classified in five stages according to the NASH-CRN system, ranging from F0 (no fibrosis) to F4 (cirrhosis). NAFLD Activity score (NAS) of STAM™ mice was calculated according to the criteria of Kleiner [15].

2.5. Liver Hemodynamics

The hemodynamic measurements were performed in fasted rats under intraperitoneal anesthesia with ketamine (100 mg/kg) plus midazolam (5 mg/kg) and body temperature maintained at 37 °C. Mean arterial pressure (MAP) was measured by catheterization of the femoral artery and portal pressure (PP) assessed by ileocolic vein catheterization using highly sensitive pressure transducers (Harvard apparatus, Holliston, MA, USA). Superior mesenteric artery (SMA) blood flow (SMABF, mL/(min × 100 g)) and portal blood flow (PBF, mL/(min × 100 g)) were measured with a perivascular ultrasonic transit-time flow probe (1 mm diameter, Transonic systems Inc, Ithaca, NY, USA). SMA resistance (SMAR) and intrahepatic vascular resistance (IHVR, mmHg/mL × min × 100 g) were calculated as ((MAP-PP)/SMABF) and (PP/PBF), respectively.

2.6. Western Blot

Rat livers were perfused with saline for exsanguination and samples were directly frozen in liquid nitrogen and stored at −80 °C until further use. Then, liver samples were crushed cold and homogenized in Triton-lysis buffer, sonicated, and centrifuged at 14,000 rpm for 10 min at 4 °C. Supernatant total protein concentration was quantified by a BCA protein assay kit (ThermoFisher Scientific, Waltham, MA, USA). Forty (40) micrograms of protein was run on a 10% sodium dodecyl sulphate–polyacrylamide gel electrophoresis (SDS-PAGE). Proteins separated by SDS-PAGE were transferred onto a polyvinylidene fluoride (PVDF) membrane (ThermoFisher Scientific, Waltham, MA, USA). Membranes were washed with TTBS 1X several times and blocked for 1 h at RT with PhosphoBLOCKERTM 5% (Cell biolabs, San Diego, CA, USA) to detect the phosphorylated proteins P-Akt (1/500, Cell signaling, Danvers, MA, USA) and P-eNOS (Ser1177, 1/250), or with skimmed milk to detect Kruppel-Like Factor 2 (Klf2) (1/200, Santa Cruz biotechnology, Dallas, TX, USA). Gapdh antibody (1/5000, Ambion, Austin, TX, USA) was used as the loading control. Membranes were developed using the ECL kit (GE Healthcare; Little

Chalfont, UK) and protein expression was finally determined by densitometry analysis bands using Image Studio Lite (Lincoln, NE, USA).

2.7. Real-Time PCR

Rat liver samples were maintained at least 24 h in RNA*later* (ThermoFisher Scientific, Waltham, MA, USA) and then stored at −80 °C until further use. Total RNA was extracted by using the RNeasy mini-Kit (QIAGEN, Venlo, The Netherlands), and retro-transcribed to complementary DNA (High-capacity cDNA reverse transcription, ThermoFisher Scientific, Waltham, MA, USA). Twenty (20) nanograms of cDNA was added to Taqman universal PCR master mix plus the specific Taqman probes for *α-Sma* (alpha-Smooth muscle actin, Reference code: Rn01759928_g1) and *Col1a1* (Collagen type I alpha 1 chain, Reference code: Rn01463848_m1) (Life Technologies Ltd., Renfrew, UK). Quantitative reverse-transcription polymerase chain reaction (qRT-PCR) was performed using the 7900HT Fast Real-Time PCR system (ThermoFisher Scientific, Waltham, MA, USA), based on a standard protocol of 40 cycles at 95–60 °C. The relative gene expression was normalized to *β-Actin*. Data were analyzed using the Relative Quantification qPCR Application in ThermoFisher Cloud. For results calculation, the $2^{-\Delta\Delta Ct}$ method was used.

2.8. Biological Parameter Analyses

Continuous variables were tested for normality using the D'Agostino–Pearson normality test and are documented as mean ± standard error of the mean (SEM). Statistical analyses were performed using GraphPad Prism software (GraphPad Software, San Diego, CA, USA). Biological parameters of treatment groups were compared by Student's *t*-test or One-Way ANOVA with Dunnett's multiple comparisons' test. A p-value < 0.05 was considered statistically significant.

3. Results

3.1. The Nine-Strain Bacterial Consortium Improves Portal Hypertension (PHT), Endothelial Dysfunction (ED), and Fibrotic Markers in the Rat NASH Model of PHT

At the end of the 2-week treatment period, body weight (BW), blood biochemistry, NASH histology, and systemic and portal hemodynamics were evaluated to elucidate the effects of the bacterial consortium treatment and FMT on the regulation of PHT and ED in NASH rats.

3.1.1. Microbiota-Based Treatments Significantly Improved Body Weight

The HFGFD intervention induced a marked increase in BW (Table 1 and Figure S1A). During the 2-week treatment period, animals in the HFGFD-VEH group continued increasing their BW to a great extent (22.08 ± 3.18 g). However, HFGFD-CON only gained on average 2.91 ± 3.55 g ($p < 0.05$), whereas HFGFD-FMT lost on average 5 ± 3.47 g ($p < 0.05$). Compared to the HFGFD-VEH, both groups receiving microbiota-based treatments gained significantly less weight during the 2-week treatment.

3.1.2. The Metabolic Profile Improved in the Treatment Groups

Both microbiota-based treatments displayed an important reduction in fasting blood glucose and insulin levels, and HOMA-IR index with respect to the HFGFD-VEH group, although these differences did not reach statistical significance (Table 1 and Figure S1B,C). Both treatments showed a significant but slight increase in triglycerides when compared to the vehicle group. Cholesterol fractions remained unchanged (Table 1). ALT levels were significantly reduced, and albumin was significantly improved in the FMT group.

3.1.3. No Treatment Group Significantly Reversed the NASH Histological Pattern

HFGFD intervention for 10 weeks resulted in a consistent reproduction of NASH histological hallmarks (i.e., co-occurrence of steatosis, hepatocellular ballooning, and lobular inflammation) (Figures S2 and S3). However, none of the 2-week microbiota-based

treatments were associated with significant improvements in overall NASH histological diagnosis or its individual features. This is in line with previously obtained results following microbiota transplantation in this particular NASH model [11]. Interestingly, no animals receiving HFGFD-CON presented inflammation or ballooning scores above 1 (Figure S2B,C). Finally, as shown in the Sirius red-stained liver sections in Figure S3, none of the groups developed fibrosis. This is also in agreement with previous results [11]. However, expression of the pro-fibrotic hepatic marker *Col1a1* was significantly reduced in the microbiota-based treatments when compared with the vehicle group; in contrast, *α-SMA* was only reduced by the consortium treatment (Figure 2).

Table 1. Biochemical characteristics after 2 weeks of intervention in the rat NASH model of PHT. HFGFD-VEH: group of NASH rats receiving sham gavage (vehicle); HFGFD-CON: group of NASH rats receiving the 9-strain bacterial consortium daily; HFGFD-FMT: group of NASH rats receiving fecal microbiota transplantation from control lean rats (1× transplantation followed by sham gavage).

	HFGFD-VEH ***n* = 13**	**HFGFD-CON** ***n* = 11**	**HFGFD-FMT** ***n* = 11**
Body weight pre-HFGFD (g)	254.46 ± 2.59	256 ± 2.1	256 ± 3.32
Body weight pre-trt. (g)	531.7 ± 10.3	543.6 ± 10.29	515.1 ± 13.48
Body weight gain with trt. (g)	22.08 ± 3.18	2.91 ± 3.55 *	−5 ± 3.47 *
Body weight post-trt. (g)	552.33 ± 11.77	546.6 ± 11.53	507 ± 12.39 *
Glucose (mg/dL)	182.45 ± 14.94	166.9 ± 14.89	171.36 ± 10.47
Insulin (ng/mL)	15.36 ± 3.6	9.24 ± 1.17	11.21 ± 1.13
HOMA-IR	7.89 ± 2.3	3.7 ± 0.54	4.68 ± 0.45
Albumin (g/dL)	2.9 ± 0.04	3.03 ± 0.05	3.13 ± 0.06*
Bilirubin (mg/dL)	0.09 ± 0.01	0.09 ± 0.02	0.11 ± 0.01
AST (IU/L)	205.56 ± 34.05	234.29 ± 45.72	172 ± 63.52
ALT (IU/L)	66.15 ± 4.36	67.1 ± 9.29	47.5 ± 31.31 *
TG (mg/dL)	27.92 ± 1.35	33 ± 1.91 *	33.54 ± 2.96 *
Total cholesterol (mg/dL)	75.54 ± 4.75	86.78 ± 3.89	78.91 ± 2.99
Cholesterol HDL (mg/dL)	41.93 ± 2.43	46.78 ± 1.97	45.54 ± 2.48
Cholesterol LDL (mg/dL)	25.27 ± 2.52	34.75 ± 3.4	27 ± 1.96

* $p \leq 0.05$ versus HFGFD-VEH. Abbreviations: ALT, alanine aminotransferase; AST, aspartate aminotransferase; HDL, high-density lipoprotein; HFGFD, high-fat, high-glucose/fructose diet; HOMA-IR, Homeostasis model of insulin resistance index; LDL, low-density lipoprotein; TG, triglycerides.

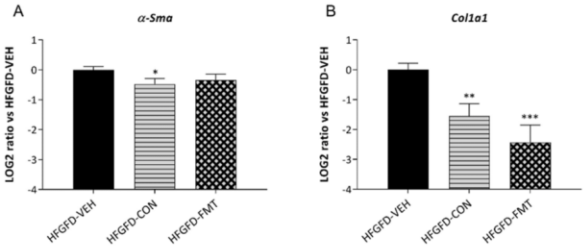

Figure 2. Relative mRNA expression of (**A**) *α-Sma* and (**B**) *Col1a1* measured by quantitative RT-PCR in the liver of NASH rats and expressed as log2 ratio. *β-Actin* was used as an endogenous control, and results were normalized to the HFGFD-VEH group. HFGFD-VEH: group of NASH rats receiving sham gavage (vehicle); HFGFD-CON: group of NASH rats receiving the 9-strain bacterial consortium daily; HFGFD-FMT: group of NASH rats receiving fecal microbiota transplantation from control lean rats (1× transplantation followed by sham gavage). Abbreviations: α-Sma, alpha-Smooth muscle actin; Col1a1, Collagen type I alpha 1 chain. *, **, *** $p \leq 0.05$, ≤ 0.01, and ≤ 0.001, respectively, versus HFGFD-VEH.

3.1.4. Microbiota-Based Treatments Significantly Reduced Portal Pressure and Improved Liver Hemodynamics

Consistent with previous findings [11,16], and despite the absence of histological fibrosis, animals in the 10-week HFGFD intervention showed values of portal pressure (PP) of 10.32 mmHg on average (Table 2). Importantly, both the bacterial consortium treatment and FMT significantly reduced PP when compared to the vehicle-treated group, even while maintaining the HFGFD during the 2-week treatment period (Table 2). This decrease in PP observed in the HFGFD-CON group was secondary to a significant decrease (80% reduction) in intrahepatic vascular resistance (IHVR) as compared to HFGFD-VEH, in a similar degree as measured in the HFGFD-FMT group (104% reduction) (Table 2). Regarding systemic hemodynamics, no relevant differences were observed between groups (Table 2).

Table 2. Hemodynamic measurements after 2 weeks of intervention in the rat NASH model of PHT. HFGFD-VEH: group of NASH rats receiving sham gavage (vehicle); HFGFD-CON: group of NASH rats receiving the 9-strain bacterial consortium daily; HFGFD-FMT: group of NASH rats receiving fecal microbiota transplantation from control lean rats (1× transplantation followed by sham gavage).

	HFGFD-VEH ***n* = 13**	**HFGFD-CON** ***n* = 11**	**HFGFD-FMT** ***n* = 11**
MAP (mmHg)	113.05 ± 4.53	119.95 ± 4.21	117.34 ± 5.14
PP (mmHg)	10.32 ± 0.22	9.58 ± 0.19 *	9.21 ± 0.12 *
SMABF (mL/[min × 100 g])	2.73 ± 0.24	2.71 ± 0.21	2.82 ± 0.17
SMAR (mmHg/mL × min × 100 g)	40.78 ± 3.25	40.79 ± 4.36	39.35 ± 2.36
IHVR (mmHg/mL × min × 100 g)	7.58 ± 1.27	4.20 ± 0.35 *	3.71 ± 0.21 *

* $p \leq 0.05$ versus HFGFD-VEH. Abbreviations: HFGFD, high-fat, high-glucose/fructose diet; IHVR, intrahepatic vascular resistance; MAP, mean arterial pressure; PP, portal pressure; SMABF, superior mesenteric artery blood flow; SMAR, superior mesenteric artery resistance.

3.1.5. Features of ED Were Improved in Animals after Receiving Microbiota-Based Treatments

ED molecular hallmarks were assessed to further characterize the changes observed in IHVR and PP induced by the microbiota-based treatments with respect to the vehicle-treated group [17,18]. As seen in Figure 3, microbiota-based treatments induced a significant increase in P-Akt. P-eNOS showed a tendency to increase in both HFGFD-CON and HFGFD-FMT when compared to HFGFD-VEH, although it did not reach statistical significance. Interestingly, only the consortium-treated group showed a marked significant increase in Klf2 (Figure 3C).

3.1.6. Microbiota-Based Treatments Improved Cecal Species Diversity and Induced Composition Shifts

To verify the effect of both microbiota-based treatments on (bacterial) species diversity and taxonomic composition, the cecum content of rats was collected at sacrifice, and microbial DNA was extracted and sequenced. The Inverse Simpson diversity index revealed that, although not reaching the microbial diversity levels of the control diet (CD) group, diversity improved over vehicle (HFGFD-VEH) in both treatment groups; this was nearly statistically significant in the bacterial consortium (HFGFD-CON) treatment group (Figure 4).

Classifier performance as analyzed through balanced error rate (BER) suggested that HFGFD-CON induced a more defined change than HFGFD-FMT (Figure S4). In addition, the corresponding feature selection (VIP > 1, $n = 123$) showed that the bacterial consortium treatment induced the suppression of 72 (58.5% of observable change) vehicle-associated taxa and promoted the emergence of 48 (41.5%) non-product treatment associated taxa, whereas FMT, according to feature selection ($n = 0$), induced the suppression of 135 (75.8%) taxa, and replacement with 43 (24.2%) taxa. Hence, both treatments produced an important replacement of the HFGFD-VEH associated microbial community, but the bacterial consortium (CON) achieved a more defined and richer replacement than FMT. Figure S4B provides the top 10 discriminant taxa according to classifier estimated variable importance (VIP) and their associations, whereas Figure S4C combines the three VEH/CON,

VEH/FMT and CON/FMT contrasts into a single Euler plot proportional to the numbers of features selected for each contrast.

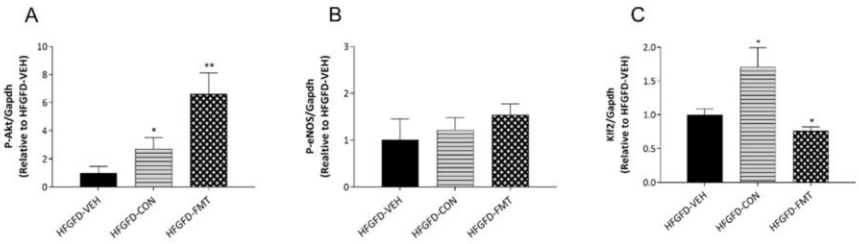

Figure 3. Expression of markers of endothelial dysfunction in NASH rats. (**A**–**C**) Western blot analysis of intrahepatic markers of endothelial dysfunction. Bar diagrams show the quantification of phosphorylated (P)-Akt, P-eNOS, and Klf2 using glyceraldehyde 3-phosphate dehydrogenase (Gapdh) as a loading control and normalized to the HFGFD-VEH group. HFGFD-VEH: group of NASH rats receiving sham gavage (vehicle); HFGFD-CON: group of NASH rats receiving the 9-strain bacterial consortium daily; HFGFD-FMT: group of NASH rats receiving fecal microbiota transplantation from control lean rats (1× transplantation followed by sham gavage). Abbreviations: Akt, Protein kinase B; eNOS, Endothelial nitric oxide synthase; Klf2, Kruppel-Like Factor 2. *, ** $p \leq 0.05$ and ≤ 0.01, respectively, versus HFGFD-VEH.

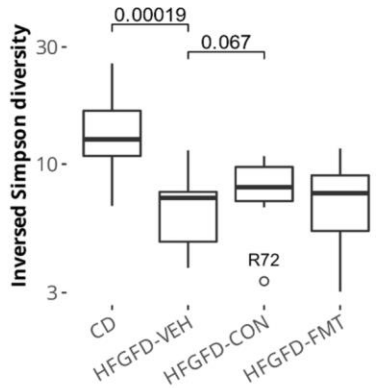

Figure 4. Microbial diversity in the cecum of NASH rats. Statistically significant differences are depicted above boxplots; these represent Wilcoxon signed–rank test ***p***-values computed without the outlier R72. HFGFD-VEH: group of NASH rats receiving sham gavage (vehicle); HFGFD-CON: group of NASH rats receiving the 9-strain bacterial consortium daily; HFGFD-FMT: group of NASH rats receiving fecal microbiota transplantation from control lean rats (1× transplantation followed by sham gavage).

3.1.7. The Nine-Strain Bacterial Consortium Induced Functional Microbiome Shifts

Changes in microbial composition, as evaluated by whole metagenome shotgun (WMS) sequencing, were used to conduct predictive pathway analysis to unravel putative biosynthetic pathways that could be modulated by treatment. The bacterial consortium (CON) treatment was predicted to drive an increase in microbial branched-chain amino acids

(BCAA) and a decrease in aromatic amino acids (AAA) biosynthesis capacities. In addition, methionine biosynthesis was also predicted to decrease. These changes over HFGFD-VEH were significant in the HFGFD-CON but not in the HFGFD-FMT group (Figure 5).

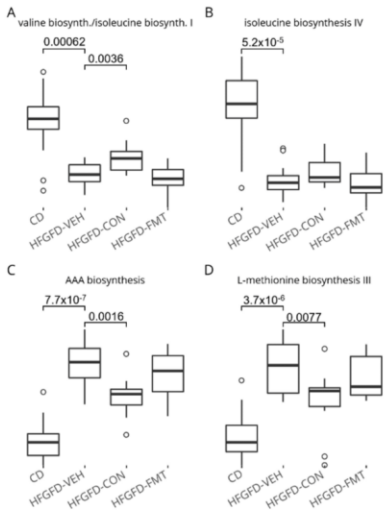

Figure 5. Predicted BCAA (**A**,**B**), AAA (**C**), and Methionine (**D**) biosynthesis pathways in the cecum of NASH rats. Statistically significant differences are depicted above boxplots. HFGFD-VEH: group of NASH rats receiving sham gavage (vehicle); HFGFD-CON: group of NASH rats receiving the 9-strain bacterial consortium daily; HFGFD-FMT: group of NASH rats receiving fecal microbiota transplantation from control lean rats (1× transplantation followed by sham gavage).

3.1.8. Microbiota-Based Treatments Induced Differential Hepatic Gene Expression

The expression of 20,359 liver genes was documented through RNA-Seq analysis of the three HFGFD groups. Of these, 444 (2.2%) were considered discriminant by sPLS-DA analysis for one or more of the CON/VEH, FMT/VEH or CON/FMT contrasts, with most genes being induced by treatment. Figure S5C depicts the breakdown on up- vs. downregulated discriminant genes. Table 3 provides details on gene expression modulation by the microbiota consortium of the top 1000 fatty liver associated genes according to the Harmonizome database, and eventual FMT equivalent. We have detected molecular chaperones to be predominantly modulated by both microbiota-based treatments. Among all modulated chaperones, we highlight the heat shock protein (Hsp) family members *Hspa1a*, *Hspa1b*, and *Hspa8*, as these were strongly downregulated by both treatments. Microbiota treatments also induced the downregulation of the endoplasmic reticulum (ER) chaperone BiP (*Hspa5*), as well as of its co-chaperone *Dnajb9*. Additional key genes downregulated by treatment were the cell division cycle *(Cdc)42* and the Rac family small GTPase *(Rac)1* (Table 3). The RNA-seq analysis also revealed that both microbial treatments enhanced the expression of several putative tumor suppressor genes (data not shown).

Table 3. Modulation of the top 1000 fatty liver disease genes in the liver of NASH rats. VEH: group of NASH rats receiving sham gavage (vehicle); CON: group of NASH rats receiving the 9-strain bacterial consortium daily; FMT: group of NASH rats receiving fecal microbiota transplantation from control lean rats (1× transplantation followed by sham gavage).

Rat Gene	Human Ortholog	CON/VEH Log2FC	CON/VEH pFDR	FMT/VEH Log2FC	FMT/VEH pFDR	Protein
Hspa1b	HSPA1B, HSPA1A	−3.48	0.002	−4.36	0.000	Heat shock 70 kDa protein 1B, and 1A
AABR07048992.1	HSPA8	−1.49	0.000	−1.50	0.000	Heat shock cognate 71 kDa protein
Hsph1	HSPH1	−0.74	0.060	−0.93	0.005	Heat shock protein 105 kDa
Pir	PIR	−0.74	0.084	-	-	Pirin
Sdf2l1	SDF2L1	−0.71	0.066	-	-	Stromal cell-derived factor 2-like protein 1
Dnajb9	DNAJB9	−0.71	0.016	−0.69	0.012	DNAJ homolog subfamily B member 9
LOC680121	HSPA8	−0.64	0.003	−0.48	0.024	Heat shock cognate 71 kDa protein
AABR07012795.1	PRDX1	−0.62	0.067	-	-	Peroxiredoxin−1
Hspa5	HSPA5	−0.61	0.058	−0.62	0.031	Endoplasmic reticulum chaperone BiP
Sult2a1	SULT2A1	−0.55	0.073	-	-	Sulfotransferase 2A1
Dusp6	DUSP6	−0.51	0.084	-	-	Dual specificity protein phosphatase 6
Calr	CALR	−0.40	0.030	−0.38	0.022	Calreticulin
Pnrc1	PNRC1	−0.40	0.081	-	-	Proline-rich nuclear receptor coactivator 1
Cdc42	CDC42	−0.36	0.000	−0.21	0.013	Cell division control protein 42 homolog
NEWGENE_620180	SLC40A1	−0.35	0.021	−0.43	0.002	Solute carrier family 40 member 1
Prdx1	PRDX1	−0.35	0.001	-	-	Peroxiredoxin-1
Litaf	LITAF	−0.34	0.000	-	-	Lipopolysaccharide-induced tumor necrosis factor-alpha factor
Atp2a2	ATP2A2	−0.32	0.065	−0.40	0.007	Sarcoplasmic/endoplasmic reticulum calcium ATPase 2
Slc10a1	SLC10A1	−0.30	0.081	−0.28	0.074	Sodium/bile acid cotransporter
Pdia3	PDIA3	−0.29	0.084	−0.29	0.051	Protein disulfide isomerase A3
Idh1	IDH1	−0.28	0.050	−0.32	0.008	Isocitrate dehydrogenase
Slc39a8	SLC39A8	−0.27	0.017	−0.19	0.093	Metal cation symporter ZIP8
Apoe	APOE	−0.26	0.067	−0.23	0.067	Apolipoprotein E
Maoa	MAOA	−0.25	0.049	−0.24	0.042	Amine oxidase
Ctsb	CTSB	−0.25	0.048	−0.34	0.001	Cathepsin B
Psmb4	PSMB4	−0.24	0.040	-	-	Proteasome subunit beta type-4
Ccnd3	CCND3	−0.24	0.051	-	-	G1/S-specific cyclin-D3
Dpp4	DPP4	−0.23	0.050	−0.35	0.000	Dipeptidyl peptidase 4
Aldoa	ALDOA	−0.23	0.067	-	-	Fructose bisphosphate aldolase A
Ctsd	CTSD	−0.22	0.069	−0.29	0.005	Cathepsin D
Rac1	RAC1	−0.21	0.000	−0.24	0.000	Ras-related C3 botulinum toxin substrate 1
Enpp1	ENPP1	−0.20	0.057	−0.26	0.004	Ectonucleotide pyrophosphatase/phosphodiesterase 1
Calm1	CALM1	−0.19	0.064	-	-	Calmodulin−1
Sdc2	SDC2	−0.19	0.064	−0.33	0.000	Syndecan-2
Akt1	AKT1	0.20	0.056	-	-	RAC-alpha serine/threonine-protein kinase
Abcg3l3	ABCG2	0.36	0.078	-	-	Broad substrate specificity ATP-binding cassette transporter ABCG2
Atm	ATM	0.39	0.006	-	-	Serine-protein kinase ATM
Abcg3l1	ABCG2	0.42	0.019	-	-	Broad substrate specificity ATP-binding cassette transporter ABCG2
Inhba	INHBA	0.48	0.099	-	-	Inhibin beta A chain
Abcc5	ABCC5	0.49	0.097	-	-	ATP-binding cassette sub-family C member 5
VEGFA	VEGFA	0.57	0.003	0.50	0.007	Vascular endothelial growth factor A
Egf	EGF	0.64	0.030	0.56	0.042	Pro-epidermal growth factor
LOC108348190	EGF	0.72	0.046	-	-	Pro-epidermal growth factor
Thrsp	THRSP	1.07	0.049	0.93	0.067	Thyroid hormone-inducible hepatic protein

Among the upregulated genes, the thyroid hormone responsive Spot14 (*Thrsp*) gene was found to be one of the main modulated genes, as both treatments considerably increased its expression. In addition, the AKT Serine/Threonine Kinase 1 (*Akt1*) was found to be only upregulated by the microbiota consortium (CON) treatment (Table 3).

Finally, over-representation analysis of differentially expressed genes induced by the microbiota consortium treatment was performed. Up- and downregulated genes were considered separately and both a restrictive (VIP > 1, pFDR < 0.1) and a relaxed (pFDR < 0.1) condition was used as input, generating respectively, 281 up- and 191 downregulated genes, and 489 up- and 326 downregulated genes. Consistent with the observed amelioration of the hepatic pro-fibrotic marker *Col1a1* (Figure 2B), liver transcriptomics identified numerous pro-fibrotic pathways being positively modulated by the two microbiome-based treatments. In this regard, we highlight the pro-fibrotic signaling pathways VEGFA-VEGFR2 (WP3888), Wnt signaling (WP428), and the Cytoskeletal regulation by Rho GTPases (P00016), all found to be putatively downregulated by the microbiota consortium (CON) treatment (Table 4).

Table 4. Putatively downregulated (as indicated by a downward arrow) pro-fibrotic signaling pathways in the liver of NASH rats treated with the 9-strain consortium.

Pathway ID	N	q-Value	Human Orthologs	Description
WP3888↓	21	0.090	RPS11, TPP1, ALDOA, PPP1CA, CTNND1, SDCBP, DNAJA1, CDC42, SSR4, DNAJB9, RAP1B, RHOA, PFN1, YWHAE, PSMD11, PAK2, SDF2L1, CALR, ATP6V0D1, HSPA1A, RAC1	VEGFA-VEGFR2 Signaling pathway
WP4656↑	8	0.067	CSPP1, CEP104, DVL1, OFD1, ATM, BBS4, PCM1, CEP120	Joubert Syndrome
WP428↓	7	0.091	RHOA, RAC1, WNT11, CCND3, PPP3R1, GPC4, NLK	Wnt Signaling
P00016↓	6	0.031	ARPC4, CDC42, ARPC5, PFN1, PAK2, RAC1	Cytoskeletal regulation by Rho GTPase
pid_21478↓	5	0.007	ARPC4, CDC42, PIR, ACTR3, RAC1	y branching of actin filaments
pid_5967↓	5	0.007	ARPC4, CDC42, RHOA, ACTR3, RAC1	Role of pi3k subunit p85 in regulation of actin organization and cell migration
R-HSA-390450↓	3	0.030	TCP1, CCT4, CCT8	Folding of actin by CCT/TriC
R-HSA-5625970↓	3	0.030	CDC42, RHOA, RAC1	RHO GTPases activate KTN1
R-HSA-389960↓	3	0.053	TCP1, CCT4, CCT8	Formation of tubulin folding intermediates by CCT/TriC

3.2. *The Nine-Strain Bacterial Consortium Delays Disease Progression and Improves NAFLD Disease Markers in the STAM™ Mouse Model*

Because liver transcriptomics performed in the NASH rats suggested that the tested bacterial consortium could be favorably modulating pro-fibrogenic pathways (Table 4), we were prompted to test the same consortium on a rodent model that displays notable signs of fibrosis at histopathology. For that, the STAM™ mouse model was used. The therapeutic effect of the nine-strain consortium was evaluated and compared to the benchmark Telmisartan. The effects were evaluated at the histopathological level and blood was collected for biochemical analysis. Because STAM animals are lean [19], as expected, the bacterial consortium did not improve BW (data not shown). As observed in the NASH rats, no significant alterations were detected in blood parameters, namely ALT and cholesterol

levels (Table 5). However, a trend of decreased whole blood levels of glycated hemoglobin (HbA1c) was observed by the end of the study (Figure S6).

Table 5. Biochemical characteristics after 4 weeks of intervention in the STAM™ mouse study. CD + VEH: group of control diet mice receiving sham gavage (vehicle); STAM + VEH: group of STAM mice receiving sham gavage (vehicle); STAM + CON: group of STAM mice receiving the 9-strain bacterial consortium daily; STAM + TLM: group of STAM mice receiving Telmisartan daily.

	CD + VEH ***n* = 8** **9 Weeks**	**STAM + VEH** ***n* = 8** **9 Weeks**	**STAM + CON** ***n* = 10** **9 Weeks**	**STAM + TLM** ***n* = 8** **9 Weeks**	**STAM + VEH** ***n* = 8** **12 Weeks**	**STAM + CON** ***n* = 8** **12 Weeks**
ALT (IU/L)	24.00 *** ± 1.27	39.38 ± 2.41	43.5 ± 3.28	35.00 ± 2.39	65.13 ± 14.04	60.63 ±12.81
TG (mg/dL)	79.63 * ± 10.46	500.9 ± 152.5	679.9 ± 91.35	465.6 ± 107.6	926.4 ± 251.6	1017 ± 248.8
Total cholesterol (mg/dL)	76.92 **** ± 3.51	125.7 ± 8.11	124.8 ± 4.32	132.7 ± 2.71	187.3 ± 41.99	186.9 ± 38.81
Cholesterol HDL (mg/dL)	57.84 ** ± 2.75	83.69 ± 7.13	75.55 ± 3.31	97.21 ± 4.73	72.24 ± 7.46	70.21 ± 6.84
Cholesterol LDL (mg/dL)	13.1 ± 0.66	14.68 ± 1.20	13.64 ± 0.74	18.78 * ± 1.10	24.35 ± 6.12	23.76 ± 5.16

*, **, ***, and **** $p \leq 0.05$, ≤ 0.01, ≤ 0.001, and ≤ 0.0001, respectively, versus STAM + VEH. Abbreviations: ALT, alanine aminotransferase; HDL, high-density lipoprotein; LDL, low-density lipoprotein; TG, triglycerides.

3.2.1. The Consortium of Nine Gut Commensals Improved NAS at Histopathology at 9 Weeks of Age

As expected [13], liver sections from the vehicle-treated STAM group exhibited micro- and macrovesicular fat deposition, hepatocellular ballooning, and inflammatory cell infiltration (Figures 6 and S7). The bacterial consortium-treated STAM mice (STAM-CON) displayed significantly reduced NAS scores when compared to the disease group at 9 weeks of age (Figure 6D). This was the result of reduced steatosis and ballooning scores (Figure 6B,C). At 12 weeks of age this was no longer observed.

3.2.2. The Consortium of Nine Gut Commensals Improved Fibrosis, and Showed Reduced Hepatic Expression of F4/80 and Serum CK-18 Levels

To evaluate collagen deposition, liver sections were stained with Sirius red (Figures 7A and S8A). As expected, liver sections from the vehicle-treated STAM group (STAM-VEH) displayed increased collagen deposition in the pericentral region of the liver lobule when compared to the control diet group. The bacterial consortium-treated group (STAM-CON) showed a significant decrease in the fibrosis (Sirius red-positive) area when compared to the disease group at 12 weeks of age but not at 9 weeks of age, when the amount of fibrosis is lesser. This therapeutic effect on fibrosis was also confirmed on fibronectin immunostained liver sections (Figure S9).

To further evaluate inflammation, macrophage F4/80 immunostaining was used in liver sections. Even though no significantly reduced general inflammation was observed in H&E-stained sections (Figures 6A and S7), the F4/80-stained sections showed a significant reduction in macrophage inflammatory infiltration in the consortium-treated group at 9 weeks of age, and a trend to decrease at 12 weeks of age (Figures 7B and S8B). Finally, CK-18 serum levels were also significantly reduced in the consortium-treated group at 9 weeks of age, and a trend to decrease was observed by 12 weeks of age (Figure 7C), a result that correlates with reduced hepatocyte apoptosis and improved histological activity [20].

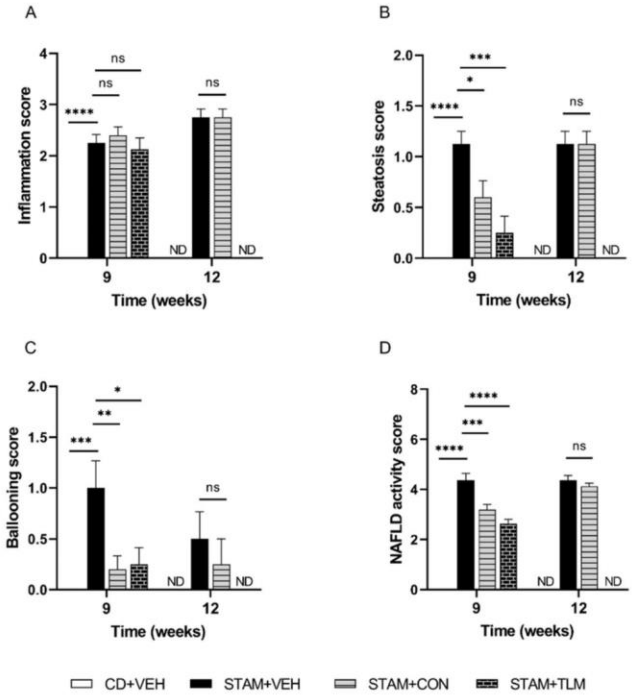

Figure 6. NAFLD activity score (NAS) in the STAM™ study. Histopathology was evaluated in H&E-stained liver sections, and the NAS score was calculated. The components (**A**) inflammation, (**B**) steatosis, (**C**) ballooning, and (**D**) the composite score, were evaluated at both 9 and 12 weeks of age (euthanasia 1 and 2, respectively). CD + VEH: group of control diet mice receiving sham gavage (vehicle); STAM + VEH: group of STAM mice receiving sham gavage (vehicle); STAM + CON: group of STAM mice receiving the 9-strain bacterial consortium daily; STAM + TLM: group of STAM mice receiving Telmisartan daily. ND: not determined for the CD + VEH and STAM + TLM groups at 12 weeks. ns: not significant. *, **, ***, **** $p \leq 0.05$, ≤ 0.01, ≤ 0.001, and ≤ 0.0001, respectively, versus STAM + VEH.

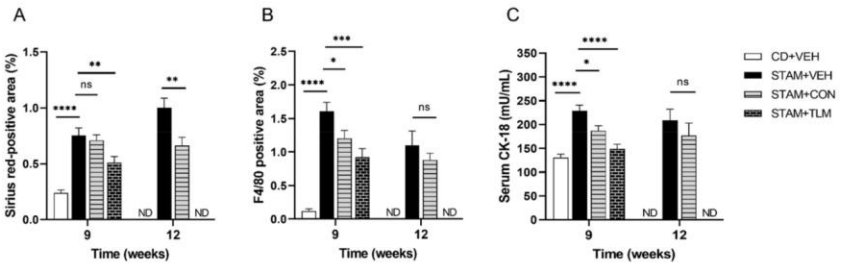

Figure 7. Hepatic fibrosis area, F4/80 positive area, and serum CK-18 levels in the STAM™ study. (**A**) Fibrosis assessed in Sirius red-stained liver sections. (**B**) Immunohistochemistry of macrophages evaluated in F4/80-immunostained sections. (**C**) Serum levels of CK-18, a marker for apoptotic hepatocytes. All markers were evaluated at both 9 and 12 weeks of age (euthanasia 1 and 2, respectively). CD + VEH: group of control diet mice receiving sham gavage (vehicle); STAM + VEH: group of STAM mice receiving sham gavage (vehicle); STAM + CON: group of STAM mice receiving the 9-strain bacterial consortium daily; STAM + TLM: group of STAM mice receiving Telmisartan daily. ND: not determined for the CD + VEH and STAM + TLM groups at 12 weeks. ns: not significant. *, **, ***, **** $p \leq 0.05$, ≤ 0.01, ≤ 0.001, and ≤ 0.0001, respectively, versus STAM + VEH.

4. Discussions

The gut–liver axis has a recognized role in NASH onset and progression, possibly fueled by the anatomo-functional crosstalk between the intestine and the liver. It is well described that a disrupted intestinal barrier integrity is frequently observed in NAFLD patients, and that the ensuing state of low-grade inflammation and endotoxemia, due to the translocation of harmful gut-born molecules, correlates with disease severity [21]. However, the effects of bacterial-derived molecules go beyond the translocation of microbe-associated molecular patterns (MAMPs) such as lipopolysaccharides (LPS), and numerous metabolites resulting from bacterial fermentation have been described to contribute to pathology [22]. Therefore, therapeutic approaches aimed to restore and balance the gut microbiome are considered a promising strategy to treat NASH and other liver diseases [23,24]. In this regard, FMT has been shown to improve disease pre-clinically in NASH rats, by restoring the insulin/p-Akt/p-eNOS signaling pathway, thereby improving IR and ED [11]. In humans, this treatment modality is also being explored [24,25], and although so far, no severe adverse events have been reported in NAFLD-FMT trials, several factors may hamper its clinical applicability such as the amount and frequency of stool transplantation, the need for bowel preparation prior to treatment, heterogeneity of fecal donors, and long-term expected effects [22]. Therefore, consortia of defined bacterial composition are a valuable alternative [22–24].

Relevant research, conducted in different animal models, has been previously performed using combinations of defined bacterial strains as therapeutic strategies in the management of NASH [23,26–28]. In the current study, we have tested a nine-strain consortium of gut commensals of defined composition and amount. Among others, the tested consortium was composed of four butyrate producers (*Faecalibacterium prausnitzii*, *Butyricicocccus pullicaecorum*, *Roseburia inulinivorans*, and *Anaerostipes caccae*) and five propionate producers (*Roseburia inulinivorans*, *Akkermansia muciniphila*, *Phocaeicola vulgatus*, *Veillonella parvula*, and *Blautia obeum*). We tested this consortium in a therapeutic setting in two rodent models of NASH: the rat NASH model of PHT, and the STAM™ mouse model. In rats, the consortium showed a protective effect on BW, a trend to improve fasting blood insulin levels and HOMA-IR, and a significant protective effect on PHT, namely a significant reduction in IHVR and PP. Similar to previous results [11] and to the FMT

group included in the current study, protection occurred through the restoration of the sensitivity to insulin of the hepatic Akt-dependent eNOS signaling pathway. In addition, an upregulation of Klf2 was observed in the liver of consortium-treated rats. This is also relevant, as the upregulation of hepatic Klf2 has been shown to ameliorate PHT in cirrhotic rats, via inactivation and apoptosis of hepatic stellate cells, together with a reduction in oxidative stress and improvement in endothelial function [17,18]. Despite these results, we did not observe improvement in NASH at histopathology. Nevertheless, this is also in accordance to previous studies testing the efficacy of stool transplantation in this model, specifically developed to evaluate diet-induced endothelial dysfunction and PHT in NASH, rather than NASH histopathology [11].

Previously, FMT has been shown to significantly alter the gut microbial composition of NASH rats [11]. However, FMT is preceded by intestinal emptying before stool transplant, which, in the current study, resulted in the suppression of numerous microbial taxa as opposed to the consortium treatment. Thus, we observed that the bacterial consortium induced more defined and richer changes in the gut microbiota than FMT. When translating these taxonomic shifts into predictive metabolic alterations, namely putative changes on microbial metabolic pathways, results suggested that the consortium was predicted to increase the biosynthesis of BCAA, and to decrease the biosynthesis of AAA and methionine. This is an interesting result, because a decreased BCAA/AAA ratio has been shown to correlate with liver dysfunction in cirrhotic patients [29]. Whether an altered fecal amino acid profile contributes to NAFLD disease progression in the current study remains to be determined. Nonetheless, BCAA treatment was shown to ameliorate liver fat accumulation in experimental animal models via increased production of acetic acid by gut microbes [30]. Therefore, this warrants further investigation, to determine whether the nine-strain bacterial consortium can effectively increase the levels of BCAA and decrease those of AAA as predicted, and thereby ameliorate disease.

The administration of the nine-strain consortium also altered the hepatic gene expression. Several disease-associated genes were downregulated by this treatment. Among these, several members of the heat shock family of proteins (HSP) were strongly downregulated by both the consortium and FMT treatments, including *Hspa1a*, *Hspa1b*, *Hspa8*, and *Hspa5*, all members of the Hsp70 family of proteins, and the Hsp40 co-chaperone *Dnajb9*. HSP are produced in response to stress and play an important role in assisting protein synthesis from the secretory pathways of the endoplasmic reticulum (ER), to ensure correct protein folding [31]. ER stress is involved in the progression of NAFLD to NASH and abnormal ER stress responses have direct pathological consequences, including fat accumulation, IR, inflammation, apoptosis, and, consequently, fibrosis [32]. Of importance, drugs targeting HSP as anti-fibrotics in NASH are currently in Phase II of clinical development (ClinicalTrials.gov NCT04267393). It is therefore conceivable that the observed downregulation of HSP by the microbiota-based treatments in our study reflects a diminished ER stress response. Among the upregulated genes, *Thrsp* (encoding Spot14) was found to be induced by both treatments. Spot14 (S14) was originally identified as a mRNA from rat liver that responded rapidly to thyroid hormone [33]. Recently, it has been described to play a key role in the tissue-specific regulation of lipid metabolism in response not only to thyroid hormone but also to dietary substrates such as glucose and polyunsaturated fatty acids, and also to other hormones such as insulin and glucagon [34]. Spot14 is involved in de novo synthesis of fatty acids, and in the export of lipids from the liver as very low-density lipoprotein (VLDL) particles [34]. Why the currently tested microbiota-based treatments would induce S14 transcription is not clear, but it may reflect the increased hepatic responsiveness to insulin, as suggested by studies performed both in rodents and obese patients [35–37].

Even though histological changes in fibrosis cannot be addressed in the NASH-PHT rat model, some pro-fibrotic markers such as *α-Sma* and *Col1a1* were found to be downregulated upon treatment with the nine-strain consortium. In addition, liver transcriptomics analysis suggested that a few fibrogenic pathways were downregulated by the treatment, such as the VEGFA-VEGFR2, the Wnt signaling, and the Cytoskeletal regulation by Rho

GTPases pathways [38]. However, because histological fibrosis cannot be adequately tested in the NASH-PHT rat model, we tested the same nine-strain consortium in a rodent model which developed liver fibrosis: the STAM™ mouse model. In this study, the consortium-treated animals showed anti-fibrotic effects, and significantly reduced collagen- and fibronectin-positive areas in liver sections at 12 weeks. Although a trend to decrease at 9 weeks was also observed, this did not reach statistical significance, possibly because of the lower fibrosis levels developed at that time point. In addition, consortium-treated animals also displayed a reduced F4/80 positive area, a marker for mouse macrophages, as well as lower levels of serum CK-18, a marker of hepatocyte apoptosis, thereby suggesting an overall beneficial effect on all key aspects of NASH pathology. Of further relevance is that the consortium dosage stopped at 9 weeks of age. This may explain, in part, the lesser protective effects observed at 12 weeks in histological steatosis, ballooning, and inflammation, especially when compared with the clear beneficial effects at 9 weeks, thus suggesting a reversal of these more dynamic readouts upon treatment withdrawal. However, it also showed that the protective effect observed at the level of fibrosis at 12 weeks of age was long-lasting, and still apparent 3 weeks after the cessation of treatment. It is still to be evaluated whether these therapeutic effects would be even more pronounced if the consortium had been administered until sacrifice at 12 weeks.

The currently tested consortium is composed, among others, of several butyrate and propionate producers. A non-significant increase in cecal butyrate and propionate levels was measured in the NASH rats (data not shown). Whether these account for the observed benefits in this study is not known. However, sodium butyrate supplementation has been shown to attenuate high-fat diet-induced NASH in mice, most likely by restoring gut dysbiosis and improving gastrointestinal barrier [39]. Interestingly, overweight and obese patients also have higher levels of propionate in their stools, suggesting that either propionate is overproduced, or it is mal-absorbed [40]. In addition, in overweight adult humans, propionate has been shown to prevent weight gain and insulin resistance [41]. Although the role of SCFA in liver health is not completely understood, it has been suggested that when the balance between caloric intake and expenditure is maintained, SCFAs would benefit liver health [42]. Therefore, it is reasonable to postulate that this consortium may improve disease partially due to increased butyrate and propionate levels in the intestine.

Further work must be performed to recapitulate the findings in the two models, namely in what concerns microbial changes in the gut lumen, as well as liver molecular alterations, to confirm the mode-of-action behind the consortium treatment. Nonetheless, the current results support the use of defined combinations of gut commensal bacteria for the treatment of NASH, so to delay disease progression.

5. Conclusions

Despite high prevalence, so far, there are no approved therapies for NASH. This progressive form of NAFLD has proven challenging to reverse with pharmacotherapies to date. On the other hand, preventing the progression from simple steatosis to steatohepatitis and fibrosis represents an attractive therapeutic target. Thus, there is a high unmet medical need to develop new effective therapeutic modalities targeting these key NASH mechanisms. Stool transplantation has been shown to ameliorate aspects related to NASH in pre-clinical models, but it does not offer a long-term solution to patients. The use of microbial consortia of defined composition may therefore represent a more patient-friendly approach at an early stage of disease. The role of the gut microbiome in NAFLD and other metabolic diseases is undisputable [2,4,42]. Intestinal microbial dysbiosis has been shown to contribute to the onset and progression of disease. Therefore, restoring eubiosis is of interest. In the current study, a specific consortium of nine intestinal commensal strains was tested in two in vivo models of NASH and shown to improve symptomatology and to prevent progression to fibrosis. This study convincingly showed that live biotherapeutic products (LBP) are a patient-friendly approach worth considering for development as therapy for NASH.

Supplementary Materials: The following supporting information can be downloaded at: https://www.mdpi.com/article/10.3390/biomedicines10051191/s1. Figure S1 depicts the body weight gain and insulin resistance in NASH rats (fasting insulin levels and HOMA-IR); Figure S2 displays the histological evaluation of the H&E-stained liver sections collected from the NASH rats in bar diagrams; Figure S3 shows representative images of liver parenchyma stained with H&E or liver fibrosis stained with Sirius red in sections collected from the NASH rats; Figure S4 shows the results on the microbial taxonomic composition in the cecum of NASH rats; Figure S5 displays the results obtained on the hepatic gene expression in NASH rats; Figure S6 shows the whole blood HbA1c measured in the STAM™ mice; Figure S7 shows representative images of H&E-stained liver sections collected from the STAM™ study; Figure S8 shows representative images of Sirius red-stained, and F4/80 immunostained liver sections collected from the STAM™ study; Figure S9 displays the immunohistochemistry of fibronectin (bar plot), and the representative images of fibronectin immunostained liver sections collected from the STAM™ study at 12 weeks of age [43–55].

Author Contributions: Conceptualization, I.P., J.G., M.M., and S.A.; Data curation, I.P., M.M., and S.A.; Formal analysis, I.P., A.B., I.R., F.E., and M.d.L.; Funding acquisition, S.P.; Investigation, I.P., A.B., I.R., F.E., M.d.L., S.B, D.G., M.T.S., M.M., and S.A.; Methodology, I.P., A.B., I.R., F.E., M.d.L., S.B., D.G., M.T.S., J.G., M.M., and S.A.; Project administration, I.P.; Supervision, N.H., S.P., J.G., M.M., and S.A.; Visualization, I.P., A.B., I.R., and M.d.L.; Writing–original draft, I.P., A.B., I.R., and M.d.L.; Writing–review and editing, J.G., M.M., and S.A. All authors have read and agreed to the published version of the manuscript.

Funding: This research received no external funding.

Institutional Review Board Statement: All procedures related to the NASH rat study were conducted in accordance with the European Union Guidelines for Ethical Care of Experimental Animals (EC Directive 86/609/EEC for animal experiments) and approved (file number: 11047) by the Animal Care Committee of the Vall d'Hebron Institut de Recerca (VHIR, Barcelona, Spain), and conducted in the animal facilities of VHIR. The STAM™ mouse study was conducted according to the following guidelines: Act on Welfare and Management of Animals (Ministry of the Environment, Act No. 105 of October 1, 1973), Japan; Standards Relating to the Care and Management of Laboratory Animals and Relief of Pain (Notice No. 88 of the Ministry of the Environment, April 28, 2006, Japan), and Guidelines for Proper Conduct of Animal Experiments (Science Council of Japan, 1 June 2006).

Data Availability Statement: Data is contained within the article.

Acknowledgments: We acknowledge International Flavors & Fragrances Inc. (IFF) for financial support.

Conflicts of Interest: I.P., M.L., S.B., N.H., and S.P. are employees of MRM Health, which produces and develops the nine-strain bacterial consortium discussed in this study. D.G. was an employee of MRM Health at the time this project initiated, and when the product was formulated for the rat study.

References

1. Qian, Y.; Fan, J.G. Obesity, Fatty Liver and Liver Cancer. *Hepatobiliary Pancreat. Dis. Int.* **2005**, *4*, 173–177. [PubMed]
2. Abdul-Hai, A.; Abdallah, A.; Malnick, S.D.H. Influence of Gut Bacteria on Development and Progression of Non-Alcoholic Fatty Liver Disease. *World J. Hepatol.* **2015**, *7*, 1679–1684. [CrossRef]
3. Arslan, N. Obesity, Fatty Liver Disease and Intestinal Microbiota. *World J. Gastroenterol.* **2014**, *20*, 16452–16463. [CrossRef]
4. Leung, C.; Rivera, L.; Furness, J.B.; Angus, P.W. The Role of the Gut Microbiota in NAFLD. *Nat. Rev. Gastroenterol. Hepatol.* **2016**, *13*, 412–425. [CrossRef] [PubMed]
5. Chen, Y.H.; Wu, W.K.; Wu, M.S. Microbiota-Associated Therapy for Non-Alcoholic Steatohepatitis-Induced Liver Cancer: A Review. *Int. J. Mol. Sci.* **2020**, *21*, 5999. [CrossRef] [PubMed]
6. Lu, V.B.; Gribble, F.M.; Reimann, F. Nutrient-Induced Cellular Mechanisms of Gut Hormone Secretion. *Nutrients* **2021**, *13*, 883. [CrossRef] [PubMed]
7. Ferreira, C.M.; Vieira, A.T.; Vinolo, M.A.R.; Oliveira, F.A.; Curi, R.; dos Santos Martins, F. The Central Role of the Gut Microbiota in Chronic Inflammatory Diseases. *J. Immunol. Res.* **2014**, *2014*, 689492. [CrossRef]
8. Wong, V.W.-S.; Tse, C.-H.; Lam, T.T.-Y.; Wong, G.L.-H.; Chim, A.M.-L.; Chu, W.C.-W.; Yeung, D.K.-W.; Law, P.T.-W.; Kwan, H.-S.; Yu, J.; et al. Molecular Characterization of the Fecal Microbiota in Patients with Nonalcoholic Steatohepatitis—A Longitudinal Study. *PLoS ONE* **2013**, *8*, e62885. [CrossRef]
9. Albillos, A.; de Gottardi, A.; Rescigno, M. The Gut-Liver Axis in Liver Disease: Pathophysiological Basis for Therapy. *J. Hepatol.* **2020**, *72*, 558–577. [CrossRef]

Appendix

10. Hu, H.; Lin, A.; Kong, M.; Yao, X.; Yin, M.; Xia, H.; Ma, J.; Liu, H. Intestinal Microbiome and NAFLD: Molecular Insights and Therapeutic Perspectives. *J. Gastroenterol.* **2020**, *55*, 142–158. [CrossRef]
11. García-Lezana, T.; Raurell, I.; Bravo, M.; Torres-Arauz, M.; Salcedo, M.T.; Santiago, A.; Schoenenberger, A.; Manichanh, C.; Genescà, J.; Martell, M.; et al. Restoration of a Healthy Intestinal Microbiota Normalizes Portal Hypertension in a Rat Model of Nonalcoholic Steatohepatitis. *Hepatology* **2018**, *67*, 1485–1498. [CrossRef] [PubMed]
12. Jojima, T.; Tomotsune, T.; Iijima, T.; Akimoto, K.; Suzuki, K.; Aso, Y. Empagliflozin (an SGLT2 Inhibitor), Alone or in Combination with Linagliptin (a DPP-4 Inhibitor), Prevents Steatohepatitis in a Novel Mouse Model of Non-Alcoholic Steatohepatitis and Diabetes. *Diabetol. Metab. Syndr.* **2016**, *8*, 45. [CrossRef] [PubMed]
13. Fujii, M.; Shibazaki, Y.; Wakamatsu, K.; Honda, Y.; Kawauchi, Y.; Suzuki, K.; Arumugam, S.; Watanabe, K.; Ichida, T.; Asakura, H.; et al. A Murine Model for Non-Alcoholic Steatohepatitis Showing Evidence of Association between Diabetes and Hepatocellular Carcinoma. *Med. Mol. Morphol.* **2013**, *46*, 141–152. [CrossRef]
14. Park, J.G.; Mok, J.S.; Han, Y.I.; Park, T.S.; Kang, K.W.; Choi, C.S.; Park, H.D.; Park, J. Connectivity Mapping of Angiotensin-PPAR Interactions Involved in the Amelioration of Non-Alcoholic Steatohepatitis by Telmisartan. *Sci. Rep.* **2019**, *9*, 4003. [CrossRef] [PubMed]
15. Kleiner, D.E.; Brunt, E.M.; Van Natta, M.; Behling, C.; Contos, M.J.; Cummings, O.W.; Ferrell, L.D.; Liu, Y.-C.; Torbenson, M.S.; Unalp-Arida, A.; et al. Design and Validation of a Histological Scoring System for Nonalcoholic Fatty Liver Disease. *Hepatology* **2005**, *41*, 1313–1321. [CrossRef] [PubMed]
16. Bravo, M.; Raurell, I.; Hide, D.; Fernández-Iglesias, A.; Gil, M.; Barberá, A.; Salcedo, M.T.; Augustin, S.; Genescà, J.; Martell, M. Restoration of Liver Sinusoidal Cell Phenotypes by Statins Improves Portal Hypertension and Histology in Rats with NASH. *Sci. Rep.* **2019**, *9*, 20183. [CrossRef] [PubMed]
17. Marrone, G.; Russo, L.; Rosado, E.; Hide, D.; García-Cardeña, G.; García-Pagán, J.C.; Bosch, J.; Gracia-Sancho, J. The Transcription Factor KLF2 Mediates Hepatic Endothelial Protection and Paracrine Endothelial-Stellate Cell Deactivation Induced by Statins. *J. Hepatol.* **2013**, *58*, 98–103. [CrossRef]
18. Marrone, G.; Maeso-Díaz, R.; García-Cardena, G.; Abraldes, J.G.; García-Pagán, J.C.; Bosch, J.; Gracia-Sancho, J. KLF2 Exerts Antifibrotic and Vasoprotective Effects in Cirrhotic Rat Livers: Behind the Molecular Mechanisms of Statins. *Gut* **2015**, *64*, 1434–1443. [CrossRef]
19. Febbraio, M.A.; Reibe, S.; Shalapour, S.; Ooi, G.J.; Watt, M.J.; Karin, M. Preclinical Models for Studying NASH-Driven HCC: How Useful Are They? *Cell Metab.* **2019**, *29*, 18–26. [CrossRef]
20. Tsutsui, M.; Tanaka, N.; Kawakubo, M.; Sheena, Y.; Horiuchi, A.; Komatsu, M.; Nagaya, T.; Joshita, S.; Umemura, T.; Ichijo, T.; et al. Serum Fragmented Cytokeratin 18 Levels Reflect the Histologic Activity Score of Nonalcoholic Fatty Liver Disease More Accurately than Serum Alanine Aminotransferase Levels. *J. Clin. Gastroenterol.* **2010**, *44*, 440–447. [CrossRef]
21. Miele, L.; Valenza, V.; La Torre, G.; Montalto, M.; Cammarota, G.; Ricci, R.; Mascianà, R.; Forgione, A.; Gabrieli, M.L.; Perotti, G.; et al. Increased Intestinal Permeability and Tight Junction Alterations in Nonalcoholic Fatty Liver Disease. *Hepatology* **2009**, *49*, 1877–1887. [CrossRef] [PubMed]
22. Dai, X.; Hou, H.; Zhang, W.; Liu, T.; Li, Y.; Wang, S.; Wang, B.; Cao, H. Microbial Metabolites: Critical Regulators in NAFLD. *Front. Microbiol.* **2020**, *11*, 567654. [CrossRef] [PubMed]
23. Meroni, M.; Longo, M.; Dongiovanni, P. The Role of Probiotics in Nonalcoholic Fatty Liver Disease: A New Insight into Therapeutic Strategies. *Nutrients* **2019**, *11*, 2642. [CrossRef] [PubMed]
24. Ebrahimzadeh Leylabadlo, H.; Ghotaslou, R.; Samadi Kafil, H.; Feizabadi, M.M.; Moaddab, S.Y.; Farajnia, S.; Sheykhsaran, E.; Sanaie, S.; Shanehbandi, D.; Bannazadeh Baghi, H. Non-Alcoholic Fatty Liver Diseases: From Role of Gut Microbiota to Microbial-Based Therapies. *Eur. J. Clin. Microbiol. Infect. Dis.* **2020**, *39*, 613–627. [CrossRef]
25. Philips, C.A.; Pande, A.; Shasthry, S.M.; Jamwal, K.D.; Khillan, V.; Chandel, S.S.; Kumar, G.; Sharma, M.K.; Maiwall, R.; Jindal, A.; et al. Healthy Donor Fecal Microbiota Transplantation in Steroid-Ineligible Severe Alcoholic Hepatitis: A Pilot Study. *Clin. Gastroenterol. Hepatol.* **2017**, *15*, 600–602. [CrossRef]
26. Li, Z.; Yang, S.; Lin, H.; Huang, J.; Watkins, P.A.; Moser, A.B.; Desimone, C.; Song, X.; Diehl, A.M. Probiotics and Antibodies to TNF Inhibit Inflammatory Activity and Improve Nonalcoholic Fatty Liver Disease. *Hepatology* **2003**, *37*, 343–350. [CrossRef]
27. Spooner, H.C.; Derrick, S.A.; Maj, M.; Manjarín, R.; Hernandez, G.V.; Tailor, D.S.; Bastani, P.S.; Fanter, R.K.; Fiorotto, M.L.; Burrin, D.G.; et al. High-Fructose, High-Fat Diet Alters Muscle Composition and Fuel Utilization in a Juvenile Iberian Pig Model of Non-Alcoholic Fatty Liver Disease. *Nutrients* **2021**, *13*, 4195. [CrossRef]
28. Xue, L.; He, J.; Gao, N.; Lu, X.; Li, M.; Wu, X.; Liu, Z.; Jin, Y.; Liu, J.; Xu, J.; et al. Probiotics May Delay the Progression of Nonalcoholic Fatty Liver Disease by Restoring the Gut Microbiota Structure and Improving Intestinal Endotoxemia. *Sci. Rep.* **2017**, *7*, 45176. [CrossRef]
29. Campollo, O.; Sprengers, D.; McIntyre, N. The BCAA/AAA Ratio of Plasma Amino Acids in Three Different Groups of Cirrhotics. *Rev. Investig. Clin. Organo Hosp. Enferm. Nutr.* **1992**, *44*, 513–518.
30. Iwao, M.; Gotoh, K.; Arakawa, M.; Endo, M.; Honda, K.; Seike, M.; Murakami, K.; Shibata, H. Supplementation of Branched-Chain Amino Acids Decreases Fat Accumulation in the Liver through Intestinal Microbiota-Mediated Production of Acetic Acid. *Sci. Rep.* **2020**, *10*, 18768. [CrossRef]

31. Raghunath, A.; Panneerselvam, L.; Sundarraj, K.; Perumal, E. Heat Shock Proteins and Endoplasmic Reticulum Stress. In *Heat Shock Proteins and Stress*; Asea, A.A.A., Kaur, P., Eds.; Springer International Publishing: Cham, Switzerland, 2018; pp. 39–78; ISBN 978-3-319-90725-3.
32. Zhang, X.Q.; Xu, C.F.; Yu, C.H.; Chen, W.X.; Li, Y.M. Role of Endoplasmic Reticulum Stress in the Pathogenesis of Nonalcoholic Fatty Liver Disease. *World J. Gastroenterol.* **2014**, *20*, 1768–1776. [CrossRef] [PubMed]
33. Seelig, S.; Liaw, C.; Towle, H.C.; Oppenheimer, J.H. Thyroid Hormone Attenuates and Augments Hepatic Gene Expression at a Pretranslational Level. *Proc. Natl. Acad. Sci. USA* **1981**, *78*, 4733–4737. [CrossRef] [PubMed]
34. Cunningham, B.A.; Moncur, J.T.; Huntington, J.T.; Kinlaw, W.B. "Spot 14" Protein: A Metabolic Integrator in Normal and Neoplastic Cells. *Thyroid* **1998**, *8*, 815–825. [CrossRef] [PubMed]
35. Jump, D.B.; Bell, A.; Lepar, G.; Hu, D. Insulin Rapidly Induces Rat Liver S14 Gene Transcription. *Mol. Endocrinol.* **1990**, *4*, 1655–1660. [CrossRef]
36. Chen, Y.T.; Tseng, P.H.; Tseng, F.Y.; Chi, Y.C.; Han, D.S.; Yang, W.S. The Serum Level of a Novel Lipogenic Protein Spot 14 Was Reduced in Metabolic Syndrome. *PLoS ONE* **2019**, *14*, e0212341. [CrossRef]
37. Ortega, F.J.; Vazquez-Martin, A.; Moreno-Navarrete, J.-M.; Bassols, J.; Rodriguez-Hermosa, J.; Gironés, J.; Ricart, W.; Peral, B.; Tinahones, F.J.; Fruhbeck, G.; et al. Thyroid Hormone Responsive Spot 14 Increases during Differentiation of Human Adipocytes and Its Expression Is Down-Regulated in Obese Subjects. *Int. J. Obes.* **2010**, *34*, 487–499. [CrossRef]
38. Cannito, S.; Novo, E.; Parola, M. Therapeutic Pro-Fibrogenic Signaling Pathways in Fibroblasts. *Adv. Drug Deliv. Rev.* **2017**, *121*, 57–84. [CrossRef]
39. Zhou, D.; Pan, Q.; Xin, F.Z.; Zhang, R.N.; He, C.X.; Chen, G.Y.; Liu, C.; Chen, Y.W.; Fan, J.G. Sodium Butyrate Attenuates High-Fat Diet-Induced Steatohepatitis in Mice by Improving Gut Microbiota and Gastrointestinal Barrier. *World J. Gastroenterol.* **2017**, *23*, 60–75. [CrossRef]
40. Schwiertz, A.; Taras, D.; Schäfer, K.; Beijer, S.; Bos, N.A.; Donus, C.; Hardt, P.D. Microbiota and SCFA in Lean and Overweight Healthy Subjects. *Obesity* **2010**, *18*, 190–195. [CrossRef]
41. Chambers, E.S.; Viardot, A.; Psichas, A.; Morrison, D.J.; Murphy, K.G.; Zac-Varghese, S.E.K.; MacDougall, K.; Preston, T.; Tedford, C.; Finlayson, G.S.; et al. Effects of Targeted Delivery of Propionate to the Human Colon on Appetite Regulation, Body Weight Maintenance and Adiposity in Overweight Adults. *Gut* **2015**, *64*, 1744–1754. [CrossRef]
42. Sikalidis, A.K.; Maykish, A. The Gut Microbiome and Type 2 Diabetes Mellitus: Discussing a Complex Relationship. *Biomedicines* **2020**, *8*, 8. [CrossRef] [PubMed]
43. Thoendel, M.; Jeraldo, P.; Greenwood-Quaintance, K.E.; Yao, J.; Chia, N.; Hanssen, A.D.; Abdel, M.P.; Patel, R. Comparison of Three Commercial Tools for Metagenomic Shotgun Sequencing Analysis. *J. Clin. Microbiol.* **2020**, *58*, e00981-19. [CrossRef]
44. Franzosa, E.A.; McIver, L.J.; Rahnavard, G.; Thompson, L.R.; Schirmer, M.; Weingart, G.; Lipson, K.S.; Knight, R.; Caporaso, J.G.; Segata, N.; et al. Species-Level Functional Profiling of Metagenomes and Metatranscriptomes. *Nat. Methods* **2018**, *15*, 962–968. [CrossRef] [PubMed]
45. McMurdie, P.J.; Holmes, S. Phyloseq: An R Package for Reproducible Interactive Analysis and Graphics of Microbiome Census Data. *PLoS ONE* **2013**, *8*, e61217. [CrossRef] [PubMed]
46. Rohart, F.; Gautier, B.; Singh, A.; Lê Cao, K.-A. MixOmics: An R Package for 'omics Feature Selection and Multiple Data Integration. *PLoS Comput. Biol.* **2017**, *13*, e1005752. [CrossRef] [PubMed]
47. Liao, Y.; Smyth, G.K.; Shi, W. FeatureCounts: An Efficient General Purpose Program for Assigning Sequence Reads to Genomic Features. *Bioinformatics* **2014**, *30*, 923–930. [CrossRef] [PubMed]
48. Anders, S.; Huber, W. Differential Expression Analysis for Sequence Count Data. *Genome Biol.* **2010**, *11*, R106. [CrossRef] [PubMed]
49. Thévenot, E.A.; Roux, A.; Xu, Y.; Ezan, E.; Junot, C. Analysis of the Human Adult Urinary Metabolome Variations with Age, Body Mass Index, and Gender by Implementing a Comprehensive Workflow for Univariate and OPLS Statistical Analyses. *J. Proteome Res.* **2015**, *14*, 3322–3335. [CrossRef]
50. Wu, T.; Hu, E.; Xu, S.; Chen, M.; Guo, P.; Dai, Z.; Feng, T.; Zhou, L.; Tang, W.; Zhan, L.; et al. ClusterProfiler 4.0: A Universal Enrichment Tool for Interpreting Omics Data. *Innovation* **2021**, *2*, 100141. [CrossRef]
51. Martens, M.; Ammar, A.; Riutta, A.; Waagmeester, A.; Slenter, D.N.; Hanspers, K.; A Miller, R.; Digles, D.; Lopes, E.N.; Ehrhart, F.; et al. WikiPathways: Connecting Communities. *Nucleic Acids Res.* **2021**, *49*, D613–D621. [CrossRef]
52. Karp, P.D.; Riley, M.; Paley, S.M.; Pellegrini-Toole, A. The MetaCyc Database. *Nucleic Acids Res.* **2002**, *30*, 59–61. [CrossRef] [PubMed]
53. Jassal, B.; Matthews, L.; Viteri, G.; Gong, C.; Lorente, P.; Fabregat, A.; Sidiropoulos, K.; Cook, J.; Gillespie, M.; Haw, R.; et al. The Reactome Pathway Knowledgebase. *Nucleic Acids Res.* **2020**, *48*, D498–D503. [CrossRef] [PubMed]
54. Nishimura, D. A View from the Web BioCarta. *Biotech. Softw. Internet Rep.* **2001**, 2, 117–120. [CrossRef]
55. Rouillard, A.D.; Gundersen, G.W.; Fernandez, N.F.; Wang, Z.; Monteiro, C.D.; McDermott, M.G.; Ma'ayan, A. The Harmonizome: A Collection of Processed Datasets Gathered to Serve and Mine Knowledge about Genes and Proteins. *Database* **2016**, *2016*, baw100. [CrossRef] [PubMed]